Pre-clinical Evaluation of the Forces During Limb Lengthening Using Manual and Automated Devices

A thesis submitted for the degree of Doctor of Philosophy

Rhona Sinclair

Brunel University,
School of Engineering and Design

September 2011

ABSTRACT

Limb lengthening procedures use fixation devices to extend the constantly regenerating bone and surrounding soft tissues. Automated devices have been developed that aim to provide a more gradual tissue extension, resulting in better quality of treatment for the patient. Benefits include pain reduction and probable enhanced tissue outcomes. The development of one such new smart lengthening device is described.

An integrated numerical model of tissue mechanics during lengthening is presented. It represents the mechanical environment in which the devices extend. The mechanism of the automated device is also modelled using Matlab software and validation was achieved through experimental testing. Validation of the tissue model includes the design of an experimental hydraulic system with the ability to control the peak loads and relaxation over time. A simplified mechanobiological model for the longer term healing effects is proposed. Calibration of the tissue model to clinical data allows for direct comparison of the load and extension of identical tissues, one being lengthened by a traditional device, the other an automated device.

This simulation can be extended to include a range of lengthening rates and frequencies of distraction alongside various patient dependent tissue properties. The models also provide the opportunity to assess the effects of iterative changes to the device parameters (such as stiffness) on its performance as well as analyse the effect that these changes have on tissue extension and loading.

Use of these models to optimise the device design alongside optimisation of the extension regime can result in improved device design and consequently improved patient outcomes.

TABLE OF CONTENTS

LIST OF FIGURES

LIST OF TABLES

ACKNOWLEDGEMENTS

I would like to thank my supervisor Mr Chris Brown for his support and guidance, not only during this work but throughout my time at Brunel University. Additionally, Professor Peter Hobson has provided further supervision and another well received opinion.

My thanks go to Dr Andy Taylor (of Finsbury Developments Ltd.) who initiated the original concept of the smart device and Dr Anne Roques for her advice and encouragement. I am grateful for the time and effort of Mr Richard Wadey (Micro-Precision Instruments Ltd) who assist in the development of the electronics and associated software of the automated device and to Keith Withers for the support in his lab over the years.

Chapter 1

Introduction

1.1 Indications for limb lengthening

Limb lengthening has been recognised as a valid technique for both congenital and acquired disorders that result in a leg length discrepancy (LLD). Congenital disorders relate to limb hypoplasia syndromes, skeletal dysplasias and hemihypertrophy or atrophy syndromes while acquired disorders can be traumatic, infectious, inflammatory, neurologic and metabolic bone diseases. (Ilizarov, 1990; Shepherd *et al.*, 2001).

Aside from being a cosmetic problem, without this intervention patients may suffer from gait disturbance, and degenerative changes in the axial skeleton. Functional loss is the main reason for surgical management. A LLD of 1-1.5cm is noticeable to the patient but can be tolerated with no real functional impairment whereas at 1.5-2.5cm there may be minor functional difficulties, correctable with a shoe wedge. Above 2.5cm, the LLD may result in hip pain, lower back pain, alteration of gait pattern and significant discomfort for the patient (Shepherd *et al.*, 2001) and at this point surgical treatment is the preferred option.

The decision-making algorithm shown in Figure 1-1 has been suggested for the preferred treatment of LLDs.

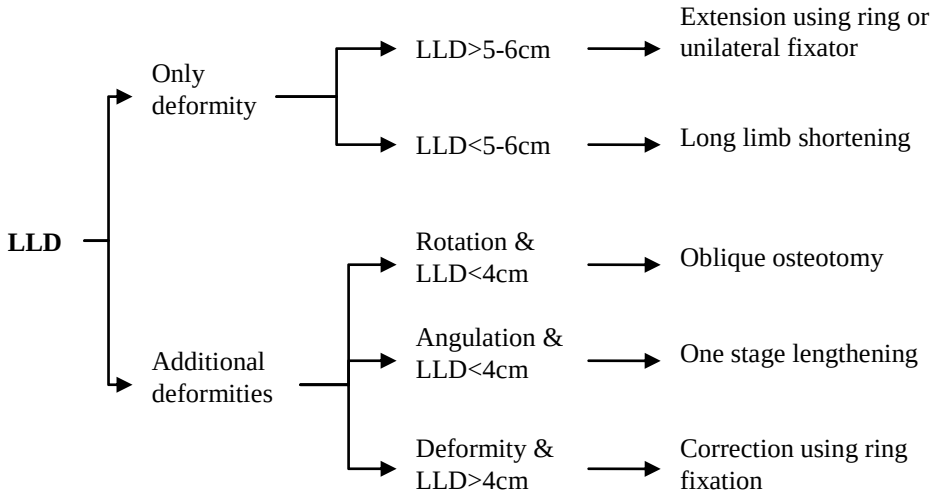

Figure 1-1 Clinical decision making algorithm (adapted from Shepherd *et al.*, 2001)

This study will concentrate on only one branch of this diagram – LLD as the only deformity. Even for small discrepancies, long limb shortening is not always appropriate and thus extensions can be as little as a few centimetres

1.2 Historical review of limb lengthening procedures

Although Codivilla is attributed with the first successful callus distraction procedure in the early 1900's (Codivilla, 1905), high complication rates led to a negative opinion of the surgery and its apparatus until the 1950's when Professor Gavril Ilizarov sought to understand the procedure more comprehensively. Ilizarov developed a 'law of tension stress' which states that "living tissue, when subjected to slow, steady traction, becomes metabolically activated in both the biosynthetic and proliferative pathways" (Ilizarov, 1990). This can be applied to a wide range of orthopaedic indications including deformity correction and lengthening. Ilizarov developed a mechanically sound external fixation system to produce these stresses within the tissues, now widely known as the 'Ilizarov frame', which has remained largely unchanged since its initial development.

Ilizarov's technique is the preferred treatment for limb length discrepancies and bilateral lengthening. This technique refers to any procedure resulting in gradual elongation of the limb using an extendable fixator (not to be confused with the Ilizarov circular frame – a

specific fixator design). Elongation can be achieved using an assortment of currently available devices of varying configurations and degrees of automation, with different mechanical and cosmetic benefits.

1.3 Testing of automated lengthening devices

A new monolateral smart device has been developed that provides continuous lengthening and has the ability to change the rate of lengthening throughout the procedure. Load measurement has been identified as a method of assessing tissue regeneration during limb lengthening (Aarnes *et al.*, 2005) and it has been proposed that this could be used to determine the optimal rate of distraction whilst reducing complications during lengthening such as premature consolidation or non-union. The new smart lengthening device was designed with load measurement and a control system so that it could make changes to the extension rate based on load readings (although much of the initial testing requires a linear extension to be maintained). Load based lengthening regimes are not specific to the device in question as other devices have used this same idea (Wee *et al.*, 2011). Even during manual lengthening, the rate does not always stay constant and decisions to change the load are currently based on radiographic evidence and patient pain levels.

To fully test automated lengthening devices of this kind, assess their impact on tissues and compare them to existing devices, standard external fixation test procedures (ASTM F1541) are inadequate. New test procedures must be developed to support the control decisions that are based on continuously changing incoming data. Animal models are commonly used because they provide a very close imitation of the tissues present during human limb lengthening, but the ethical issues surrounding animal testing are such that this is undesirable as a frequent test method.

1.4 Research aims

Consequently, the aim of this work was to develop a simulated environment for the testing of limb lengthening apparatus including automated devices. This was broken down into objectives:

- Simulate the manual and automated device mechanisms using a numerical model
- Validate the model using experimental techniques
- Simulate the resistive forces of the tissues during lengthening

- Devise a method of validation for the tissue model using experimental methods
- Use these models to predict the resistive loads developed during limb lengthening by different devices in order to aid their development

With improved designs of lengthening devices it is hoped that patient outcomes would be improved. A longer term objective is that, through use of additional clinical data collected from automated devices, the model could suggest an optimal lengthening regime for individual devices whilst also identifying abnormalities in tissue growth.

As a consequence of these aims, the structure of this work flows from description of the device development and the numerical model built to simulate the mechanics (Chapters 4 and 5) through to its experimental validation (Chapter 6). The tissue model is designed and tested (Chapter 7) before adding the complexity of pins (Chapter 8) and a basic mechanobiological healing model (Chapter 9). Finally the full model is applied using clinical data (Chapter 10). Conclusions are then drawn and future work is defined (Chapter 11).

Chapter 2

Background of limb lengthening

2.1 Introduction

The biological process involved in lengthening limbs is often referred to as callotasis or distraction osteogenesis (from the Latin ‘distractus’ meaning to draw apart, the Greek ‘osteon’ meaning bone and the Latin ‘genesis’ meaning formation). The use of distraction osteogenesis (DO) was first introduced by Ilizarov in the 1950’s for the lengthening of limbs and, although the process was implemented at other anatomical sites shortly after (for example maxillofacial reconstruction by Snyder *et al.*, 1973), this current study is concerned with the use of devices for DO specifically on limbs. During limb lengthening, the focus is on bone formation, but care must be taken to ensure the preservation, as well as formation, of the softer surrounding tissues such as muscle, tendon, skin and nerves.

This Chapter introduces the clinical procedure for limb lengthening, describes the tissues involved in the process and discusses the types of apparatus used by clinicians to distract the tissues.

2.2 Anatomy – bone and soft tissue interactions

2.2.1 Long bone anatomy

Lengthening can take place on upper and lower limbs but the functional penalty of a leg length discrepancy (LLD) is more significant. Consequently surgery is more likely to be considered as a treatment option for LLDs. The femur and tibia are viable lengthening sites, and depending on the indication, one or both of these may be treated.

The femur is the longest and strongest bone in the human body forming part of the hip joint proximally and the knee joint distally. The tibia is the second largest bone and is the larger of the two bones distal to the knee, the other being the fibula. The proximal end of

the tibia acts as an articulation surface of the knee joint, while the distal end (along with the fibula) forms part of the ankle joint. The arm is composed of the humerus and radius; the proximal end of the humerus creating the shoulder joint with the scapula and the distal end joining with the radius and ulna of the lower arm to form the elbow joint.

The femur, tibia, humerus and radius are considered 'long' bones and have a similar composition, described in Figure 2-1. The ends of the bone (epiphysis) consist of spongy trabecular bone; a lattice arrangement of small bone struts, covered by compact cortical bone. The diaphysis, or shaft of the bone, consists of a thick walled cylinder of cortical bone with a medullary canal at its centre, containing marrow. A membrane of connective tissue with osteogenic potency lines the internal surface of this canal, and is named the endosteum. A similar membrane, the periosteum, covers the external surface and, like the endosteum, is also highly vascular. The contact surfaces of the epiphysis are covered with hyaline cartilage; a complex arrangement of mainly collagen fibrils permitting low friction articulation.

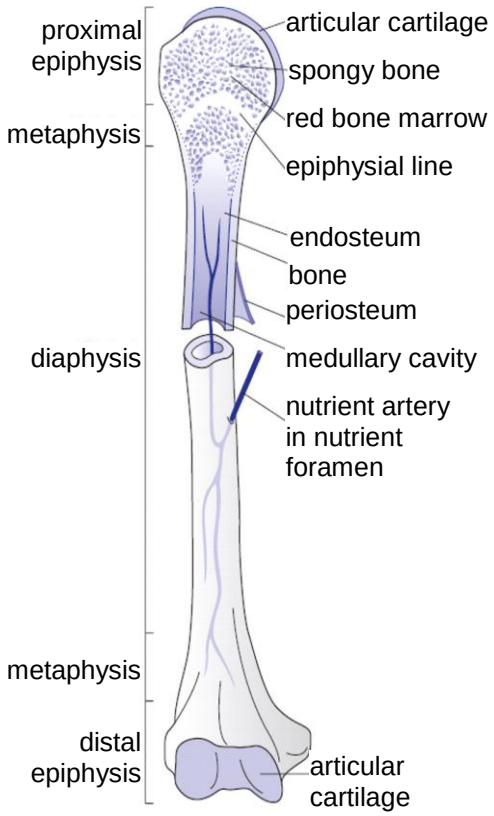

Figure 2-1 Partially sectioned humerus (adapted from Tortora and Grabowski, 2002)

Each long bone has a mechanical and anatomical axis (Figure 2-2). The mechanical axis is a line joining the proximal and distal joint centres while the anatomical axis is the mid-

diaphyseal line. The exact angle between axes is patient specific but particular care is given to these axes when lengthening leg bones to avoid additional deformities influencing gait.

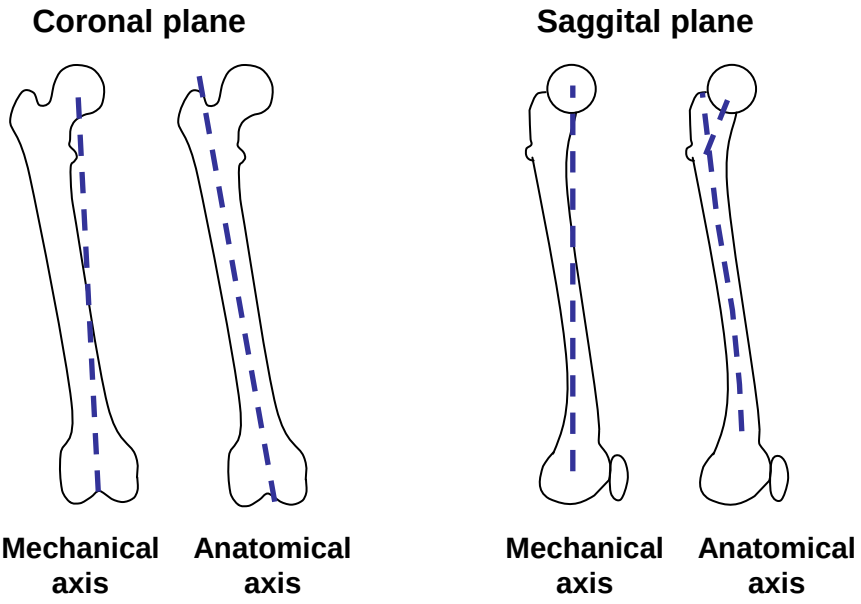

Figure 2-2 Anatomical and mechanical axis of the femur

A ridge known as the linea aspera can be found on the posterior surface of the femoral shaft onto which several muscles are attached. The major muscles of the lower limb are shown in Figure 2-3. Surgeons carefully consider these muscle groups during preoperative planning, ensuring positioning of external fixator pins minimises damage.

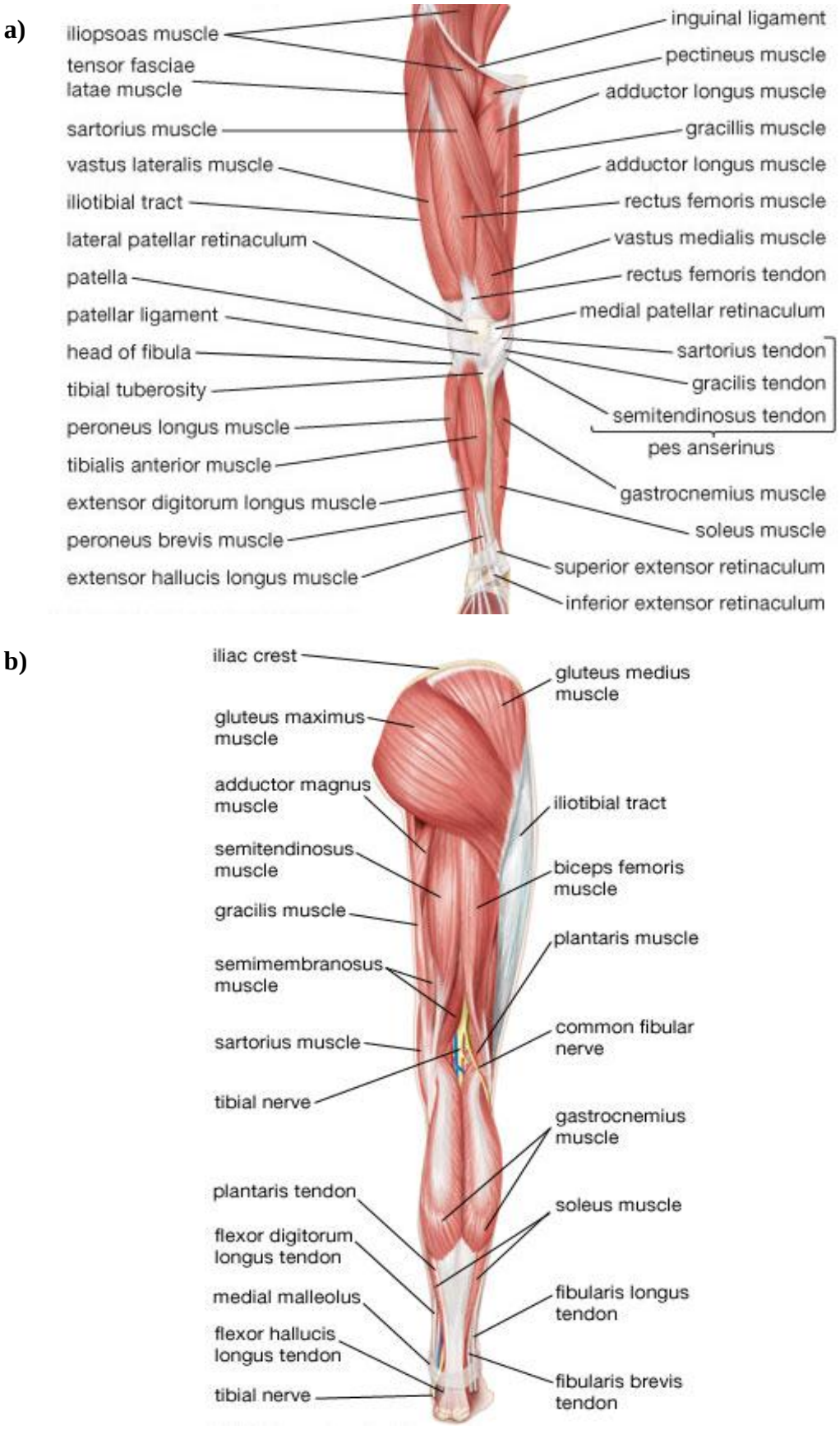

Figure 2-3 Muscle groups in the leg a) anterior b) posterior

(from Encyclopaedia Britannica Online)

2.2.2 Callus tissue physiology

Limb lengthening achieves new bone formation as a result of stretching a healing callus formed between two bone ends. A variety of connective tissues form throughout the procedure. These are similar to the tissues present during bone healing and include bone, cartilage, fibrous tissue and granulation tissue. They can be referred to as 'connective tissue', one of the four types of tissues under the traditional classification of tissues (the others being muscle, nervous and epithelial). Connective tissue provides the structure of the human body in the form of bone, ligament, tendon and cartilage. In fact, these structural tissues are all from a common origin (mesenchyme – an embryonic tissue), have a degree of vascularity and are comprised primarily of a non-living extracellular matrix which allows for a greater degree of loading than any other tissue. The matrix is comprised of cells, ground substance and fibres (primarily collagen fibres), which are exceptionally tough and have high tensile strength, even higher than steel fibres of the same size (Marieb and Hoehn, 2010). The main tissues involved in bone lengthening are now described.

Bone tissue:

In addition to having an abundance of strong fibrous collagen proteins, bone tissue has a dense surrounding of an inorganic component – calcium salts (specifically calcium phosphate). These crystals are deposited on and between the fibres giving the tissue increased rigidity and hardness in order to provide support and protection to body structures. A number of different cells permeate the bone; osteocytes which are the most abundant cell in compact bone and responsible for routine turnover of cells; osteoblasts which are responsible for bone formation by laying down a collagenous matrix upon which the mineral is later deposited; and osteoclasts whose purpose is destruction of the bone. Bone tissue takes two main forms known as woven and lamellar bone. This distinction is particularly important in callus formation as both will exist at different times in the healing process and have different mechanical properties. Woven bone is non-oriented, with collagen fibrils and crystals found randomly placed. It is highly mineralized and is laid down at a fast rate of 4microns/day. This can be contrasted to lamellar bone which is laid down much more slowly, at a rate of less than 1micron/day, is much more organized is its arrangement of fibrils and mineral and is consequently stronger (Currey, 2002).

Fibrocartilage:

Rows of chondrocytes alternating with rows of collagen fibres provide the structure of fibrocartilage and it can be described as a cross between cartilage and dense regular connective tissue. Its structural properties mimic this combination, which allow it to resist tension well whilst also being compressible.

Granulation tissue:

As the first fibrous connective tissue to be formed during the wound healing process, granulation tissue replaces the initial fibrin clot. It is soft and moist in texture and consists of a variety of cells such as fibroblasts, new blood cells, mesenchymal stem cells (MSCs), endothelial cells and immune cells alongside a provisional extracellular matrix (Marieb and Hoehn, 2010).

2.2.3 Muscle properties

Limb lengthening requires the elongation of soft tissues alongside hard tissues. Although focus is given to the bone and its ability to regenerate, clinical complications can arise due to the response of some soft tissues to the lengthening process (Nakamura *et al*., 1997). The muscles and tendons in the system are not severed prior to stretching and will provide some immediate resistance to lengthening. The level of resistance may depending on the clinical indication i.e. if the cause of the shortened limb is trauma then the original length of the muscles is nearer to the final length and, as such, may not provide as much resistance to lengthening compared to muscle in a patient with insufficient bone growth.

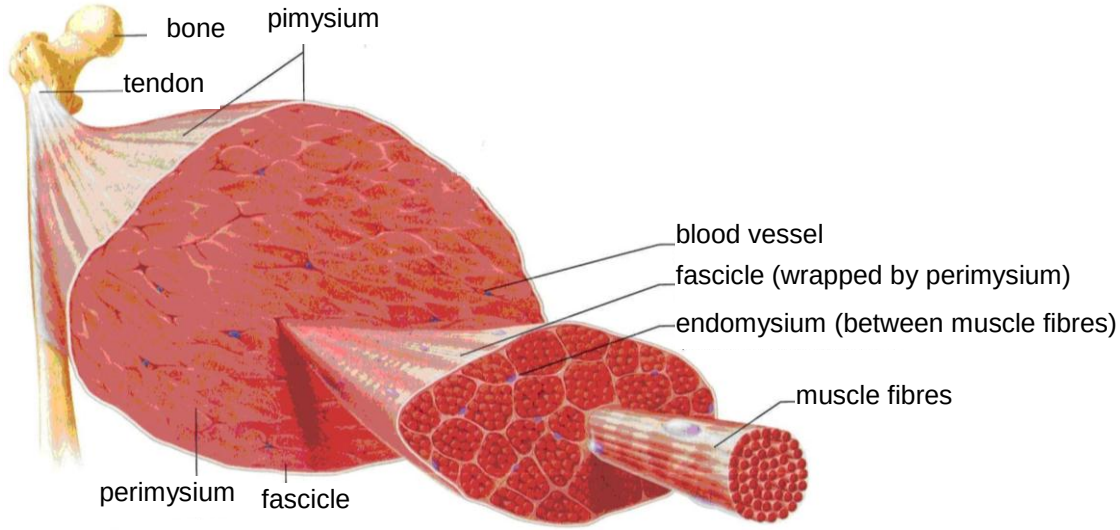

Figure 2-4 Composition of muscle tissue (adapted from Marieb and Hoehn, 2010)

Figure 2-4 shows the composition of muscle tissue. The construction is cellular and each muscle is a made up of individual muscle fibres bundled into fascicles by the perimysium. Inside the fibres are sarcomeres, composed of actin and myosin, the active proteins. Skeletal muscle fascicles are connected to the bone by tendons. Tendons are largely composed of tenocytes, water and fibrous collagen proteins which weave together to form strands of flexible tissue. They form a mineralised connection by growing into the bone, creating a permanent bond.

2.3 Biological principles of distraction osteogenesis

2.3.1 Bone healing

It is well known that bones can self-heal following a fracture if it is stabilised sufficiently. This regenerative nature of bone is the basis for DO, therefore it is important to understand the physiology of fracture healing with particular reference to the types of tissues forming at the various stages.

The four major phases in the healing process are described below and shown in Figure 2-5:

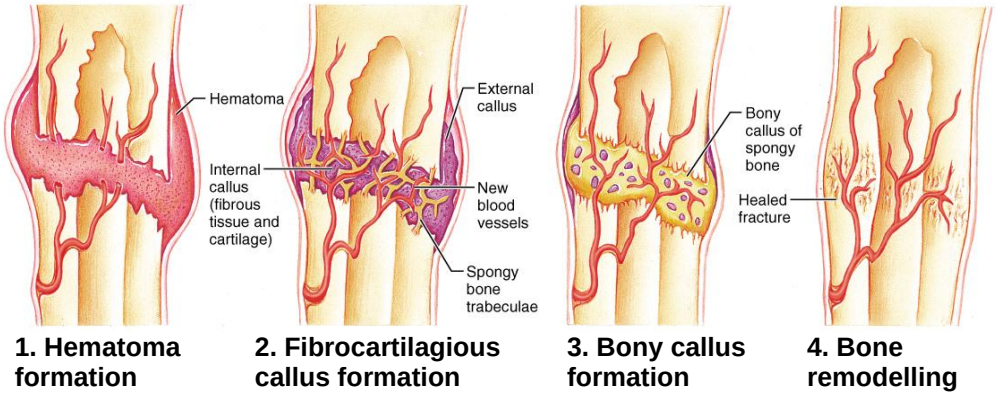

Figure 2-5 Stages of fracture repair (from Marieb and Hoehn, 2010)

<u>1. Reactive – Hematoma formation</u>

This is the inflammatory phase following the fracture. Immediately blood cells are seen around the site and within a few hours a blot clot is formed (hematoma). These cells eventually die but fibroblasts interspersed with newly formed capillaries make up the granulation tissue as described in 2.1.2.

2. Reparative – Fibrocartilagious callus formation

Within a few days, the periosteum adjacent to the fracture begins to aid chondroblast activity alongside the granulation tissue, forming hyaline cartilage. The cells of the periosteum at the existing bone ends transform into osteoblasts and begin to form woven bone which reach out to the corresponding tissue on the other side of the fracture gap.

3. Bony callus formation

A callus is formed when the hyaline cartilage and woven bone have been laid down between the bone ends. Some of the strength is now restored and the tissue is ready to be replaced by lamellar bone in the form of trabecular bone. This replacement starts with the woven bone, moving inwards to the hyaline cartilage.

4. Remodelling

This phase is a replacement of the trabecular bone with compact bone. Osteoclast activity removes the trabecular bone while osteoblasts lay down the compact bone, eventually remodelling the callus into a shape more similar to the original cylinder.

This process is known as 'indirect' healing - the bone ends are slightly separated and are permitted some micromotion relative to each other- as opposed to 'direct' healing which involves securing the bone ends together such that no motion is permitted and the callus does not form. It has been recognised that indirect healing provides a more stable environment during the healing process, a more satisfactory long-term outcome and takes less time compared to the direct healing method (Goodship and Kenwright, 1985).

2.3.2 Law of tension-stress

This healing process can be used to further advantage using the biological principle of distraction osteogenesis. During the repair process, approximately one week post-fracture, the gap tissue is comprised of spongy bone trabeculae, fibrous tissue and cartilage which, instead of being allowed to ossify, can be slowly stretched in the axial direction. This tension has been found to promote activity and growth according to Ilizarovs 'law of tension stress' (Ilizarov, 1990).

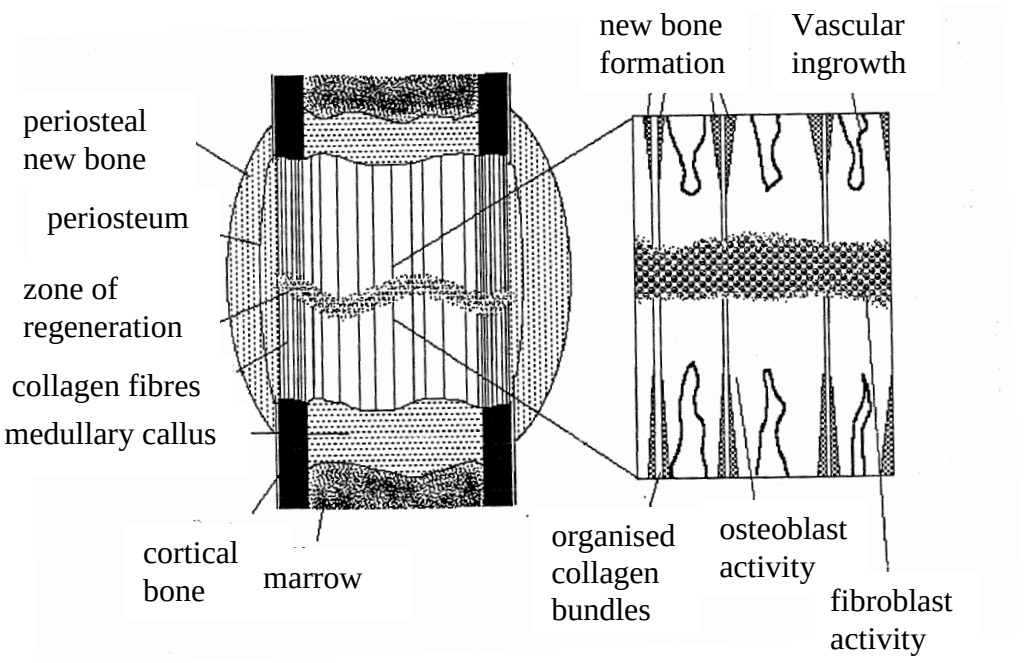

Figure 2-6 Composition of distraction callus taken from histology (from Younger, 1990)

Within the distraction site is a central growth zone (CGZ) made of cells similar to fibroblasts, responsible for producing the collagen fibrils that act as a matrix for osteoid formation (Figure 2-6). These columns of osteoid are laid parallel to the direction of distraction and turn into lamellar bone containing osteocytes towards the proximal and distal ends of the distraction site. Under ideal conditions, this central growth zone is almost nonexistent, however it is typically 2-4mm wide and gradually ossifies during the period of neutral fixation (Ilizarov, 1989a, 1990).

2.4 Clinical method

2.4.1 Introduction to clinical method

There are commonly four stages in the lengthening process:

1. Surgical procedure

    a. Fixation – An adjustable frame is fitted to both ends of the bone in order keep the ends at an optimal separation for bone growth. This frame is traditionally an external frame with pins or wires through the bone segments but more recently has been introduced intramedullary (i.e. an extending nail through the medullary canal), usually with some external components.

b. Osteoclasis – A 'fracture' is induced in the form of an osteotomy. Preservation of the medullary canal can be accomplished by instead performing a corticotomy (or closed osteoclasis). The fracture site can be metaphyseal or diaphyseal and the precise location will be influenced by muscle attachment points near the preferred location.

2. Latency period

Post-operatively there is a 3-10day latency period depending on the patient, during which the space between the bone ends fills with the fibrocartilaginous gap tissue seen during 'normal' bone healing. If distraction were to take place immediately there would be a significantly lower quantity of bone filling the gap.

3. Distraction period

After tissue formation in the latency period, the distraction site is ready to be stretched, typically over a period of several weeks or months relating to the degree of extension required. The distance between the bone pins is increased by gradually adjusting the frame such that the gap tissue is tensioned and will respond by regenerating as described in section 2.3.2.

4. Consolidation phase

Thereafter a period of neutral fixation, usually at least as long as the distraction period, allows complete ossification of the CGZ resulting in regenerate bone filling the whole distraction site and mechanical stability returns. Only after this period is the frame removed.

5. Remodelling

After frame removal the newly formed bone undergoes Haversian remodelling. The large callus of bone is slowly reduced and replaced by cortical bone in a cylindrical geometry. Some authors have shown that the medullary canal may not exist immediately prior to frame removal and that full remodelling of bone material to original condition may require as much as one year (Tjernstrom *et al.,* 1992).

2.4.2 Factors affecting the quality of osteogenesis

Many factors have been found to affect the quality of the tissues formed during limb lengthening and some of these are outlined below.

1. Surgical procedure

a. Osteotomy - In 1989, Ilizarov showed that the preservation of the medullary canal increased the rate of bone formation due the preservation of the soft tissue, bone marrow and the nutrient artery including its branches (Ilizarov, 1989a). Intraoperatively this has not been completely verified; moreover some authors have proved a complete restoration of the intramedullary artery just ten days after the complete osteotomy (Yasui *et al.*, 1991; Fink, 1996). Krawczyk *et al.*, (2007) performed a comparative study between various osteotomy techniques on ovine tibia and their influence on bone regeneration. The five techniques used different chisel sizes or drilling techniques and ranged from subcutaneous (classical) corticotomy to osteoclasia using a modified Kirschner wire to drill multiple subcutaneous holes in the cortical layer. All techniques except the classical corticotomy resulted in normal regenerate formation although the osteoclasia technique appeared to speed up the rate of osteogenesis.

The location of the induced fracture has also been shown to affect osteogenesis, with metaphyseal bone transsection being preferred over diaphyseal transsection (Fink, 1996). Other authors found this to be true (Antoci *et al.*, 2006), with metaphyseal sites having a decreased lengthening index (days/cm). One study (Fischgrund *et al*., 1994) found this to be more significant with shorter lengthenings, suggesting that this could be due to the minimum diaphyseal bone consolidation time of four to five months.

b. Fixation – A variety of fixation solutions exist for different indications, many that can be used simultaneously for deformity correction. The choice of frame design and interface with the tissue through pins or wires is similar to other orthopaedic devices where the surgical preference is derived from previous experience, new research and peer group discussion.

There are many factors relating to these systems which can be said to influence the quality of the regenerate, the main one being the stability of the frame itself and the interface with the bone. The gap created by the induced fracture and subsequent frame fixation allows indirect bone healing to occur. Thus stability is an important

consideration because too much movement between the bone ends would result in an undesirable grossly enlarged callus. Stiffness can be influenced by frame arrangement, component materials, pin number, proximity to osteotomy and proximity between pins in a group. The optimal level of stability changes throughout the different phases of the procedure. This will be discussed in section 2.5 during the evaluation of currently available devices.

2. Latency period

The time delay before distraction commences has been shown to affect the volume of callus tissue, the degree of vascularisation (White and Kenwright, 1991) and bone mineralisation (Singare *et al.*, 2006). Although latency periods of 5-7days are common, this factor is highly related to patient demographics. Bones of young patients, whose metabolic processes are faster, are likely to heal more quickly than those of an adult smoker and thus the latency period should be reduced to avoid over-consolidation before distraction begins.

3. Distraction period

The rate and frequency of distraction are critical factors affecting osteogenesis. Again, optimum conditions are patient dependent and rates are often altered during the procedure if indications suggest that the callus is not forming or that premature consolidation is taking place.

Rate – Ilizarov experimented with different rates of distraction and concluded that a daily distraction rate of 1mm was optimal (Ilizarov, 1989b). He found rates lower than this led to premature ossification of the gap tissue, indicating osteogenesis overtaking the elongation, especially when the closed osteoclasis technique was used. Conversely he found that higher rates could not only lead to reduced bone formation (most likely due to the tearing of endosteal and periosteal vessels), but could also have a detrimental effect on the surrounding soft tissues. This average rate of 1mm/day has subsequently been adopted as an absolute standard by the industry. As discussed, the rate of bone formation and healing can vary between patients and one would expect that this distraction rate should vary according to the osteogenic activity of the tissue in order to maintain tissue quality.

Frequency – the most commonly used frequency of distraction, used alongside a number of fixation systems, is four times daily. A 1mm distraction rate performed in one step

proved unfavourable to osteogenic activity; the gap tissue was found to be of very low density (Ilizarov, 1989b). The large step resulted in tearing of the periosteum, similar to the results of a short latency phase. Additionally allowing 24hrs between distraction times permitted over-consolidation of the little tissue that had been laid down. At the same rate but distracting every six hours (0.25mm x 4), relatively dense bone was found to fill the distraction space with a CGZ of around 2-4mm. Ilizarov further tested the effect of distraction frequency by using an automated distraction device in an animal model to provide 0.017mm of elongation every 24mins. The results showed increased osteogenic activity while the growth zone was hardly visible and the resulting cortex was "almost identical to the original bone in both thickness and density" (Ilizarov, 1989b). Not only that but the fascia, capillaries, arterioles and nerve tissue also showed a much greater resemblance to the control (undistracted) tissue (Ilizarov, 1989b). These results in conjunction with a more recent clinical example (Aarnes *et al*., 2002b) indicate that a high frequency distraction is preferred but the clinical norm remains at four times per day. The reasoning behind this apparently conflicting information comes down to practicality. Patients or their carers would not be expected to remember to adjust their frame more frequently than the regular pattern of 'morning, noon, evening, night', therefore higher frequency elongation would require an automated distraction device.

4. Consolidation phase

The optimum consolidation phase must be at least as long as the distraction phase to ensure complete restoration to sufficient bone quality. The fixator should only be removed when the patient is close to full weight bearing. However, determining the load sharing between the fixator and the callus is often difficult. Bone quality can be assessed radiologically but this is a qualitative technique and surgeons are likely to err on the side of caution as opposed to removing the frame too early. This is often termed the 'neutral fixation' period, however many authors (Goodship and Kenwright, 1985; Shepherd *et al.*, 2001) suggest that compression forces providing axial micromovement during this phase can speed up the healing process.

5. Patient Factors

Patient age has been found to have a considerable influence on the speed of osteogenesis, with bone formation being more rapid in patients under 20yrs old (Fink *et al*., 1996). Fischgrund *et al.*, (1994) also found significantly slower healing for those over 30

compared to patients in their 20's. Interestingly there was no significant difference in bone healing rate between patients groups aged 1-10 and 11-19. Existing conditions (or lifestyle choices such as smoking) can also affect the outcome of the distraction procedure and each case must be dealt with individually to ensure that the most suitable treatment is being given.

2.5 Lengthening techniques

2.5.1 Apparatus development

The traditional circular frame developed by Ilizarov became the standard fixator used in limb lengthening procedures. More recently other devices with mechanical, cosmetic and functional benefits have been designed and used with varying levels of success. Very high complication rates are common for this procedure, some relate to specific frames or equipment while others are procedure related. Problems can arise during and after the procedure itself and range from pin-tract infections and neurologic injury (during pin insertion and distraction) to muscle contractures and joint stiffness.

As mentioned previously, osteogenesis is greatly influenced by frame stability and many studies have been carried out comparing the mechanical characteristics of these fixation types to enable enhanced bone healing (Fragomen and Rozbruch, 2007). This data is also worthwhile when considering limb lengthening, but it must be acknowledged that although fracture healing and bone lengthening are similar in many respects, they may have different optimal mechanical environments. It has been suggested that the ideal lengthening system should:

- have low axial stiffness, promoting some axial micromovement (Yasui *et al*., 1991)
- have high bending and translational stiffness, preventing shear and bending
- have high torsional stiffness, as rotation would correspond to shear tangential to the outer cortex

Additionally, it has been said that a more rigid fixation phase is preferred in the initial stages of the distraction (e.g. for the first few weeks) and thereafter some limited axial motion should be permitted to reduce stress shielding effects (Yasui *et al*., 1991). It has been reported that excessive micromovement during the distraction period may limit the total achievable lengthening and that it should perhaps only be applied during the post-distraction phase where it can enhance the consolidation of the regenerate bone (Figueirdo *et al.*, 1993). Towards the preset time for fixator removal it may be advantageous to allow

some dynamisation, allowing the bone to anticipate the forthcoming lack of support as premature frame removal can result in deformity and bone shortening (Fragomen and Rozbruch, 2007).

2.5.2 External Fixation

The most commonly used techniques for limb lengthening use external fixation in the form of ring fixators or unilateral fixators.

Ring Fixators:

The Ilizarov frame has become the most widely regarded system for lower limb lengthening, using a circular external fixator which provides the biomechanical advantage of stability, and can be used to correct multiplanar deformities as well as provide simple lengthening (Shepherd *et al*., 2001).

Figure 2-7 Ilizarov circular frame (from Smith and Nephew)

The frame, shown in Figure 2-7, comprises a number of rings connected by vertical rods and thin (1.5-1.8mm) crossed wires which are inserted through the soft tissues and centre of the bone, therefore connecting the two sections to be separated. The rods are extendable and provide the means of stretching the tissues, loading via the wires. The patient is responsible for the lengthening regime, accomplished by the turning of a screw on each of the three/four rods. Frame stability is greatly dependent on properties such as ring diameter, ring width, ring height, wire positioning, ring spacing and number of fixation points. An advantage of the technique is the potential for modification of angle,

rate and frequency of distraction throughout the process without the need for further surgery. This is of particular value when correcting deformities (Shepherd *et al.*, 2001). Moreover, the non-uniformity of muscle surrounding the bone is such that the bone is prone to valgus deformation during the distraction process, combated by pivoting the fixators about the transverse plane. Full rings can be replaced by partial (open) rings, or arches and although stability is reduced, partial rings and arches are better for use near joints for increased mobility (Fragomen and Rozbruch, 2007).

An intramedullary nail (IMN) can be combined with the Ilizarov frame, allowing the bulky external frame to be discarded directly after the distraction period. This is of cosmetic benefit to the patient, while aiding functional rehabilitation and reducing pin-site infection but a second surgery is required to remove the nail after consolidation. To insert the nail, the medullary canal is reamed, percutaneous holes are drilled and an osteotomy is performed. After placement of the nail, it is locked by the insertion of the proximal screw only and the external fixator is then applied. The nail is locked distally on reaching the desired length and the external fixator is removed. An increased mechanical protection of the regenerate is a main advantage of the technique, amounting to fewer refracture and malunion complications as well as accelerating the return of joint mobility. Alongside the increasing the number of operations required, drawbacks relate to high infection rates as a result of the intramedullary spread of infection and close proximity of the external pins to internal screws. Infection can be minimised by ensuring at least 1mm gap between the rod and any pins or wires (Shepherd *et al.*, 2001).

Paley *et al.* (1997), regarded as one of the main advocates of the technique, conducted a 32 patient comparative study in which lengthening over an IMN was performed alongside matched case standard Ilizarov techniques. Increased blood loss and higher cost were associated with the study group but there were no refractures, fewer pin-tract infections and range of motion within the knee returned to normal twice as fast compared to the control group.

An alternative ring fixation system is the Taylor Spatial Frame (known as the TSF, made by Smith and Nephew). This system uses wires or half pins connected to the bone, but instead of 3 or 4 vertical rods, it has 6 oblique struts that can be lengthened independently thus allowing for correction of translational, rotational and angular deformities simultaneously. Pre-operative planning is performed using the complex software provided with the system, but this can be a drawback as an internet connection is required for full functionality of the software.

Biedermann *et al.* (2006) attempted to show the benefits of the TSF over the Ilizarov but concluded that although the TSF was easier to manipulate, in clinical use it did not show superior results. Fadel & Hosny (2005) also published results showing the TSF to be less favourable than using the Ilizarov. Conversely, a comparative study by Manner *et al*. in 2007 showed that the TSF produced more accurate results due to the computational aid and reiterated the advantage of simple handling of the system for deformity correction. These conflicting findings might be attributed to the learning curve associated with the apparatus, the degree of deformity correction as opposed to only axial lengthening, and simple surgical preference.

Both Ilizarov and TSF rings are most commonly manufactured from stainless steel, titanium or aluminium, but newer carbon fibre rings provide advantages of decreased frame weight and radiolucency for enhanced evaluation of the distraction site. They are also compatible with imaging systems such as MRI and CT. Baidya *et al.* (2001) state that although values for stiffness of the new rings are lower, they remain within the strength and deformation limits required for a ring fixator. Short chopped carbon composite and knitted Kevlar were both evaluated in their clinical study and the short chopped carbon produced improved results. It was revealed that this may be due to the larger volume fraction achieved during assembly in the mould. Other carbon fibre reinforced ring designs have been patented, detailing the orientation of the reinforcement fibres (Smith and Nephew Richards Inc., 1991).

Unilateral Fixators:

Unilateral frames are commonly used for fracture fixation, but the method is not as well documented as a method of distraction when compared to ring fixators. This type of fixator gives an alternative to the circular frame, which allows for technically easier insertion and is generally better tolerated by patients owing to the reduced bulk of frame (particularly on the femur and humerus). Two sets of pins are inserted, with two or three pins in each set, separated using a single extendable rod or sliding mechanism.

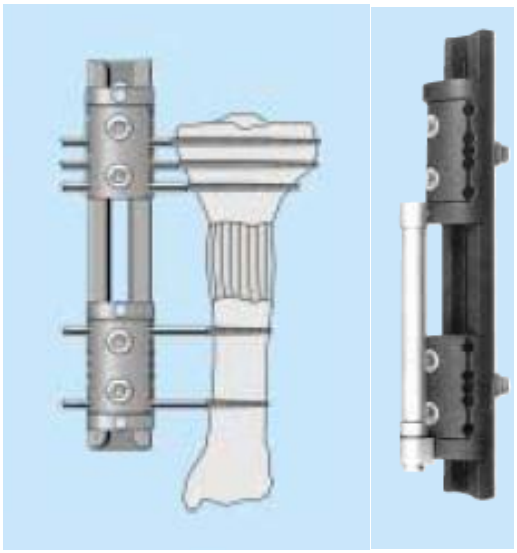

Figure 2-8 Unilateral fixator used in the limb lengthening configuration (from Orthofix, 1999)

One of the few monolateral distraction devices in clinical use is the Orthofix Limb Reconstruction System (Figure 2-8) which can be used for a variety of segmental (multi-level) complications including bone transport, compression-distraction and bifocal lengthening (Orthofix, 1999). The system is comprised of clamps (two for monofocal lengthening, three for bifocal) which are able to slide on a rigid rail connected by distraction units.

Briefly,

1. Clamp templates are assembled on the rail. Locking screws are loosened to allow free movement.
2. Precise positions of clamps and cortical screws are determined
3. Template is used to ensure alignment to long axis of bone
4. Clamp templates are locked to rail then templates are replaced by straight clamps
5. Osteotomy of bone
6. Distraction unit screw gets turned 90deg every 6hrs (1mm/day)
7. Sliding clamp is then locked to rail for consolidation period

Documented advantages include the ability to begin with a very small distance between proximal and distal clamps (although in practice, there is a minimum desirable distance between osteotomy site and the screws). Additionally the increased structural stability of the rail is of particular value for lengthenings in excess of 10mm.

The stiffness of non-symmetrical constructs is of greater significance as bending could result in malformation of bone during the axial lengthening. It has been found that for tibial procedures, anterior mounted frames best neutralise bending forces in the bone while femoral frames tend to be mounted laterally for more practical reasons (Fragomen and Rozbruch, 2007). The stability of all unilateral frames is improved by the use of larger-diameter half pins with more points of fixation; reduced distance between the frame and the bone; and placing the pins out-of-plane to one another.

Noonan *et al.* (1998) conducted a review of 261 lengthening procedures using monolateral distraction, comparing results for femora and tibia, different indications for lengthening, and varying age. Lengthening was achieved through two distractions of 0.5mm per day which is half the frequency suggested by Ilizarov. Percentage increases in length were impressive (as much as 86%) but complication rates were high, particularly in tibial distraction and in patients over 14yrs old. Femoral malalignment was due to varus angulation whereas malalignment in the tibia was due to increased valgus angulation. The precise positioning of the fixators was not disclosed although x-ray images suggest mediolateral placement.

The Institute for Limb Lengthening and Reconstruction in New York (one of the most recognised lengthening and reconstruction clinics in US), uses circular and unilateral fixators and states that both have "provided excellent stability and helped us accomplish fracture union and bone lengthenings very successfully" (Fragomen and Rozbruch, 2007).

Figure 2-9 The EBI monolateral fixator used clinically (from Institute for Limb Lengthening and complex reconstruction, 2007)

There are other unilateral fixators on the current market including the EBI monolateral lengthening frame (Figure 2-9) and all work on a similar principle.

2.5.3 Internal Fixation

Totally intramedullary gradual elongation can be accomplished using the Albizzia Femoral Elongation System (Figure 2-10, developed by Guichet and Casar, 1997), the more recent Intramedullary Skeletal Kinetic Distractor (ISKD), designed by Cole and Justin, and other early stage technologies.

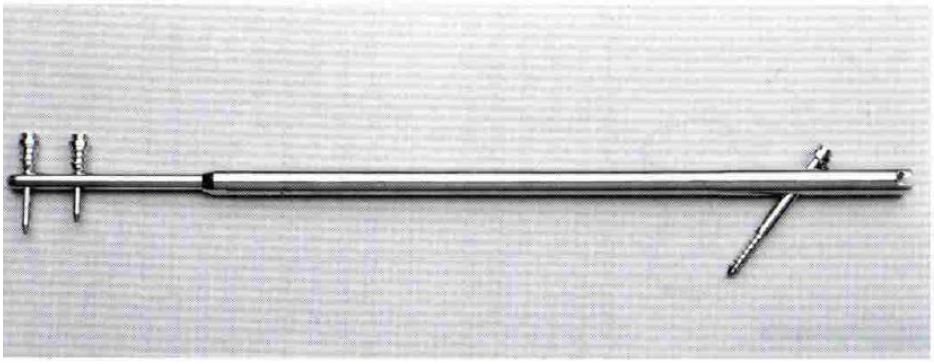

Figure 2-10 Totally intramedullary elongation system, or Albizzia (from Guichet and Casar, 1997)

The most obvious advantage for the patient is the lack of external frame for cosmetic benefit and comfort during daily activities and sleep. Pin site infections are also eliminated but scars from surgery for implantation will be present. A main disadvantage of these systems is the inability to reduce the length of the nail after it has been increased via the racheting. Another drawback is that both of the devices mentioned can only be used for patients whose growth plates have fused i.e. those over approximately 16yrs old, due to the required rotation of one bone section relative to another. Guardians of patients under this age may either choose to wait to receive this treatment or to use more traditional external fixation methods.

Three current devices are described in this section. Case studies relating to the use of these devices are increasing in number and sample sizes are also increasing. The author is frequently linked to the device designer and promising results are often portrayed despite contraindications but it appears that complication rates are in line with those reported when using standard Ilizarov fixators.

Using the Albizzia system (Figure 2-11), elongation is achieved through a "simple rotary manoeuvre across the osteotomy site". The nail consists of a solid distal rod which rotates and slides within a proximal cylinder, while an internal ratchet mechanism controls the sliding and extension of the rod from the cylinder. An osteotomy is performed and

reaming of the medullary canal takes place. Thereafter the nail is inserted and locked distally with two screws then proximally with one screw (Guichet and Casar, 1997).

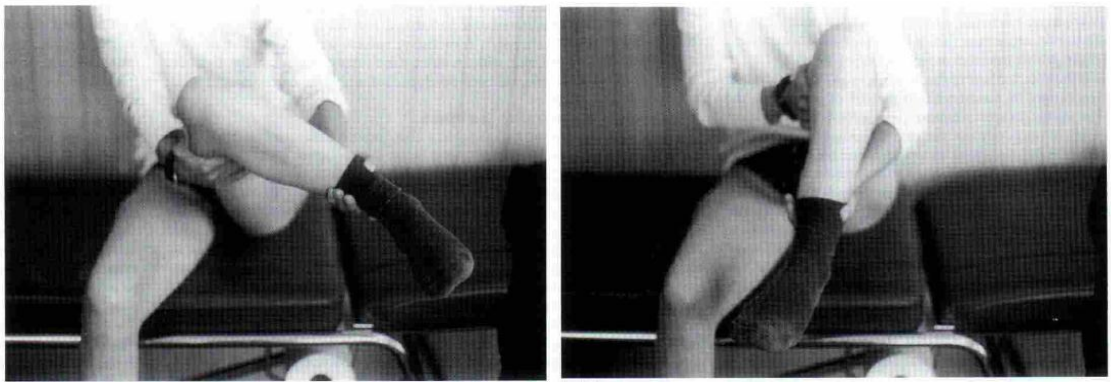

Figure 2-11 Distraction process using the Albizzia ratcheting mechanism (from Guichet and Casar, 1997)

After a suitable latency period, distraction is initiated by holding the patient's thigh and knee whilst rotating the distal section of the femur 20° beyond its neutral position then returning back to neutral (Figure 2-11). Each rotation provides 1/15 mm elongation, thus to stay in line with common distraction rates, the limb must be rotated 15 times per day (distributed between 3 or 4 sessions). It has been observed that although complications such as pin-tract infections are eliminated, others in the form of intramedullary infection and excessive pain are very common. Levels of pain are not often reported in research of lengthening, but this study found patients to be in most discomfort if not in a fully relaxed state when manoeuvring or if they had not regained full motion in adjacent joints. Patients are advised to undertake regular exercise in order to reduce the likelihood of discomfort, as this promotes muscle relaxation which prevents contracture and spasm during ratcheting (Guichet and Casar, 1997). Ratcheting problems have been one of the main reasons for the reluctance to use the device. This group have performed several studies (although it is unclear whether entirely separate patient sets were used) in which they record the clinical experience with the device. It may be expected that results would be exceptional due to Guichet himself being the designer of the system but post-operative complications are numerous. In 1995, 48 patients underwent lengthening using the Albizzia procedure (52 bones) with a mean age of 21yrs. Pain was elevated significantly in the second and third weeks due to the healing response and considerable inflammation. Despite 31% of cases suffering post-operative complications (25% of whom required additional surgery) and a pain score for ratcheting from 1.5-2.4 on a four point scale, the patient satisfaction score was a considerable 8.8/10 (Guichet and Casar, 1997). A similar

publication of clinical results by the same authors, recorded that 39% of (12/31) cases required readmission and general analgesia for ratcheting, nevertheless the clinical outcome was said to be 'excellent' in 75%. This was based on a set of six criteria including lengthening obtained, range of movement and pain (Guichet *et al.*, 2003).

ISKD employs a very similar system but the angle of rotation required for the ratchet mechanism is only 3-9°. This means that elongation can be achieved during regular daily activities, monitored by a magnetic external system, and is only 'topped up' by additional rotations if required. With reduced manipulation required, pain levels were expected to be significantly reduced compared to the Albizzia system, as was indeed found by Cole *et al.* in 2001. The group studied 18 patients treating a combination of femora and tibia achieving a mean lengthening of 49mm at a rate of 0.82mm/day. The authors state that no complaints of pain during lengthening were recorded and that patients who had previously used external fixators for distraction found the ISKD to provide a 'better quality of life', although methods of assessment of this quality were not stated in the publication. A larger study was completed by Thonse *et al.* in 2005 of 91 tibia and femora but Cole's high quality of outcome was not equalled. Approximately 20% of patients experienced difficulty inducing traction with some requiring analgesia during manipulation exercises for additional lengthening. This same need for manipulation and additional analgesia has been found by other authors such as Hankemeier *et al.* (2005) and Leidenger *et al.*, (2006) with 25% and 31% of patients requiring additional assistance respectively. Thonse *et al.*, (2005) found that distraction was too rapid for 10% of patients whilst a more recent study Kenawey *et al.* (2011) recorded 9 'runaway nails' out of 57. As a result of this mechanical problem, insufficient bone regeneration is a likely and further surgical intervention is required, highlighting the need for better control of the internal mechanics.

Other innovations include a totally intramedullary motorised distraction device reported by Baumgart *et al.* (1997). Although the device has been implanted in hundreds of patients, it has not yet been approved by the FDA. The system consists of an implanted nail with antenna which, during close proximity to the high FM electric energy transmitter, controls the lengthening process by activation of motors within the nail (Figure 2-12). It is programmed externally and, once the device has been inserted, the distraction program cannot be modified. Currently the nail is only in use by specially appointed surgeons who have adequate training but is being marketed as both a medical and cosmetic device for the lengthening of shortened limbs.

Figure 2-12 Fitbone -motorized distraction device (from Wittenstein Intens, 2008)

Baumgart's clinical study reported the outcome of 12 cases, in which the intramedullary canal was large enough to contain the device. The average rate was 0.8mm/day and in all cases the desired lengthening was achieved. Post-operative complications included re-operation in 25% (3/12) of cases. It was stated that patients could not feel the motor moving and that the distraction was pain free. Pain during lengthening by the Fitbone device was monitored in a separate study by Zimmermann *et al.* (2007). The type and level of pain was found to vary of the course of treatment, starting from a more acute pain from post-surgical healing tissues through to a more protopathic pain from the deep soft tissue. After 4-5cm lengthening the pain was found to change again to a "stretching-pain" associated with the soft tissues. It is unknown whether these are specific to the use of the Fitbone device or could characterise tissues under lengthening by alternative devices.

Singh *et al.* (2006) and Krieg e*t al.* (2011) have both reported their experience of the Fitbone for tibial and femoral lengthening in 24 and 32 cases respectively. The outcomes were generally regarded as positive although complications included replacement of device components in both studies (lack of power from internal gears, motor replacement, bolt loosenings) resulting in problems such as insufficient callus formation and delayed union. Such a degree of error within the mechanics of the device is unusual when compared to traditional external fixators.

Only one study has compared all three fully implantable intramedullary devices and agreed that the ISKD is difficult to control, finding the Fitbone device had similar control issues (Betz *et al.*, 2008). It suggests that the Albizzia has the best cost-performance ratio

based on its controllability, early weight bearing capability and high lengthening ability (100mm).

A report from the UK National Institute for Clinical Excellence (NICE) was published in March 2006 aiming to assist the Interventional Procedures Advice Committee (IPAC) in making recommendations regarding the use of intramedullary methods of limb lengthening (NICE, 2006a). This document summarises a number of European (outside the UK) and American case studies featuring the new techniques, some of which have been mentioned previously in this section. Its 'efficacy' analysis included the extent of lengthening, rate of lengthening and range of movement of the knee joint while the 'safety' analysis related to complications intra-operatively and post-operatively.

Data from the case studies indicated that the extent and rate of lengthening were in line with existing techniques. Range of knee movement was not significantly altered as a result of the procedure. Few intra-operative complications were experienced but the post-operative findings were the main concern. The high levels of pain were found to be the most common adverse event and the use of anaesthesia to achieve the lengthening due to extreme pain during the ratcheting process was noted. Other problems involving bone fractures or mechanical failure of the nail such as nail bending, ratchet wear and motor failure were also considered. Specialist advisors to the NICE (Mr C Bradish, Mr M Laverick, Prof. H Simpson) thought the technique to be 'novel' but warned that the lack of control could result in delayed or premature consolidation, as has been found.

Although the report does not itself make any recommendations, its findings were used in a guidance document published by NICE in December 2006 (NICE, 2006b). The guidance states that 'current evidence on the safety and efficacy of intramedullary distraction for lower limb lengthening does not appear adequate for this procedure to be used without special arrangements for consent and for audit or research'. Although this advice does not support widespread use of the technique, it does not exclude its use so surgeons planning on using this technique are advised to inform their trust, ensure the patient understands the safety implications and has read patient guidance documents and comprehensively document the procedure.

Comments on this guidance document raised questions relating to the inclusion of the now withdrawn Albizzia – due to high ratcheting pain and highlighted the fact that Fitbone is not yet CE marked (or FDA approved) and should be considered 'under development' (NICE, 2006c).

These recommendations were for UK only. The FDA has approved the use of the ISKD and its use is growing in the U.S.

2.5.4 Summary

It has been shown that the range of available apparatus for the clinical lengthening of limbs have varying properties alongside varying complications. Table 2-1 summarises the key characteristics of each device.

Feature and Function	Ilizarov frame	Taylor Spatial Frame	Orthofix LRS	ISKD	Albizzia	Fitbone
external fixator	✓	✓	✓			
internal fixator				✓	✓	✓
manually actuated	✓	✓	✓	✓	✓	
automatic actuation						✓
small increments				✓		
visual length indicator	✓	✓	✓			
other length indicator				✓		✓
deformity correction	✓	✓	✓			
reversal of extension	✓	✓	✓			
reduced bulk			✓	✓	✓	✓
suitable for paediatrics	✓	✓	✓			✓
large elongation	✓	✓	✓			

Table 2-1 Summary of fixation methods

2.6 Biomechanical testing of limb lengthening devices

2.6.1 Requirements for testing

For the purposes of fulfilling regulatory requirements for MHRA/CE/FDA approval, the mechanical testing of fixators used for limb lengthening come under the same class as static external fixators, commonly used for stabilising fractures. The stiffness of a fracture fixation device influences the micromovement at the bone ends which, as stated previously, has been shown to affect the type of callus formation and healing, particularly in the initial phase of repair (Carter *et al.*, 1988). In the case of distraction osteogenesis, fixator stiffness influences not only the micromovement but also, and perhaps more importantly, the tissue extension increments. For example, a 0.25mm change in length of the device may only result in 0.2mm of tissue extension due to bending of the device or pins. Consequently, testing the axial stiffness of distraction devices is of increased

importance in order to analyse the effect its stiffness may have on the extension of, and resultant forces within, the callus and soft tissue. Furthermore, tissues are known to exhibit time-dependent properties which means that the loading through the device changes between distraction increments. Although this may not affect traditional manual devices, changes in load may affect the functioning of an automated device so this should be kept in mind. Additionally, automated devices require further testing of the control system in addition to mechanical testing to ensure that the device is lengthening at the desired rate and is not over or under extending.

2.6.2 Device stiffness

Existing methods for determining the stiffness characteristics of a frame construct range from *in-vivo* strain measurements to laboratory based materials testing machines to computational models (e.g. Watson, 2002; Matsuura *et al.,* 2003; Gardner *et al.,* 1997a; Guichet and Casar, 1997; Podolsky and Chao, 1993). Static loading is commonly used to test devices even though they are likely to be under dynamic loading conditions for much of their use. The axial stiffness is often assumed linear for a device within the elastic range of its constituent materials. This may be incorrect as demonstrated by Podolsky and Chao (2003), and Gasser *et al.* (1990) who found that Ilizarov fixators had a non-linear load deformation curve. They found that at lower loads the stiffness was reduced and greater axial motion was permitted (which may stimulate fracture callus), while at higher loads the frame stiffened (protecting the tissues from excessive motion which may cause non union). This is, in fact, similar to the properties of tendons and ligaments (see Chapter 3).

Uniaxial loading is used in many test regimes but loading direction may be important, especially for unilateral devices which have orientation dependent stiffness. If loading is indeed uniaxial, then the pins are cantilevered and the compression of bone segments is not symmetrical (Gasser *et al.,* 1990).

Although not directly related to stiffness, fatigue testing has been used to assess the potential for re-use of devices; using both low and high load regimes with high and low cycle numbers respectively (Matsuura *et al.,* 2003). Gardner *et al*. (1997a) used cyclic axial testing of five different unilateral devices to determine the failure mode (slippage, plastic or fatigue failure).

2.7 Implications for testing and modelling

Limb lengthening is a difficult procedure involving complex tissues and many different factors have been shown to affect the quality of the outcome. Numerous device manufacturers are trying to create a device that will provide the optimal environment for tissue growth and yet problems remain common. The challenge in designing lengthening devices is that they are operating within an 'active' system unlike the passive system of fracture healing. Within fracture healing, the device is 'constant' and the tissues are 'changing' but in the case of DO, it may be preferential to have the tissues under 'constant', ideal conditions (prior to consolidation) and design a device that can change to maintain this environment.

There is a need to look more closely at the tissue mechanics to understand the environment that the fixator is attempting to change, how lengthening of a fixator affects the tissue, if the tissue characteristics affect the loading on the device and how a smart device may be able to provide a solution to the 'optimal' environment problem. It is proposed that experimental testing and numerical models can be of use in this process.

Chapter 3

Studies in tissue mechanics – a review

3.1 Introduction

In order to build representative models of the limb lengthening process, there is a need to understand the changing mechanical characteristics of the elongated tissues. This Chapter presents a review of the mechanical properties of tissues, followed by an examination of previous published work relating to clinical data for these properties measured during lengthening. Finally, a summary is given of models that have been proposed for the simulation of tissue forces, both experimentally and numerically.

3.2 Tissue mechanics

3.2.1 Callus – bone healing

Tissues formed during distraction osteogenesis (DO) were histologically examined by Ilizarov at various time points throughout the lengthening of canine tibia (Ilizarov, 1989, 1989b, 1990). Cell features that are seen in embryonic and neonatal development of limbs were found, proving the stimulation of osteogenesis. Osteogenesis also occurs during fracture healing and results in a callus with a similar structure and composition of tissue, thus examination of the mechanical properties of healing tissue can be of use in determining the properties of the callus during limb lengthening. As a fractured bone heals, the stiffness of the newly formed tissue rapidly increases due to mineralization. Consequently it is only the initial stages of fracture repair that can help to characterise a callus during lengthening.

Stiffness of the fracture callus has be found using varying non-mechanical methods such as resonant frequency analysis (Benirschke *et al.*,1993) and acoustic emission (Watanabe

et al., 2006) but these methods often give a stiffness value relative to that of healed tissue. Absolute values for stiffness can be obtained using indentation analysis which has been performed *in vitro* on different sections of the healing callus (Leong and Morgan, 2008). In one study (Markel *et al*., 1990) gap tissue was found to have a stiffness of 15N/mm at weeks two and four, rising to 150N/mm at week twelve. Bending stiffness is often used as an indicator of overall callus stiffness and has been measured using various methods (Richardson *et al*., 1992; Hente *et al.,* 2003; Ogrodnik *et al.,* 2007). Axial stiffness of the callus is more relevant to the current work and was measured during fracture healing by Cunningham *et al.* (1987) using force plates and a transducer on the fixator along with the pin stiffness and a known loading. Results at 4 weeks postoperatively (which would be close to the upper limits of stiffness for a distracted callus) gave a stiffness value of approximately 50N/mm. However, other studies have shown axial stiffnesses over 50N/mm at week two, dependent on the rigidity of fixation (Mora and Forriol, 2000).

Many biological tissues have been found to possess time-dependent characteristics and boney callus tissue is no different (Fung, 1983). When measuring the stiffness of the callus *in vivo*, many authors neglect the features of viscoelasticity e.g. measured stiffness is related to loading rate, and creep, where constant loading results in further deformation (Moorcroft *et al.,* 2001). In a recent *ex vivo* study, healing callus was found to exhibit high stress relaxation following an applied stretch (McDonald *et al.,* 2009). Additionally, a feature known as reverse stress relaxation was also observed, where a step reduction in loading to a specific point was followed by an increase over time towards the basal tension (Figure 3-1), although it was noted that not all fracture sites will display identical behaviour.

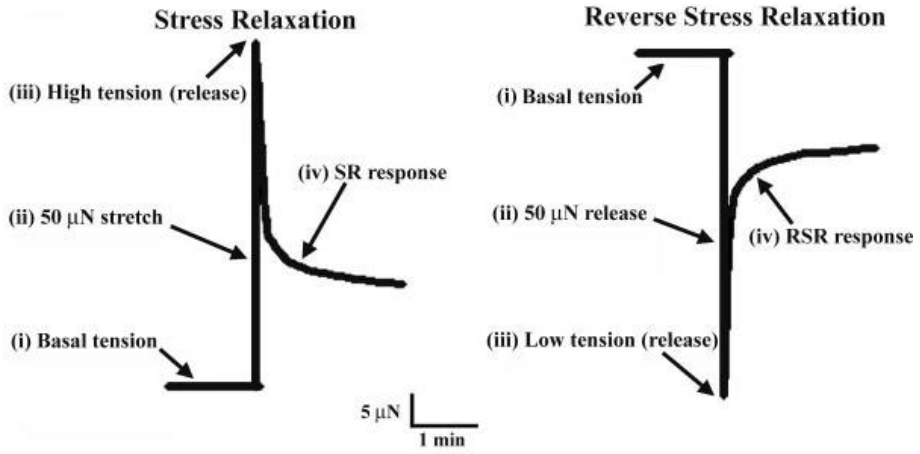

Figure 3-1 Stress relaxation (SR) and Reverse Stress Recovery (RSR) of callus tissue (from McDonald *et al*., 2009)

It can be concluded that callus tissue should be considered a highly viscoelastic material with a stiffness in the range of 10-50N/mm in the early stages post-fracture. Examination of studies performed on lengthened callus is likely to bring further clarification.

3.2.2 Soft tissues

In general, soft tissues exhibit similar mechanical properties to that of immature callus tissue, but with lower tensile stiffness and higher stress relaxation. This can be attributed to the different proportions of the structural components (e.g. collagen, smooth muscle, elastin etc.) and the arrangement of these elements within the tissue (McDonald *et al*., 2009; Fung, 1983). Measurement of muscle and tendon properties *in vitro* is common but these values are not representative of their *in vivo* state, thus their significance for a limb lengthening model is limited. Consequently only *in vivo* studies are mentioned here.

Fukashiro *et al.* (2001) compared their results for the tendon and muscle fibre stiffness to those from previous studies (Table 3-1), noting also the technique used to measure the stiffness, which in their case was the *in vivo* 'free vibration technique'.

	Stiffness				
Author	Tendon (kN m^{-1})	Fibre (Nm^{-1}) N^{-1}	MTC	Method	Young's modulus (GPa)
Present study	364	611	Human triceps surae	The free vibration technique	–
Morgan (1977)	13–33	910–1140	Cat soleus		–
Morgan *et al.* (1978)	25	1060	Kangaroo GM		–
Walmseley & Proske (1981)	20–50	1550	Cat soleus	The α method	–
	20–51	2500	Cat GM		–
Proske & Morgan (1987)	17–50	670	Cat solues		–
Hurley *et al.* (1977)	1215	–	Rat tail tendon		9
Cusack & Miller (1979)	690	–	Rat tail tendon		5.1
Shadwick (1990)	102	–	Pig digital extensor tendon	Calculating from Young's modules	0.76
	225	–	Pig digital flexor tendon		1.66
Voigt *et al.* (1995)	165	–	Human Achilles tendon		1.2
Sasaki & Odajima (1996)	390	–	Bovine Achilles tendon		2.9
Benedict *et al.* (1968)	250	–	Human Achilles tendon		–
Cavagna (1970)	170	–	Human triceps surae	The natural frequency of free oscillations	–
Shorten (1987)	440	540	Human triceps surae	The free vibration technique	–

GM: *Gastrocnemius medialis*. Values of Cavagna (1970) and Shorten (1987) were calculated as r_b = 0.05 m.

Table 3-1 Muscle and tendon stiffness coefficients from various studies (taken from Fukashiro *et al.*, 2001))

Selecting only human studies from this list, the stiffness of the tendons ranges between 165-440N/mm while the muscle fibre has a stiffness of 540-611Nm^{-1} N^{-1}. At loads clinically relevant to those found in limb lengthening (200N), this stiffness equates to

around 120N/mm. These results are slightly lower than those measured by Magnusson *et al.* (2001) for the human triceps aponeurosis (350-740N/mm). When the muscles (soleus and gastrocnemius) are included (such as in the study by Babic and Lenarcic, 2004), the values are lower, with muscle tendon complex (MTC) stiffness ranging from 150-300N/mm depending on the muscle load (ranging from 200-1000N). They propose that the variance in stiffness with load can be attributed to the muscle, while the Achilles tendon stiffness remains constant over the load range. This is shown graphically in Figure 3-2 where the contributions of the Achilles tendon (ka) and the soleus muscle (ks*fs) are represented with dashed lines

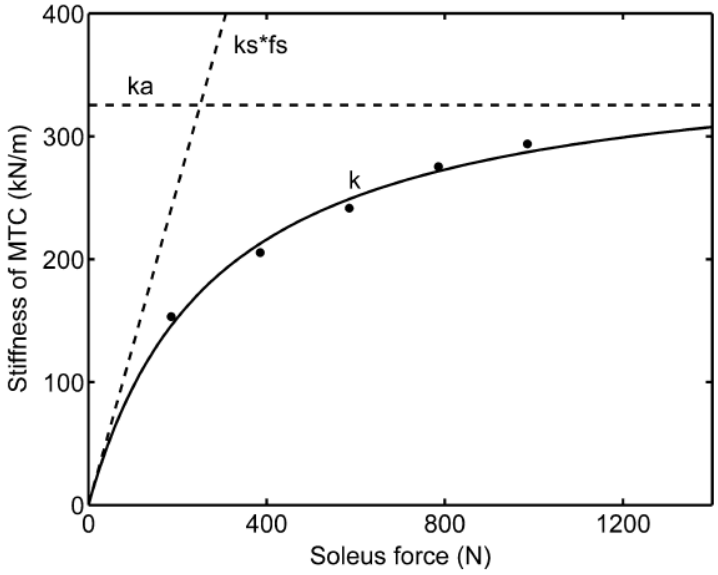

Figure 3-2 Elastic stiffness of MTC (human triceps surae) as a function of the muscle load. (from Babic and Lenarcic, 2004)

Tendon and muscle stiffness has been shown to be within a similar range to early fracture callus and should therefore be considered when assessing the reaction forces during limb lengthening.

3.3 Tissue mechanics – clinical lengthening

3.3.1 Forces within tissue

In an attempt to further understand the mechanical and biological processes involved in limb lengthening, the stress within the distracted tissues has been measured quantitatively by various authors. This has been accomplished using apparatus attached to the external frame during lengthening. One early clinical study was published in 1990 by Wolfson *et*

al. who used a modified tibial Ilizarov frame with force transducers in each of its three columns to collect weekly data from an 11yr old female patient with an initial 50mm LLD originating from poliomyelitis.

Pre-distraction forces were found to increase linearly to a maximum of 245N though post-distraction peaks were not disclosed. The first femoral study was conducted by Younger *et al.* (1994), which involved three subjects. Peak forces for each subject were higher than recorded for the tibia, at 428N, 447N and 675N. Simpson *et al.* (1996) used unilateral frames on ten patients with varying pathologies on both femur and tibia. They recorded similar resting forces at under 300N for post traumatic indications, whereas those with congenital indications had higher resting forces (above 400N) and considerably higher peak forces; in one case reaching 1300N resulting in an angular deformity of the tibia. Table 3-2 provides a list of published clinical studies relating to the forces present within the tissues during limb lengthening.

Researcher	Force across callus site	Stiffness of limb	Methodology	Notes
Wolfson *et al.* (1990)	Range = 49-245N	Increases by 3.9% per mm	One case study. Patients using Ilizarov lengthening on tibia	No post-distraction or stiffness values presented
Aarnes *et al.* (2002a)	Peak 431-542N	Average 72N/mm	Four short statured patients, tibial lengthening	Decay/hour was less overnight when performing bifocal
Aarnes *et al.* (2002b)	Peak = 472N	n/a	Two patients, bilateral and bifocal	High frequency distraction peak = 307N
Younger *et al.* (1994)	Peak = 673N	n/a	Three patients using force transducers on Ilizarov femoral frame	'Sawtooth' varied by 95N between readings
Ohnishi *et al.* (2005)	Peak = 600N	n/a	Twenty patients, ten acquired femoral shortening, ten achondropalsia. Unilateral fixator with load measurement	Lengthening frequency does not significantly affect load increment rate of 1.3-1.5N/mm
Simpson *et al.* (1996)	Peak = 1300N in one case	Range 50-450N/mm	Ten patients, unilateral fixator on femur/tibia. Callotasis/Wagner techniques both used	Peak in most cases = 600N
Gardner *et al.* (1998)	Peak = 380N	Range 0-1650N/mm (mean =372N)	Two tibial lengthenings. Ilizarov ring fixator	Muscles – plastic response Regenerate – viscoelastic response
Lauterburg *et al.* (2006)	Peak = 737N 14N/kg of body mass.	One patient: approx 24N.kg/mm	Ten femora, eleven tibia. Ages 6-22yrs. Unilateral fixator	
Pouliquen (1994)	Peak 2450N in 4 cases	n/a	Unilateral fixator used	
Waanders *et al.* (1998)	Peak 45N	Range 20-80N/mm	Rabbit study. Unilateral fixator, bilateral lengthening of tibia	Only 18days post operative
Aaronson and Harp (1994)	Peak 200N	n/a	Canine study	
Taylor (2005)	n/a	334Nm/degree of torsional stiffness	Digital torque wrench technique for stiffness measurement- rabbits	

Table 3-2 Force and stiffness measurements during limb lengthening

Some of these studies focus on tissue stiffness, suggesting that it is it not the absolute force within the tissues that gives an indication of the condition of the callus, but instead the change in load with respect to elongation. Similar to load values, the stiffness of the resisting system has been found to vary greatly, not only between patients but over the length of the procedure. The study by Wolfson *et al.* (1990) suggested that stiffness increases gradually at 3.9% per mm of distraction while Gardner *et al.* (1998) found stiffness to be more irregular as seen in Figure 3-3.

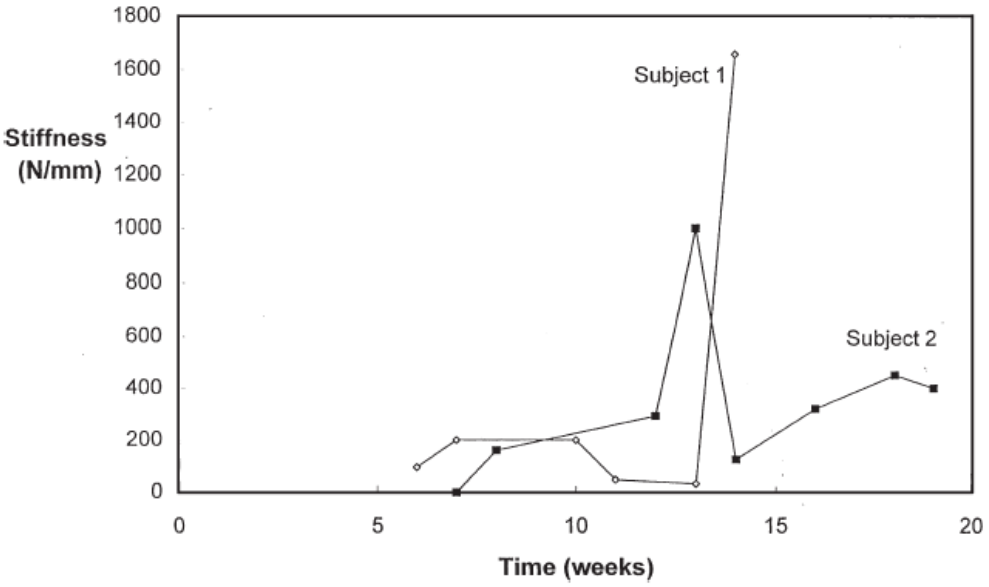

Figure 3-3 Distraction gap stiffness during the procedure shown for two patients (from Gardner *et al.*, 1998)

In attempting to find the axial stiffness of the regenerate during consolidation, Aarnes *et al.* (2005) used similar methods to Cunningham *et al.* (1987) when measuring fracture callus stiffness. By using a force plate and the calculated stiffness of the Ilizarov fixator, they were able to determine the load share ratio between the frame and the tissues. During weight bearing the loading is compressive thus load is taken through the bone not soft tissues. Consequently the ratio was used to determine a suitable frame removal time such that the bone could provide enough structural support. Stiffness calculation by an automated device is readily achievable if the distraction distance and load are being monitored already. This is something that is of great interest to clinicians (McNally, 2008) who are keen to remove the bulky frame from the patient as soon as the bone is mechanically stable.

3.3.2 Sources of resistance to distraction

Measurements taken using a transducer on an external fixator during lengthening are a total of the resistance of the two types of tissue in the composite system - bone regenerate and soft tissue. Great difficulty lies in finding the origin of the resistive force or the independent contribution of each tissue type. It has been said that a reduction in resistive response from the soft tissues can be attributed to better tissue adaptation (Aarnes *et al.*, 2002b). The converse is true with hard tissue i.e. a low stiffness can represent poor bone mineralization. Excessive stiffness from the callus can therefore signify over-mineralisation or early consolidation. The difference in the 'optimal' state of each tissue demonstrates the importance of finding the source of the resistance to distraction if attempting to maintain favourable conditions for each.

In an attempt to do this, Younger *et al.* (1994) measured the ground reaction force during weight bearing, attributing any changes in the force through the frame to callus stiffness. In fact, they found only a small change in frame loading suggesting that the load was being taken mainly by the callus. This was contradictory to Wolfson's theory that the callus was mechanically insignificant.

Gardner *et al.* (1997b, 1998) attempted to differentiate between the stiffness of hard and soft tissue after attributing the variation in location of the dominant stiffness of the system over the length of the procedure to the constantly changing source of resistive forces. CT images were used alongside force recordings to find the main tissues resisting lengthening and, although the results showed that muscle groups such as the flexor and extensor digitorum longus and the gastrocnemius could be the focus of resistive force, the study was not large enough for a conclusive outcome. Other authors have also taken radiographic evidence alongside force measurements. For example, Aarnes *et al.*, (2002a) studied 8 femora and concluded that poor bone healing was not the source of low loadings, but instead that low force must be attributed to better soft tissue accommodation. Simpson *et al.* (1996) found no correlation between callus formation shown on radiographs and force readings.

Animal studies cannot give comparable quantitative load values for forces during human limb lengthening due to tissue mass disparities, but they may be valuable in determining the relative contributions of the hard and soft tissues. Using a canine tibial model, Aronson and Harp (1994) measured loads through the fixator along with cross sectional area of the osteogenic zone and concluded that the main source of distraction load was the collagenous bridge within the callus. This hypothesis was confirmed by Cai *et al.* (2004)

who performed tibial lengthenings on sixteen rabbits, monitoring the passive distraction resisting force and the contribution of the gastrocnemius (which has been shown to be the cause of knee and ankle contractures during DO). By severing the Achilles tendon post-sacrifice, they concluded that the gastrocnemius and surrounding muscles provide much less resisting force than the callus itself, both at the end of the distraction phase and five weeks post-distraction. Other authors agree that the most resistance is from callus (Taylor *et al.,* 2005) but some also confirm that there will be some stiffness contribution from the muscle (Waanders *et al.,* 1998). In contrast, the load patterns seen by Forriol *et al.* (1997) in their lamb model suggest that the soft tissue is the major source of resistance.

It is obvious that there is no conclusive opinion on the main source of the resistive load during limb lengthening and that both the hard and soft tissues contribute to some degree. Force transducers on fixators have provided useful information, yet patterns recorded have been used to support various viewpoints. By monitoring the forces more frequently and building up a larger picture of the mechanical responses of tissues to distraction throughout the clinical procedure, it may be possible to attribute distraction resistance to specific tissues based on their properties, with specific regard to their time-dependent relaxation properties. This is something that may be achievable with an automated distraction device.

3.3.3 Time-dependent mechanical characterisation of tissues

The difference between pre- and post-distraction forces has been shown to give an indication of tissue stiffness. The same data can be used to provide information of tissue relaxation, using the difference between post-distraction force from one step and the pre-distraction force from the following step. Given that callus, muscle and tendon all have viscoelastic characteristics (as discussed in section 3.2), one could expect that after the step increase in displacement and load, there will be a degree of load relaxation. If the relaxation after each step is incomplete, pre-distraction forces will increase as the treatment progresses, resulting in tension accumulation. The degree of accumulation was shown by Simpson *et al.* (1996) to be dependent on the indication for lengthening. Figure 3-4 shows that for a patient with congenital shortening, they measured a maximum pre-distraction value of 750N and a maximum of 1300N post-distraction. For post-traumatic cases the tension accumulation was significantly lower.

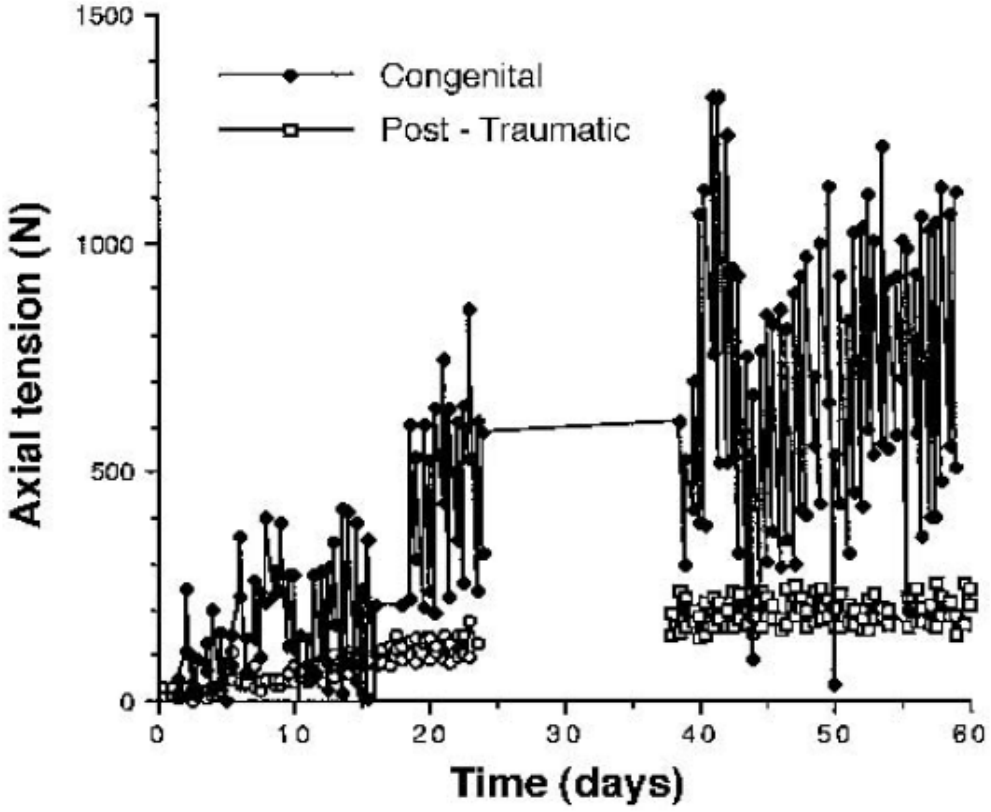

Figure 3-4 The distraction forces over time for two patients with different pathologies (from Simpson *et al.*, 1996)

The large difference in these values showed that, not only was the tissue stiffness higher than previously described, but that there was considerable load relaxation after each cycle. This highlighted the highly viscous nature of the tissue. Figure 3.5 plots a typical force reading after 0.25mm lengthening, showing the time-dependent response to a step elongation; a typical viscoelastic relaxation curve, plateauing at about two hours leaving some unrecovered tension accumulation after three hours.

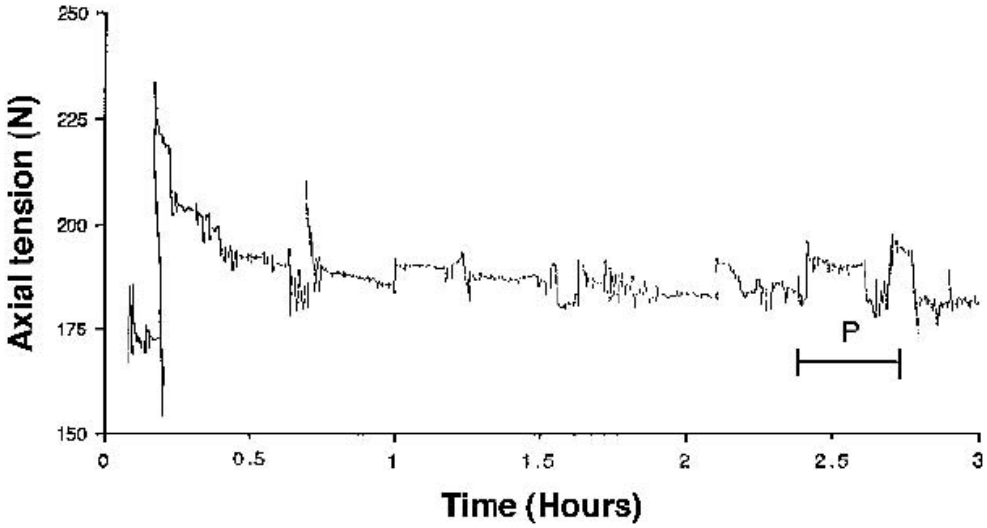

Figure 3-5 Typical load relaxation following distraction increment (from Simpson *et al.*, 1996)

Ohnishi *et al.*, (2005) also observed a viscoelastic response, but contrary to Simpson's findings, the tissues appear to be relaxing right up until the next distraction (Figure 3-6).

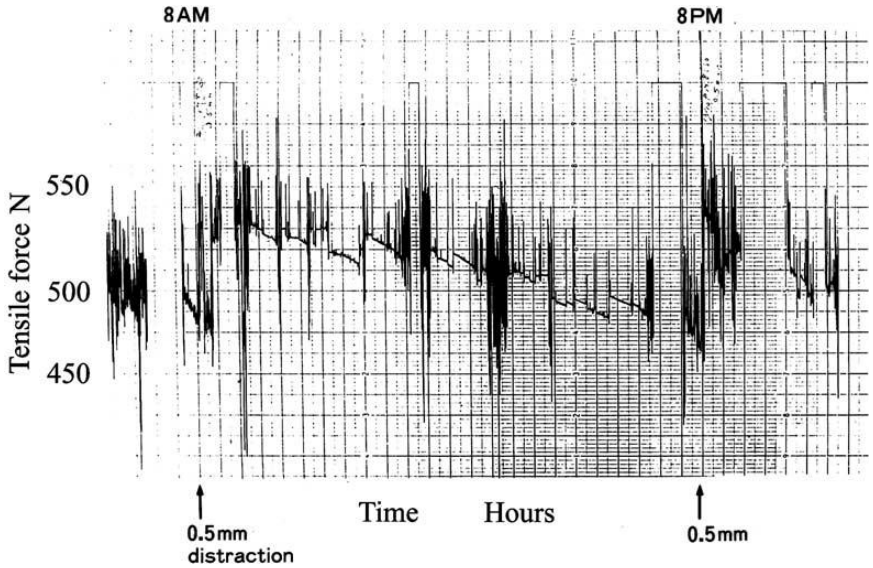

Figure 3-6 Forces measured overnight between distractions (from Ohnishi *et al.*, 2005)

Younger *et al.* (1994) found the change in load following a distraction to be related to the time of day. They found the force reading to increase after lengthening to a peak two hours after distraction, at midnight. This was found to be representative of all 3 subjects, reducing to its minimum around 6am, before the next lengthening. No firm explanation was given for these findings, but potential contributors such as hormonal, osmotic or cellular effects were identified. Additionally, the study found that 0.25mm lengthening

resulted in no significant immediate load increase; contrary to all other studies. Aarnes *et al*. (2002, 2002b) did detect an immediate force increase as a result of distraction, but also found that more relaxation per hour occurred overnight than during the day. The profile of the decay was not available because only pre and post-distraction forces were recorded thus the decay may not have been truly viscoelastic. Additionally, it is possible that the overnight forces did, in fact, increase but then decreased again prior to the next lengthening.

Gardner *et al.* (1998) found a very inconsistent relaxation, attributing this to the changing source of the resistive forces, while Lauterburg *et al.* (2006) found consistently high relaxations throughout the procedure. However, this was only in one subject as the remaining patients were only monitored on a weekly basis.

3.3.4 The role of high frequency distraction

In 1989, Ilizarov published the findings of a study that used quasi-continuous distraction on animal limbs and highlighted the osteogenic benefits of higher frequency distraction compared to the usual extension regime of four steps per day. A comparative study by Aarnes *et al.* in 2002 showed that this new method can be used more widely in the clinical setting. Their automatic distraction device extended by increments of 1/1440mm every minute, maintaining the rate of 1mm/day. It was found, through measuring compression forces in the frame, that the tension accumulation was significantly less (approximately 35%) in the high frequency distracted region than in the stepwise (low frequency) region, thus supporting the use of this method of distraction (Figure 3-7).

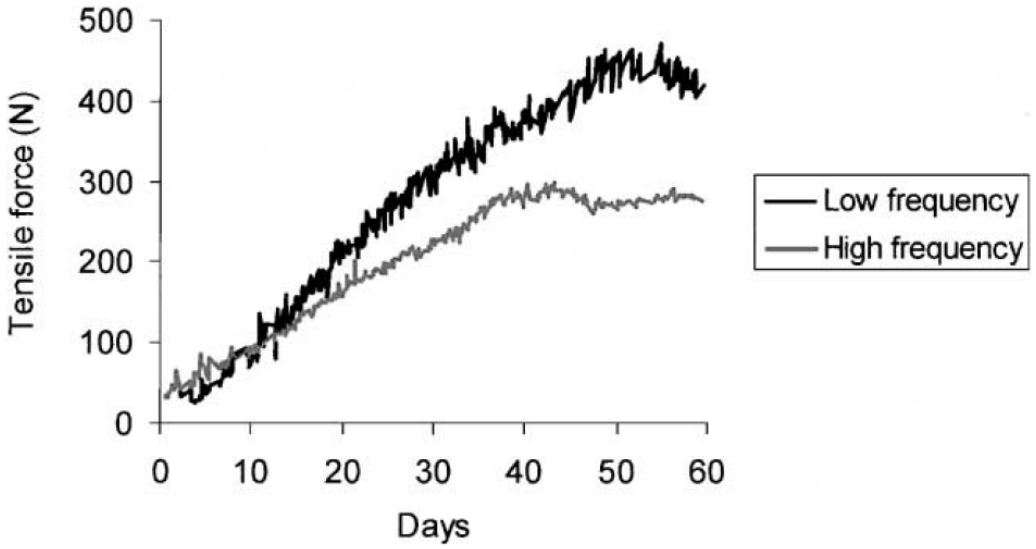

Figure 3-7 High frequency vs low frequency distraction (from Aarnes *et al*., 2002b)

This contradicted the findings of Ohnishi *et al.* (2005) who found that the lengthening frequency did not significantly affect the load increment rate, which in all cases was measured as 1.3-1.5N/mm. However, they did find that the circadian changes were very slight compared to standard step lengthening. Figure 3-8 shows the forces measured for different frequencies of lengthening, illustrating the closer distribution of data points for the higher frequency case.

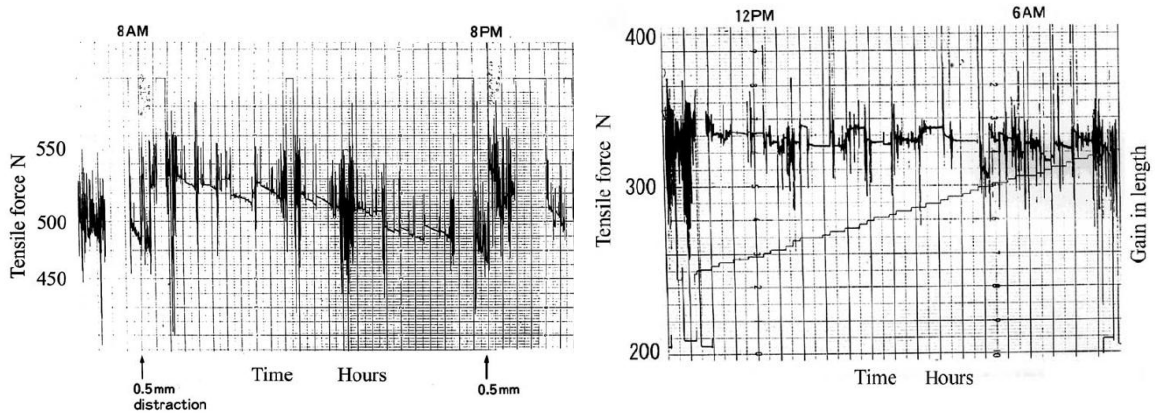

Figure 3-8 a) Forces measured during stepwise distraction b) high frequency distraction (note different scales, from Ohnishi *et al.*, 2005)

Reduction in this daily variation of forces results in less overstretching of both hard and soft tissues and consequently less pain, as was experienced by those undergoing higher frequency distraction. The immediate force increases shown in Figure 3-4 and Figure 3-8

are reduced when automated continuous lengthening is used in place of the stepwise method.

3.4 Tissue modelling studies

3.4.1 *In vitro* bone models

Bone substitutes are commonly used in the testing of orthopaedic devices. A popular choice is a product manufactured by Sawbones (Pacific Research Laboratories Inc.) and is made of polyurethane foam. The mechanical properties of these bones and the test blocks are consistent and stated to be within the range of human bone (cancellous and cortical) but they are not intended to replicate the precise mechanical properties of human bone in that they provide little or no time-dependent response. Consequently this makes Sawbones unusable for the testing of bone lengthening devices, as does the high stiffness values of the test blocks which, at their lowest end, represent osteoporotic bone, not newly formed callus.

Eveleigh (1997) simulated bone healing for the purposes of testing an IM nail as a fracture fixation method. Glass fibre cloth sheets (with an epoxy resin) were layered at specific time intervals and allowed to harden to simulate the increasing stiffness of the bone during healing, starting with a stiffness relating to callus and gradually increasing until full stiffness was achieved but even the early stage material stiffness was too high for newly formed bone regenerate.

Studies using callus mimics were found to be limited, particularly for the early stage of callus formation, therefore investigation was required into alternative solutions for providing a bone model with appropriate mechanical properties.

3.4.2 *In vitro* soft tissue models

Love *et al.* (2003) attempted to simulate the soft tissues effects during lengthening using a neoprene rubber sheeting to provide passive stretch response to lengthening. They found the tension in the stretched material to be similar to that of lengthened muscle with consistent viscoelastic behaviour. Urethane rubber has also been used to model tendons while strings linked to motors were used for muscle forces (Takano *et al.*, 2008). Rubbers tend to have short relaxations times in the order of a few minutes and have high levels of tension accumulation which are not consistent with the results shown from clinical studies for lengthening.

3.5 Tissue modelling studies – numerical

3.5.1 Mechanical modelling of tissues

Numerical studies are commonly used in tissue mechanics research to further understand the parameters associated with biological materials and processes. Finite element models often use linear elastic material properties as an approximation for bone callus, while different stages of healing can be analysed by changing the modulus of callus, taking the stiffness from the sources described in section 3.1 (Gardner *et al.*, 2000). The viscoelasticity of both hard and soft tissue is often overlooked in finite element studies of fracture fixation but this cannot be ignored when simulating the dynamic nature of DO.

General viscoelastic models based on various arrangements of springs and dashpots are shown in Figure 3-9 and have been applied to biological tissues (Fung, 1983). The arrangement of the components in series or parallel describes the most well known models - the Maxwell and the Kelvin-Voigt respectively.

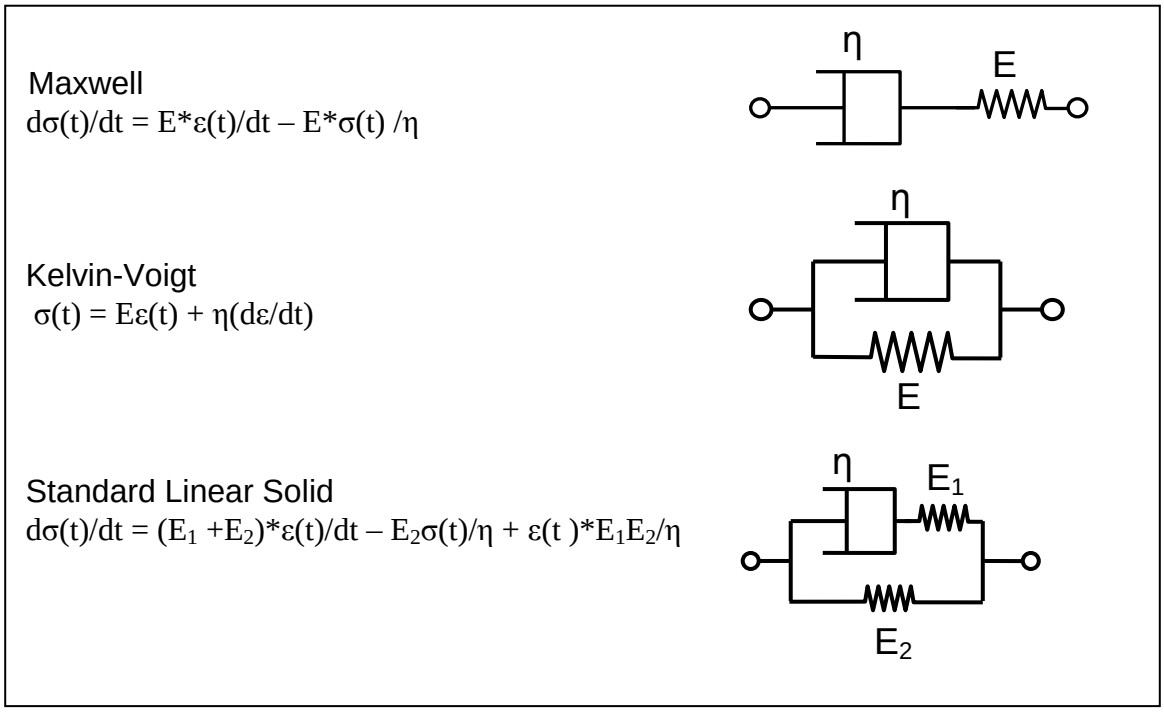

Figure 3-9 Models of viscoelasticity (where the viscous component is defined by the value of η, the elastic by E).

The mechanical response to a step stress input and step strain input varies greatly between the models; the response of a viscoelastic system to a step increase in stress is described correctly using the Kelvin-Voigt method whereas a viscoelastic step strain response is better described using the Maxwell model. The Standard Linear Solid model is a combination of the two i.e. a Maxwell with a spring in parallel, or a Kelvin Voigt with a

spring in series. It correctly represents both step stress and step strain. More accurate curve fitting to experimental data may be achieved by combining these units in more complex arrangements or using further generalisation (Fung, 1983). A generalised Maxwell model consists of a spring element with many Maxwell elements in series and has been used by authors to broadly describe tissue viscoelasticity (Dhar and Zu, 2007), or more specifically tendon (Machiraju *et al.*, 2006). Babic and Lenarcic (2004) illustrated how the tendon unit must be put in series with the muscle units in order to start to build a model that describes the whole system, particularly applicable to the case of lengthening where many tissues are involved (Figure 3-10). Fukashiro *et al.* (2001) also combined muscle and tendon models, this time including the viscous component but using only one muscle unit.

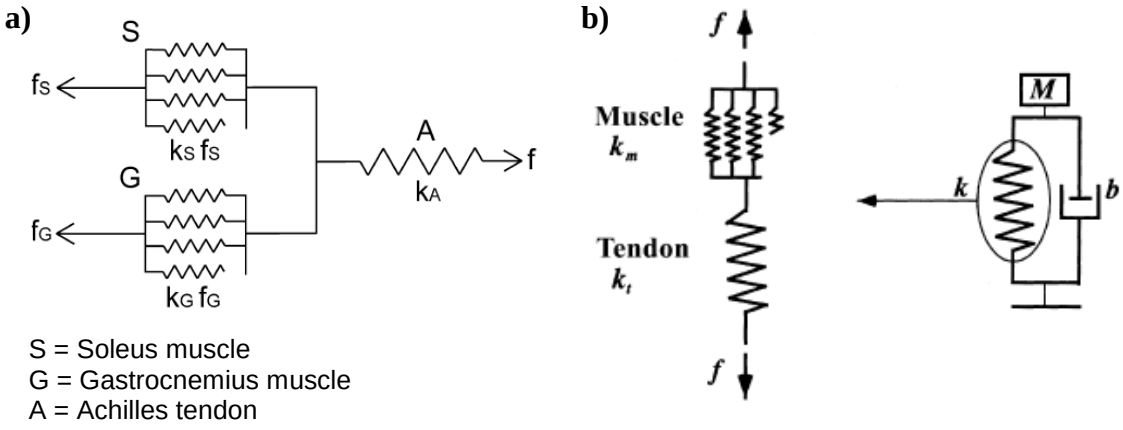

Figure 3-10 Two examples showing the ability of muscle and tendon models to be assembled together to describe the full muscle tendon complex (MTC)
a) Babic and Lenercic, 2004 and b) Fukashiro *et al.*, 2001

These models give the immediate response of tissue to a distraction step and subsequent relaxation, but in order to find the longer term tissue characteristics and influence of rate and frequency of distraction, it is important to understand the changes occurring in the tissue at a biological level, as any change in tissue type over time will in turn affect callus stiffness. Only then would a smart controlled device be equipped to make decisions about future events and tissue condition in order to prevent premature consolidation and/or refractures.

3.5.2 Fracture healing models

The stress within the callus tissue has been found to influence the types of tissues formed during fracture healing and DO (Pauwels, 1960). As discussed, the initial stages of

distraction osteogenesis mirror the physiological features of the fracture healing process. Both are dependent on specific mechanical conditions for optimal clinical outcomes and the limited models describing distraction are, in fact, further iterations of fracture healing models.

The mesenchymal tissue rapidly produced after a fracture (or after an osteotomy) can be described as pluripotent i.e. it has the potential to become one of many skeletal tissue types. Local stresses and strains were identified as the possible stimulus for the differentiation of this mesenchymal tissue in the 1960s, with Pauwels being one of the first to propose a concept of tissue differentiation, described by Figure 3-11.

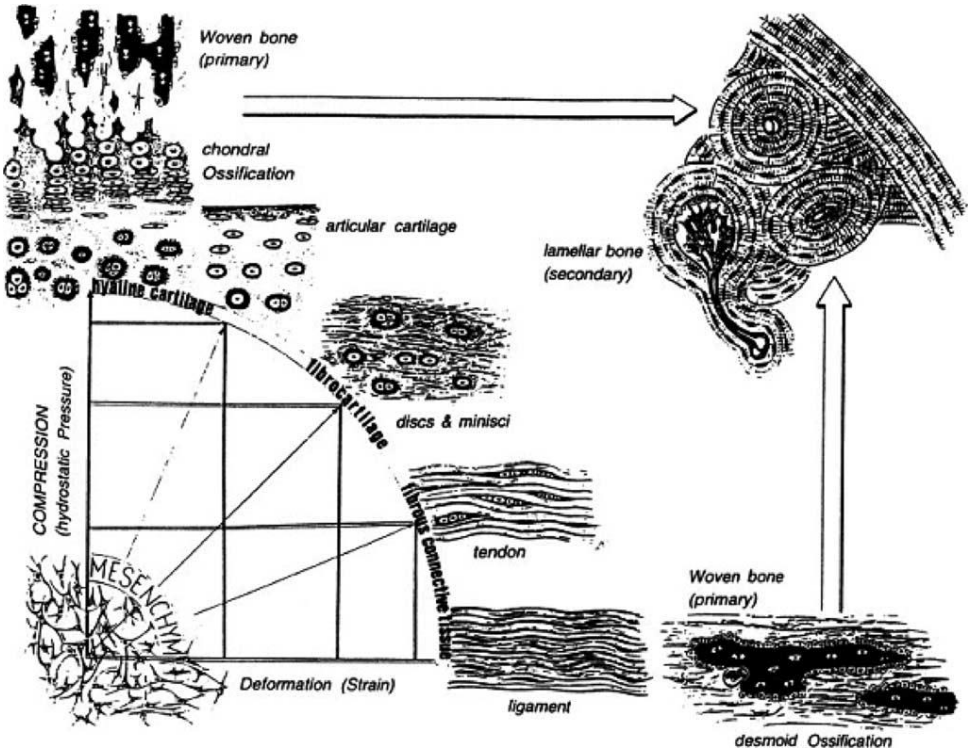

Figure 3-11 Pauwels concept of tissue differentiation (from Pauwels, 1960)

Having studied various *in vivo* differentiation patterns and estimating the applied loads in these situations, Pauwels proposed that high distortional strains in the mesenchyme result in a more fibrous tissue while hydrostatic pressure is the stimulus for a cartilaginous structure (Pauwels, 1960). No specific stimulus was suggested for bony tissue formation but it was supposed that bone could only form after the soft tissues had sufficiently stabilised the mechanical environment (Lacroix *et al.,* 2002).

Claes *et al.* (1998) investigated this hypothesis further by performing numerical modeling and experimental analysis attempting to quantitatively determine the strain and stress

acting on the cells *in vivo* and the biological consequences of fracture gap size and stability of the fixation by comparing patterns of tissue formation. They simplified the geometry to an axisymmetric representation of a fractured long bone, divided into seven distinct regions and five material types. Three healing stages were examined at 1, 4 and 8 weeks after the fracture, when one would expect significant changes in the tissue types and in the degree of interfragmentary strain. By loading these models, computing resultant stresses and pressures using the finite element method and comparing patterns to histological data, their results suggested intramembraneous bone formations at local stresses under 5% and hydrostatic pressures under 0.15MPa. Endochondral ossification was found to relate to regions of strains below 15% and compressive pressures larger than 0.15MPa while connective tissue or fibrous cartilage was found in all other cases.

Carter *et al.* (1988) also used Pauwels concept as a basis for their mechanoregulation model, extending it to include cyclic loading history (Figure 3-12). This was thought to be an important factor as opposed to focussing on the instantaneous tissue conditions.

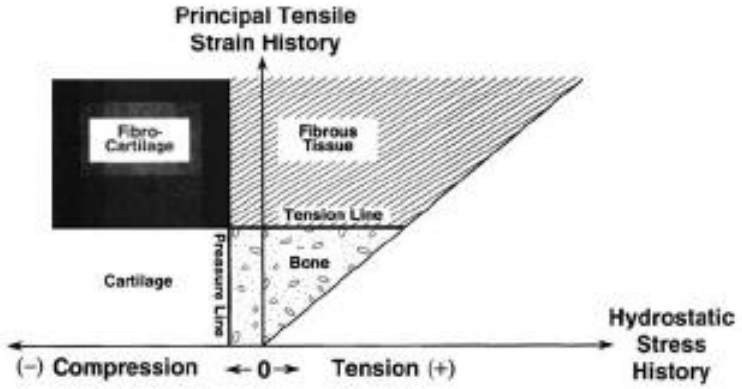

Figure 3-12 Relationship between tissue differentiation and mechanical stimuli (from Carter *et al.*, 1988)

Carter *et al.* (1988) tested this hypothesis using the finite element method, predicting patterns of tissue differentiation during secondary fracture healing in a long bone subjected to cyclic axial loading. They too used an axisymmetric model of the fracture site, consisting initially of diaphyseal bone and callus/medullary tissue which was subjected to a unit axial force and compared patterns of tensile strain and hydrostatic stress with histologic observations. This model supported their hypothesis for mechanoregulation and outputs were similar to that of Claes *et al.* (1998); that in areas of low tensile strain, bone formation is more likely, whereas in regions of moderate tensile

strain a more fibrous tissue can be expected. Chondrogenesis was seen to occur in areas of hydrostatic compressive stress.

An assumption in both of these finite element models is that the material is a non-porous solid. Yet, the (shear) stress on the cells as a result of fluid flow has been identified by some authors (Kuiper *et al.,* 2000; Lacroix and Prendergast, 2002; Gomez-Benito *et al*., 2005) as being a potential stimulus for tissue differentiation. In order to test this assumption, models have been developed that include both a solid phase and fluid phase allowing analysis of shear stresses as a result of fluid flow.

Basic concepts of biomechanical models first developed for understanding and predicting fracture healing have been extended to be applicable for the case of DO.

The biomechanical model of Morgan *et al.* (2006) was based on that used by Carter *et al.* (1988) but included further parameters such as fluid velocity and tissue dilation. Their goal was to characterise the biological environment within the distraction gap during one 2mm simulated distraction. Comparison was made between four stimuli (total pressure, tensile strain, tissue dilation and fluid velocity) immediately following distraction and after 12hrs. The temporal nature of fluid flow through poroelastic materials means that pressures and strains change over time following a step displacement. It was found that within the first 20mins, total pressures reduced to around a third of instantaneous values and fluid velocities decreased to zero after 10mins. Tensile strains also decreased but were dependent on the specific region, the largest being a 43% decrease. Conversely tissue dilation increased over the 12hr period from near zero to 43% strain. This was coupled with a contraction of the regenerate perpendicular to the distraction vector which completely dissipates leaving pure elongation. This model provides interesting insight into the types of mechanoregulation exhibited during simulated tissue lengthening, especially when tensile strains are evaluated, however it is limited by the fact that only one distraction step is used for analysis, and as such, it is difficult to gain understanding of how factors such as rate and frequency of distraction will affect tissues in the longer term.

3.5.3 Mechanobiological healing models

Many of the aforementioned models have been developed into more complex mechanobiological models which update the material properties (i.e. tissue type) as a result of the particular mechanical stimuli at each time period in that area or element. A key aspect of these models is the ability to relate biological changes to mechanical

properties that influence the stiffness of the regenerate as the process develops. The cyclic nature allows analysis at various time points as the procedure continues.

A mechanobiological model developed by Lacroix and Prendergast (2002) is shown below (Figure 3-13), taking tissue shear strain and fluid shear stress as the stimuli.

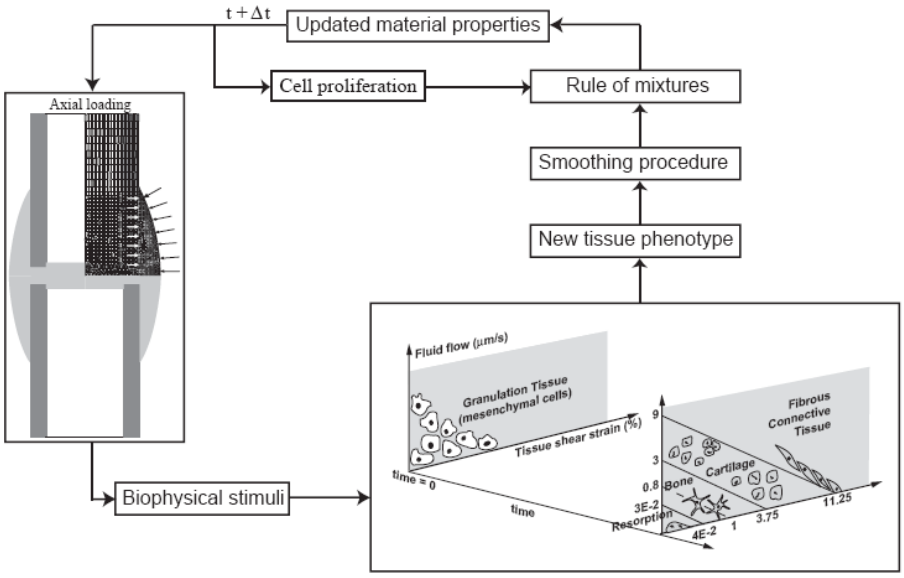

Figure 3-13 Flow chart of iterative model, including mechanoregulation (from Lacroix and Predergast 2002)

An initial set of conditions is prescribed (geometry, boundary conditions, material properties) and following each load step in the FEA, biophysical stimuli are computed. If under the new conditions, a new phenotype is favoured according to their mechanoregulation diagram, the material properties for that element are changed. The delay for the process of tissue differentiation is accounted for by averaging the previous ten tissue types. Spreading of cells through the callus is simulated using a diffusion law based on cell density. Their model successfully predicts several well known features of the fracture healing process. Initial iterations show fibrous connective tissue filling the fracture gap and intramembranous ossification proximal and distal to the fracture site. The callus is then seen to stabilise initially by endochondral ossification in the external callus which reduces the strain in the fracture gap, followed by ossification between the bone ends. Subsequently the strain through the remaining callus is reduced and because low levels of both stimuli result in resorption due to lack of mechanical stress, the original shape of the bone is restored. Validation of the model was carried out using the experimental model of Claes *et al.* (1998). Thresholds used in the model were taken from original studies and have been used by other authors (e.g. Huiskes *et al*., 1997).

Although this model predicts callus resorption at the end of the healing process, it does not predict the state of the initial callus formation, the growth of which will determine interfragmentary strain and thus influence the mechanical stimuli acting on the cells. Gomez Benito *et al.* (2005) developed a model that simulates the process of callus growth through cell proliferation, migration and differentiation from mechanical stimuli and time (Figure 3-14).

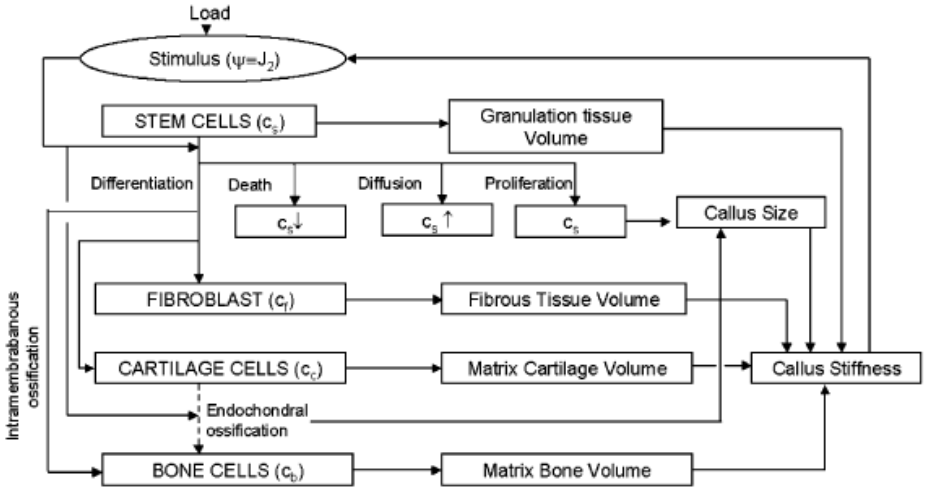

Figure 3-14 Flow diagram of mechanobiological model (from Gomez Benito *et al,*. 2005)

Three different finite element analyses are performed. Firstly the poroelastic analysis computes the mechanical stimulus on each cell as a result of external load input. Using predetermined threshold values, subsequent analyses predict the differentiation, proliferation and death of cells. The second analysis is the diffusion process, required for finding migration and ossification of cells. Lastly the thermoelastic analysis is performed which is responsible for callus size. The outputs from each of these separate processes are used to update variables such as material properties (using mixture rules) and geometry, allowing the finite element model to be remeshed ready for the next iteration. Evaluation of the model was performed using a range of gap sizes from 1-6mm, demonstrating that the callus would be enlarged with an increased gap size but that there is a point at which the gap size is too large for endochondral ossification to take place and thus very little bone is formed in the callus.

In order to establish the best numerical representation of the fracture healing process, Isaksson *et al.* (2006) designed a 3-dimensional finite element model with the ability to compare the results of three different algorithms (Carter *et al.*, 1998; Claes and Heigele (1999); Lacroix and Prendergast, 2002) to *in vivo* experimental data. The study included

torsional loading in addition to the axial loading used in the authors original analysis. Algorithms whose stimuli for tissue differentiation were hydrostatic pressure and strain failed to predict the healing and bone formation when torsional load was applied.

One study (Gomez Benito *et al.*, 2005) shows the relevance of these mechanobiological models, not only to clinical parameters but also to device testing and design. They used their 3D model to find the influence of the stiffness of the external fixator and, in line with experimental results, they found that decreasing the stiffness of the fixator delayed fracture healing and increased callus size.

3.5.4 Distraction osteogenesis models

Isaksson *et al.* (2007) performed the first study including tissue differentiation during the complete distraction process, aiming to optimise treatments by finding information about local stress and strain magnitudes. Based on the mechanobiological FE model developed by Prendergast *et al.* (1997), the distraction was applied (over 1 second per 24h period) and biophysical stimuli were calculated (octahedral shear strain and fluid velocity) to determine the specific phenotypes the precursor cells would become. Differentiation from one phenotype to another was not modelled but matrix production and tissue growth over time were dependent on the type of cell. New elastic modulus for each of the elements was then a function of the new cell density. The model predicted well the bone formation pattern seen experimentally, including results for different rates and frequencies of distraction. Interestingly, comparison was also made between experimental reaction forces and those found numerically. Reaction forces in the experiment were found to increase linearly for the first 3weeks; conversely the computational model predicted forces to drop over the course of lengthening due to the increasing proportion of low stiffness regenerate, a phenomenon not seen clinically. Relaxation values were closer to model outputs. This author along with others (e.g. Boccaccio *et al.,* 2008) takes into account the temporal nature of the cell differentiation; by averaging the tissue material properties from previous iterations. This is an important consideration because the consequences on the stiffness of the model would be an immediate step change in stiffness which is not seen in reality.

Reaction force to tissue distraction have been predicted (Reina Romo *et al.,* 2009a) using a development of the fracture healing model of Gomez Benito *et al.* (2005). Three different distraction rates were applied - 1mm/day, 2mm/day, 0.3mm/day and the effect each rate had on the cell distribution was analysed. Cells underwent proliferation,

differentiation and migration depending on the level of mechanical stimulus – a consequence of the distraction. Similar to previously described studies, they also employed a temporal component to the model by computing the cells maturation level, calculated from the number of days each cell took to mature at a specific stimulus level. Patterns matched well to experimental data, predicting non-union at high rates and premature consolidation at low rates. In contrast to Isaksson *et al.* (2007), the reaction forces for clinical rates of lengthening were found to increase over the period of distraction. One limitation is the assumption of a free stress state at the beginning of each distraction phase. This presumes that the tissue relaxes fully after each distraction which is not necessarily the case in clinical practice (Simpson *et al.*, 1996). Their next model tackles this issue, analysing the effect of pre-traction stresses (Reina-Romo *et al.*, 2009b). These residual stresses are taken to be as a result of incomplete stress relaxation following an elongation.

It is clear that computational modelling can be helpful in understanding the impact of the mechanical state of tissue on complex biological processes (Doblare, 2004). Some validation has been achieved, particularly with regard to tissue pattern during fracture healing. Conversely, the more recent distraction osteogenesis simulations include a large number of model parameters, some of which cannot be directly validated through in-vivo measurement. There have been some attempts to use these models to assess the increase in reaction force as a result of each distraction and it is clear that pre-traction forces cannot be ignored.

3.6 Summary

Characteristics of hard and soft tissue have been explored. This indicates of the type of loading environment that the distraction devices are working within. Loads during distraction have been measured and found to have a highly dynamic loading profile suggesting that devices ought to be able to withstand continuously changing loading conditions. Tissue stiffness not only varies between patients due to demographics or indication for lengthening, but has been found to change throughout the limb lengthening procedure. Mechanobiological modelling can be useful in explaining why these changes take place.

It has been shown that the standard regimes using traditional devices do not necessarily provide optimal patient outcomes, thus there is a need for more advanced devices with the

ability to change distraction rates and frequencies. These new devices require rigorous testing to ensure complication rates are kept to a minimum when used clinically, some of which can be done through experimental and numerical means.

Chapter 4

Development of a smart device

4.1 Introduction

A distraction rate of 1mm/day provided in four steps has been adopted by clinicians as the standard lengthening protocol. However, it has been suggested that this may not be the optimal regime; for instance high frequency distraction has been shown to have significant benefits over traditional stepwise lengthening, improving the regenerate tissue quality and reducing patient pain during the procedure (Ilizarov, 1989; Aarnes *et al*., 2002). Any deviations from this standard are directed by the clinician following radiological inspection or physical examination. Monitoring of the forces within the tissue has been suggested as a method of determining the mechanical (and consequently biological) conditions of the tissues and can therefore be used to influence decisions to optimise the regime (Claes, 2007). Consequently the proposed smart lengthening device provides automated continuous lengthening whilst also having the capability to control the lengthening rate based on tissue reaction force or calculated stiffness. It must be stated here that Wee *et al.* (2008) attempted the first force-controlled distraction in an ovine model using an automated device. Their design was patented six years after this smart autodistractor, and many features distinguish the two, particularly their methods of actuation (Patent numbers US 2002/0143344, US 2008/0051779).

This Chapter explains the mechanics of the smart device and some key research and development activities, including exploration of methods for load and displacement measurement and the influence these have on the control decisions.

4.2 Actuation method

The actuation of conventional lengthening devices involves manual rotation of a screw or nut on a threaded rod to achieve separation of the pin clamps. Alternative methods of actuation include the one-way ratchet mechanisms of the Albizzia and the ISKD (previously described in Chapter 3), which are rotationally activated. The Fitbone device uses an external power supply to activate a motor driven mechanism within the intramedullary nail.

Based on current literature (see Chapter 3), the design specifications for the new smart device required a method of actuation that could achieve quasi-continuous extension (~10microns per step) over a wide range of loads (0-500N). High frequency distraction has been shown to reduce peak loads, thus the maximum loading requirement did not take into account some of the peaks recorded in literature. Piezo actuators were selected over conventional motors due to their near infinite resolution and low power consumption - of particular importance for a portable device.

When voltage is applied across the piezoelectric material, the crystal arrangements within the layers of ceramic are altered, resulting in a minute change in dimensions with very high precision (Physik Instrumente, 2005). Along with their high load capability and low current, this makes them ideal for providing the small but accurate displacements required for limb lengthening.

Performance characteristics of this type of actuator can be defined by the following:

1. No load displacement – maximum travel from actuator
2. Block force – force required to prevent any travel
3. Linear relationship - between displacement and load
4. Constant load – same travel as ‘no load’ but change in initial position

As described by Figure 4-1 , the maximum travel at no load for actuator (preloaded stacked actuator - P212.80) is 120microns while the maximum load (block force) is 2kN assuming no displacement (blue line). Between these two points the actuator output is theoretically linear i.e. if the actuator extends by 30microns then the maximum load will be reduced to 1.5kN. This occurs when the device is driving against an elastic load such that it is under increasing resistance with increasing extension. The red and green lines on the graph represent two different springs, the crossing point relating to the maximum load/displacement of the piezo actuator against these spring stiffnesses.

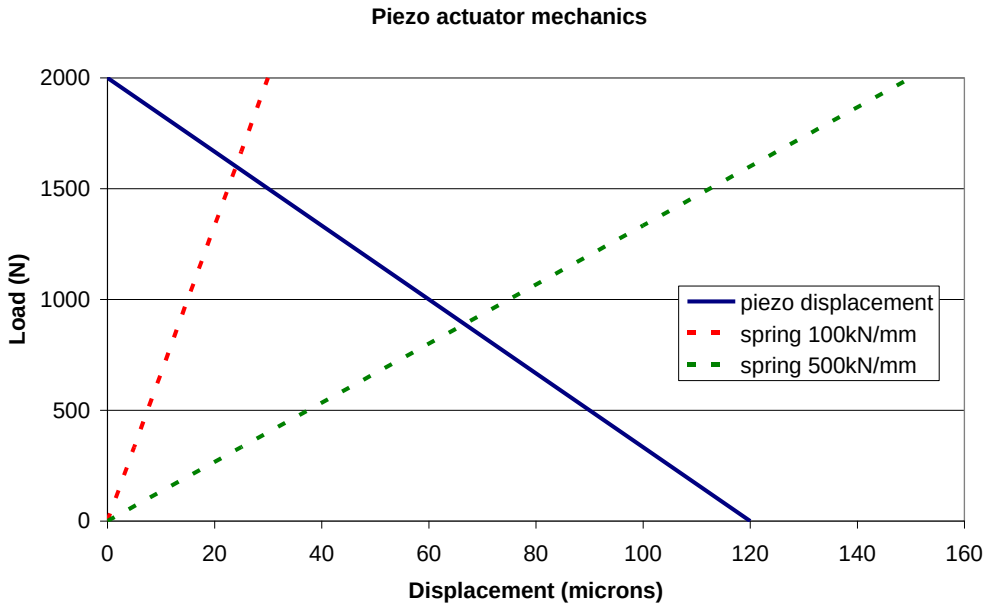

Figure 4-1 Force/distance characteristics of the piezo actuator and effect of spring load

Interestingly, if actuation is against a constant load then its total extension remains unaffected. Only the initial length of the actuator will be reduced while the change in displacement when actuated will match the unloaded case (Figure 4-2). The following equation can be used to find the maximum possible force on an elastic body as an alternative to the graphical intersection of load displacement lines.

$$F_{max} = k_t \Delta L_o (1-(k_t/(k_t+k_s))$$

where F_{max} = maximum actuator force, k_t= spring stiffness, k_s = actuator stiffness and L_o = no load extension of the actuator.

Figure 4-2b shows the reduced actuator extension against a spring load.

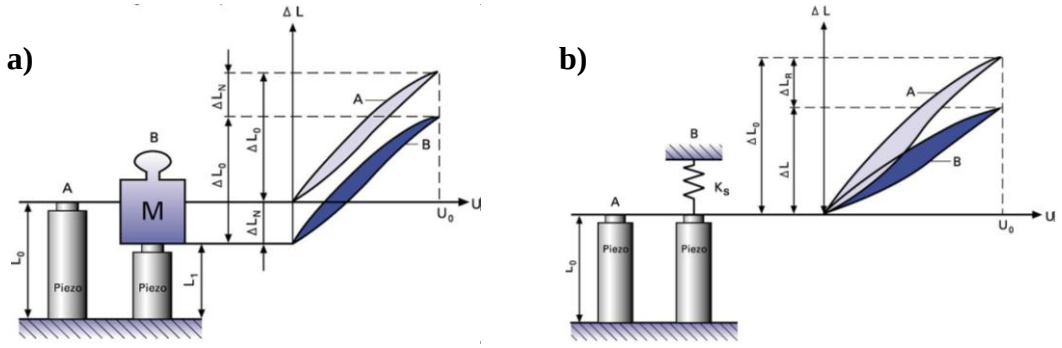

Figure 4-2 Piezo actuator mechanics against constant load and spring load. (Physik Instrumente, 2005)

4.3 Concept for new device

Similar to traditional manual unilateral devices (e.g. Monotube Triax, Stryker Trauma), the smart device design comprises two pin clamps attached to two body sections which undergo separation. Figure 4.3 shows the complete proof of concept device (and close up with the cap removed to reveal the motors and nuts on the threaded shaft).

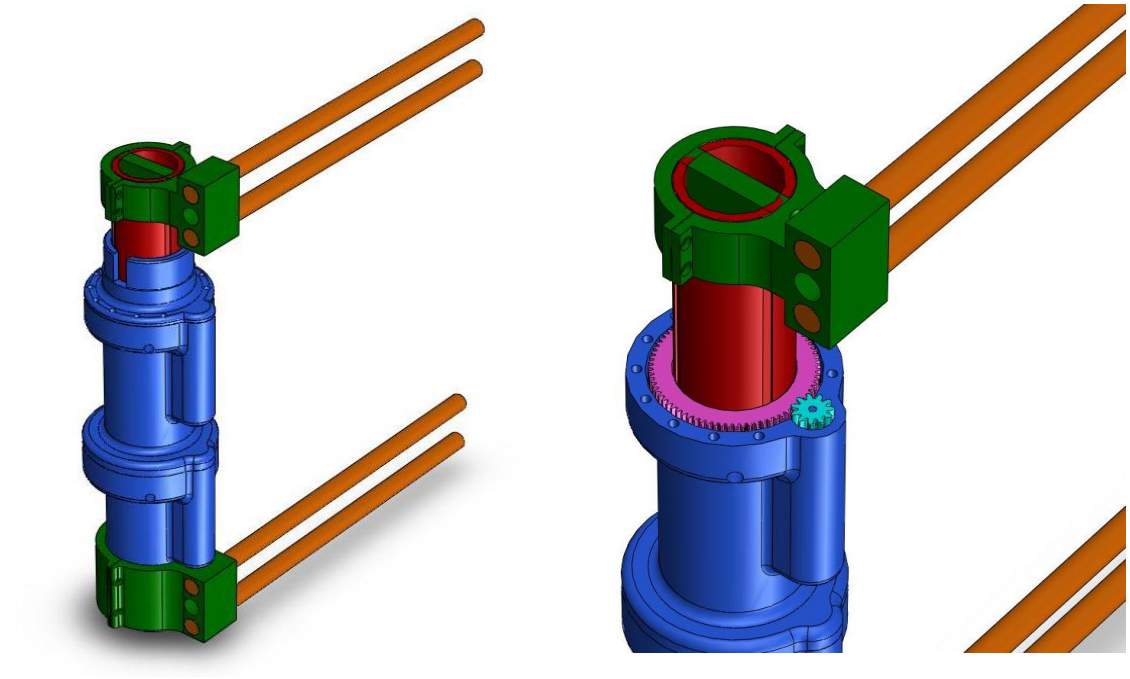

Figure 4-3 Device with pin clamps and front cap removed

Instead of a manual rotational mechanism, the shaft is driven forward by the charging of the piezo actuator and is combined with a one way inch-worm mechanism to prevent backward movement during the discharge of the piezo actuator. Miniature motors are used to drive nuts on a threaded shaft as explained in Figure 4-4. These are controlled by a PIC microprocessor which collects inputs (geartooth counter, actuator feedback voltage, motor current) and provides outputs (actuator voltage, motor signals). A program flow diagram for the PIC is provided in Appendix A.

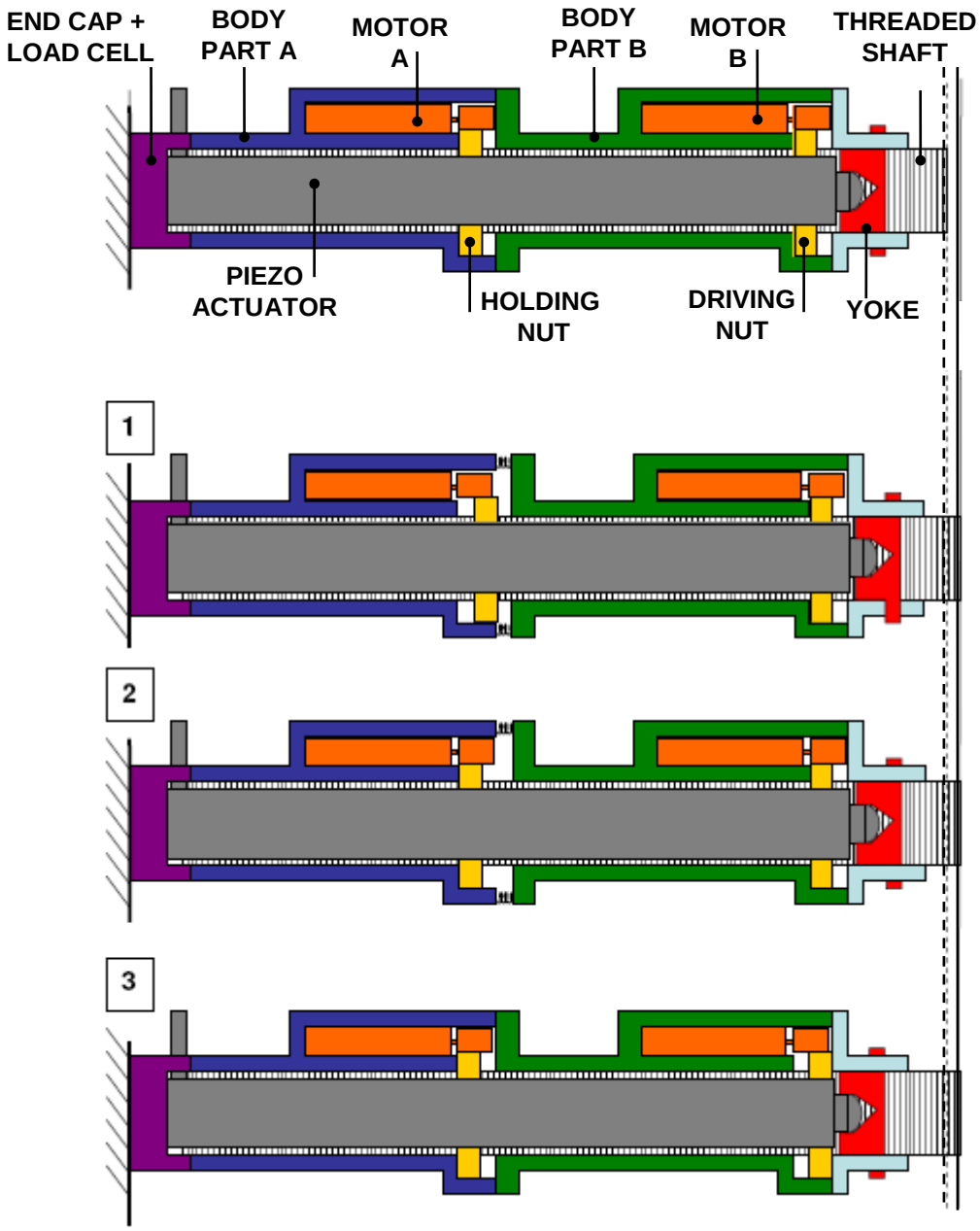

Figure 4-4 Device mechanics

The mechanism for each stage is as follows:

1. *Electrical* - By means of an inductor and oscillator, the voltage is incrementally increased across the piezo actuator (i.e. it acts as a capacitive load).

   Mechanical – The actuator is charging and therefore extending relative to the applied voltage. Body part B, threaded shaft and nuts all displace.

2. *Electrical* - In this high voltage state and before discharge, miniature motor A is switched on, rotating the pinion and nut (acting as a spur gear set). When the motor stalls the resultant current peak acts as a switch to turn the motor off.

   Mechanical – The holding nut is rotated and eventually hits the surface of body part A, tightening against it.
3. *Electrical* – Another oscillator is used to switch the transistor and thus the discharging circuit on. The voltage is dissipated across a resistor. It may be possible at a later stage to recover the loss by discharging back into a battery.

   Mechanical – The actuator discharges and body part B retracts. The position of the holding nut prevents the threaded shaft and driving nut from retracting with it.
4. *Electrical* – In this discharge state, motor B is switched on again until the motor stalls and the resultant current peak switches off the motor.

   Mechanical – The driving nut is rotated against the surface of body part B, back to the initial position ready for the cycle to repeat.

The presence of small springs between the two body parts results in a small preload that, in theory, compresses the piezo actuator, reducing its initial length but not changing the total possible extension. This relates to the 'constant load' case of actuation mentioned in section 4.2.

When used clinically, pins are used with pin-clamps to attach the device to the bone. One is situated at the end of the threaded shaft and one on body part A. These pins introduce bending into the device which was found to increase frictional forces between the threaded shaft and body parts. Channels on the outer surface of the shaft allowed 0.5mm diameter guiderods to be fitted and used as the bearing surface to assist the sliding of the threaded shaft inside the body parts.

4.4 Improving device performance

During charging, the load path between the piezo actuator and the pins fixed into the bone involves many additional components. It was found that any load dependent 'compliance' within the device from interfaces or component deformation (due to strain or bending) had to be overcome by the piezo actuator during charging before any load was transmitted to the external (tissue) environment. Thus the actual displacement or load transferred to the bone was significantly reduced from the theoretical value. Additionally, when the

actuator discharged, any compliances within the secondary load path incurred losses and resulted in a backwards movement of the shaft from the maximum position reached during the cycle. This is referred to as 'setback'. Load paths and compliances are summarised in Figure 4-5.

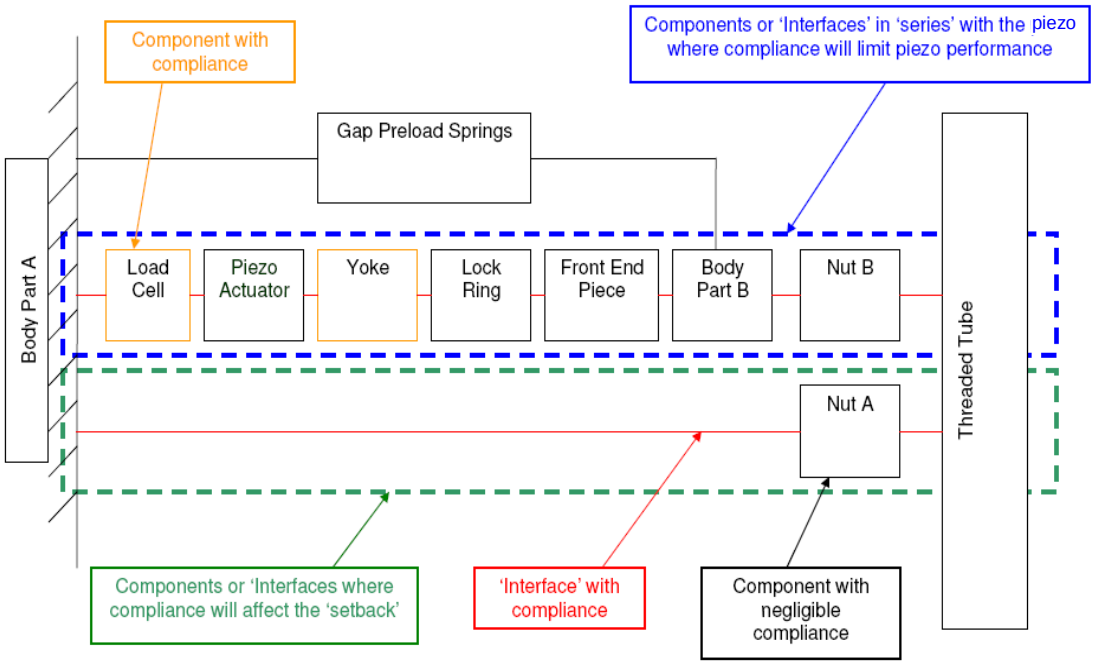

Figure 4-5 Compliances and interfaces that will influence device performance

Although the maximum voltage for the piezo actuator was 1000V providing 120microns of free displacement, the voltage limit for continuous operation was given by the manufacturer as 800V (to increase actuator lifetime) which limited the maximum travel to 96microns, or maximum load to 1600N. Environmental influences (such as humidity) are sighted as the cause for degradation in low frequency operation thus the cost of replacement actuators should be balanced against the cost of actuators with enhanced case sealing. Alternatively it may be that short-term peaks over this voltage level may be acceptable and show no degradation of the actuator. For the purposes of this testing the voltage was kept to 800V to ensure no changes in actuator performance.

Figure 4-6 explains the mechanics of the charging sequence and suggests a combined stiffness of interfaces and components of 12.5N/micron. Assuming zero initial charge, the piezo actuator always starts in the same initial unloaded state i.e. (from Figure 4-2) L_0 is always the same, no matter what load the device is under. During period A the piezo actuator charges and extends against a spring load (Figure 4-2), provided by the compliance of the interfaces and components detailed above (Figure 4-5). With a

12.5N/micron stiffness this theoretically results in 20microns of 'lost' extension under a load of 250N. 'Lost' extension is described as piezo actuator extension which is not transferred to the shaft. Additionally, the piezo actuator stiffness itself was 16.67N/micron therefore the actuator contracts by 15microns due to the 250N load increase. Any additional movement is then dependent on the elasticity of the external load. In this case the elastic load was 200N/mm or 0.2N/micron. During 'B' the actuator is loaded from 250-262N due to a piezo actuator and shaft displacement of 60microns (elastic load).

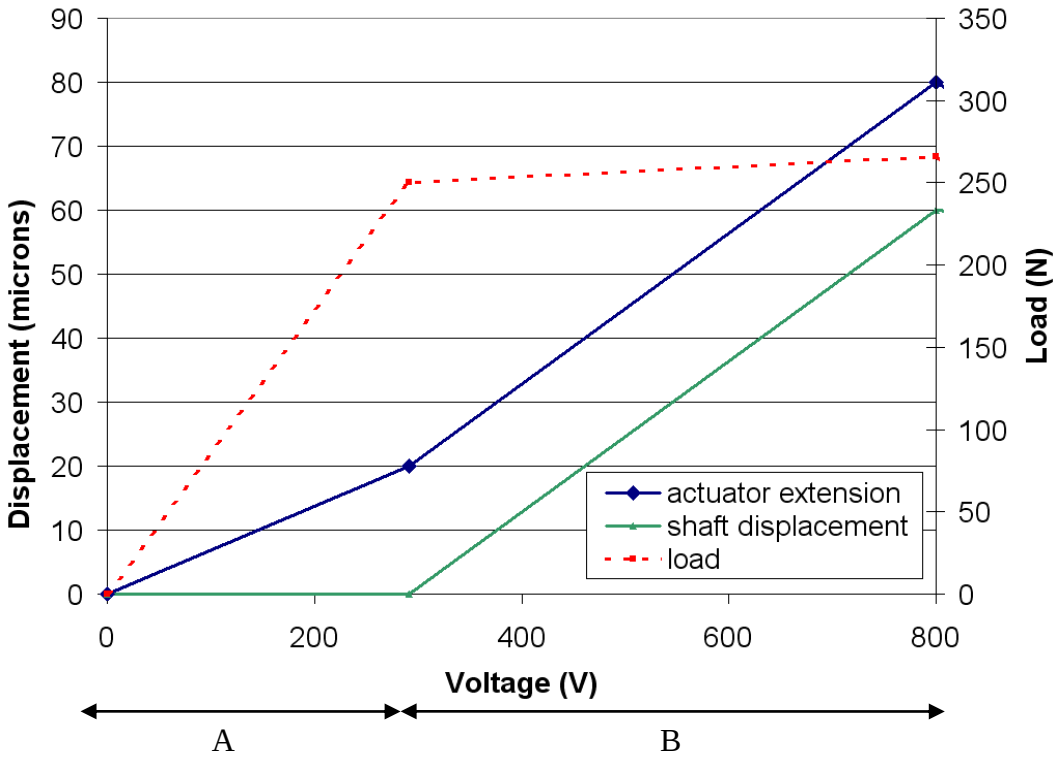

Figure 4-6 Illustration of an initial external load of 250N and a tissue stiffness of 200N/mm.

The final shaft displacement here is shown as 60microns. The motor then tightens the nut against the surface of the housing but the additional compliances (detailed in Figure 4-5) result in some setback of the shaft (e.g. 10micron) such that its final displacement is reduced (Figure 4-7).

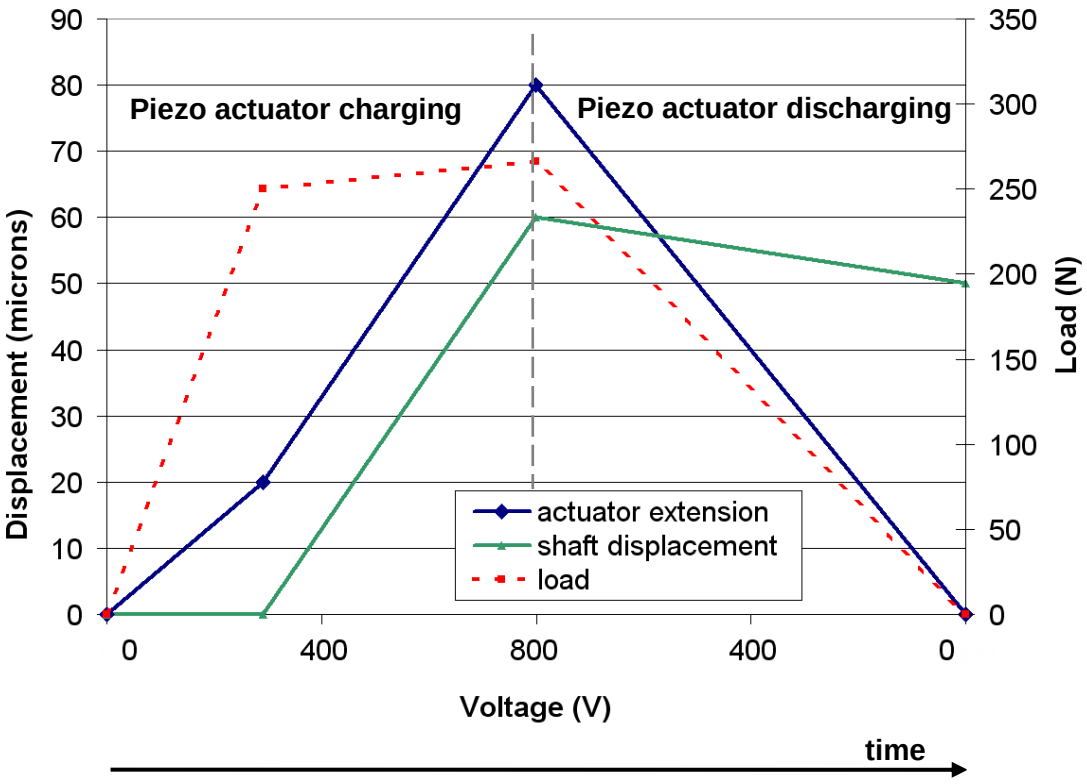

Figure 4-7 Illustration of the influence of setback on shaft displacement

Undesirable compliances within the proof of concept device included interface problems as well as deflections of parts themselves. Analysis was performed of the original device in order to determine the most significant contributors to this problem. Dial gauges were set up at specific locations, pressure film was used to find the contact points of the nuts on the thrust surface and small adjustments to the components were completed, with less than 5% improvement on performance.

Using the results of this analysis of the proof of concept model, a new prototype was designed and manufactured during this piece of research. Firstly, thought was given to the arrangement of the components and the possibility of a more substantial change to the device construction. The author established that a significant change in the mechanism assembly could result in elimination of some components. This, alongside design changes to others, was found to improve the stiffness of the structure considerably. In this new arrangement, the two-part housing was replaced by a single part, reducing bending when under an offset load (using pins).

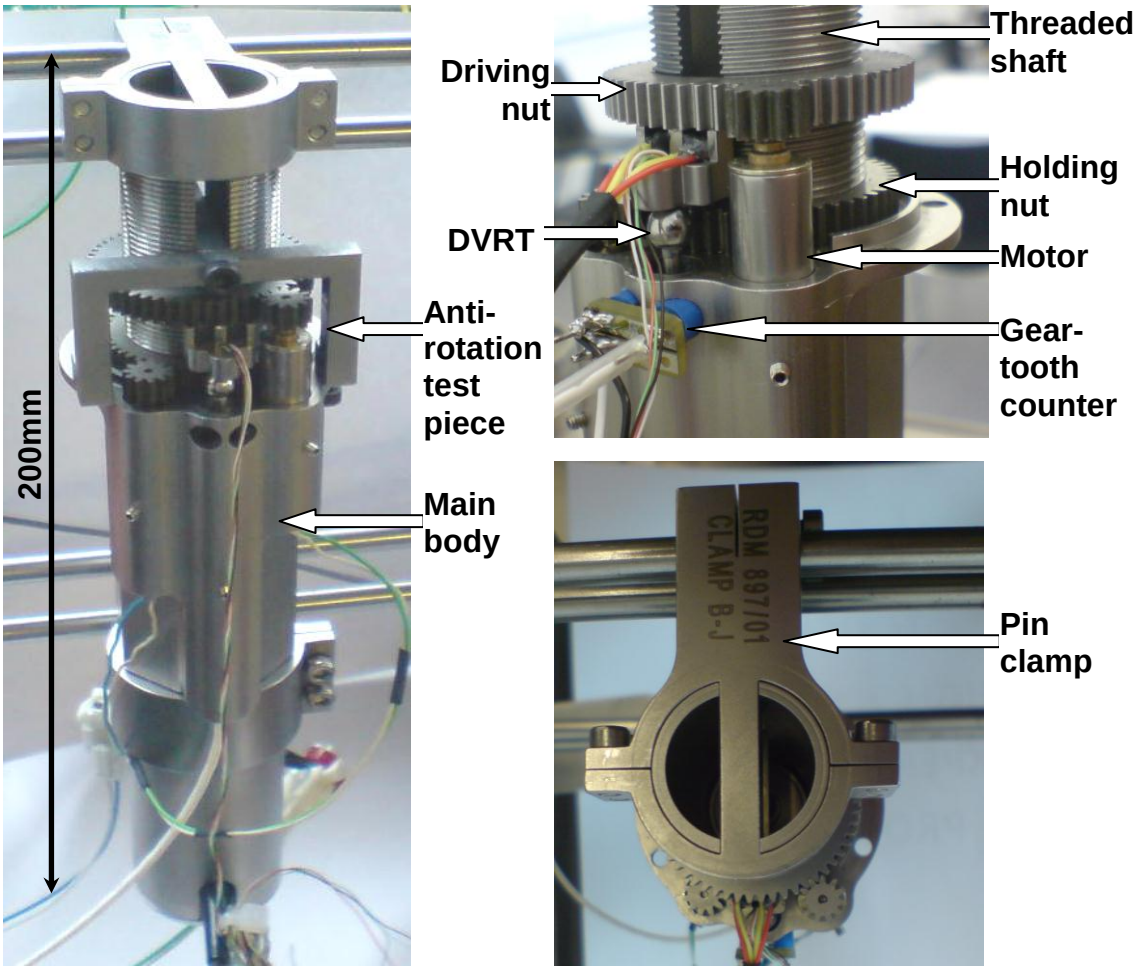

Figure 4-8 New improved concept for smart device

The second main advantage was the ability to have a smooth shaft as a bearing surface instead of using guiderods, allowing a threaded section to run inside the smooth inner surface of the housing. Another benefit was the ability to move both nuts to one end, which allowed easy viewing of the mechanism during running. This was previously hidden within the housing (Figure 4-8). Capacitance sensing between the two body parts was originally to be used in the proof of concept model to measure extension per cycle, but for the new prototype, this was replaced by a small DVRT (Microstrain, SG-DVRT) with a resolution of 1micron. The original design for the geartooth counting as 'global' displacement measurement was modified - the emitters were re-housed in the yoke piece and counting was performed when the holding nut was rotating. The yoke was also used for load measurement via strain gauges. The new design is shown in Figure 4-9 and drawings for the prototype can be found in Appendix B. The steps of the cycle are very

similar to that of the proof of concept model (Figure 4-4) but in this case the actuator extension does not affect the body parts.

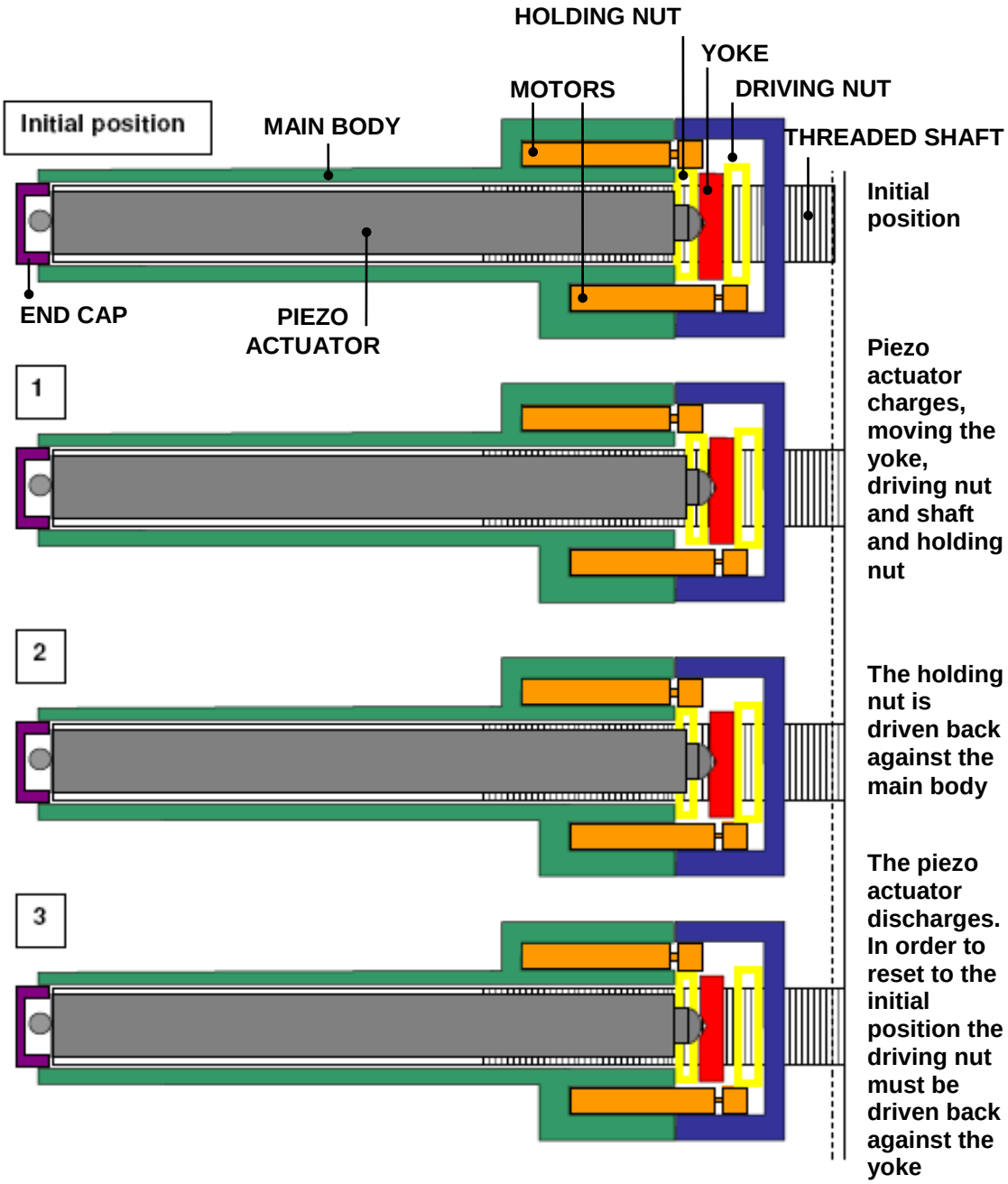

Figure 4-9 New prototype design with reduced parts and compliant interfaces.

As part of the reset procedure, the driving nut moves the yoke piece into contact with the piezo actuator and this is now the source of any 'preload' on the device as opposed to the spring load of the proof of concept model. The value of this preload was measured as around 20N.

4.5 Control system development

1. Continuous distraction – linearization during each cycle

During initial testing the piezo actuator was charged to full capacity as quickly as possible. The charge curve was analogous to a capacitor and took around 90 seconds for charging and 30 seconds for discharging. The aim of the device was to have continuous lengthening and therefore the voltage increase required linearization (see ramp in Figure 4-10). This was most important when testing the response of the device to a system with time-dependent loading characteristics.

Similar to capacitors, piezo actuators have a leakage voltage that, in this case, presented problems due to the high frequency pulse circuit that was being used to charge the actuator. Leakage, especially at high voltages, meant that the frequency of the charge pulses had to be increased considerably to maintain the linearity during charging. This accounts for any discrepancy between the target voltage (ramp) and the measured voltage (piezo voltage) in Figure 4-10.

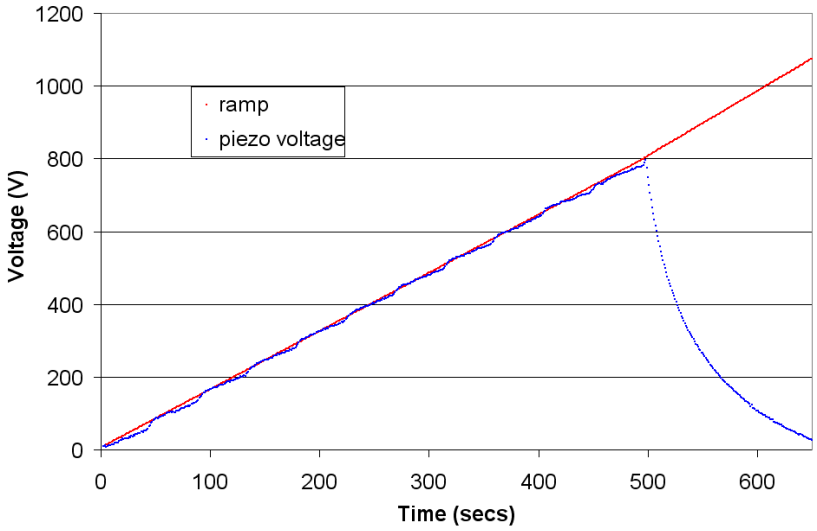

Figure 4-10 Voltage linearised - following 'ramp' signal, then discharging

A linear voltage ramp did not result in exact linear movement of the shaft due to aforementioned compliances (Figure 4-7) and, although an attempt was made to use the DVRT signal for control, voltage control coding was less complex so it was preferred at this stage of testing.

2. Linearisation of extension over a number of cycles

As the load increased, the number of microns of device extension per cycle was expected to reduce. To maintain long term linearity of lengthening, the device was programmed to change the piezo actuator ramp rate (volts per second, i.e. speed of charge) if the extension per cycle was found to change. If the extension per cycle reduced such that it would not manage to lengthen by the preset daily amount (e.g. 1mm) the ramp rate was increased and the cycle would be faster, increasing the total number of cycles.

The geartooth counter was used to measure the overall extension of the device by counting the holding nut teeth as they rotated, and broke the infrared beam between the emitters and collectors. Each geartooth count represented a shaft movement of 20microns (the thread pitch was 1mm and the holding nut had 50 gearteeth). This method of measurement limited the maximum absolute error to ~20microns, assuming no errors within the counting circuit. Although this may seem large, the total percentage error reduced dramatically over the lengthening period (i.e. max error after one geartooth count ~100% but after 50 counts = 20/1000 ~ 2%).

Linearisation of extension was done by implementing a function within the coding that used the stated extension requirement per day (e.g. 1000microns), the timer count (total time), the total geartooth distance and the geartooth distance from the previous cycle to calculate the required charging rate. A parameter was created within the code (named p_param), defining the number of volts required per micron of extension during charging. This was calculated using data from the previous cycle and controlled the ramp rate which ranged from a minimum of 8 (= 800/8 = 100microns per 800V) to a maximum of 160 = (800/160 = 5microns per 800V).

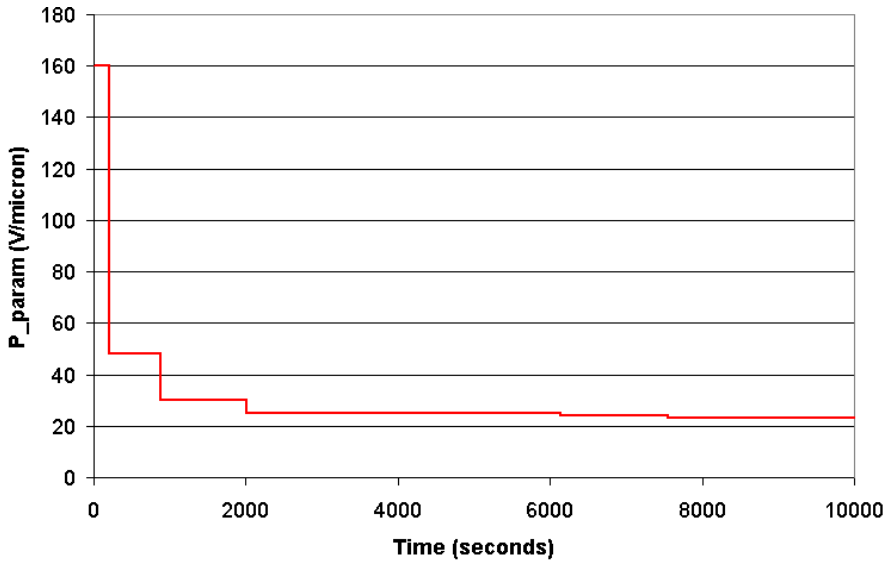

Figure 4-11 P_param changing over first few cycles using damping coefficient to approach smoothly

Any discrepancy between the required geartooth distance and the actual extension resulted in an error. This error value was then used along with a damping coefficient to change the parameter (p_param), allowing the ramp rate to smoothly approach a value that linearised extension (Figure 4-11).

Clinically, the parameter value (p_param) would initially be set to the minimum value i.e. assuming low load. However during testing it was preferable to have faster charging rates (assuming there were no time-dependent loading effects) which could either be controlled by setting a high extension requirement per day or by setting the parameter to maximum, resulting in an initial cycle time of approximately 8mins.

4.6 Capability for smart distraction

As discussed in Chapter 3, load measurement during distraction can be used to provide an indication of the tissue quality. Claes (2007) considers regular monitoring of forces as having the potential to be of "great help when optimising the distraction regime". Another research group (Wee *et al.*, 2008) is involved using the forces found in tissues to control the lengthening and have performed animal studies to examine this theory. Full understanding of the tissue behaviour involved has not yet been achieved but there is certainly promise in this area, especially for the early identification of premature consolidation or non-union.

In order to measure forces during distraction, the initial proof of concept model was fitted with a load cell, screwed into the base of the piezo actuator and seated against the end cap. When the configuration of the device was changed to one main body it was decided that, in order to reduce compliance, an existing component in the load path should be used for strain measurement as opposed to an additional (dedicated) component. The shaft was investigated as a potential option, but lack of space and difficulty in finding a suitable area rendered this solution unsuitable. The yoke piece was then designed such that it acted as a beam in bending and load could be measured using strain gauges positioned top and bottom (Figure 4-12b). Finite element analysis was used to assess different designs of the yoke piece and find the optimum gauge positions i.e. areas of high strain with low strain gradient. This allowed various geometries to be analysed without additional manufacturing and testing. The strain plot (Figure 4-12a) shows potential areas of around 200microstrain but the strain gradient was still reasonable high so small strain gauges of just 1mm length were used (Vishay Instruments) to prevent averaging reducing the strain value.

a)

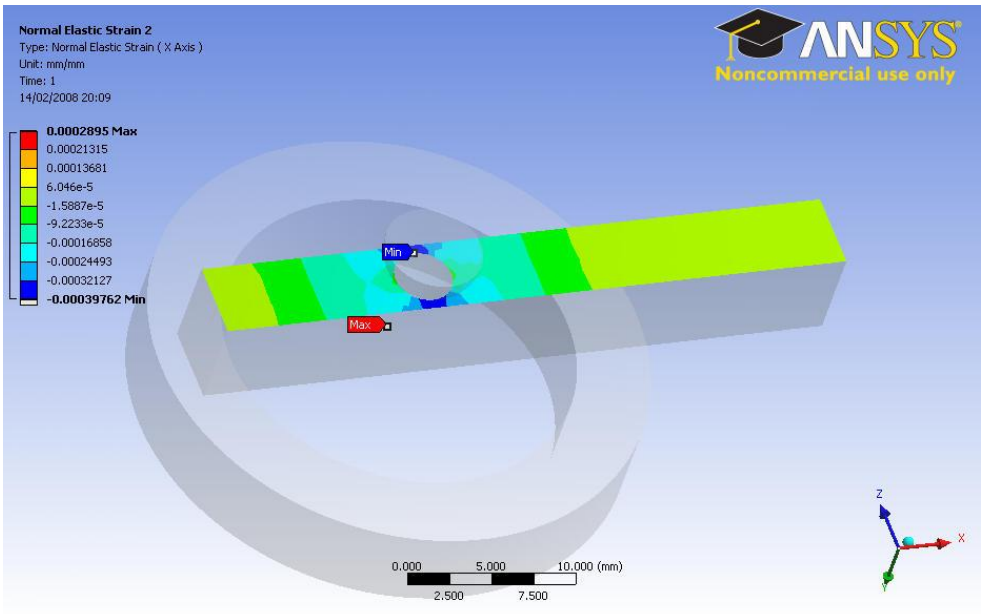

b)

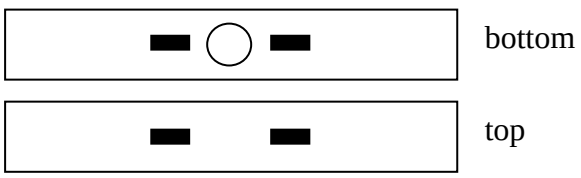

Figure 4-12 a) Finite Element Analysis of yoke b) Final positions of yoke

Rapid changes in load are often a more significant indicator of tissue problems than absolute load. Therefore it was proposed that an accurate measure of absolute load may not be required to detect problems and that an approximate method using only the displacement measurement signal could be possible. This theory is now explained.

The extension of the piezo actuator per cycle reduces with increasing load, thus if the extension is known, the approximate loading through it can be calculated using Figure 4-1 from section 4.2.

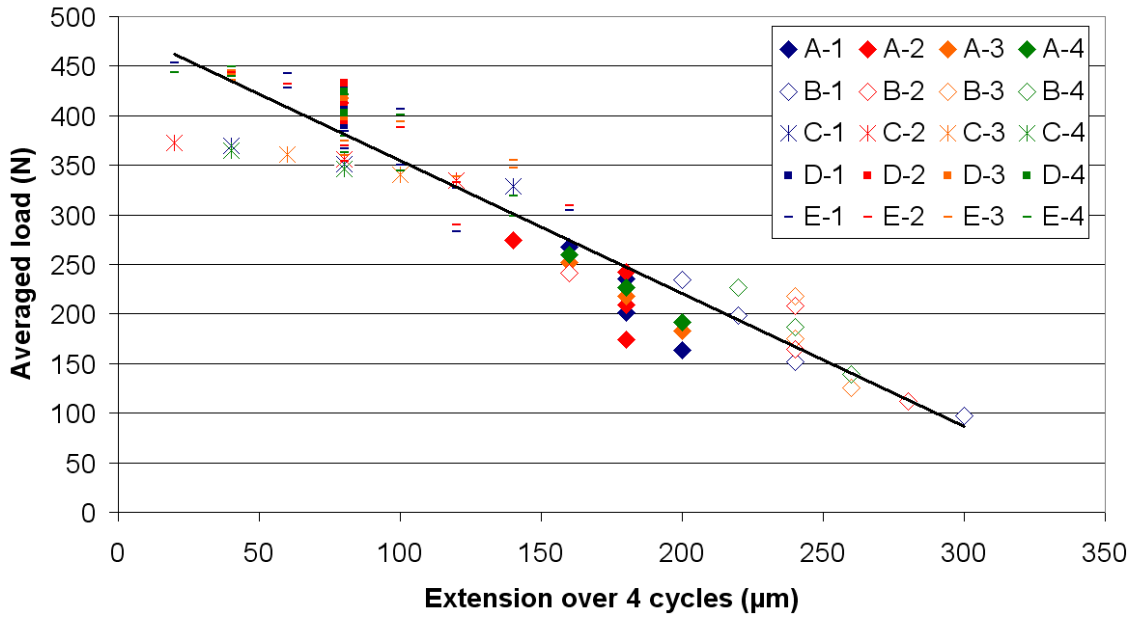

Figure 4-13 Relationship of load to the displacement of the device.

To test this theory, the first analysis involved five typical sets of data (A-E) of around sixteen cycles, covering a range of loads. Each data set was split into subsets with four cycles in each and the total extension per subset (four cycles) was plotted against the average load over those four cycles (Figure 4-13). The total extension was taken over four cycles instead of one to reduce errors from the low resolution of the geartooth signal.

The same data was then split into different subsets of four cycles starting from the second cycle (subset 2, e.g. A-2), then the third cycle (subset 3), then the fourth cycle (subset 4), allowing another three subsets per cycle to be extracted for analysis (as explained in Table 4-1).

	Data Set A			
Cycle number	A1	A2	A3	A4
1				
2				
3				
4				
5				
6				
7				

Table 4-1 Explanation of data sets

The first results were promising, showing a good linear correlation between average load and total extension over each set of four cycles (R^2 value of 0.89). The extension over four cycles became very low at higher loads and the geartooth resolution was dominating. Consequently a different method of splitting the data into subsets was used. Instead of taking 'number of cycles' as the method of division for each subset, a limit of 250microns was selected such that when the extension became greater than 250microns, this became a new subset and the average load was calculated over the distance since the last measurement. (This was not exactly 250microns due overshoot – geartooth can increase 80microns in one cycle).

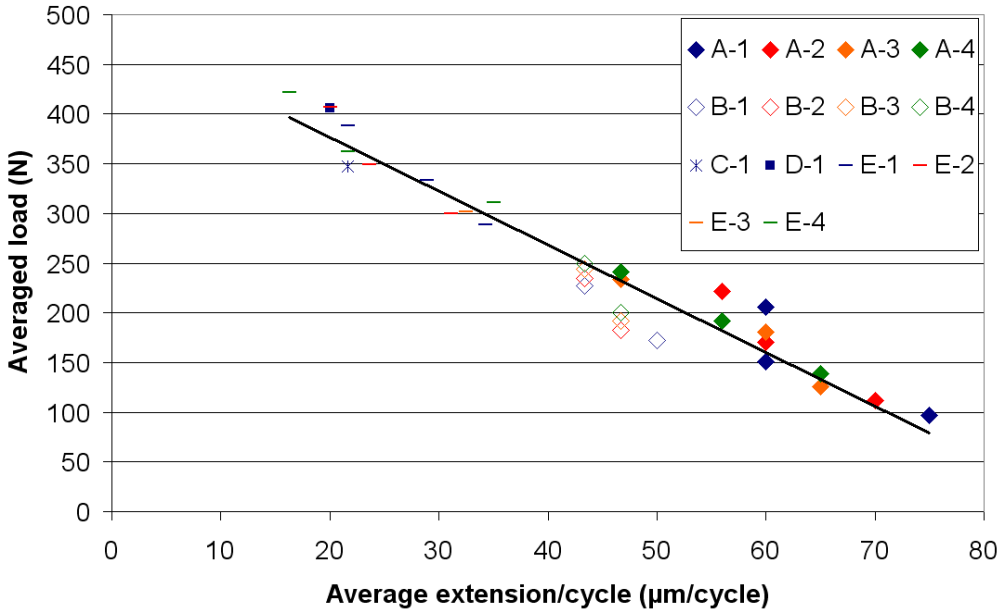

Figure 4-14 Load approximation using displacement measurements. Using the same data from Figure 4-13, this time plotting the average load over each 250micron displacement

From Figure 4-14 it can be seen that the linear correlation was stronger ($R^2 = 0.94$) using this method, although there are fewer data points and the load range is slightly narrower (100-425N).

Using this method, approximate load values are calculated and compared every 250microns i.e. approximately 4 times per day if lengthening at the standard rate. Any significant changes that may correspond to tissue problems would be identified within 12hrs, which is generally less than expected with manual techniques.

Thus, with the load and extensions available to the PIC processor, the stiffness of tissue can be calculated and compared to stiffness values throughout the procedure. Ultimately, these values will be used when the 'smart' nature of the device is utilised. This will involve a decision making algorithm which will specify a change in rate or frequency based on the tissue characteristics or trends. Currently the device simply maintains a linear extension by means of assessing the geartooth signal and adapting the subsequent cycle length accordingly.

4.7 Testing a smart limb lengthening device

Evaluation of a smart automated limb lengthening device not only requires the standard assessment of the mechanical stability/integrity of the device (as described by ASTM

F1541 - Standard specification and test methods for external skeletal fixation devices), but also thorough examination of the means by which the system is controlled.

The piezo actuated device is, as previously described, comprised of a main cylindrical body with sliding threaded shaft, to which the pin clamps are attached. The influence of pin bending is significantly larger than any deflection of the body itself and although examination of these deflections would be included within the submission for regulatory body approval, the focus here is on the non-standard testing of the device during controlled elongation. Smart devices require feedback from the local environment and consequently sensors or measurement systems are involved. The input signals are gathered and processed then a decision making algorithm controls one or more output signals. These decisions are particularly important in the case of this piezo actuated device because the elongation of the device during charging is load dependent. Therefore the monitoring systems are required to ensure that the correct elongation has been achieved and these monitoring systems need thorough assessment. Other complications arise from the dynamic mechanical environment experienced by the device during limb lengthening and, as a result, testing of such devices requires more than simple static loading tests.

In light of these complexities and because testing all possible conditions is difficult and time consuming, the numerical model was developed to allow for the testing of a range of design iterations/permutations and to help identify the limits of device.

Chapter 5

Development of numerical model

5.1 Introduction

European and International regulatory authorities require external manual fixators to be put under a static load testing regime to ensure that they can withstand the forces developed during limb lengthening (ASTM F1541, 2007). For a dynamic electromechanical device with a control system however, the required testing is significantly more extensive (e.g. IEC 60601-4 relating to programmable medical electrical systems).

As an additional resource, validated numerical models of devices allow for faster design of the control systems and evaluation of their limits along with prediction of the expected mechanical device performance under a wide range of changing clinical conditions and extremes of operation.

Given these benefits, a model developed of a smart limb lengthening device can be used for design optimisation, particularly focussed on the reduction of compliances of components and interfaces for better efficiency. Available contact models were analysed and an appropriate model implemented. Additionally, friction modelling was included as the high friction between moving components reduced efficiency. This was not only in terms of losses through heat, but it also greatly affected the degree of tightening of the nuts and, consequently setback in the system during the discharge cycle. The development of both of these models is explained in this Chapter with reference to parameters that allowed for correlation with experimental results.

This device model is part of the full system numerical model which includes the resistive force, i.e. simulation of the tissue, against which the device was evaluated. This is described more fully in Chapters 6, 7 and 9.

5.2 Modelling the device

5.2.1 Numerical representation of device

The device was modelled using a similar numerical method to that of Loverich *et al.* (2007) whose piezo actuator powered device is similar in function but not in purpose to this smart limb lengthening device. Their research focussed on reducing the weight of an actuator that changed the lift of aircraft wings, requiring fast operation against a constant load with motors in continuous operation. This is in contrast with the varying and offset loads that the smart device must function under. Matlab's Simulink was used to develop both the device model and the tissue models, described in Chapter 7, ensuring compatibility and allowing for analysis of the system as a whole. Firstly the component parts of the device were represented in two dimensions with positional constraints, then as free body diagrams to allow characteristic equations of motion to be written. These were then constructed as Simulink models with inputs (e.g. force) and outputs (e.g. displacements). Figure 5-1 shows the first basic model with 6 components and the component equations can be found in Appendix C(i).

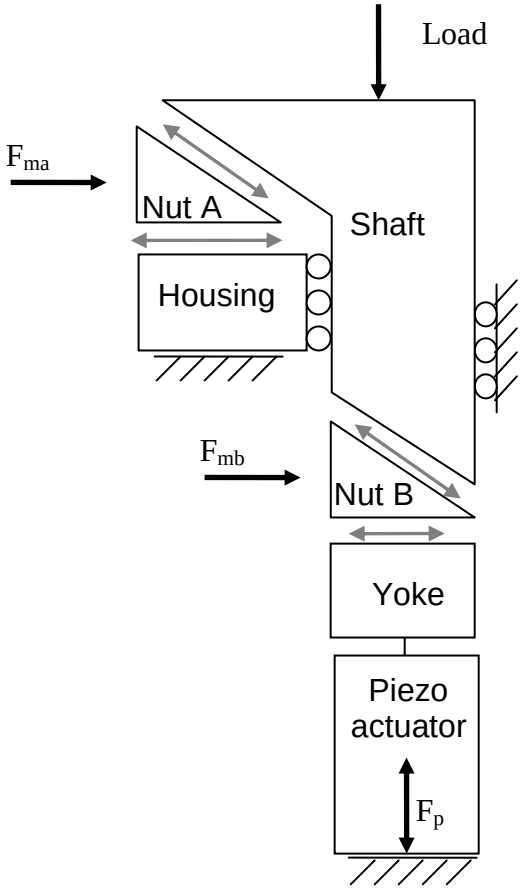

Figure 5-1 Basic device model with positional constraints

The nuts were represented by wedges for the purposes of the 2-D model; the wedge angle related to the thread pitch and circumference which were 1mm and 24mm diameter respectively, resulting in a wedge angle of 0.76degrees. Contact and friction models describe the relationship between components.

5.2.2 Contact Modelling

The first contact stiffness models were developed by Hertz in 1881 (Hertz, 1896). Contact stiffness was found to depend on the surface profile, specifically the height and distribution of asperities. In their well regarded theories, Greenwood and Williamson (1966) and Onions and Archard (1973) suggested that elastic contact can describe well the contact of the opposing asperities (assumptions include spherical tipped asperities, linearly elastic surfaces, zero traction stress between the asperities and small contact deformations compared to the asperity radius).

In order to successfully calculate the contact stiffness there are constants that must be known, such as the average radius of asperities and distribution of asperities, which are difficult to ascertain. Conveniently, one of these models (Greenwood and Williamson, 1966) can be greatly simplified into a lumped parameter model with just one parameter, K_c allowing for correlation with experimental results which, in this case, was far more important than the theoretical contact stiffness. The force then becomes:

$$F(\delta) = K_c * \delta^{5/2}$$

Loverich *et al. (*2007) simplified this further to a two stiffness model for use in their actuator simulation, taking two critical force points in the cycle and ensuring that these fell on the continuous curve, with linear stiffness between. They argue this had the benefit of reducing the complexity of governing equations without significantly reducing accuracy.

To quantify the error introduced in this linear approach if applied in this device model, a small study was conducted which compared the displacement output of the linear models with the continuous model. A subset of the full device was selected which included the shaft, one nut and the nut thrust surface (Figure 5-2).

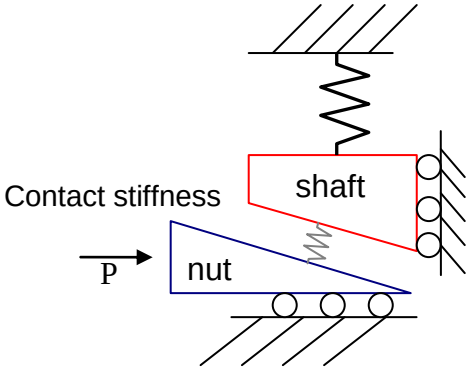

Figure 5-2 Subset of the full device model used for analysis of contact models

Because the compressive load varied for the device model, one fixed point was taken as the maximum load (500N) and the other was adjusted so that there was a minimum discrepancy between the two models (Figure 5-3).

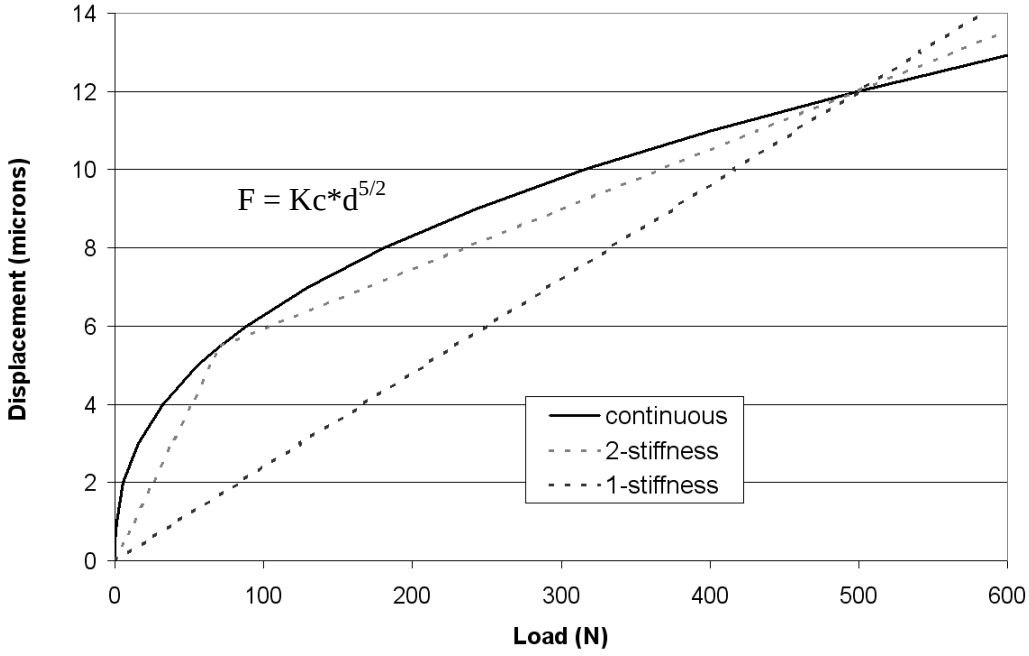

Figure 5-3 Difference in nut and shaft displacement using three contact stiffness models

The difference in vertical displacement between nut and shaft under the range of loads was plotted for each of the models. The maximum percentage difference between the continuous model and the linear stiffness models was approximately 20% for the two stiffness model or 200% for the single stiffness model across the clinically relevant range (50-500N). This error at each contact point would result in a maximum cumulative error of 6microns per cycle (at loads of 50N or 250N) which was deemed unacceptable. It was

concluded that the model must match over the full load range (0-500N) and as limited additional computational capacity was required the continuous model was chosen for use in further analysis.

Contact surfaces could not be assumed to be aligned as would be the case for the theoretical model. Thus, in order to ensure that the contact model represented the specific case, it was decided to make the contact model a two parameter model. The value for 'g' was determined through experimental means, i.e.

$$F(\delta) = K_c * \delta^g \qquad \text{where } g > 1$$

During charging the load path - piezo actuator>yoke>nut>shaft - was simplified from three to two contact regions as the yoke stiffness could be incorporated into the compliances for the nut component (Chapter 4). Similarly, the contact regions were reduced in the discharge loadpath - shaft>nut>housing>ground – by representing the housing component as an additional compliance at the interface of the holding nut and 'ground'. For simplicity all interfaces were initially assumed to have the same value of stiffness ($K_{c1}=K_{c2}=K_{c3}=K_{c4}$) but the contact models could easily include individual component strain or deflection (as an additional spring in series) and thus each model stiffness (K_{cn}) was later adjusted to match the specific interface. Appropriate damping values were chosen alongside the stiffness values to reduce instabilities in the system.

A Simulink subsystem block was developed for each interface that calculated the normal force from displacements and velocities of the bodies (see Appendix C(ii))

5.2.3 Friction modelling

The tangential force opposing motion between two contacting surfaces is commonly called the friction force and can reduce the efficiency of mechanical systems. Friction models are often specific to the surface conditions of the contacting components, which for the device were dry sliding contact at low speeds (<0.05m/s) with no lubrication. The Coulomb friction model is one of the most commonly used models and defines the force as being dependent on the normal reaction force (F_n), the coefficient of friction (u), and the sign of the slide velocity (v) (Figure 5-4a).

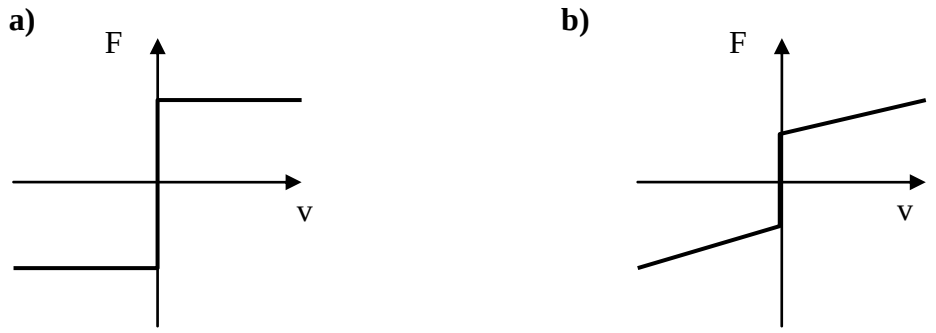

Figure 5-4 a) Coulomb friction model b) Coulomb-viscous friction model

The simplest model to include velocity dependent friction is the viscous model where Friction = F_v*v and is often combined with the Coulomb model as shown in Figure 5-4b. These are often termed Classic models, where the force is either constant or linear in relation to velocity. Some authors proposed that the frictional force was not linearly related to velocity (Stribeck, 1902, referenced in Jacobson, 2003). Originally, Morin (1833) suggested that the friction force at rest can be higher than the dynamic friction level. Thus, the excitation force must exceed this static friction force (or 'stiction') before sliding occurs and velocity increases, where dynamic friction force is in opposition. These friction models can be described more generally using the following form:

$$F = \begin{cases} F(v) & \text{if } v \text{ not equal to } 0 \\ F_e & \text{if } v = 0 \text{ and } |Fe| < Fs \\ F_s sgn(v) & \text{otherwise} \end{cases}$$ (Olsson *et al.*,1998)

where F(v) can be a non-linear function.

Non-linear dynamic friction force, F(v) was modelled by Stribeck who suggested a gradual reduction in force from static friction to dynamic friction as the velocity increases (Figure 5-5a).

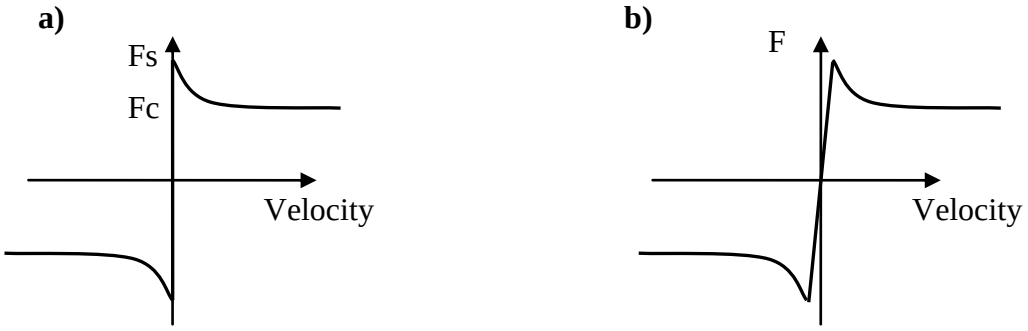

Figure 5-5 a) Stribeck friction model b) Stribeck-Dahl friction model

Using the Classic models, at zero velocity the force can be positive, negative or zero. Dahl (1968) suggested that there is a small degree of elastic resistance to displacement at low input loads that must be overcome before permanent dislocation occurs. This is often called pre-sliding stiffness (or microslip) and gives rise to the increased force before release. This increase in force at very low velocities has been modelled using elastic bristles to represent the asperities which must deform before sliding occurs (Haessig and Friedland, 1990). The device mechanism involves regular transition from zero to non-zero velocity of sliding surfaces and it follows that the model should be able to describe this transition well. Although the Dahl model was the first to account for pre-sliding behaviour, using their model the friction is not velocity dependent (instead is displacement dependent) and does not account for the high static forces seen before sliding takes place. The Stribeck effect was incorporated into the Dahl model by Canudas de Wit *et al.* (1995) which results in a function similar to Figure 5-5b. A variation of the Dahl-Stribeck model was developed by Gaul and Nitsche (2000) for use in their piezoelectric semi-active joint model that includes bristle stiffness and static and dynamic coefficients of friction as independent variables.

In order to determine the most practical model for use in the current simulation, a comparative study was performed using the simple Coulomb friction model, a combined Coulomb and viscous model, a version of the Dahl-Stribeck model and the Gaul model. The same subsection of the device was modelled as used for the contact model analysis, using the nut, shaft and nut thrust surface, with frictional forces present at both contacts (Figure 5-6).

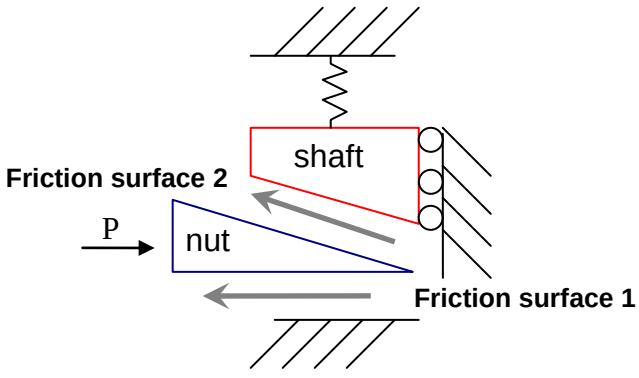

Figure 5-6 Subset of the full device model used for analysis of contact models

Following the application of force P, the final shaft displacement values were within 0.6% for all four models although profiles varied (Figure 5-7). The Coulomb model became

unstable at around 9secs because the slide velocity dropped to zero resulting in a friction coefficient that could be positive, negative or zero. The Gaul model closely followed the Coulomb model but maintained stability. Both the Coulomb-viscous model and the Stribeck model suggested a more damped system i.e. when the force became constant the shaft tended more gradually towards its final displacement. These damping factors can be determined using experimental data.

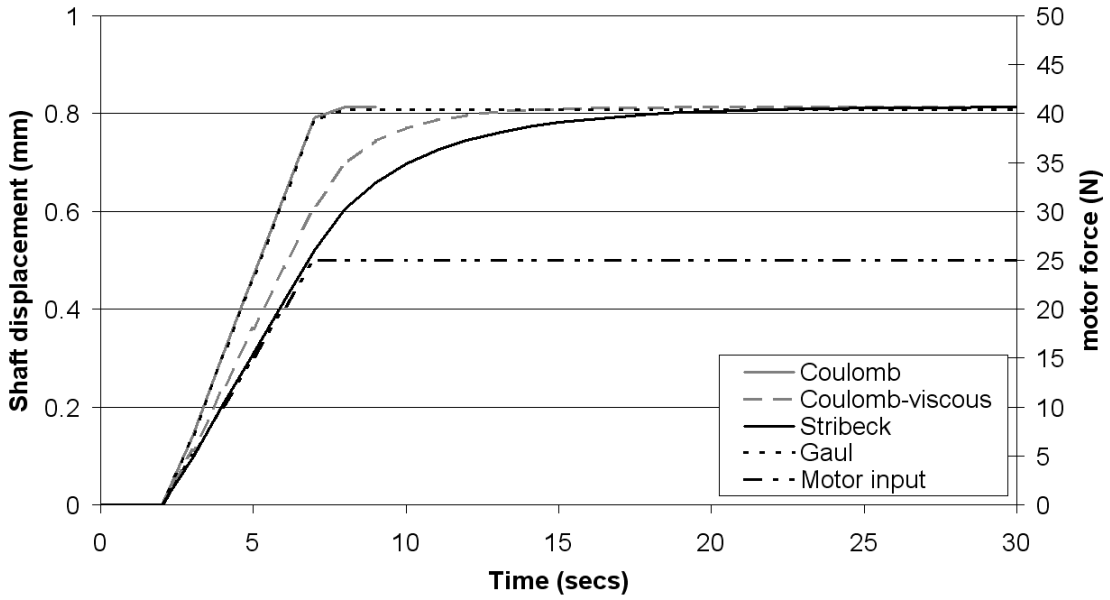

Figure 5-7 Comparison of friction models

In order to select the most appropriate model, experimental characteristics of the device function were analysed. During testing, frictional forces opposed nut rotation while the motors were driven and also prevented backwards rotation of the nuts when the device was under a static load (without friction, any compressive load would have caused the nuts to rotate anti-clockwise and thus displace the shaft backwards). In the case of the Coulomb and Coulomb-viscous models, any force imbalance caused a sliding velocity and consequently the nut rotated backwards. This proved these models were unsuitable for implementation in the device simulation without additional restrictions. Conversely the Stribeck and Gaul models did prohibit large movement with static loads and in order to fully investigate the two they were both implemented into the full scale model. It then became apparent that the simulation speed improved using the Gaul model due to the computational efficiency over the discontinuous nature of the employed Stribeck model. Some differences were seen between the outputs, such as the displacement pattern at

transitions, but these were at levels that were not large enough to influence the shaft output (horizontal nut movement of 1micron) though were kept in mind for any future model adaptations.

During experimental analysis it was noted that at low loads (<20N) the motor torque could rotate the nuts freely and drive the shaft forward. This feature of the motors was useful in the selection of parameters for the friction model by identifying the maximum load at which the motors were able to drive the shaft via the nuts. Experimentally this was dealt with by putting a 2second limit on the run-time of the motors during the start up and reset sequence. It is proposed that in future designs there be some identification of this error using current levels in order to reduce the driving time or eliminate completely.

5.2.4 Simulating the control system

The phases of each cycle have been described in Chapter 4, with detailed description of the motion of the component during each stage. Activation of these different phases was controlled by the PIC processor. Essentially, the holding nut motor was activated when the piezo actuator voltage ramp count reached 800 (which did not necessarily relate to 800V as a PI controller was attempting to match the measured voltage to the required ramp value). The piezo actuator voltage was maintained at this value until the motor had stopped, which was identified by a peak in the current i.e. the motor had stalled. The discharge cycle then began. When the actuator voltage ramp dropped below 20V the driving nut motor was activated until stall condition, whereupon the charge cycle began again. These phases were included in the model using Simulink switches and the output for extension against a 400N static load is shown in Figure 5-8.

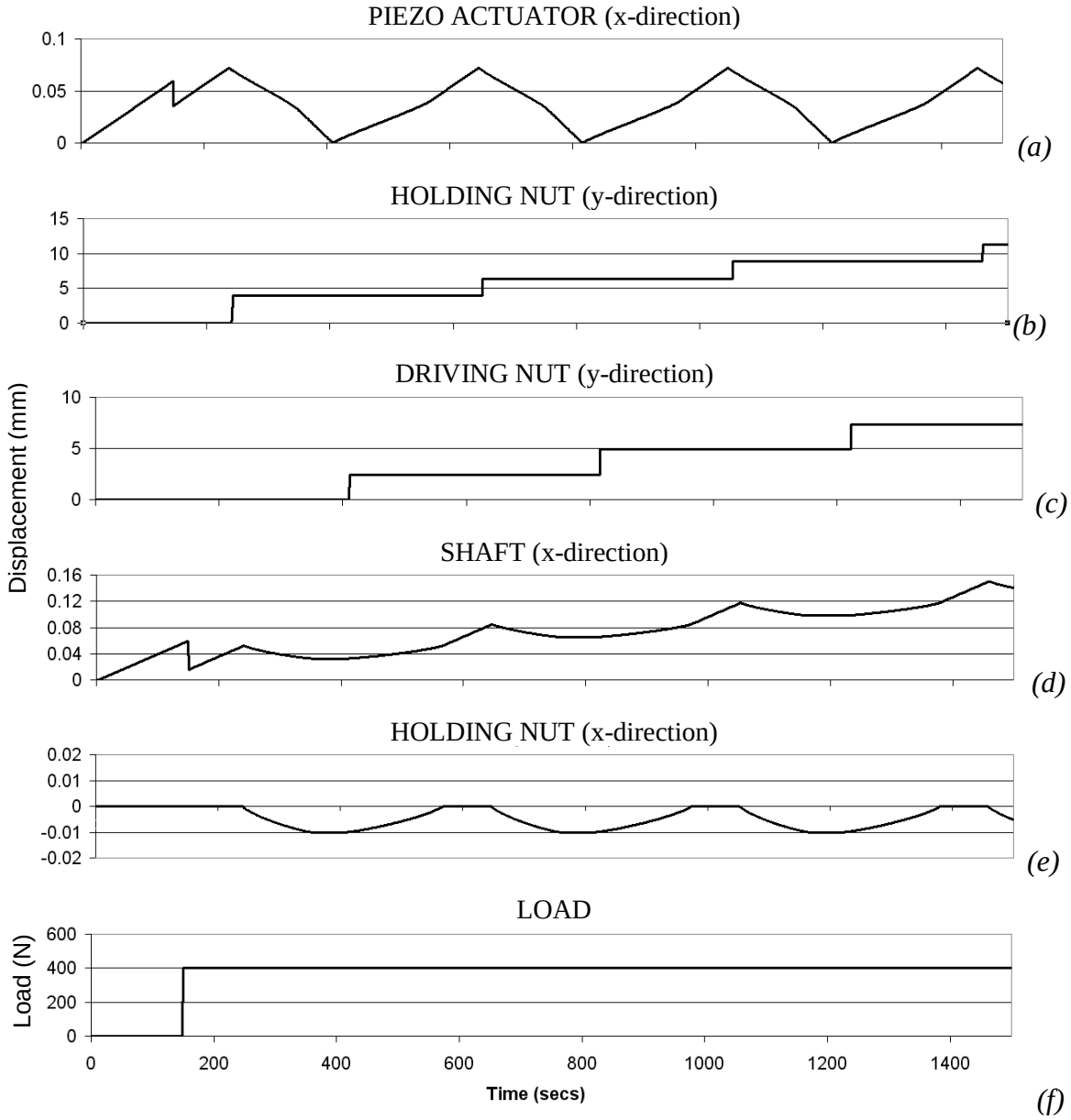

Figure 5-8 Displacement of components during extension against a 400N static load applied during the first cycle

The increase in length of the piezo actuator was represented as a displacement. The movement of the nuts was primarily in the y-direction due to the wedge mechanics explained in section 5.2.1. Static load was applied while the device was running (as opposed to prior to extension), avoiding negative displacements of the piezo actuator and shaft. Each cycle contained four phases:

1. Piezo actuator charge - Increase in the displacement of the piezo (a), yoke, driving nut and shaft (d).

2. Holding nut rotates - Y-direction displacement (b), impact and torquing of the holding nut = potential for small x-direction displacement of the piezo actuator (a), yoke and shaft (d), change in the normal forces.
3. Piezo actuator discharge – Decrease in displacement of the piezo actuator (a) and yoke but shaft displacement remains fairly constant other than small setback.
4. Driving nut rotates – Fast y-direction displacement (c), small x-direction displacement of the piezo, yoke and shaft due to impact and torquing of the holding nut resulting in change in the normal force.

5.3 Detailed design parameters

The model outputs have been shown to represent the function of the device. This includes dynamic components and their interactions. In order to validate the model, quantitative comparisons of component displacements were required. To do this, parameters for modification after analysis of experimental results were specified as:

- Contact stiffnesses (k_{c1}- k_{c4}) and the associated damping coefficients (c_{c1}- c_{c4})
- Contact parameter ‘g’
- Friction model parameters (Gaul parameters include bristle stiffness, static and dynamic coefficients of friction, damping factors)

Additional external input signals that were variable included motor torque and the ramp rate of piezo actuator voltage or voltage profile i.e. linear, step change. Values for these parameters were modified in the following Chapters to achieve numerical model validation.

Chapter 6

Axial testing and initial validation

6.1 Introduction

Final design of the numerical model was achieved by selecting values for the contact model parameters (described in Chapter 5) that provided the closest correlation of simulation outputs to experimental testing results. This was done using a simple static loading condition. Thereafter validation of the numerical model began by comparing predicted results to experimental test results when the device was extended against an elastic load.

The experimental testing technique is described in this Chapter, focussing on methods for extracting the data required for validation.

6.2 Static load test method

Experimental testing of the device was used to define the:

1. extension per cycle under different static loads
2. degree of setback during actuator discharge under different static loads
3. variation between different tests at the same load
4. sources of loss in efficiency i.e. attributable to specific or series of components or interfaces

Static load testing through the axis of the device was used to negate any friction or additional compliance effects from offset loading. The data collected during testing and used for analysis was primarily:

external LVDT signal – Linear Variable Differential Transformer

measured the total extension of the device, (microns)

microDVRT on yoke – Differential Variable Reluctance Transducer
measured the extension per cycle of the device, (microns)

geartooth signal - internal diodes to count rotating gearteeth
measured the total extension of the device
(microns, in 20micron intervals)

actuator voltage - feedback into the PIC processor for control of charging and discharging, (volts)

All signals except the LVDT were used as inputs to the processor and could be used for control purposes. A high stiffness test rig was designed using two steel rods with plates between which the device was positioned. One plate was fixed using nuts on the threaded section while the other plate was allowed to slide using linear bearings for low friction movement.

Loads up to 430N were used to represent the clinical range seen during the limb lengthening process. Static loads were applied by hanging weights from either side of a length of angled steel section attached to the top (sliding) plate ().

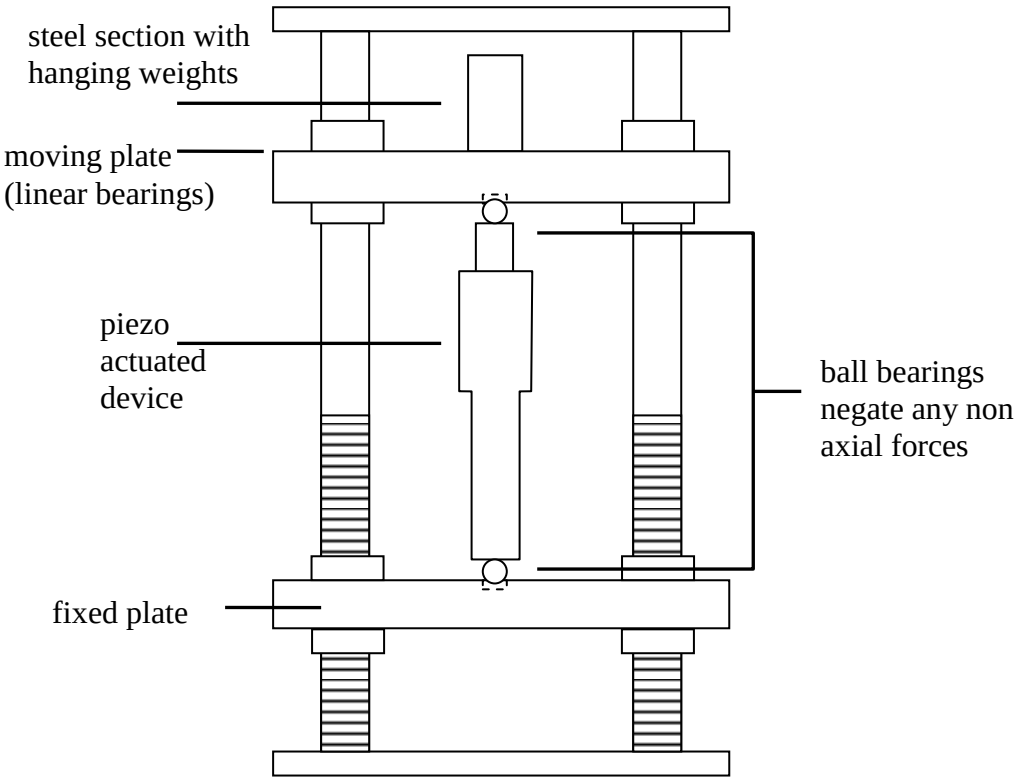

Figure 6-1 a) Schematic of test rig for static loading

Figure 6.1 b) Image of device in test rig for static loading

The LVDT was attached to the moving plate and measured the total extension of the device. In the static load case, shaft movement = plate movement. This could not necessarily be assumed for any testing where the load was increasing (due to compliances resulting from ball bearing interfaces etc.) but a reasonable assumption made was that differences were insignificant compared to device movement.

Initially four different loads were applied. The total load included the weight of the moving plate and linear bearings. The maximum time per cycle was reduced to save total test time (~6min per cycle) which could only be done where the test material had no time-dependent loading effects. Each test was repeated to give two data sets per load.

In order to analyse the variation in extension of the device under constant load, one central load (200N) was applied and repeated five times. However, after some preliminary testing, it became clear that the variation over a number of cycles was dependent on load value so this was changed to two points towards the extremes of loading, 80N and 430N.

6.3 Results

6.3.1 Experimental

The geartooth signal after each cycle across the range of static loads is plotted in Figure 6-2. Linear regression analysis based on the least squares method shows the high degree of linearity within each series as expected under static loading (minimum $R^2 = 0.96$).

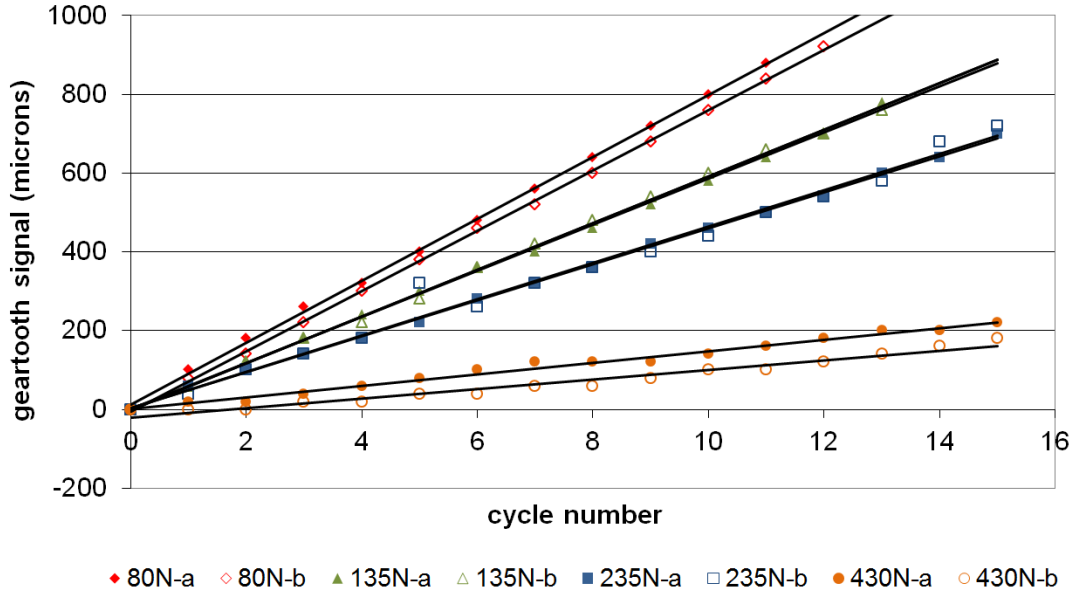

Figure 6-2 Device extension under varying static loads with trendlines for each test

Tests were highly repeatable for all loads except the 430N where there was a 16% reduction in the average extension per cycle between test a and test b. This data was then used to plot the average increase in geartooth signal per cycle across the range of loads (Figure 6-3). The trendline was forced through the 96micron extension of the device under no load. An offset exponential relationship was established with a high R^2 value of 0.99.

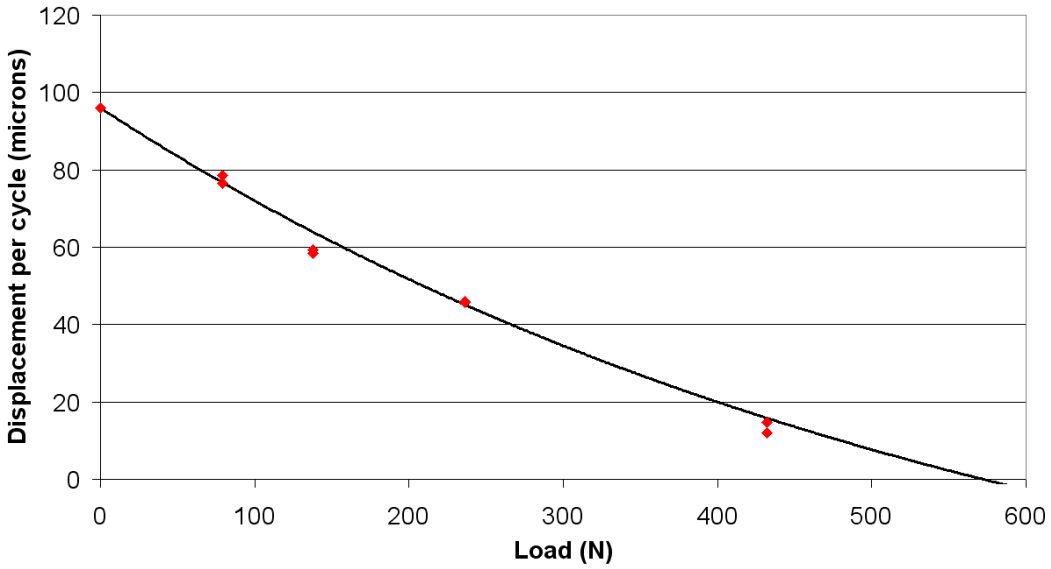

Figure 6-3 Displacement per cycle across range of static loads with trendline

To evaluate the variation between tests at extremes of static loading (80N and 430N), the device was tested to 10 cycles under the same static load 5 separate times, being fully unloaded and reset after each test. Figure 6-4 shows the average geartooth signal after each cycle over all 5 tests and the measured extremes of signal at each cycle. Variation in the 80N testing was low with a maximum difference of 60microns = 8% after 10 cycles. Although for the 430N test there was larger variation between elongations at each cycle (100microns = 125%), within each test the increase per cycle was reasonably linear (minimum R^2 = 0.91).

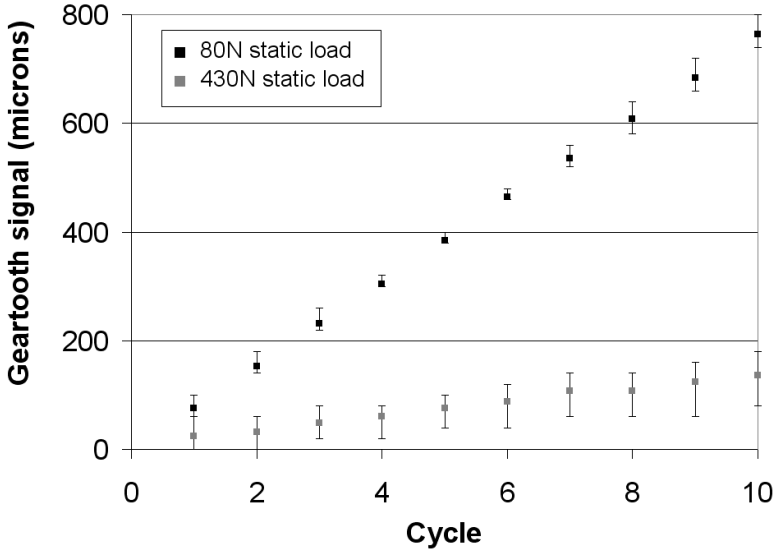

Figure 6-4 Variation analysis at 80N and 430N static load

It was established that this variation was attributable to losses incurred during tightening of the nuts as explained below (6.3.2).

6.3.2 Identifying sources of variation and loss

To identify the reason for variation at this high load, the displacements of some individual components were analysed and losses quantified. This was done by comparing the total device extension (measured by the external LVDT) to the yoke displacement (measured by the internal DVRT). The DVRT signal was a cumulative signal that summed the displacement of the yoke during each charging period. Therefore, this signal was indicative of what the extension would have been if there was no setback during the discharge periods.

One series of load data, at 80N static load, showed that at this low load all three signals (LVDT, DVRT, geartooth counter) correlated very well, taking into account the 20micron resolution of the geartooth signal. This was compared to the data during extension with a 430N static load (Figure 6-5). At high static loads the displacement signals diverged immediately. The DVRT signal was used to quantify losses between the yoke and the shaft during charging while the LVDT signal was used for setback quantification during discharging of the actuator.

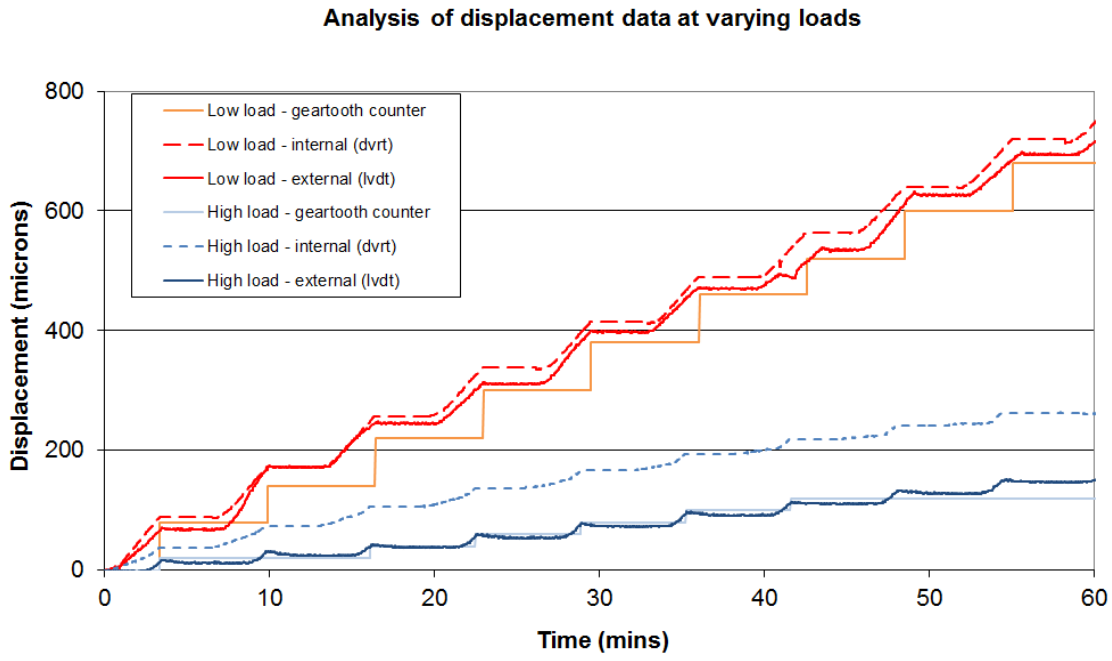

Figure 6-5 Displacement measurements at low (80N) and high (480N) static loads.

Losses during charging

The theoretical piezo actuator extension at both loads was calculated:

$F = (-K_p * \Delta L_{50N}) + F_b$ $\quad$ $F = (-K_p * \Delta L_{400N}) + F_b$

$80 = -16.667* \Delta L_{50N} + 1600$ $\quad$ $430 = -16.667* \Delta L_{400N} + 1600$

$\Delta L_{80N} = 91$microns $\quad$ $\Delta L_{400N} = 70$microns

Average shaft displacement measured during charging (LVDT):

80N load = 78.4microns, s.d. 15.1microns (16 % loss compared to theoretical)

430N = 23.microns, s.d. 2.6microns (68% loss compared to theoretical)

The average DVRT signal (measuring yoke displacement) over 8 cycles was used to quantify the loss occurring between the yoke and shaft, involving the yoke-nut interface, the nut-shaft interface and the compliances of both the yoke and shaft components.

At 80N:	Loss	= DVRT – LVDT	At 430N :	Loss	= DVRT – LVDT
		= 79-78microns			= 28-23microns
		= 1% (negligible)			= 18%

This indicated that the sources of the remaining loss of actuation (70-5microns = 67microns) at 400N were:

- piezo actuator and the yoke interface
- piezo actuator and housing interface
- component compliance

One component likely to have had a significant contributory compliance was the yoke. Finite Element Analysis suggested that between 5-10microns was lost from bending of the yoke under a load of 400N depending on the boundary conditions used.

Losses during discharging

During an additional 430N test, the setback during discharge was so large that the average extension per cycle was reduced to around 2N (Figure 6-6).

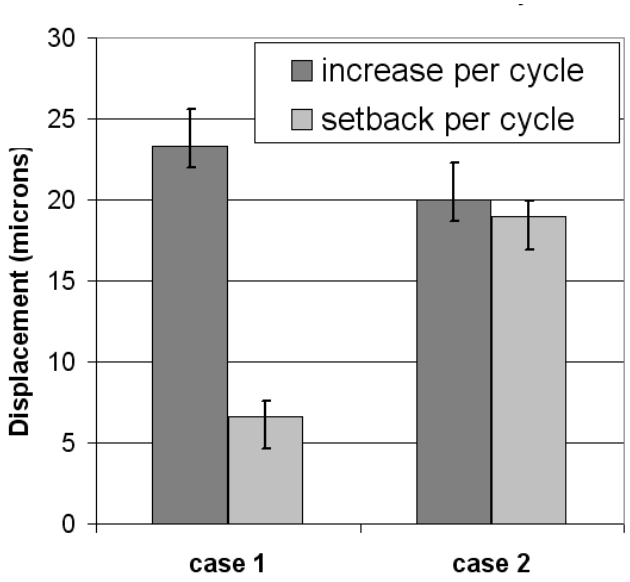

Figure 6-6 Variation in setback between tests at the same load (430N)

The variation was found to be cyclic (over 1mm of extension = thread pitch) and thus the main contributor thought to be the alignment of the faces during tightening of the nuts. Misalignment of the face resulted in one edge of the nut making contact with the thrust surface, as discussed in Chapter 5, effectively changing the contact stiffness value. This affected the interface between the holding nut and thrust surface and thus the degree of setback during discharging.

6.3.3 Refinement of numerical simulation

These findings were used to refine the simulation i.e. by changing the contact stiffness values K_{c1}-K_{c4} and the value of stiffness profile 'g', the results can be matched to experimental data.

The values of K_{c1} and K_{c2} determine the displacement of the shaft during the charging of the piezo actuator. The values of K_{c3} and K_{c4} determine the degree of setback while the actuator is discharging. Parameter 'g' was used in the model development to give a non-linear contact profile as proposed by many authors (see 5.2.2) and the experimental results (Figure 6-3) confirmed that this was the case.

A value of 1.3 for 'g' was found to best fit (R^2 = 0.99) the static load results along with stiffness values of:

$K_{c1} = K_{c2} = 6.5$

$K_{c3} = K_{c4} = 100$

allowing the simulated results to follow the experimental trendline (Figure 6-7).

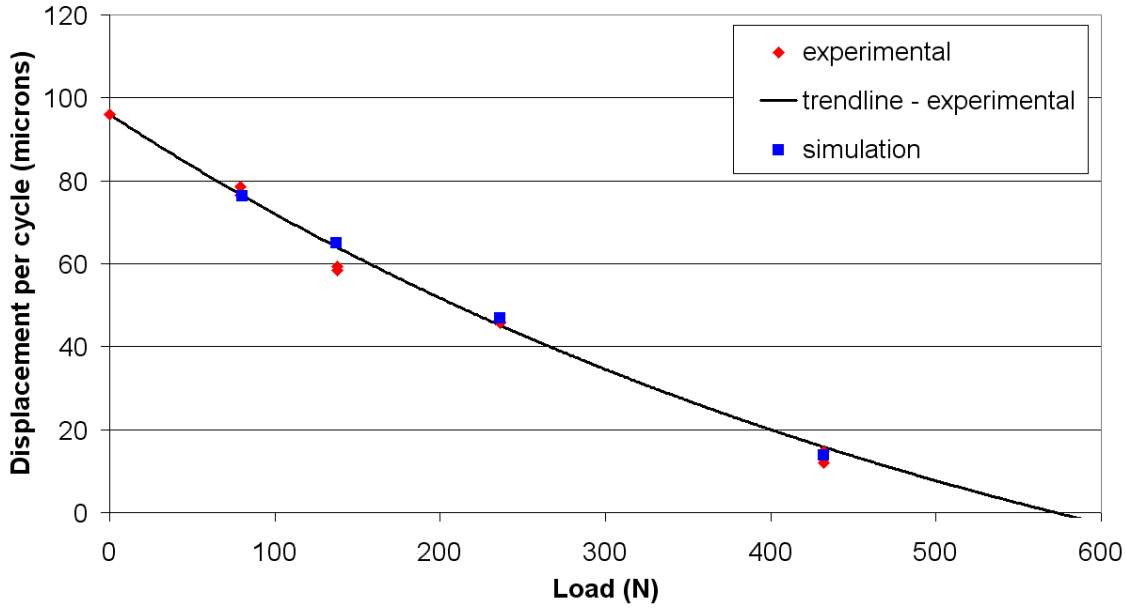

Figure 6-7 Simulation variables adjusted to match to experimental results.

Displacements of the nut and shaft were compared to experimental values throughout the cycle. Comparisons were first made at a static load of 430N.

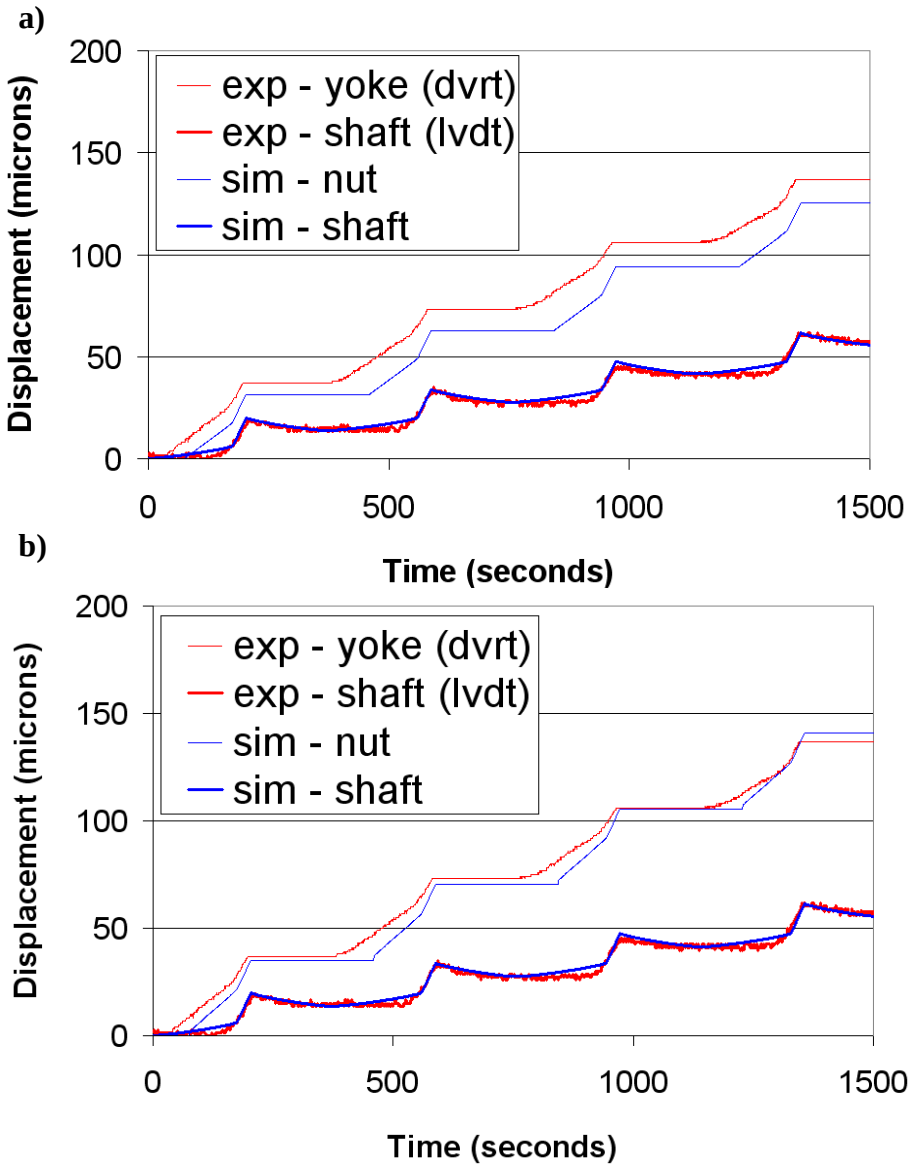

Figure 6-8 Profiles during extension for a) $k_{c1}=k_{c2}=6.5$ and b) $k_{c1}=8$, $k_{c2}=5.4$

Both output profiles from the model for shaft movement and nut movement were similar to experimental findings although the predicted vertical movement of the nut was lower than measured experimental by around 17% per cycle (Figure 6-8a). Until this point, the contact stiffnesses K_{c1} and K_{c2} (actuator-yoke-nut and nut-shaft respectively) were identical. However, this direct comparison indicated that the value of K_{c1} should be lower than the value of K_{c2}, so that the vertical nut movement was reduced while maintaining the relative shaft movement (Figure 6-8b). New stiffness values were:

$K_{c1} = 8$, $K_{c2} = 5.4$, $K_{c3} = 100$, $K_{c4} = 100$.

Comparison was also made at the low load and proved that the values were acceptable across the load range (Figure 6-9).

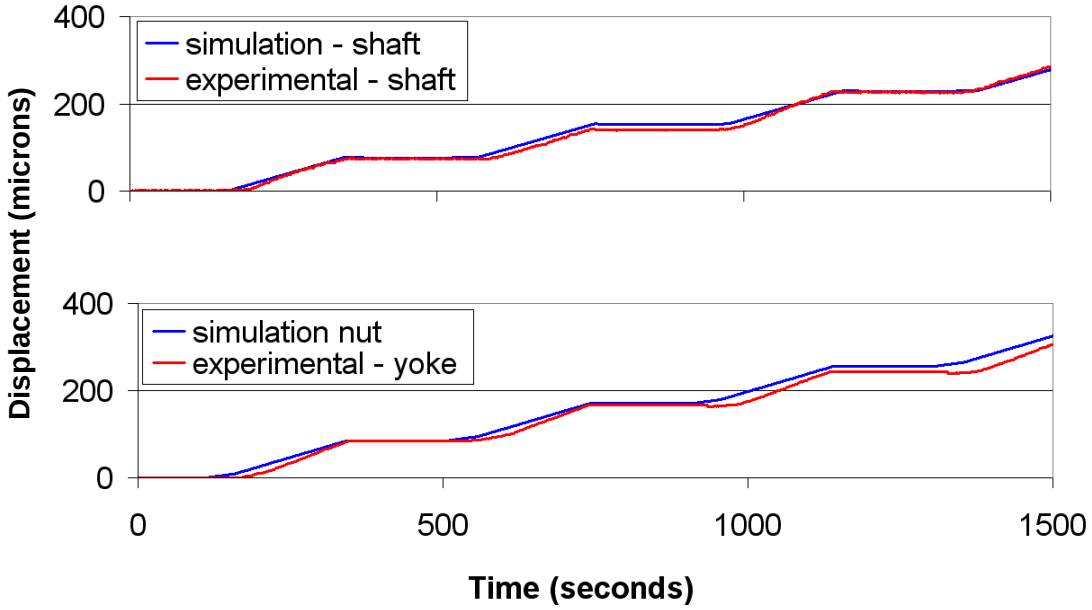

Figure 6-9 Low load validation of profile matching

The variation in the experimental results was not mirrored in the simulation. Under static loads the extension per cycle remained the same as the simulation progressed and the device extended. This changed under elastic loads where the extension per cycle reduced as the device extended as modelled in 6.4.1.

6.4 Initial validation of device model

6.4.1 Elastic load test method

The first validation of the model using these new values was performed by extending the device against specialised springs with ratings in the range of tissue elasticity (k= 5-350N/mm). To ensure that the motors did not drive the threaded shaft at the low loads, a static load was also applied during the elastic tests, selected to be in the midrange (220N). The spring was positioned between the moving plate and top plate of the rig, along with a load cell to measure additional load from compression of the spring as the plate was displaced (

Figure 6-10). A small preload (around 50N, depending on the spring stiffness) was used to ensure the spring was aligned such that the flat end of the spring was flush with the

plate, reducing 'settling' effects. Variation analysis was performed on this loading system using the 200N/mm spring.

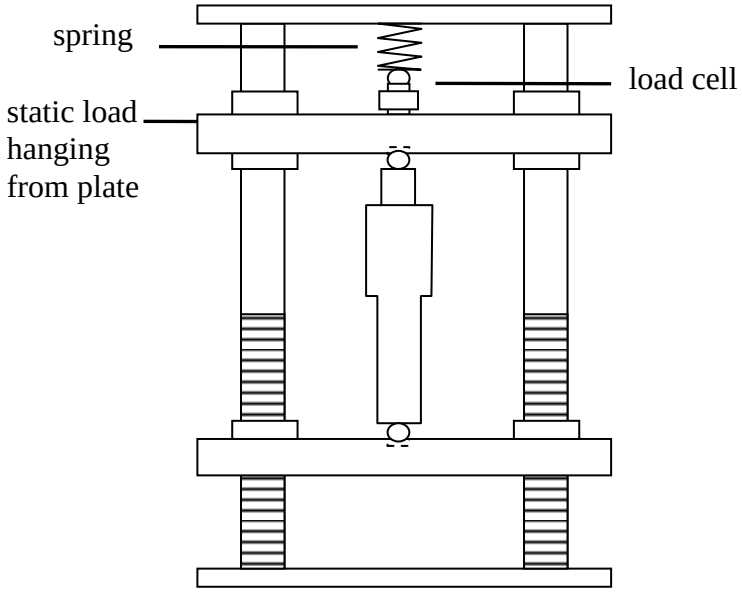

Figure 6-10 Axial test rig for spring loading.

6.4.2 Comparison between predicted and experimental outputs

As the device extended, compression of the springs resulted in an increased load through the device. Thus as time progressed, the displacement per cycle was expected to reduce with the curvature of the line (number of cycles to blocking load) relating to the spring rating. For a mid-range rating of spring (167N/mm) over 18cycles this was predicted to within 9% by the simulation, inside the variation levels expected at this load (Figure 6-11). Additionally the 20micron resolution of the geartooth signal accounted for some discrepancy.

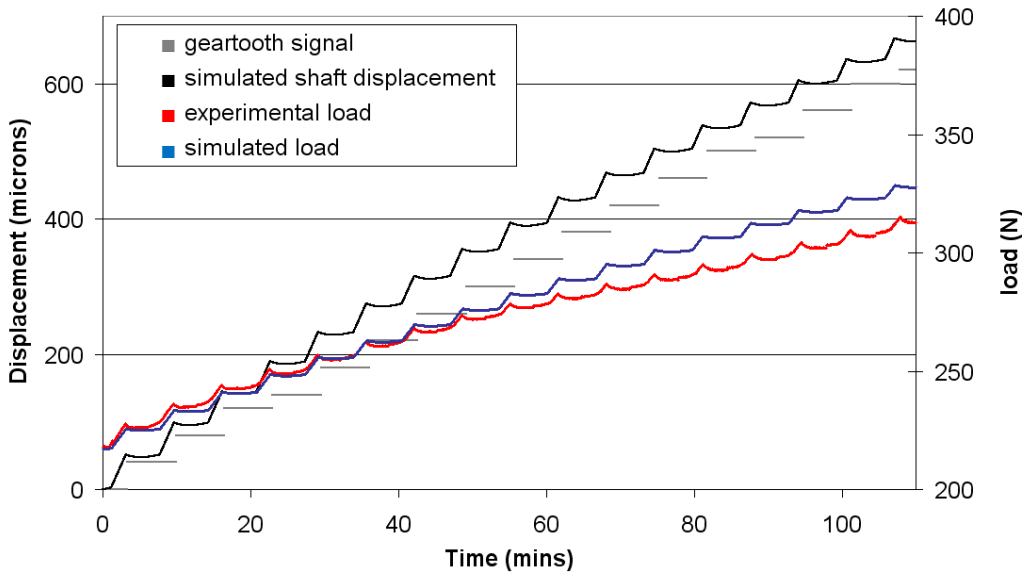

Figure 6-11 Spring load testing using a 167N/mm spring starting at 215N preload

To ensure that the simulation could predict across the clinical range of tissue stiffnesses, four spring stiffnesses were used for evaluation. A central load range was selected (220-250N) and the distance extended to cover this range was measured when distracting against each of the spring stiffness. The results, shown along with the results from the simulation, suggest that the simulation could accurately predict the device progress under a range of spring stiffnesses (Figure 6-12).

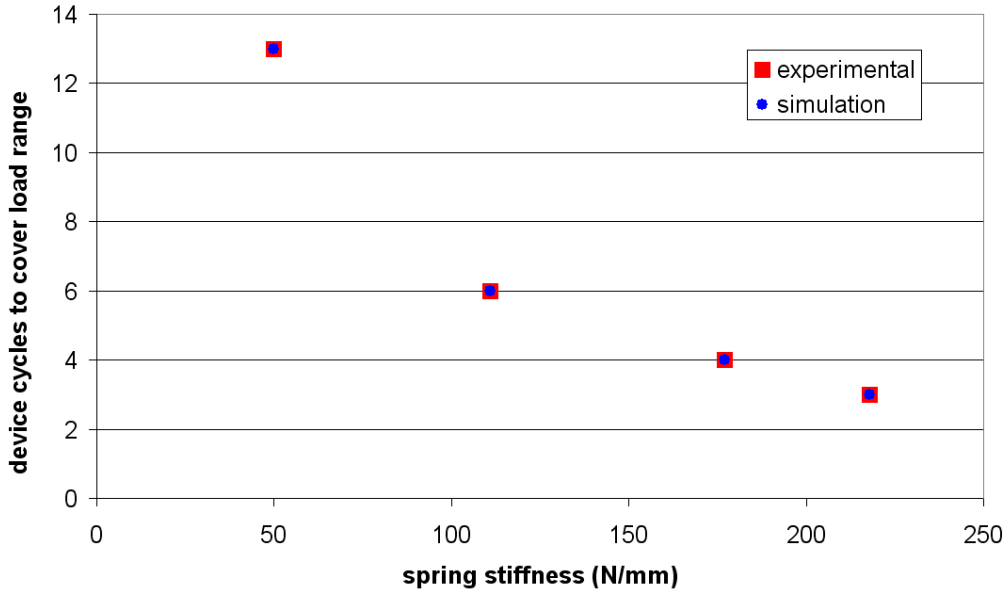

Figure 6-12 Device cycles to cover load range for a variety of spring stiffnesses

6.5 Summary

The numerical model developed could closely predict the extension of the automated lengthening device over a range of static loads from 80-430N. The first stage in the validation procedure used elastic loading and the model was found to predict well within the limits of variability found in experimental testing.

Chapter 7

Modelling of time-dependent materials

7.1 Introduction

Initial validation of the numerical model was performed using linear elastic springs to mimic the tissue resistance to extension, but literature suggests that the time-dependent characteristics of the tissues strongly influence the reaction forces experienced by extension devices during limb lengthening (Chapter 3). It follows that lengthening apparatus, particularly automated devices, should be tested in this dynamic, non-linear environment, and the control system must be designed using expected tissue behaviours. This Chapter describes the further validation of the numerical model by predicting the device performance within an innovative viscoelastic loading environment. Analysis included tissue forces for both manual and automated device distraction devices. The model could then be used to help define control parameters for smart devices.

The design of experimental and numerical models was based on the findings of Chapter 3 which investigated data from literature on the stiffness and time-dependency of tissues during DO. Of special interest were the range of values for tissue stiffness, the time over which the stress relaxation occurred following a distraction, and the percentage relaxation (i.e. how much of the step load increase was an elastic response and how much was viscous). Data including the forces measured during the time immediately following a distraction was found to be limited, as was pre- and post-distraction data throughout a full lengthening procedure. However, available data was used to build models that are adaptable across a range of values.

A good example of the type of relaxation data required was published by Simpson *et al.* (1996) which shows an immediate increase of around 50-60N following a 0.25mm distraction (relating to a 200-240N/mm stiffness) which then relaxes by around 75% after

1hr (Figure 3.5). Aarnes *et al.* (2002) found the increase to be 10-25N after each 0.25mm distraction and, although they did not monitor the relaxation curve, after 4hrs the load relaxation was found to vary from 20-88%. Gardener *et al.* (1998) reported a 40-50N increase with a 0.25mm distraction of the tibia, relaxing by 10N after 15mins and remaining at that value.

7.2 Proposed numerical model

Viscoelastic units comprised of springs and dashpots have been used previously to represent the mechanical characteristics of tissue, as described in Chapter 3. Basic viscoelastic models are described in Appendix C. The generalised Maxwell model (or SLS) was chosen as it has been used by other authors (Dhar and Zu, 2007) and is the simplest model that has the ability to represent both stress relaxation and creep. For this one dimensional model the force equation becomes:

$$F(t) = K_1*\delta + K_2*\delta*e^{(-K_2*t/\eta)}$$

This viscoelastic model was a subsection of the complete system that was developed to have the following capabilities :-

1. Incomplete relaxations between distractions were accounted for.
2. Distractions could be step or ramp to allow for manual lengthening and continuous lengthening from smart devices.
3. The distraction ramp could be variable across the charging sequence.
4. Immediate force reaction, percentage relaxation and relaxation time could be altered using the variables η, K_1, K_2 to fit with experimental data.

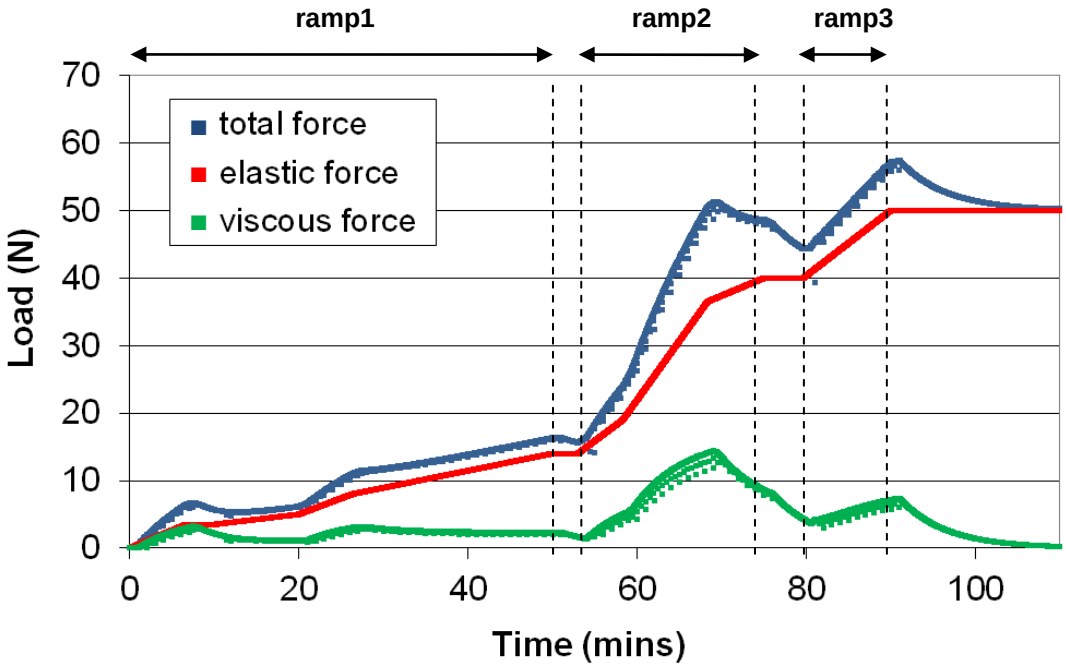

Figure 7-1 Load output from model with 3 variable ramped inputs

The Simulink model outline can be found in Appendix C(iii). Model outputs are shown in Figure 7-1 for three ramped extensions. These are not clinical inputs, rather they are used to show the capabilities of the model to deal with varying ramped inputs followed by pauses, mimicking the function of the device during charging and discharging. There is an elastic component (which is directly proportional to the extension) and a viscous component which relaxes to zero. Changing the elastic stiffness varies the percentage relaxation. Inclusion of residual relaxations can be identified by noting that although the viscous component does not fall to zero after the first two cycles, it does so after the third. This is discussed more fully below in 7.2.1, followed by more detail on the other model features (1-4).

7.2.1 Incomplete relaxations

Aarnes *et al.*, (2002) suggest that full stress relaxation between step distractions does not always occur and, as a result, the estimated peak force in each step must take into account previous distractions. Figure 7-2 shows how inaccuracies occurred if residual relaxation loads were not included i.e. if the total load was simply the addition of the elastic component (= resting load, calculated using total extension) and the new viscoelastic component (calculated using step change per extension).

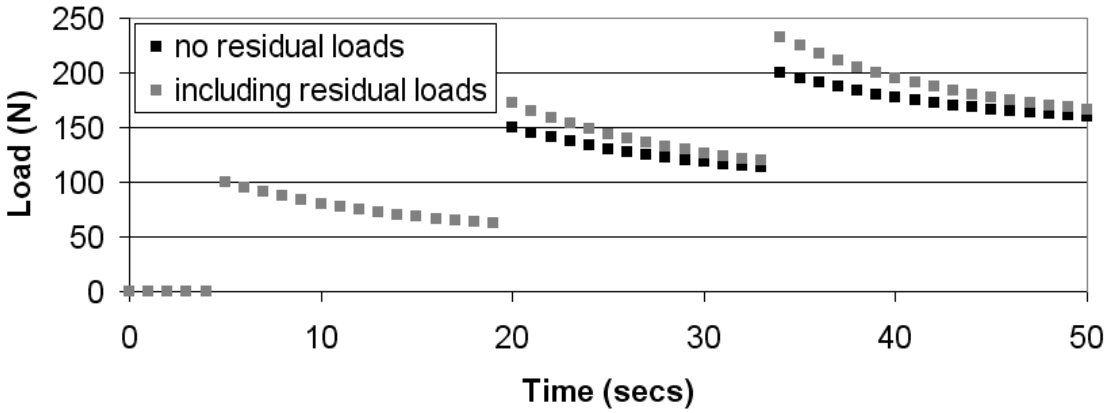

Figure 7-2 Incomplete relaxations

It was possible to ensure that residual loads were included by adding the outputs of the new cycle onto the existing, decreasing load results. Each subsequent step increased the length of the function (as all relaxation functions were on different time bases) and the computational requirement increased with every step.

A more efficient method was designed which, instead of dismissing or fully incorporating the incomplete relaxation from the previous step, used an approximation for the relaxation curve and added this to the viscoelastic load from the new step. The relaxation curve from the previous step change was characterised as an exponential relaxation function Ae^{-Bt}, starting at each new step, where constants A and B were determined using two data points on the previous curve, y_{t-10} and y_{t-20}.

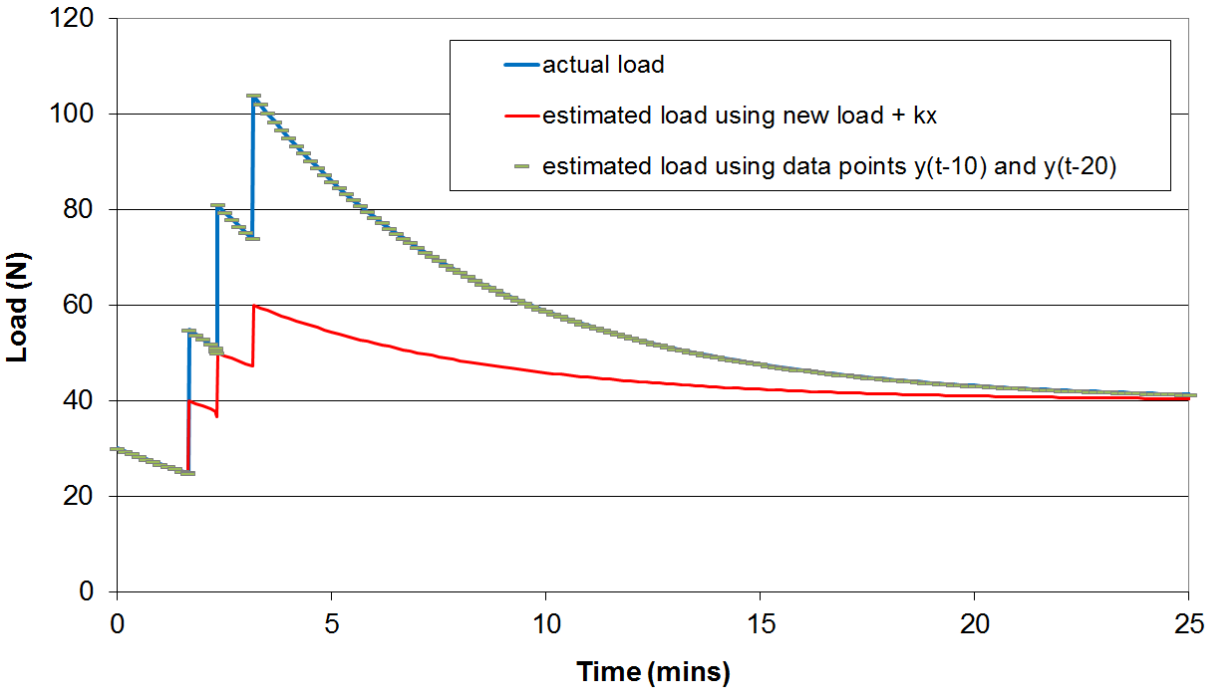

Figure 7-3 Actual load compared to estimated loads using two different methods of calculation

Figure 7-3 shows the actual load output compared to the two methods and clearly depicts the loss of accuracy when disregarding residual relaxations (error of 41% by peak 3), contrasting with the high accuracy of the residual function method. In fact, in this case, the maximum percentage difference between the estimated load (using data points y_{t-10} and y_{t-20}) and actual load at the final peak was almost zero. The two data points were taken to be 10 seconds apart, (y_{t-10} and y_{t-20}). Analysis of the influence of data point separation revealed that as little as two second separation still gave an accurate result to within 1.06E-12%. Yet, this is only over only 4 peaks and the tenfold decrease in accuracy could have implications later when dealing with longer simulations, thus the larger separation was kept.

7.2.2 Ramp inputs

Although the device extended in incremental steps in the order of one per second (quasi-continuous), the distraction pattern was similar to several ramp inputs, with a pause between each for piezo actuator discharge. It was hypothesised that the ramp input would reduce the peak force but not necessarily eliminate the tension accumulation. The first model calculated the ramp rate from the size of the first distraction step and held this same ramp rate until the next discharge cycle when the ramp rate became zero. The output is

shown in Figure 7-4 (Total Load) and the ramping input is in black (distraction in mm). The input signal is directly proportional to the elastic load which is a component of the Total Load.

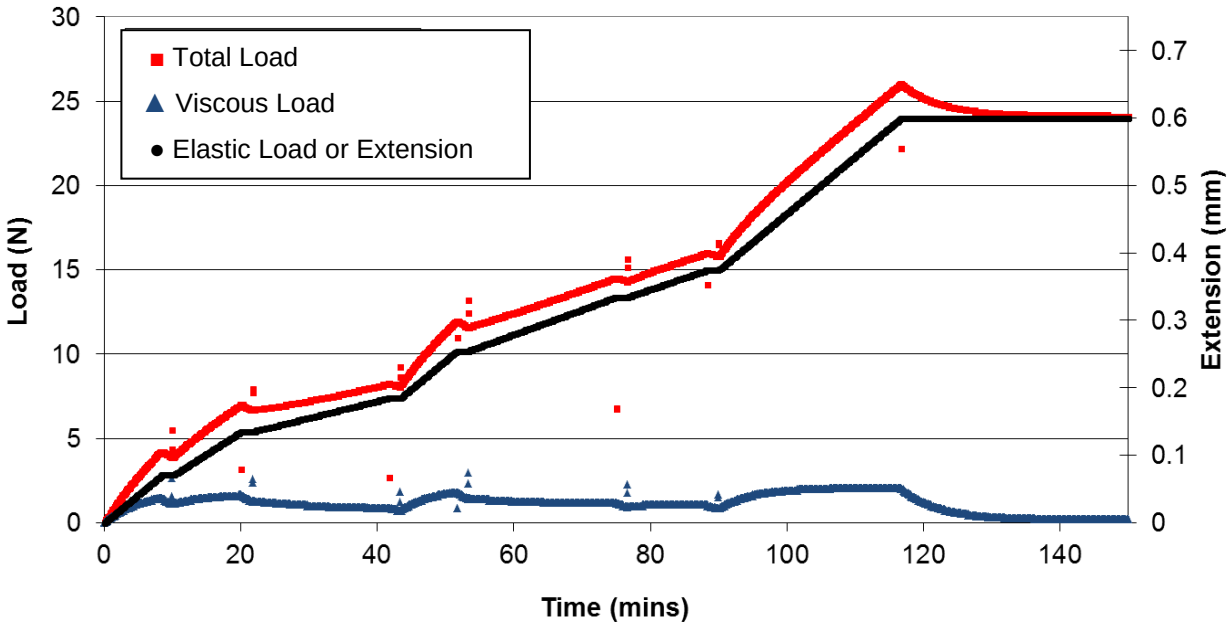

Figure 7-4 Ramped distraction resulting in viscous load output

The other component of the Total Load is the Viscous Load which is an addition of three signals,

1. the force from the current ramped elongation, 'ramp'
2. the residual relaxation from the previous ramp, in the form Ae^{-Bt}, 'residual'.
3. the force at which the new ramp started from, 'held'

This plot shows the horizontal asymptotic force response of a viscoelastic system to constant ramped extension input. This happens because the relaxation per second begins to match the increase in load per second. Once the input had stopped increasing, there was a relaxation of the force tending to zero. If the ramp increased again before the relaxation was complete then a relaxation function Ae^{-bt} was created (residual), the force at that moment was recorded (held) and both were used to calculate the total force during the next cycle.

7.2.3 Variable ramp rates

As seen from previous experimental data (Chapter 6), the extension of the device during charging was non-linear. Thus, to allow device extension as an input to the tissue model, a non-constant ramp rate had to be considered.

If each step (assume one step per second) were to be analysed individually then the viscous load would be:

$t=1: \quad \delta_1 K e^{-b*1}$

$t=2: \quad \delta_2 K e^{-b*1} + \delta_1 K e^{-b*2}$

$t=3: \quad \delta_3 K e^{-b*1} + \delta_2 K e^{-b*2} + \delta_1 K e^{-b*3}$

i.e. from t=1 to t=n $\sum \delta_t K e^{-b*1} + \delta_{t-1} K e^{-b*2} + \delta_{t-2} K e^{-b*3} .... + \delta_1 K e^{-b*n}$

where δ_1 *is the distraction at t=1 etc*

Computationally this would be extremely heavy, with a new exponential added every second of distraction, similar to addition of relaxations discussed in 7.2.1. Instead a compromise was made that split the ramp into 30second sections and computed the expected relaxation from each of these 30second ramps (note: this does not assume a step every 30seconds, instead each charge cycle is broken down into 30second sections each with a constant ramp rate).

Each 30second calculation for total force consists of:

1. Current ramp
2. Relaxation from previous ramp

To continually calculate relaxation, the method of combining relaxation curves into one exponential decay function was used as discussed in 7.2.2. The combined signals then became:

1. Current ramp
2. Relaxation from previous 30sec ramp

Note: two ramp inputs exist and run consecutively, ramp A and ramp B. This allows for the relaxation of ramp A to be used while ramp B is increasing and vice versa.

3. Residual relaxation from pre-30sec ramps
4. Held value

These signals are plotted independently in Figure 7-5.

a)

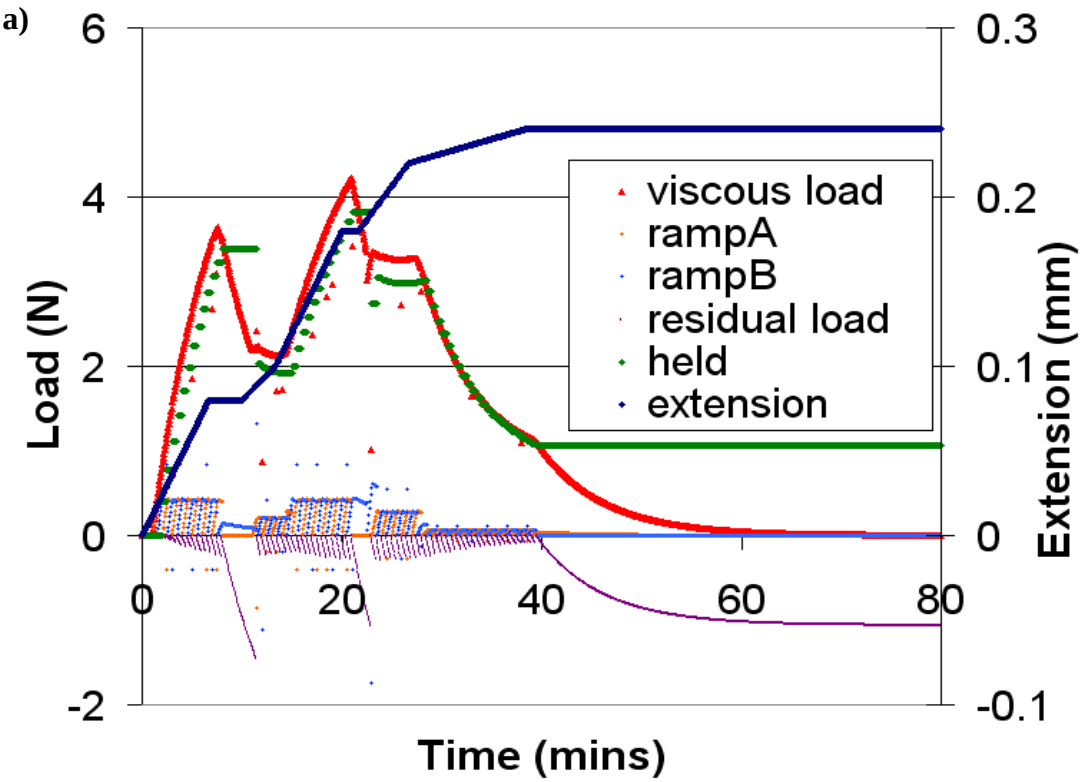

Figure 7-5 a) Varying rate of distraction (input) and the resulting output (viscous force) along with the signals used to make up the output force

b)

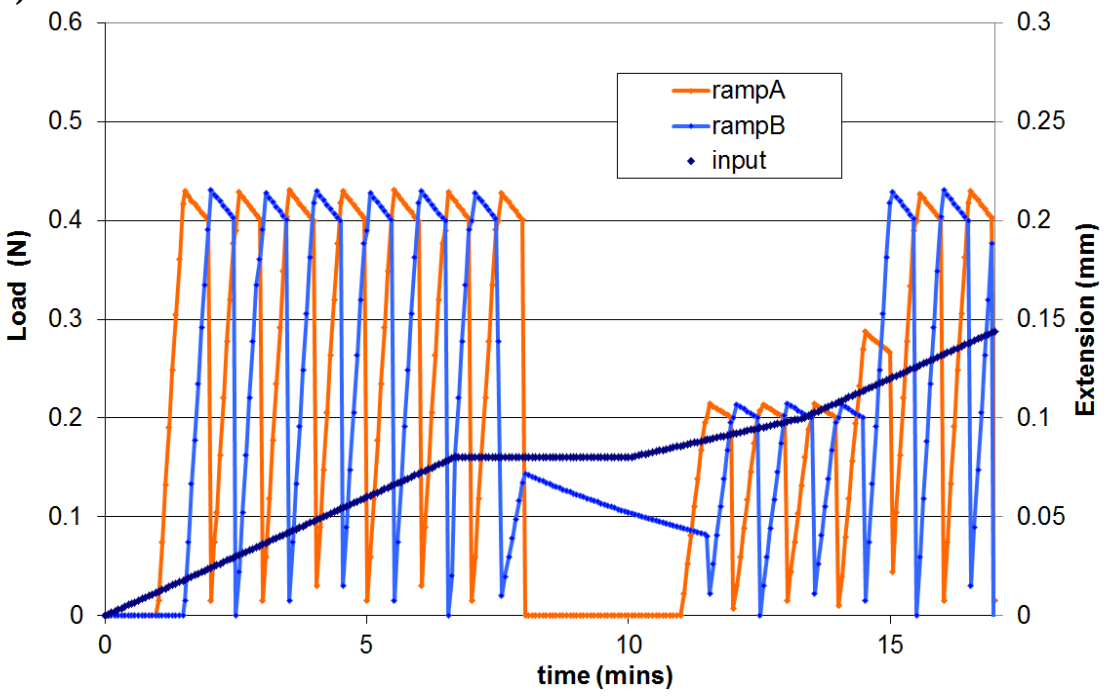

Figure 7-5 b) Closeup of the 30second ramps A and B and their variation based on input signal.

Interestingly, at times the load relaxation from previous extensions became larger than the load increase from the new ramp, resulting in a decrease in load even during times of extension. This was the case between 22-40mins, where the extension was increasing but the viscous load decreased towards zero.

7.2.4 Altering variables

Three parameters can describe the total load profile, defined as V, T and E (Figure 7-6) where:

V = viscous load

T = time for relaxation to decrease to 10% of peak

E = elastic load

These were varied by changing the values K_1, K_2 and η in the model. This gave the model flexibility in its use, allowing for closer matching of results to clinical data.

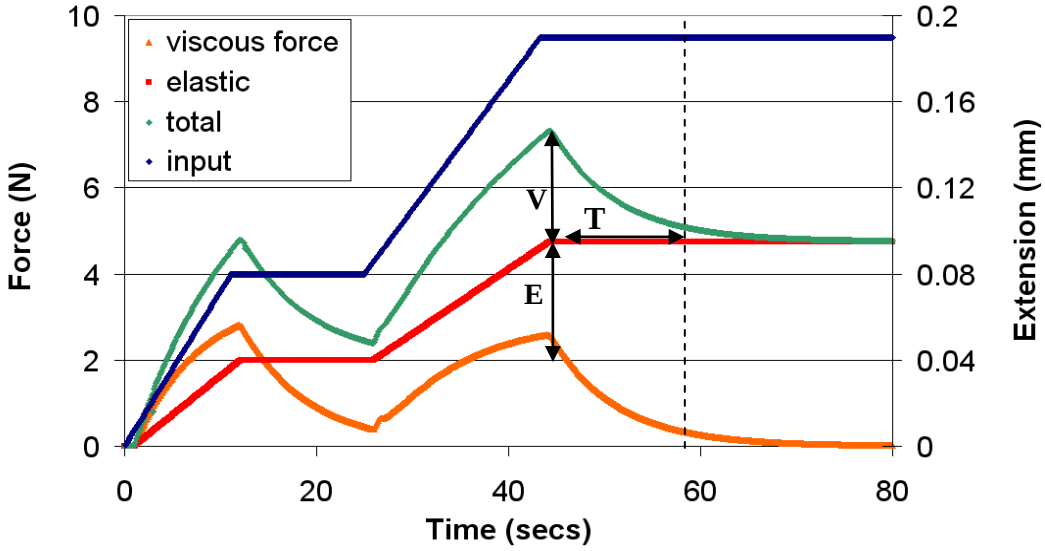

Figure 7-6 The input extension (blue) and resulting elastic, viscous and total forces defined by V, T and E.

7.3 Experimental model validation

In order to validate the model outputs, primarily resistive force and device extension, an experimental representation of the time-dependent characteristics of tissue was developed. The types of materials that have some potential for use in tissue simulation include rubbers, urethane polymers, elastomers etc. as used by Love *et al.* (2003). Materials used for damping within machine workshops were considered as they display a degree of viscoelasticity, but relaxation times were short – in the order of milliseconds. An

alternative concept was proposed that evolved from load dampers in the form of shock absorbing pistons. The creation of experimental representations of the two viscoelastic system components - springs and dashpots - allowed for a more controllable analytical approach. Varying the volume of liquid within a mechanical piston and dashpot whilst changing the spring stiffnesses arranged in series or parallel, gave a completely controllable system that predisposed itself to a more precise equivalent system to the numerical model.

7.3.1 Materials

Iterations of the dashpot system included evaluation of piston and dashpot materials, different compression liquids (oils and water), sizes of cylinders, sizes of orifice and the type of seal. These were assessed using step loads and step displacements on an Instron materials testing machine. It was found that a reduction of the flow rate could not be achieved through control of piston-dashpot clearance as fluid flow between these parts allowed load relaxation to occur very quickly. Therefore a needle valve was used to control the flow rate out of the piston, increasing the relaxation time. This allowed water to be used as the hydraulic system fluid, negating using oils of varying viscosities to achieve a range of flow rates. A rolling diaphragm seal was used to eliminate the erratic load behaviour seen during initial testing, attributed to friction between the o-rings and cylinder. This also gave a better seal, preventing flow between the piston and cylinder, instead forcing flow out through the valve and achieving more repeatable results. The cylinder was made from transparent perspex to allow detection of any air bubbles trapped in the system which would influence the results, by giving a false (low) representation of the stiffness. The final configuration is given in Figure 7-7.

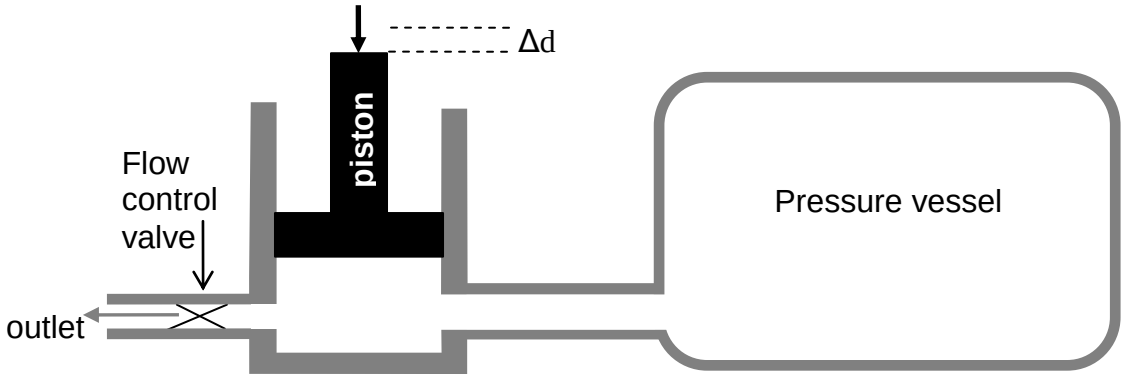

Figure 7-7 Schematic of experimental system

Spring stiffness (K_2)

The spring stiffness in series with the dashpot (K_2) was directly related to the compressibility of the fluid and the flexibility of the dashpot. If the liquid were incompressible and the dashpot perfectly rigid then the increase in force from any displacement would be infinite. In this case, the fluid was water, which has a bulk modulus of 2200MPa and the dashpot was a thin walled steel pressure vessel which expanded when the internal pressure increased. Selection of the size of the pressure vessel was based on achieving an increase in load from a 0.25mm displacement of the piston head of between 10 and 100N. The expected increase in force from a perfectly rigid system was:

$$\begin{aligned} Force &= A * P \\ &= A * E_{bulkwater} * volumetric\ strain \\ &= A * E_{bulkwater} * \Delta L/L \\ &= 19425 \text{ N} \end{aligned}$$

where A=706mm2, L=20mm, $E_{bulkwater} = 2200MPa$

This value was reduced by increasing the volume of liquid to reduce the volumetric strain, and ensuring that the expansion of the vessel was taken into the account. The resulting pressure vessel volume was 5l. Copper tubing was used instead of plastic due to high pressures and air pockets in-line were flushed out (using high pressure) to prevent measurement of air compression instead of vessel expansion.

The stiffness of the system (K_2) was quantified by measuring the increase in force from a known displacement of the piston head of the closed system. This was done by displacing the piston head and recording the associated load change. There was a load at zero displacement from the weight of the plate and bearings on the top of the piston head, but this did not influence the measurement of the gradient. A pressure gauge was used to monitor the system pressure to ensure it did not go above the safety limits for the equipment. Figure 7-8a shows the effect of having a small amount of air in the system – the compression of the air was more apparent at low loads (up to around 100N). By separating the load points during compression and release some hysteresis became apparent (energy lost in heat).

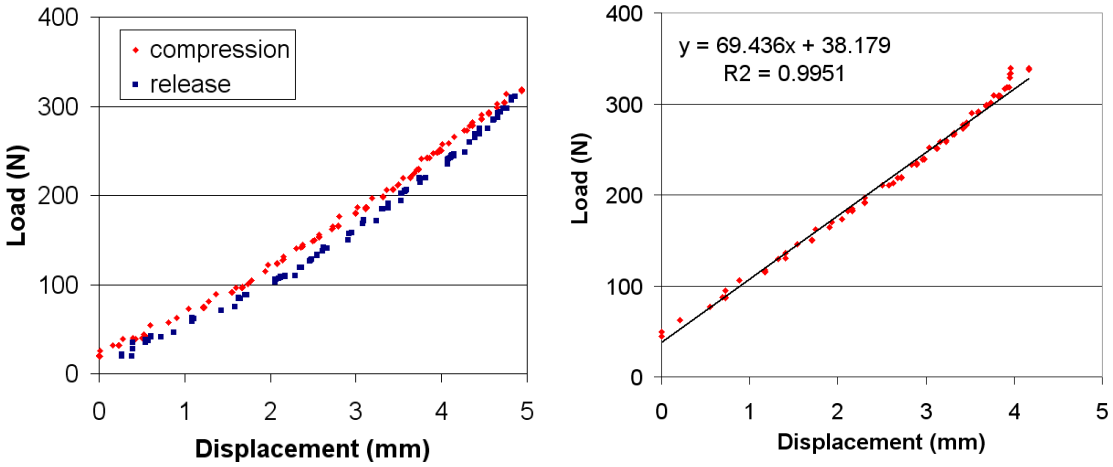

Figure 7-8 a)Non-linearity of system and hysteresis of piston system. b) Lower air content = higher stiffness and more linear

When the air content was reduced there was greater linearity at low loads (Figure 7-8b). The stiffness of the system was measured as 69N/mm, equating to around 17N increase for a typical 0.25mm clinical distraction which was within the 10-100N range set originally. This was the portion of the reaction force increase that relaxed to zero over time and was not easily changed using this experimental setup. However, when combined with springs in parallel, the proportion of releasable load was altered by changing the parallel spring stiffness. The system required refilling once the piston had reached its full travel and so the closed system became an open system during the refill, exposing it to change. Consequently the stiffness of the system was confirmed after each refill.

Stress relaxation (η)

The flow control valve provided the means to control the viscous characteristics of the system i.e. time taken for complete relaxation. Following a step displacement of the piston head, the load relaxed to zero over time. An exponential best fit line was then added to the load-time (Ae^{-bt}) and the value of b compared for different steps. In the case of tests a and b, the correlation values were very high (>0.99) showing good predictability with exponential functions giving a relaxation time of nearly 4minutes and 2minutes respectively (Figure 7-9). This relaxation time was fast in comparison to data from literature (Chapter 3). Therefore the valve position was altered.

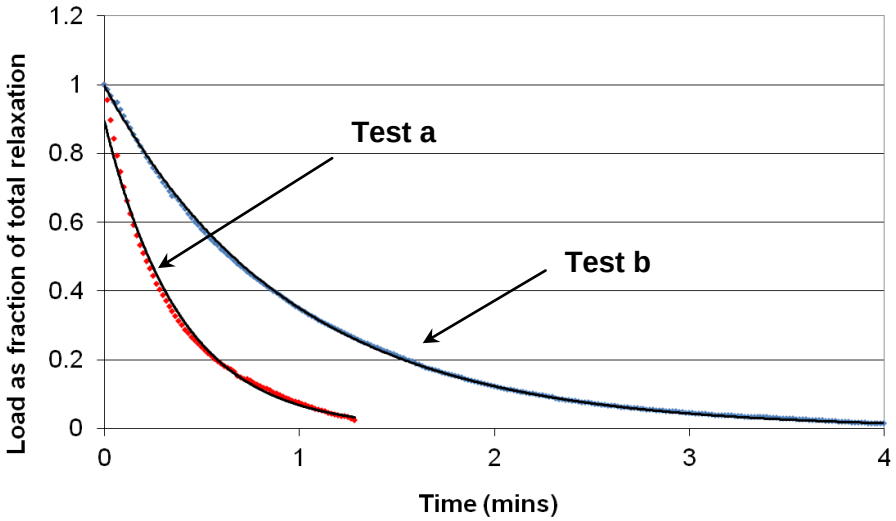

Figure 7-9 Fitting exponential functions to experimental load relaxation curves

Tests were repeated for 0.25mm step displacement and high variability was found. The cause was found to be imprecise valve setting i.e. the rotational position was extremely sensitive and it was difficult to repeat tests at specific valve settings. Consequently valve position remained constant while an additional stop valve was put in place to prevent flow between tests.

Parallel elastic component (K_1)

In order to create a SLS model of viscoelasticity, a spring was added to the system in parallel with the existing spring and dashpot. This provides the pre-distraction forces at full viscous relaxation that are seen clinically. For practical purposes two springs are used, one either side of the dashpot, bringing the total spring stiffness to $K_1 = K_{spring1} + K_{spring2}$ (Figure 7-10). The plate and rods were also expected to have a stiffness, which was in series with the springs, but was essentially integrated into total stiffness K_1.

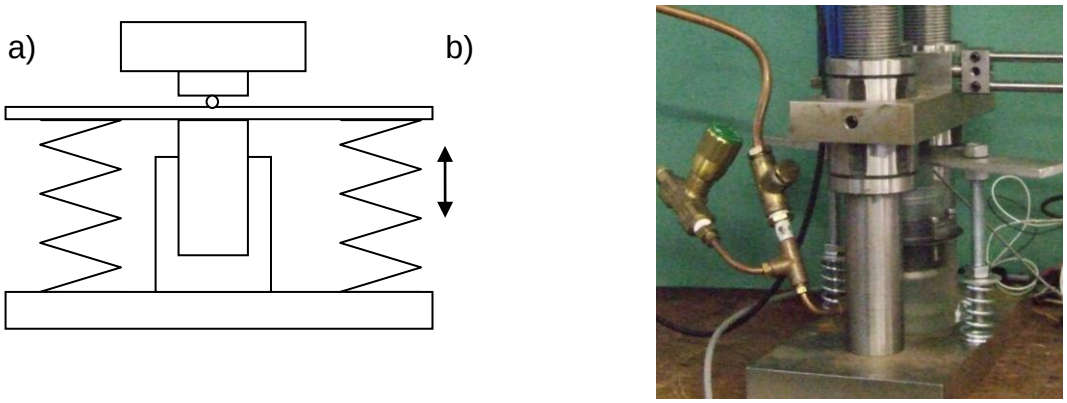

Figure 7-10 a) Schematic and b) photograph of the experimental spring arrangement

Experimentally, the response of this setup to a step displacement was an immediate load increase followed by a time-dependent reduction to a constant value (Figure 7-11).

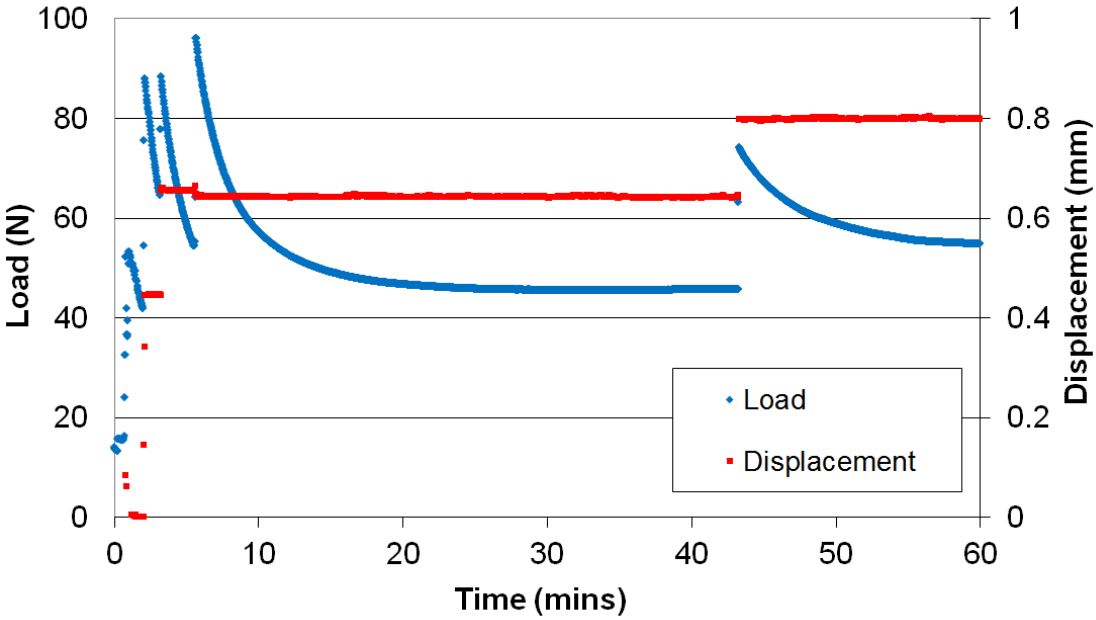

Figure 7-11 Load response to a piston displacement showing both the viscous and elastic response.

Figure 7-11 shows a typical test where the piston was displaced until a resting preload of around 45N was gained after stabilisation. The piston was displaced by 0.16mm and a partial load relaxation was seen, the resting load depending on the spring stiffness. In this case the load increase due to the springs was 11N and the immediate viscous load increase was 18N which relaxed to zero after around 18minutes.

The influence of air temperature on the loading (see Appendix E) led to the requirement of increasing the rate of testing so that any temperature related fluctuations were reduced. Daily lengthening in 5 steps (1.25mm extension) was completed over 2.5hrs on the basis that full relaxation had occurred before the next step took place (around 30mins). Additionally, the maximum extension rate of the device was ~10mins/cycle. Depending on the extension achieved per cycle the total extension over 2.5hrs (or ~15cycles) ranged from around 0.3-1.5mm.

7.3.2 Methods

Two different validation tests were performed:-

1. prediction of device performance and resistive load in a characterised viscoelastic environment
2. prediction of device performance and resistive load in viscoelastic environment with varying percentage relaxation

The first validation required calibration of the model to the experimental viscoelastic tissue environment. This was done using five manual distractions of around 0.25mm over 2.5hrs. Once calibrated, the device model was used alongside the tissue model to predict the extension and load outputs. These simulated outputs were then compared to the experimental results for the device in a viscoelastic environment. The second validation used the same calibrated tissue model but, in order to change the percentage relaxation, the elastic constant k_1 was increased to 80N/mm. Simulated results for both manual and automated device extensions were compared to experimental results.

7.3.3 Results

Results for the experimental manual distractions are plotted in Figure 7-12 and show the immediate load increase and exponential relaxation following each distraction.

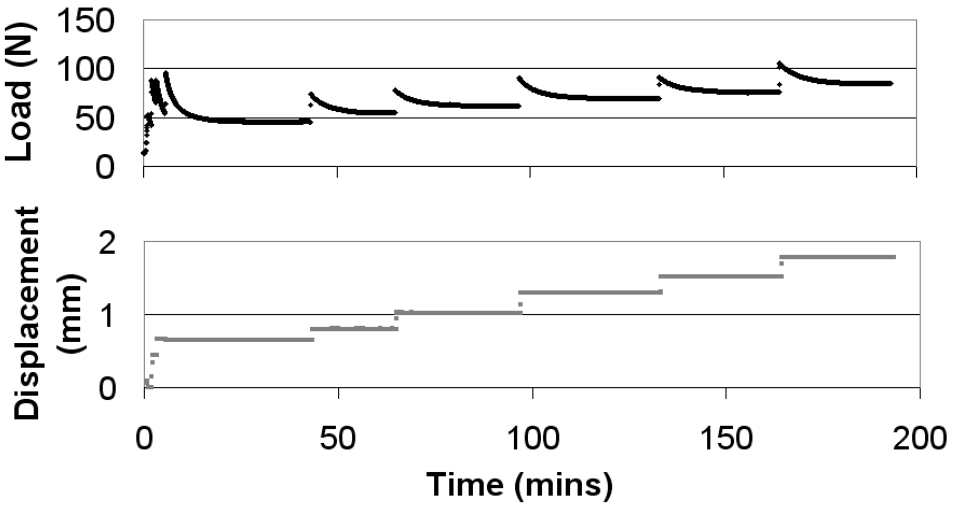

Figure 7-12 Load response to manual displacement of ~0.25mm

Each of the relaxation curves was analysed individually through the use of curve fitting to an exponential trendline, $y = Ae^{-Bt}$. An example is given in Figure 7-13. Values for A ranged from 20-21 and were dependent on the displacement while values for B ranged

from 0.003-0.0034 and were found not to be dependent on displacement. The minimum R^2 value was 0.98.

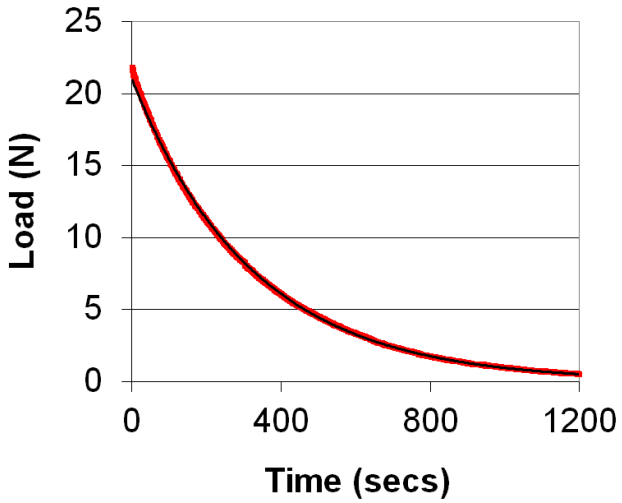

Figure 7-13 Exponential trendline fitted to step 5 of the manual distractions

Conversion of experimental data to units used in the numerical simulation (Load = $K_1*\delta + K_2*e^{(-K_2/\eta)t}$) resulted in K_1=30000N/m, K_2= 80000N/m, $\eta = 2.67x10^7$ Nsm^{-2}.

These material properties were used in the tissue model providing resistance for the device model during extension. Figure 7-14a shows that the predicted device extension followed the experimental extension against the viscoelastic material to within 110 microns after 23 cycles (= 6% error).

a) b)

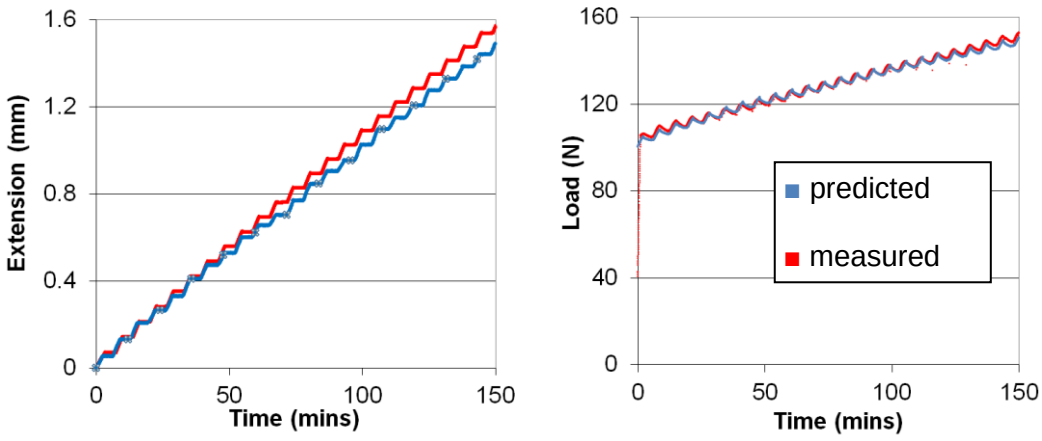

Figure 7-14 Comparison of predicted and experimental device extension and load when lengthening viscoelastic materials

Load data from the same test indicated that the relaxations during the discharge phase were predicted more accurately by the device and suggest incomplete force relaxation after each cycle (Figure 7-14b).

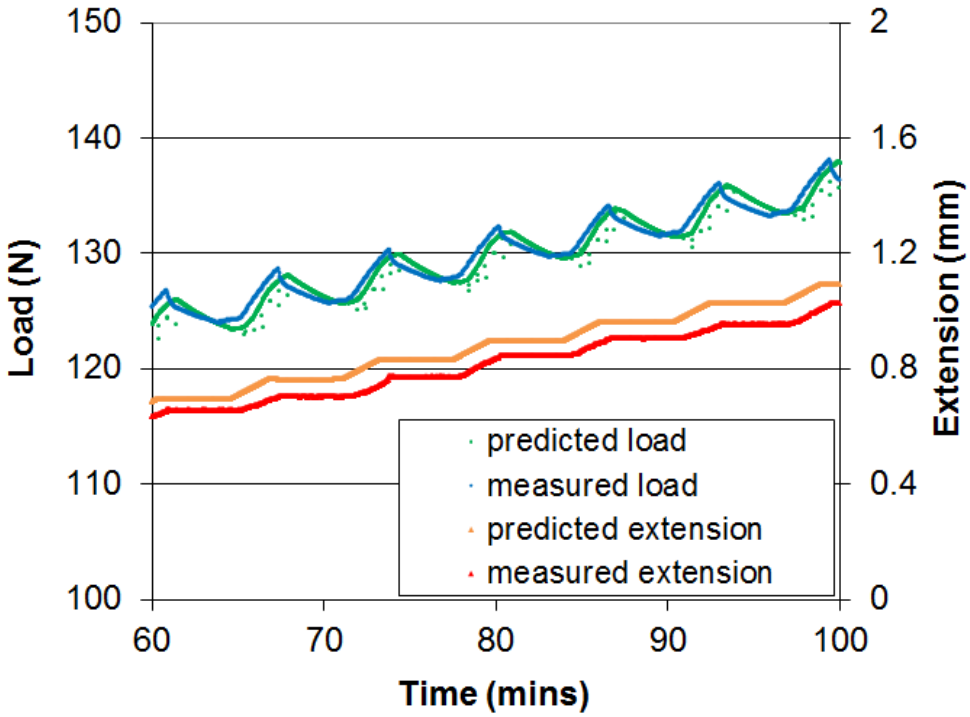

Figure 7-15 Close up of predicted and experimental loads and extensions when lengthening viscoelastic materials

Focussing on a smaller time range to view the profile highlights the load reduction during the actuator discharge phase even with no lvdt movement (Figure 7-15). The average increase in load during charging was 4.6N while the device predicted 4.3N, a 6% difference. The simulation also under-predicted the relaxation load by the same absolute error. The smoother profile of the simulated force was due to the 30second intervals of the simulation which means the peak force may have been missed, though it is clear that this error is minimal. Other than the slight smoothing the profile matched well under these conditions.

The second validation involved assessing the effect on force response of changing the percentage relaxation of the tissue model. The load data from experimental manual stepped extensions were compared to simulated results and the simulation was able to predict four out of the five peak loads to within 6%. This resulted in a relaxation of 50% compared to the previous relaxation of 70%. For the automated device over 3hours (27cycles), where the experimental extension was 1.2mm, the predicted extension was

higher by 0.11mm (9%), but the predicted load was more accurate with only 1.7% error. The profile suggested that the predicted setback per cycle was too low and that there was an immediate setback upon discharge that was not seen during testing against elastic materials (attributed to additional components within the new setup). Timing offset was due to the inconsistent cycle times experimentally whereas the cycle times for the simulation were constant. Again, focussing on the profiles gives a better indication of the simulation accuracy for the viscous load component and the device characteristics (Figure 7-16). Alongside this a comparison was made between the accuracy of load and extension predictions for both the existing high percentage relaxation (70%) and this new lower percentage relaxation test (50%).

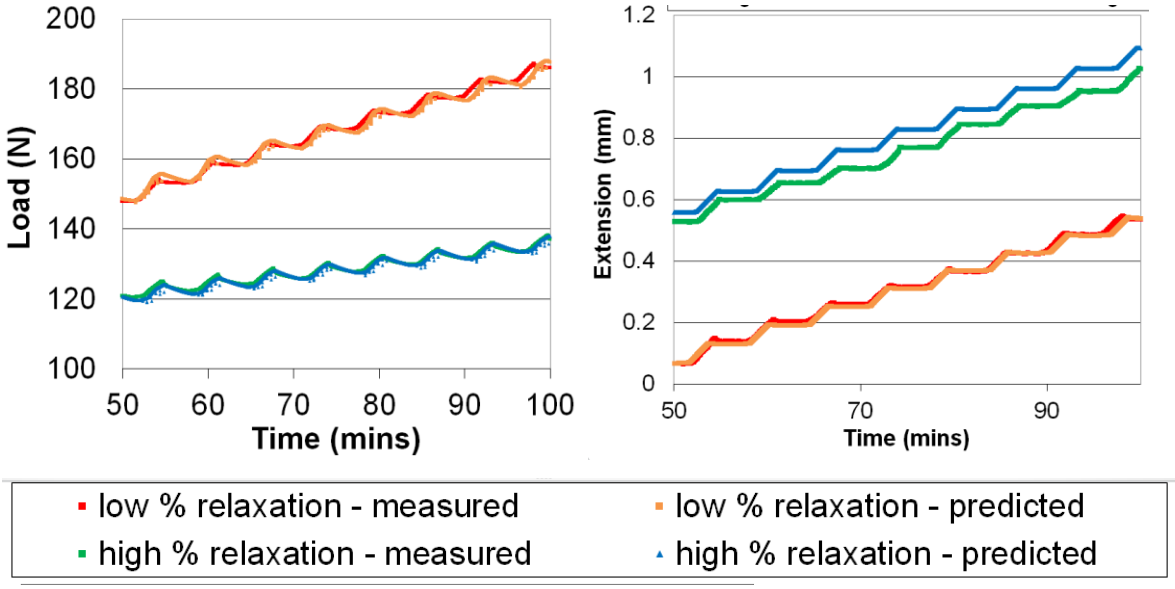

Figure 7-16 Comparing the how well the simulation predicts the load and extension profiles with different relaxation percentages

Load profiles both matched well, particularly the high relaxation. The load at the end of the actuator charging phase for low relaxation was overestimated by a maximum of 1.5N per cycle but the higher relaxation compensated over the longer term. Extension profiles appear better matched for low relaxation compared to the high relaxation. However, over the course of the extension, the error was higher for the low relaxation and the variation was also large - a range of 0.048-0.076mm per cycle just in this small section. Elevated extensions in the model were a result of too low a stiffness value of the tissue model, therefore tissue stiffness was increased which maintained the current load even when extension was reduced. Interestingly the extension per cycle of the device under viscoelastic loading was reduced compared to the elastic case, across the same load range.

For an average load of 130Nm, the extension was expected to be 63mm whereas under viscoelastic loading it was 58mm. It is suggested that this was due to the temporary increase in resistance from the viscous component.

7.3.4 Simulation characteristics

As has been shown there exists a smoothing in the predicted load reaction due to the 30second averaging of the input signal (7.3.2). It was important to assess the influence of this averaging and quantify any reduction in peak load that may be occurring and to identify the most accurate step length for simulation of an immediate extension. For a typical 0.25mm extension, the theoretical peak was:

$$F = \delta * K_2 * e^{-bt}$$

$$At\ t=0,\ K_2 = 75000,\ \delta = 0.00025m$$

$$F = 18.75N$$

The predicted peak loads using the numerical model were found to range from 17.3N to 19.0N (92.5-101.5% compared to the theoretical value) for step times between 1 and 90seconds (Figure 7-17). Any extensions under 30seconds resulted in a 17.4N peak (93% of theoretical value). For a 32second step, the peak increased to 102% of the theoretical value, reducing as the step time increased to 60seconds, where it increased again to 18.6N (<1% error). This pattern continued as the step became longer and was split between more and more 30second intervals. As expected, the peak load gradually reduced and for steps of over an hour (such as expected from the smart device) the peak was <11% of the immediate load value. Consequently a 60second step time was used in the simulation to represent an immediate manual extension as it had the most accurate prediction, suggesting that the simulation required the input to be non-zero for three ramp intervals (= minimum 61seconds). Additionally the size of the error was influenced by the rate of discharge (determined by 'η') which, for this period of testing, was faster than the clinical case (because of the need for faster testing due to temperature effects). Thus the percentage error was expected to be reduced when using a more standard rate of lengthening.

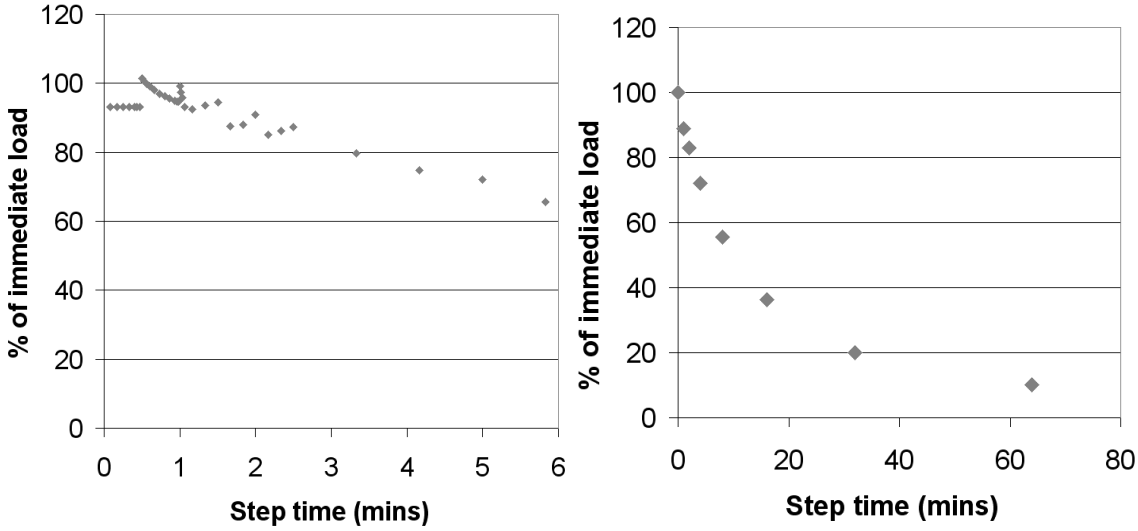

Figure 7-17 Variation of peak loading with step time

A second effect of the 30second interval was on the period of discharge. It was concluded that a discharge time less than 30seconds simply lowered the rates of ramp A and/or ramp B i.e. reduced the average increase/sec. A discharge time between 30 and 90seconds created inaccuracies i.e. if either ramp became zero, the other was also required to. This particular feature did not create any problems in the device simulation as the minimum ramp rest, determined by the piezo actuator discharge time, was 200 seconds. This may need further development if the influence of short term weight bearing were to be included in the simulation.

The simulation was then examined for its ability to work to the extremes of clinical distraction. The maximum limit of the ramp rate testing was selected as 4mm in one (manual) step. This excessive extension gave an immediate viscous force reaction of 50N and although is far beyond the clinical recommendations shows the ability of the simulation to manage large inputs. The minimum limit was chosen as a rate which would provide 0.25mm throughout one day of lengthening (Figure 7-18)

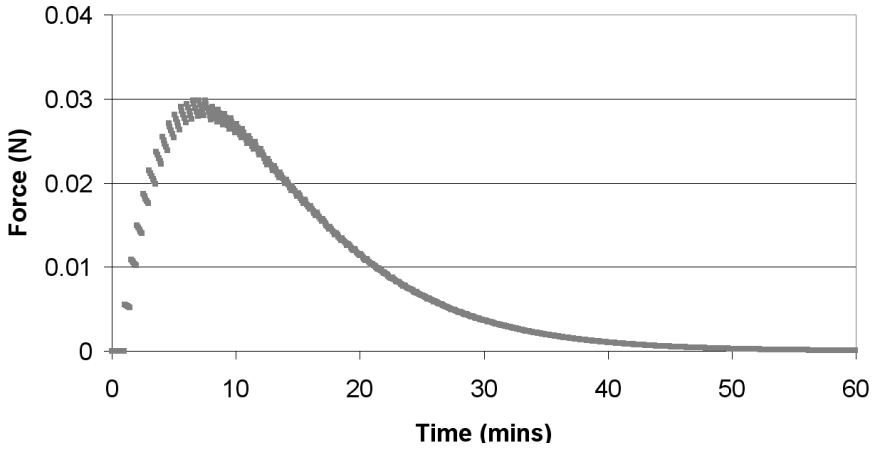

Figure 7-18 Load response to 2.89E-9 m/sec ramp rate, =0.25mm over 24hrs of continuous lengthening

The force levelled at 0.03N which was a negligible increase in viscous loading. A more standard rate of 1mm/day (=1.16E-8m/sec) resulted in a maximum viscous force of 0.34N.

7.4 Summary

The numerical model of tissue viscoelasticity described in this Chapter provides a simple method of predicting the level of force expected during tissue extension when performed using either manual or automated devices. This validated model can then be used to aid device development for both manual and automated devices. Automated devices may provide constant or variable extensions (model input) and these have both been accounted for in the model. Alongside variations in the device, validation included varying the characteristics of the tissue due to the wide range of tissue characteristics seen clinically. This was done through changing the proportion of relaxation from each load increase. Although the current predictions are short-term it is understood that the longer-term healing effects are likely to influence the mechanical properties of the tissue over time i.e. the model variables K_1, K_2 and η are likely to vary over the course of treatment and across patient groups. This will be discussed in greater detail in Chapter 9.

Chapter 8

Modelling the use of pins in fixators

8.1 Introduction

For the purposes of identifying device characteristics and developing the tissue model the device has been loaded along its axis (Chapters 6 and 7). However, clinically the load is carried through pin sets attached to the bone on either side of the osteotomy. The pins are an integral part of the load path between the device and tissues and will undergo some degree of deflection relative to the resistive forces following extension and adding an important component to the system.

Although a traditional manual device undergoes a step increase in length, the tissue may not immediately extend by the same amount due to load transferred into the pins causing pin-bending. The time-dependent characteristics of tissue (described in Chapter 7) add to the complexity of this situation, resulting in, not only stress relaxation in the tissue, but also some viscoelastic creep effects i.e. extension under constant load. This Chapter describes the influence of the pins on the load within the tissues, both in the case of a traditional manual lengthening device and for the automated device. The numerical model of the tissue was updated to include these effects, enabling better prediction for control purposes. The numerical model of the device was modified appropriate to the influence of these effects on performance.

8.2 Proposed Numerical model

The pins were represented as an additional stiffness in series with the tissue stiffness. When the time-dependency of tissues was not included in the model, the resultant stiffness k_{total} was calculated as:

$k_{total} = 1/(1/k_t + 1/k_p)$

where k_t *= tissue stiffness*

and k_p *= pin stiffness*

In the case of viscoelastic loading, the model could be represented as shown in Figure 8-1. It was expected that a step increase in length would induce not only load relaxation as seen in Chapter 7 but also time-dependent tissue extension. Pins were not the only source of additional compliance as components such as the pin clamps can contribute for both manual and automated devices.

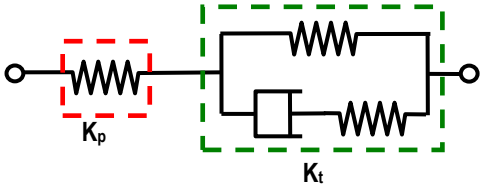

Figure 8-1 SLS model components with pin stiffness K_p shown in series with existing viscoelastic tissue stiffness model K_t

The input into the viscous Simulink model was tissue extension. Therefore the tissue extension had to be extracted from the total extension. Using basic extension and load equivalence relationships:

$F_p = F_t$

$K_p*\delta_p = K_2*\delta_2*e^{(-K2*t/\eta)} + K_1*\delta_2$

$\delta_p + \delta_2 = \delta_t$

then,

$\delta_2 = K_p*\delta_t/(K_p + K_2*e^{(-K2*t/\eta)} + K_1)$

This was implemented into the simulation, requiring a one second delay due to an algebraic loop (i.e. the values of the inputs depended on the output, δ_t depended on δ_2). This was the only change implemented in the tissue model although it was expected that there may be a change in the device performance which is explained in section 8.3.2.

8.3 Experimental model validation

8.3.1 Materials and method

Firstly, the influence of the pins on the device must be understood. Two clamps on the device (one attached to the main body, the other on the threaded shaft) were used to hold the pins (Figure 8-2).

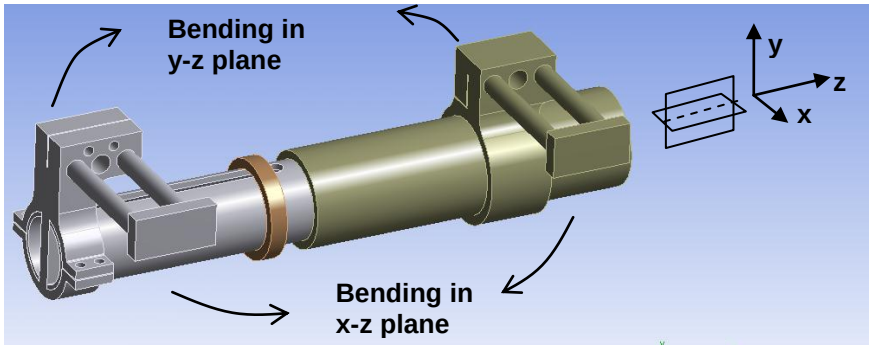

Figure 8-2 Pin clamps and their effect on device bending orientation

It was found that alongside deflection along the length of the device (δ_{zz}) and the expected bending in the x-z plane (θ_{xz}), there was additional bending in the perpendicular plane (θ_{yz}) as shown in Figure 8-2 . This was due to the offset of the pin clamp to the axis of the device (by 29mm). The clamp on the shaft could be oriented in two ways, either the pins were in-line with the gear mechanism (position 1 in Figure 8-3) or opposite (position 2 in Figure 8-3). Initial testing showed that if the clamp was positioned with the pins in-line with the gear, any bending of the device reduced the distance between the pinions and spur gears and could prevent rotation, depending on the applied load. If the deflection was in the opposite direction and the distance increased then rotation was still possible. This situation was preferable to locking although the power transmission may have been reduced.

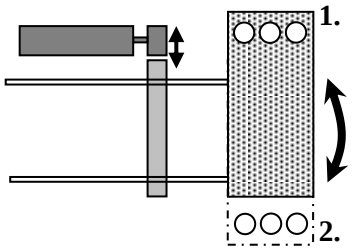

Figure 8-3 Drawing of the effect of shaft bending on the motor mechanism

The first test frame for the proof of concept model consisted of a linear bearing with two sliding plates to which the pins could be clamped. Bending of the pins produced a twisting of the plates resulting in a higher frictional force than anticipated. This gave a stepped movement of the sliding plate and a reduction in maximum force achievable. As a result, the offset rig was incorporated into the new axial rig through the use of additional pin clamps as shown in Figure 8-4.

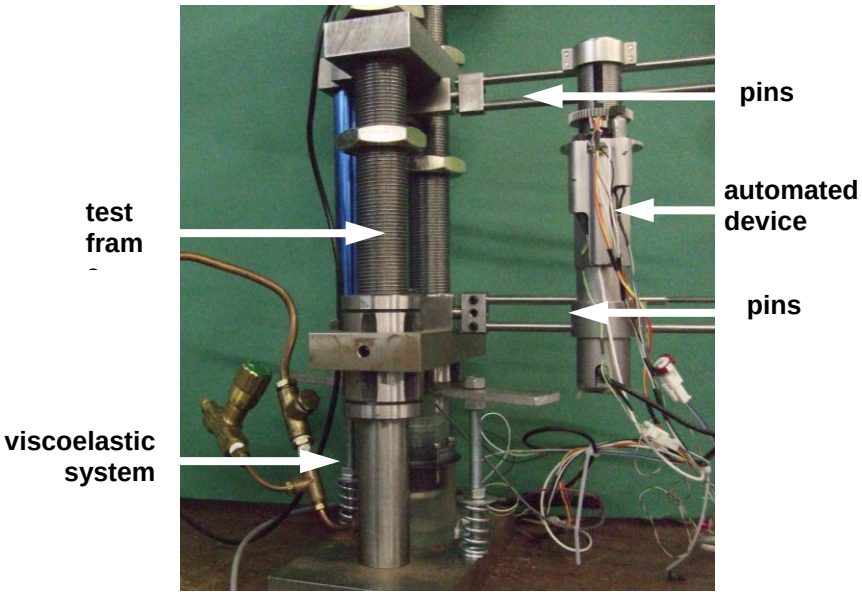

Figure 8-4 Offset test rig with viscoelastic loading

Pins of 6mm diameter were chosen as these are one of the most commonly used sizes clinically. Two pin lengths were tested – 50mm and 70mm, which represented the distance between the device and the bone. This distance would be determined in clinical practice according to patient limb size. The extension and load through the plate were measured as in the axial testing using a load cell and LVDT (Chapter 6).

In order to measure pin stiffness, deflection measurements were taken with digital callipers (with a resolution of 10microns) at the positions shown in Figure 8-5 and were repeated three times during each measurement to reduce operator error. If the variation between the three readings was greater than 20microns another reading was taken. Once within limits, an average of the three readings was taken.

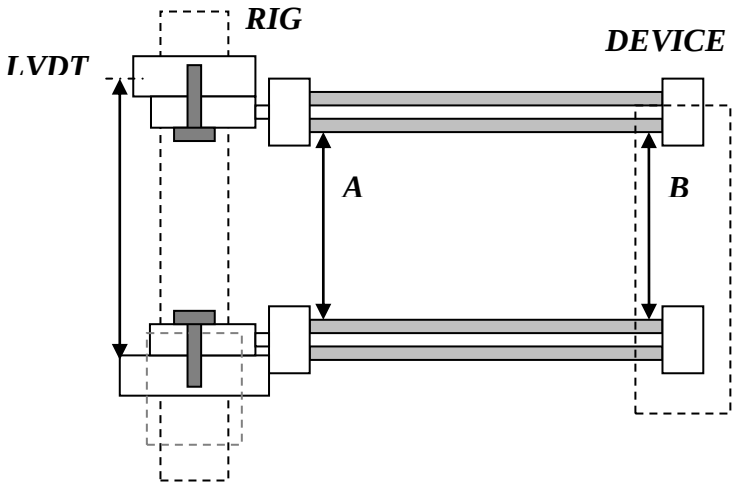

Figure 8-5 Positions of measurements for pin deflections

In the static load case, the initial pin deflection was expected to be proportional to the applied load but with no further deformation during the lengthening process. Therefore with no further load increase, the extension of the device was expected to equal the 'tissue' extension. Conversely, in the elastic load case the deflection of the pins was expected to increase as the load increased such that the extension of the device would not equal but instead be proportional to the extension of the tissue. In the viscoelastic case the load transfer mechanisms were more complex and were expected to depend on the relaxation time of the system, where immediate device extension would not necessarily result in immediate extension of the tissue.

The performance of the device under offset loading was, for comparison, assessed using the same method as that used with axial loading (Chapter 6) – finding the extension per cycle of the device at various static loads.

8.3.2 Static and Elastic load results

The findings of these two studies (pin stiffness and change in automated device performance) were used to update the model. Further validation was completed by predicting device performance and tissue mechanics when using different pin lengths and varying the proportion of relaxation. The first testing phase required finding the approximate pin stiffness for the model. The second phase analysed the effect of offset loading on the device performance.

Factors affecting pin deflection (and therefore stiffness) include pin length, diameter, separation and number of pins in each pin set, most of which are patient specific (Fragomen and Rozbruch, 2007). In order to change the stiffness for this test, the variable selected was pin length and was reduced to 50mm from 70mm.

Theoretical calculations used both traditional bending theory and an approach used by Huiskes and Chao (1986) to characterise the rigidity of unilateral or bilateral external fixation systems with any number of pins at any radius or length:

$$k_p = 6*(n*m*E*I/s^3)$$

where k_p = stiffness, n = number of side bars, m = number of pins, E = modulus, I = second moment of area of pin and s = length of pin

Pin stiffness for 70mm pin length was calculated as 411N/mm. This assumed the pins were rigidly connected at both ends (Figure 8-6a) and did not include stiffness from the adjoining clamps. Consequently the stiffnesses were overestimated compared to

experimental values where a degree of slip and clamp bending could occur. Rotation of the pin ends during initial testing indicated that the rig plates should be constrained. Clinically, malformations of the limb can occur with unilateral devices as the pin loads the bone in a way that induces bending (Figure 8-6b).

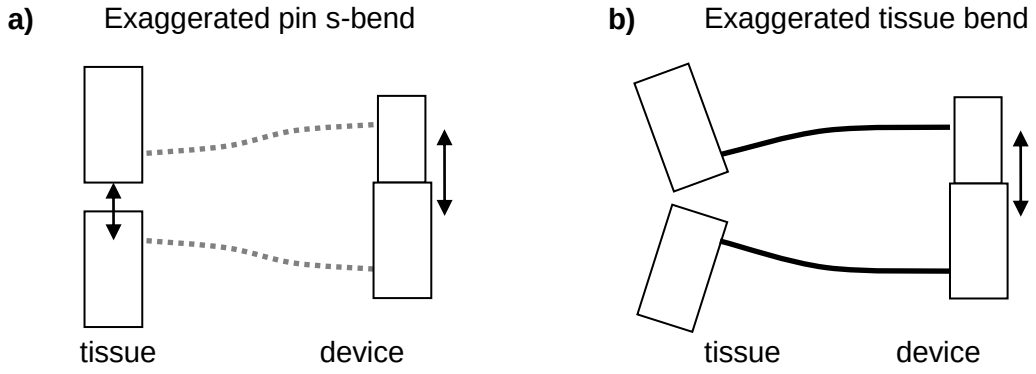

Figure 8-6 Influence of pin bending

Using nuts to constrain the plates, reducing rotation (Figure 8-6a – although in practice infinite stiff cannot be achieved and some rotation will still occur), the experimental stiffness (load increase per mm movement of the lvdt) was increased from 42N/mm to 72N/mm. Physiologically there are muscles keeping the bone segments aligned and, although they will not provide a rigid fixation, the restrained plate position is more representative of this than free rotation. In order to account for the stiffness of clamps, an additional measurement was taken, using the lvdt to measure plate displacement as a result of device extension. Experimental pin stiffnesses (k_p = 72N/mm for 70mm pin, k_p = 84N/mm for 50mm pin) were found to be less than half of the stiffness suggested by theoretical calculations.

The theoretical calculation suggests that the distance between the pins at each pin site is of no significance. This is a notable assumption as a large separation would significantly increase the stiffness compared to small separation. Experimental values remain low and the difference in stiffness between the two pin lengths is smaller than expected. Additional reasons for the large disparity between theoretical and measured values were suggested as:

- theoretical assumptions included idealised rigid connection between the pins/clamps and clamp/shaft, clamp/body
- there remained some small degree of plate rotation although the plates were manually locked

- there was some possibly some compliance/bending of the clamping components

The extension per cycle of the device was determined by compliances at interfaces which were expected to change when loading moved from axial to offset due to non-parallel surfaces at component interfaces. Figure 8-7 shows initial results which indicated a higher degree of variability than the axial case.

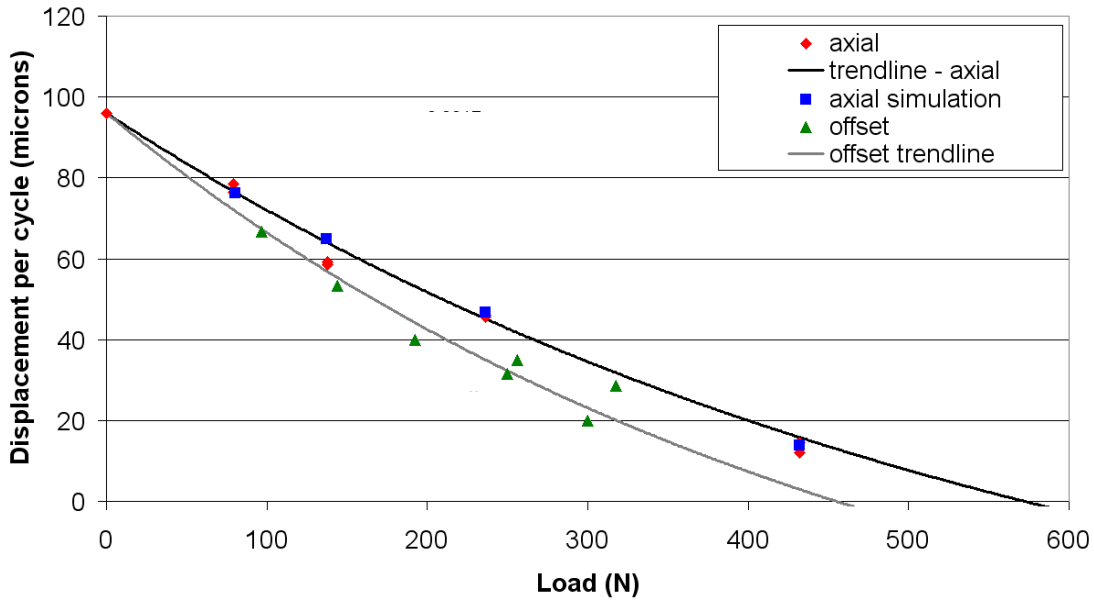

Figure 8-7 Comparison of axial and offset extension per cycle

As a result of the high variability, testing was extended in length and it became apparent that there was a cyclic pattern to the variability as shown in Figure 8-8. This pattern was repeated every 1mm, equal to the pitch of the driving and holding nuts within the device. This suggested that offset loading induced bending into the shaft which changed the angle of the nut relative to the thrust surface. It then accentuated the effect of any tolerancing error or slack in the nut/thread interfaces changing the contact stiffness and inducing a rotational pattern of extension per cycle. Figure 8-8 shows the device loading against a spring load from 110-250N and so the load was also increasing but with the 1mm pattern evident.

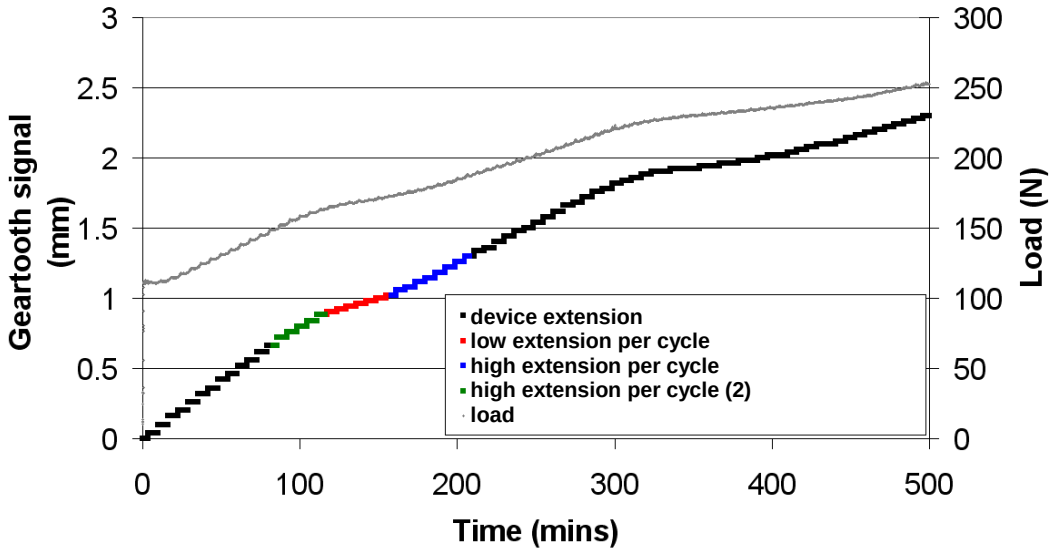

Figure 8-8 Highlights the cyclic variability of the device when loading is through pins

Table 8-1 shows the average extension per cycle of four sections taken from Figure 8-8, across the first 210minutes of the test:

Load range (N)	Extension (microns)	Average extension per cycle (microns)	Error from geartooth resolution (%)
110-142	520	52	4
142-164	320	45.7	6
164-172	140	20	1
172-187	280	40	7

Table 8-1 Analysis of coloured sections of Figure 8.8

Consequently, the model was run at two extreme load cases where the contact stiffness was changed to allow 20-52microns/cycle at loads under 200N. Analysis of setback was not viable as the DVRT signal required for analysis (see Chapter 6) used the nut which had been found to be variable in position.

8.3.3 Viscoelastic load results

Four different tests were performed with time-dependent loading; with the manual device, the smart device, varying pin lengths and varying the percentage relaxation.

The first objective was to confirm that the model could predict the tissue load and extension when using a manual lengthening device with pins. With axial loading, tissue extension occurred simultaneously with device extension, but when pins were used the

experimental tissue extension became time-dependent and an immediate increase was followed by a gradual asymptotic curve as shown in Figure 8-9. This was seen previously in the Standard Linear Solid model of viscoelasticity in Chapter 3. In the first case, using the manual device, the immediate extension was around 62% of total extension (Figure 8-9a). Although the device extensions were the same for each step, the immediate load increase varied between 8.3N and 10.4N. The immediate tissue extension did not relate directly to this load increase nor did the percentage relaxation. In fact the extremes of relaxation (44% and 65%) were related to load increases within 0.02N.

a)

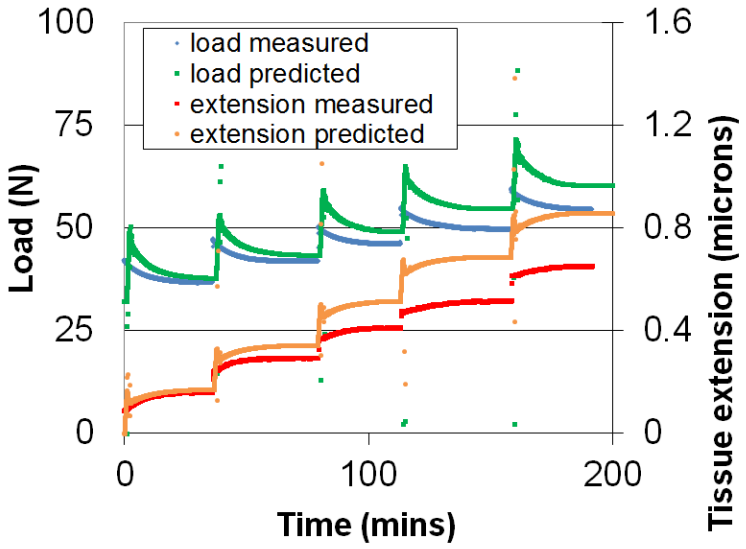

b)

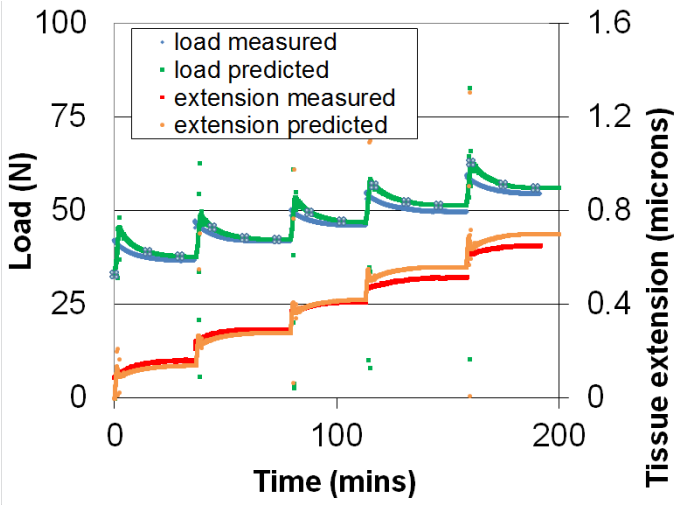

Figure 8-9 The measured values compared to the predicted load and deflection when pin stiffness was the theoretical 72N/mm and an additional device stiffness was added.

This highlighted the variability of the manual device, again attributed to a variation in device stiffness from the changing nut angle and shaft bending. When a pin stiffness of 72N/mm was used (from section 8.3.2) within the numerical simulation of the manual device, the predicted load and extension was considerably higher than the measured values (Figure 8-9). This suggested there were additional compliances that must be accounted for in order to fully characterise the device and pin combination. Finding the value of this stiffness, represented by k_d (Figure 8-10) was done by assuming 0.25mm of total extension and by noting the pre-distraction tissue extension and load increase. Thus the value of the additional spring in series was a combination of the pin stiffness and device stiffness.

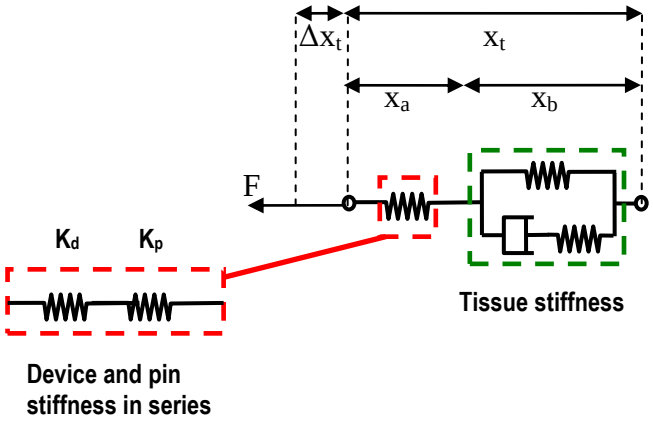

$$1/k_d = (\Delta x_t - \Delta x_b)/F_1 - 1/k_p$$

Figure 8-10 Additional spring stiffness from manual device

This calculation was performed for the 5 steps using k_p = 72N/mm for 70mm pin length. Values for F_1 ranged from 2.9-5.1N and x_2 0.11-0.16mm. This gave the additional manual device stiffness to be 69.2N/mm. If this stiffness was placed in series then the simulation prediction was more accurate, to within 50microns (8%) after five steps (Figure 8-9b). Peak loads were predicted to within 4N for each step.

The next objective was to determine the ability of the model to predict the smart device performance and resulting tissue mechanics with offset loading. With the simulation updated to use the new contact stiffness values as suggested in section 8.3.2 and a pin stiffness of 72N/mm, the simulated extensions and loads are shown in Figure 8-11a. The predicted tissue extension was 19% lower than the measured value and hence the simulated load increase per cycle was significantly lower than the experimental value. This implied that the simulated pin stiffness was too low and when increased to 160N/mm

the tissue extension was significantly closer to the measured value (Figure 8-11b). This highlighted the importance of individual analysis of devices as it had been previously assumed that the pin stiffness of the two devices would be the same. In fact, the manual device had a significantly lower offset stiffness (likely to be related to clamp stiffness) than the automated device. The measured load increase was considerably higher than predicted.

a)

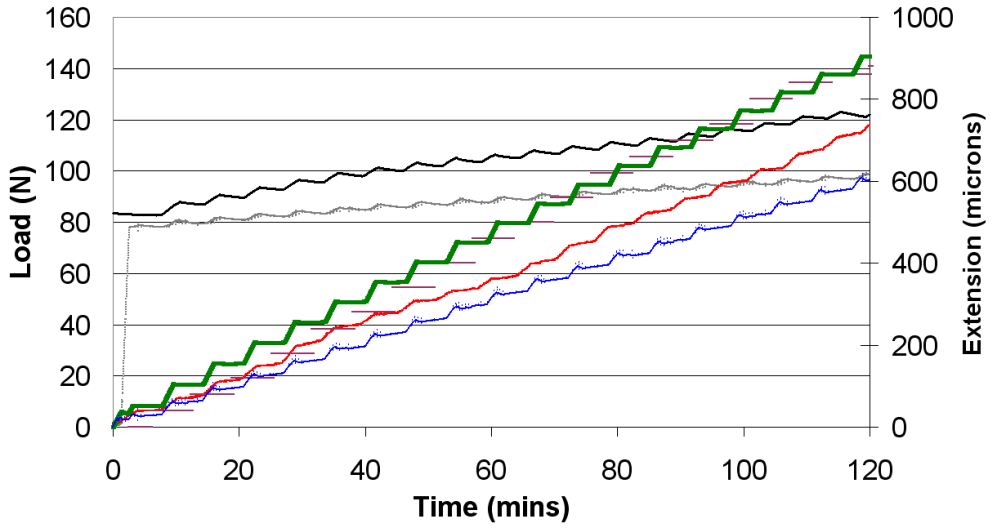

b)

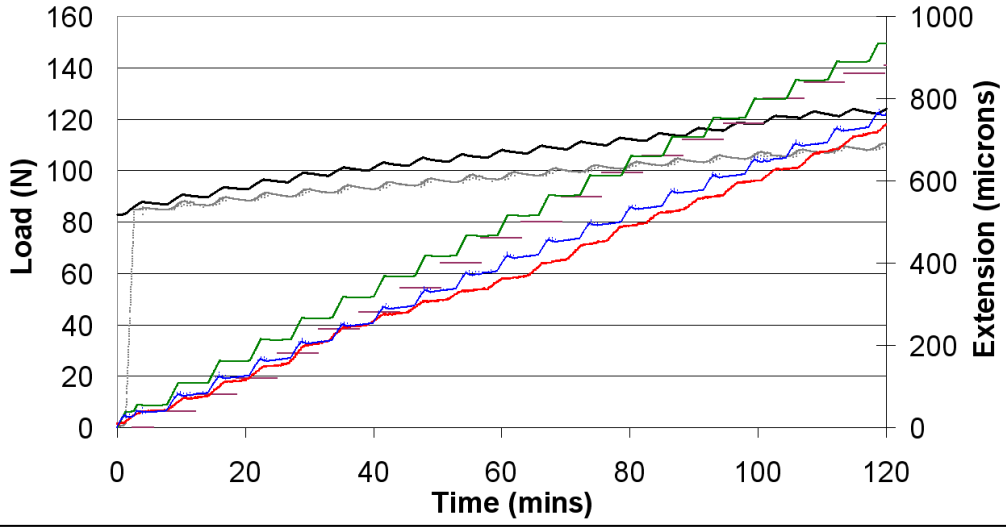

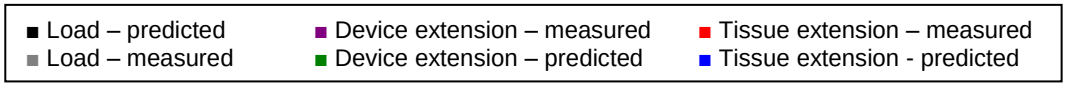

Figure 8-11 Comparison of predicted and experimental output. a) 72N/mm pin stiffness in model b) 160N/mm pin stiffness in model

Inspection of the profiles during charging and discharging of the actuator provided information on the source of the inaccuracies (Figure 8-12). It was deduced that

specifically the elastic stiffness (k_1) within the tissue model was too low, as the magnitude of relaxation was correct. Comparison of the values for tissue extension revealed that the proportion of creep response to total extension was 27% and the gradients of extension over time matched very well for some cycles, although there was variability in the measured data shown clearly in Figure 8-12b.

a)

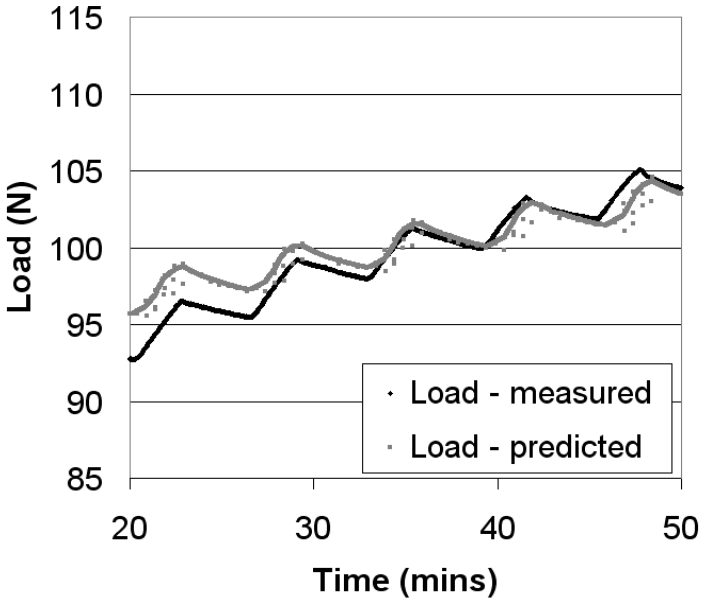

b)

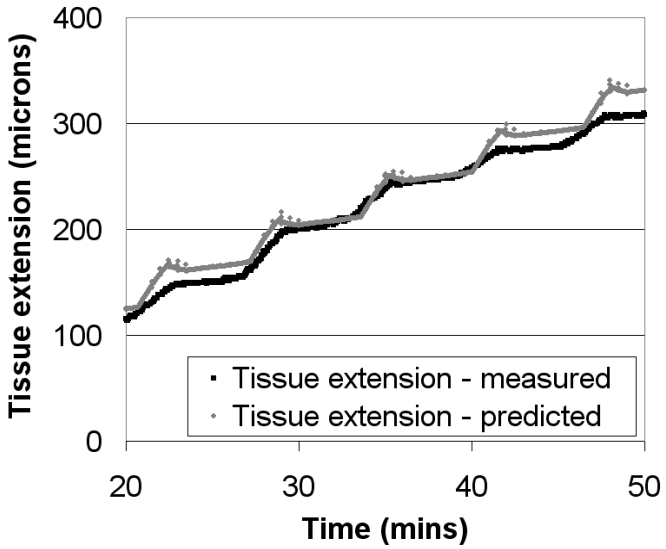

Figure 8-12 Analysis of (a) load and (b) extension profiles for predicted and measured device outputs.

The third study analysed the influence of changing one of the model variables – the pin length. A reduction in pin length was expected to be accompanied by an increase in stiffness. The measured pin and device stiffness for 50mm pin length was 84N/mm. This

was when the plates were not restrained. Interestingly, the pin stiffness measured during extension using the manual device was higher (110N/mm) than this previous test has suggested. Figure 8-13 compares the profiles of measured and predicted loads and extension. The profiles are very similar, including the creep response of the tissue extension.

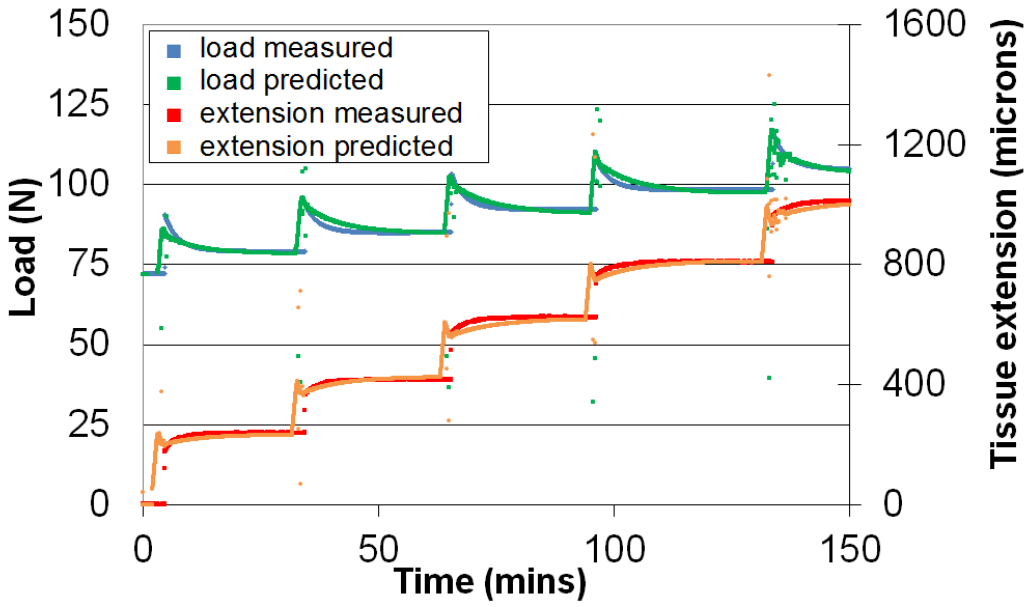

Figure 8-13 Comparison of predicted and experimental load and displacement when varying pin length using manual device

The immediate extension per cycle was, as expected, higher than with the shorter pins, at 75% of the total extension. Theoretically the percentage load relaxation for shorter pins (i.e. higher stiffness) would have been slightly reduced, but interestingly it was also slightly higher at 62% compared to 54% for longer pins. This could have been due to a change in the resting load from spring positioning or previously identified temperature effects.

When calculated from data during testing, the pin stiffness for the smart device was found to be much higher, at ~300N/mm. The load profile matched very well, to within 1N for 60% of the cycles while the displacement profile and values were within 11% after 800microns of extension (Figure 8-14). (Note: the experimental load increase for this case was considerably lower than for the longer pins, only 24N over an 800micron distraction. Therefore it was suggested that the load readings from the longer pin case were inaccurate.) In order to accurately predict the loads and extensions when using pins in the model, the importance of quantifying pin and clamp stiffness for individual devices

has been highlighted. It is suggested that calibration should take place at both extremes of pin length in order to better estimate the stiffness of the range of pin lengths used across patient groups.

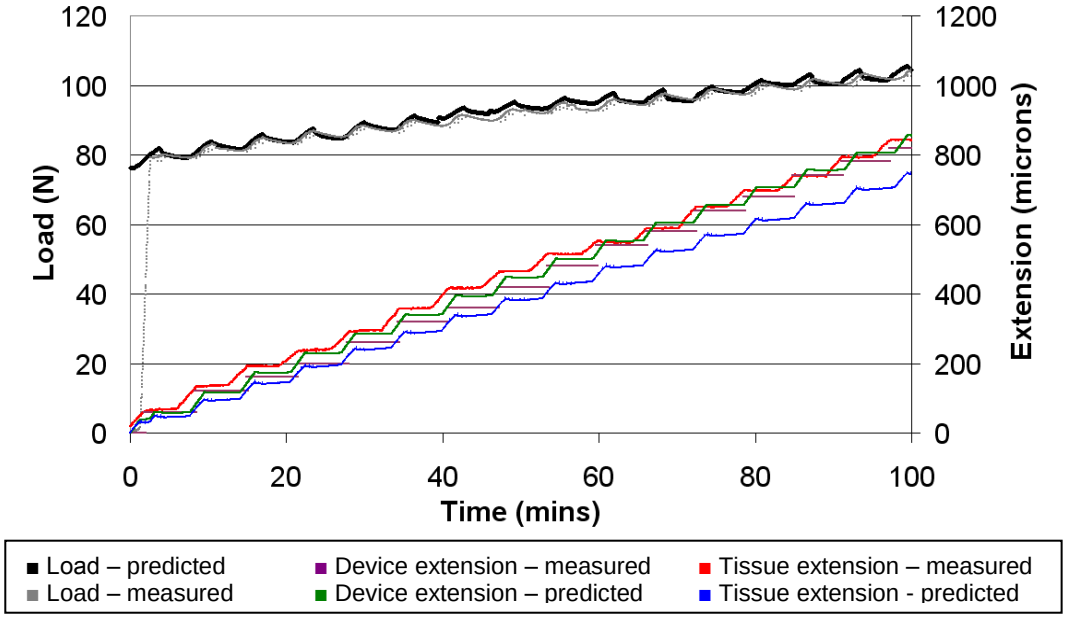

Figure 8-14 Comparison of predicted and experimental load and displacement when varying pin length using manual device

The final investigation was to analyse the effect of changing the percentage relaxation (as in Chapter 7) and assess the ability of the model to predict the tissue mechanics. The pin stiffness was set to the previously used 160N/mm and the spring stiffness used was 80N/mm as used in Chapter 7. With increased spring stiffness it was hypothesised that there would be an increase in the immediate load increase and lower percentage creep over time. This was found to be true, both in the experimental results and model predictions.

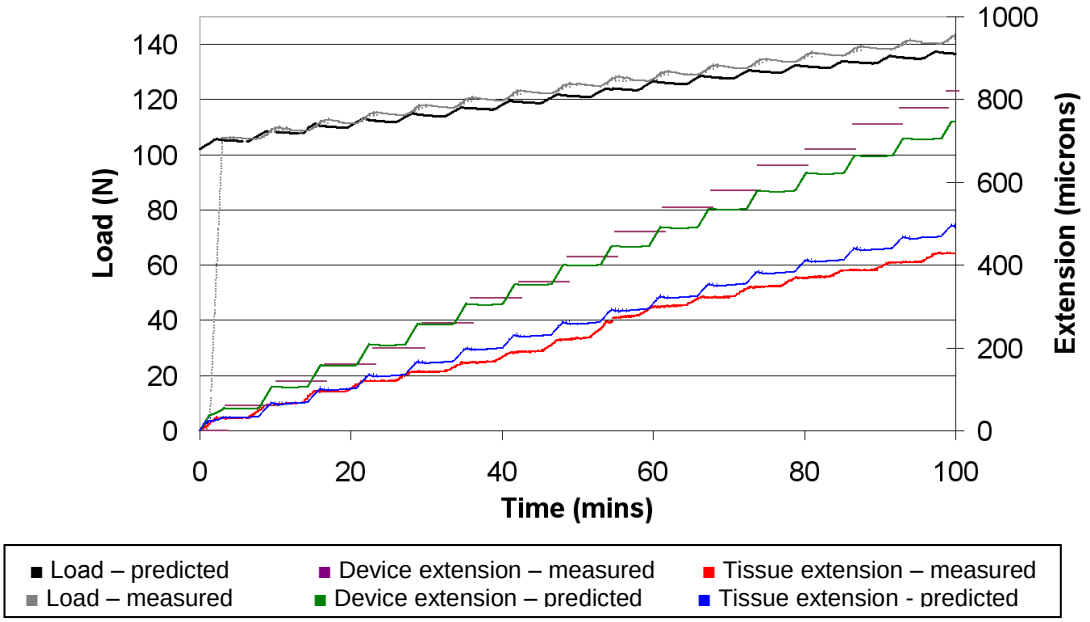

Figure 8-15 Comparison of predicted and measured outputs with a change in percentage relaxation

The shaft extension was slightly lower than the measured values (by about 6%) and the tissue load and extensions were within 17%. This suggests that the pin stiffness was not exactly the same as the previous test which may have been due to a difference in the tightening of the pin clamps on either the device or rig, or a slight difference in pin length. Load profiles matched very well as seen in Figure 8-16 but interestingly the extension profile revealed that as well as being low in gradient, the measured increase in extension was slightly slower than predicted, with a reduced final value. Extension of the tissue was the driver for load increase so this was an unusual and unexplained outcome.

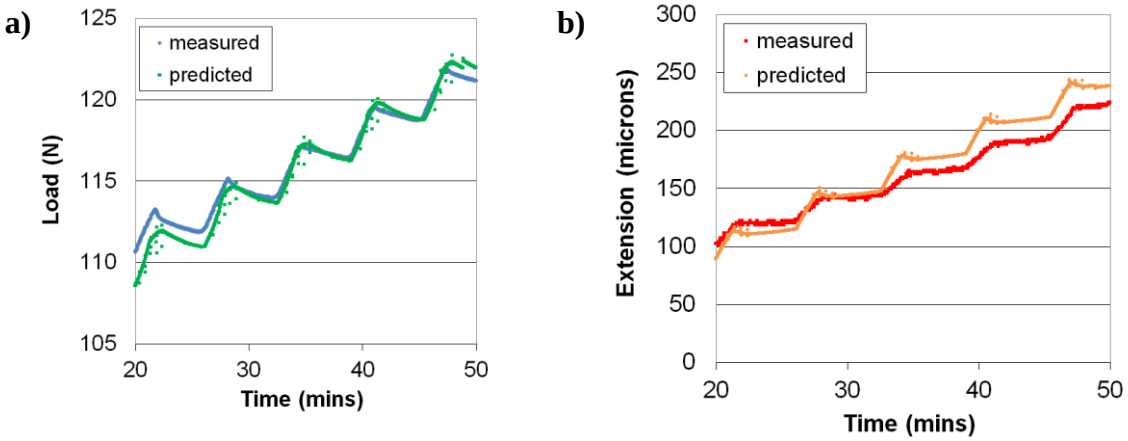

Figure 8-16 Examination of the a) load and b) extension profiles for model predicting output with change in percentage relaxation

The short peak at the end of the device charging phase was simply a feature of the model due to the 60second delay in the tissue model in recognising a discharge and thus was ignored.

8.4 Discussion

The aim of this Chapter was to determine the ability of the model to predict the response of the device to offset loading and the associated tissue response during manual and automated lengthening. The model was very specific to the mechanics of the device and as such required a full evaluation of the mechanical characteristics before it was able to predict device performance and the influence on tissues. However, once these were quantified, the predicted extension of the device and the load through the tissue were similar to experimental measurements. The shape of the extension and load profiles of the tissue was of particular interest as these provided information as to the dynamics of both the device and the tissue deformations. These were predicted well by the model and were found to change in accordance with the pin length and percentage relaxation of the tissue model.

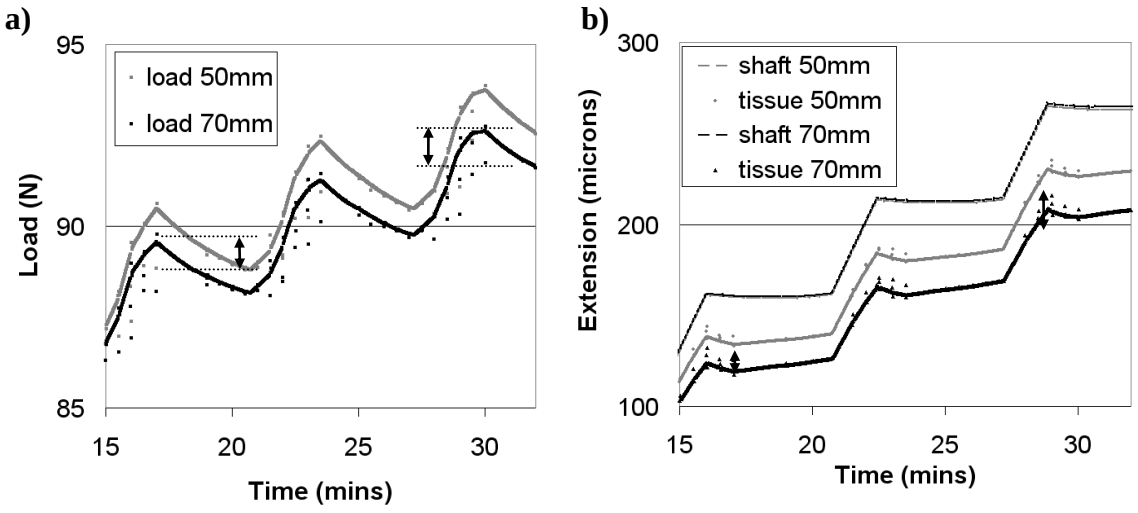

Figure 8-17 Comparison of simulated a) load and b) extensions for models with different pin lengths

For a change in pin length there was little difference between the shapes of the load and shaft extension profiles but the tissue extension was more interesting (Figure 8-17b). As

the device was charged the extension of the tissue was found to increase almost linearly for shorter pins compared to the more curved response of the longer pin length. This curve resulted in lower tissue extension per cycle compared to the shorter pin length and was due to the lower stiffness and therefore increased pin deflection. Although increasing the pin length was found to reduce the peak load through the tissue following an extension (i.e. a positive clinical effect), very low stiffness pins permit tissue deformities and can allow excessive load through the tissue during load bearing and as such should be avoided.

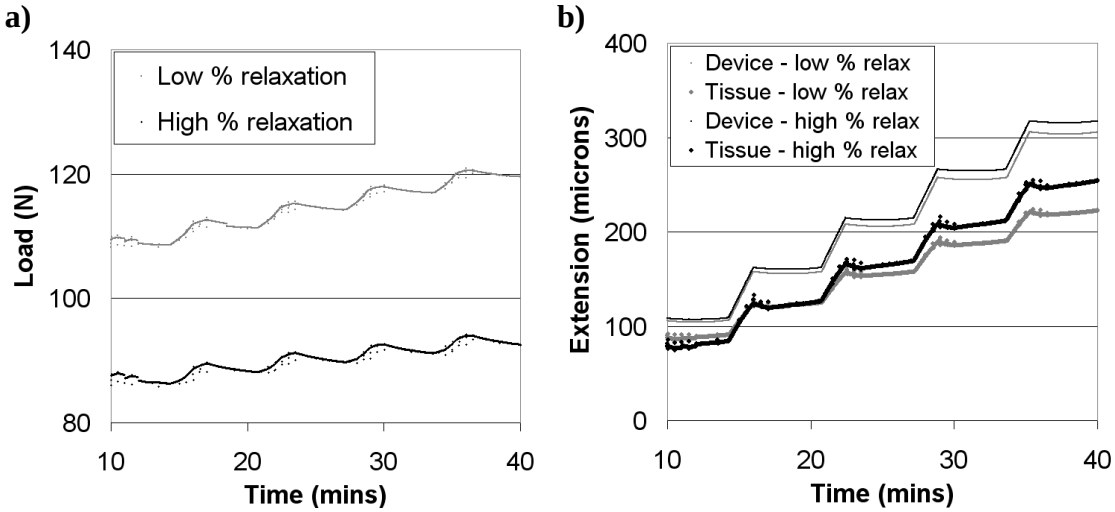

Figure 8-18 Comparison of simulated a) load and b) extension for models with different percentage relaxation

In terms of the comparative profiles, as expected, there was a higher percentage relaxation and therefore a lower value of total load increase over the cycle when the tissue spring stiffness was decreased (Figure 8-18). There was also a higher extension during charging, which still had the curved profile but was of a higher gradient. A higher relaxation required more device cycles to achieve the extension - this has implications on power requirements.

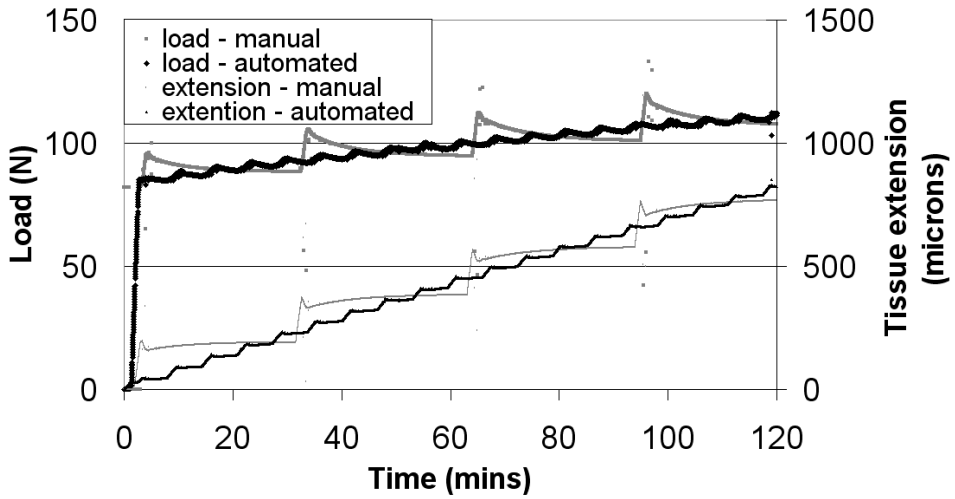

Figure 8-19 Comparison between simulated manual device and automated device outputs for same extension

The final comparison to be made between results was for the manual and automated device loads and extensions. For the same extension (0.8mm) the final load increase was almost identical but the peak load for the manual device was 13N greater than the automated device (Figure 8-19). This was dependent on the specific tissue characteristics and could be much larger in the clinical situation.

This modeling highlighted the cyclic variability within the device. The quantitative difference this made when comparing 50mm pins to the extremes of device extension per cycle is shown in Figure 8-20.

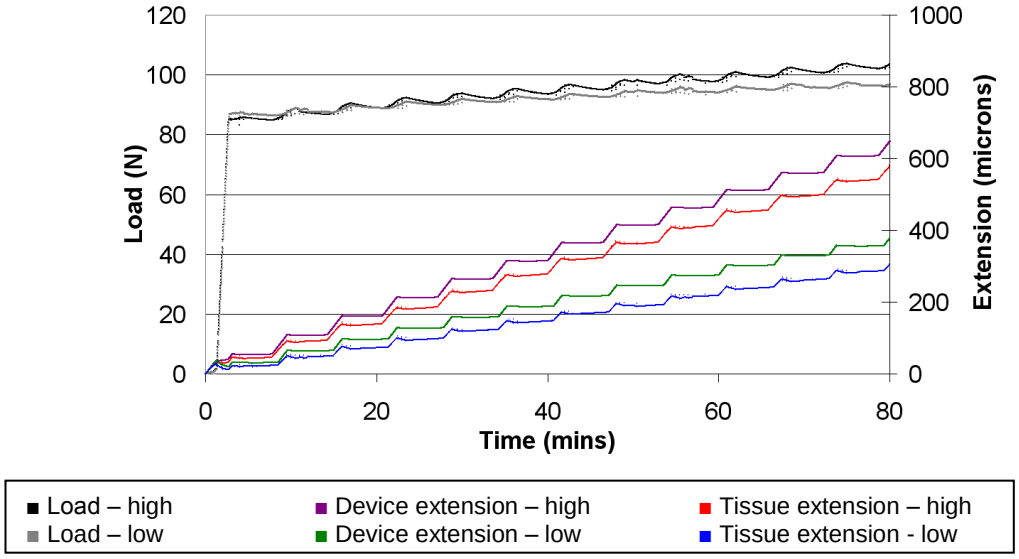

Figure 8-20 Comparison of device outputs with extremes of extension per cycle under same initial load – rotational variability.

As expected, extensions were more than doubled and the load increase was reduced, emphasising that this large variation in device performance must be reduced where possible. This should include assessment of the interfaces and tolerance values for the threaded components. The pin clamps were found to contribute substantially to the bending and further analysis may determine the specific impact this had on the device performance and the improvement that might be possible were design changes to be made. Additionally, the design of the control system could take into account some of the findings from this study, such as the delayed tissue extension. For example it might be beneficial to increase the initial extension rate of the device for each cycle to maintain a more constant increase in tissue extension that would result in lower tissue loads and improved outcomes.

It has been shown that the inclusion of pins, resulting in offset loading, has introduced effects such as creep that change both the value and timing of load through the tissue. Therefore they play an important role in the successful modeling of a system through which to evaluate limb lengthening devices.

Chapter 9

A simplified model for bone healing

9.1.Introduction

The present study has used viscoelastic models to represent the immediate stress relaxation in the tissue that follows step distractions in limb lengthening procedures. It has been suggested that, alongside this short-term response, there is also a longer-term change in the resistive response of tissue to distraction (Simpson *et al.*, 1996; Gardner *et al.*, 1998; Wolfson *et al.*, 1990), referred to here as a 'healing' response. In order to fully represent the loading conditions on the device, these changes were to be included in the model.

The viscoelastic numerical model has assumed that the resistance to extension during limb lengthening is as a result of both hard and soft tissues. Both of these tissues undergo longer term changes over the course of the lengthening procedure. However, the complex biological process of DO, i.e. the formation of bone tissue, has been more closely examined and the changing mechanical characteristics of newly formed tissues have been linked to these biological processes through histological examination. Consequently, this section will focus on the long term healing of the regenerated bone tissue (the newly formed tissue between the two bone ends).

Alterations of tissue properties within the bone regenerate are as a result of cell birth (proliferation), maturation and differentiation. It is these cell processes that have been modelled numerically by various authors in order to try to simulate the distraction osteogenesis process. Using Finite Element methods, they predict the transition from newly formed low stiffness regenerate through to calcified bone cells after the consolidation period (Isaksson *et al.*, 2007; Reina-Romo *et al.*, 2009a). These models are

updated at discrete time intervals throughout the complete DO process, modifying the mechanical properties and geometry according to the mechanical stimulus at each step.

Current mechanobiological methods are complex and costly in terms of software and time and do not always focus on the resistive forces. Instead attention is given to the pattern of developing tissues and biological processes.

Therefore, a simplified numerical model was built to represent the healing processes that exist within the bone tissue. This model focussed on the effects these have on load as a result of tissue extension over time. The aim is that, following validation, this model can then be coupled with the short-term viscoelastic model to provide a fully representative model of the distraction process for the evaluation of devices and/or control regimes (Figure 9-1).

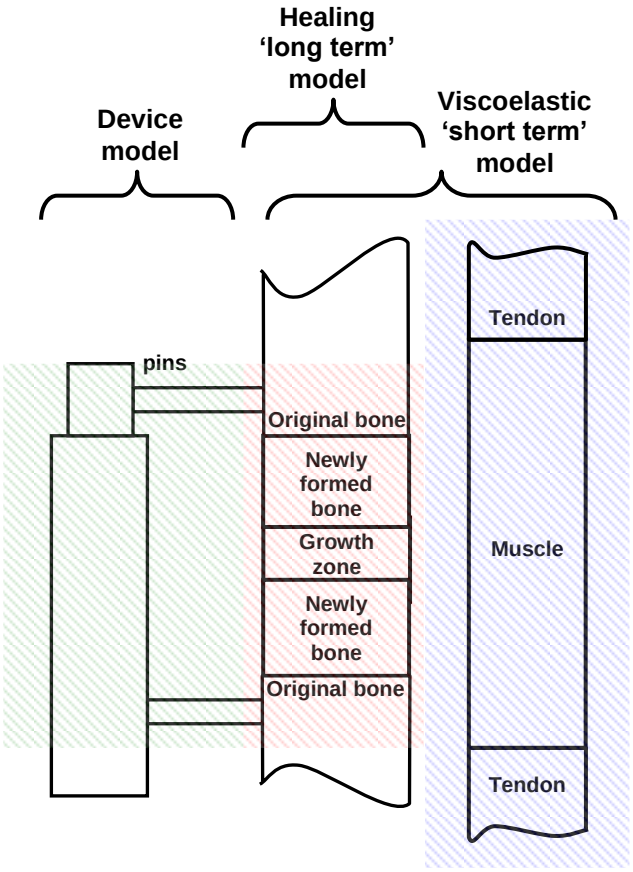

Figure 9-1 Model components and construction

The main assumption for this model was that the longer term effects were a result of bone healing and that the soft tissue relaxations were more accurately predicted by the short term viscoelastic healing model.

This model was developed as an initial representation of the healing process of the bone for the purposes of integration with the full limb lengthening model, describing the mechanical environment for both the distracted tissue and extension device. As such, it was designed to be 'simple' alternative and not a challenge to the larger complex models.
This Chapter describes the development of potential models, their characteristics and outputs, with focus on the global parameters that affect the load seen by the device such as tissue stiffness rather than the specific biological changes and tissue patterns seen during healing.

9.2 Model characteristics

The first requirement was to simulate the cells changing from one tissue type (and stiffness) to another over time. The way in which this has been achieved in previous models varies. Mechanobiological models have been used to predict the stimulus that affects differentiation from one cell type to another throughout fracture healing. They use FE to model a section of bone with the fracture gap filled with undifferentiated callus, subject it to forces and predict the tissue differentiation from the resultant stress and strain magnitudes and patterns (including shear strain) (Carter *et al.*, 1998). Although not strictly true, a reasonable simplification used in fracture healing models is to suppose that all the cells required for complete healing are in existence at the beginning of the model and that over time these change into higher stiffness phenotypes. Although the same differentiation process can be used in the DO model, it is obvious that there is a growth in the tissue on a macro level and that the number of cells between the bone ends is, in fact, increasing over time. This requires cell birth, or proliferation of mesenchymal stem cells (MSCs). More sophisticated mechanoregulation models use stimulus-dependent cell proliferation alongside differentiation to change the number of cells as well as cell location, predicting the progression of tissues in fracture healing or distraction osteogenesis over a number of time periods.
The mechanical stimulus must be chosen to control the rate of cell proliferation and differentiation. The level of stimulus determines which tissue phenotype the cell will become as well as the rate at which that transition occurs. Most authors use a stimulus related to the strain or hydrostatic stress within the tissue, proposing these as the precursor for communication between cells and subsequent biological events to occur (Pauwels, 1960; Carter *et al.*, 1998; Claes and Heigele, 1999). One hypothesis is that mechanical

strain invokes fluid flow within the tissues which results in a shear strain on the cells and that this shear strain influences the sensory pathways of the cells (Cowin and Moss, 2001). For this simplified model the stimulus was chosen to be the strain in the axial direction. The input for the model is longitudinal growth which is the same for the viscoelastic tissue model.

9.3 Model 1 – cell differentiation

9.3.1 Model description

A preliminary model was created to allow for problems in the modelling process to be identified. The symmetrical nature of the bone allowed for half of the growth zone and newly grown tissues to be represented as a series of springs with different stiffnesses (Figure 9-2).

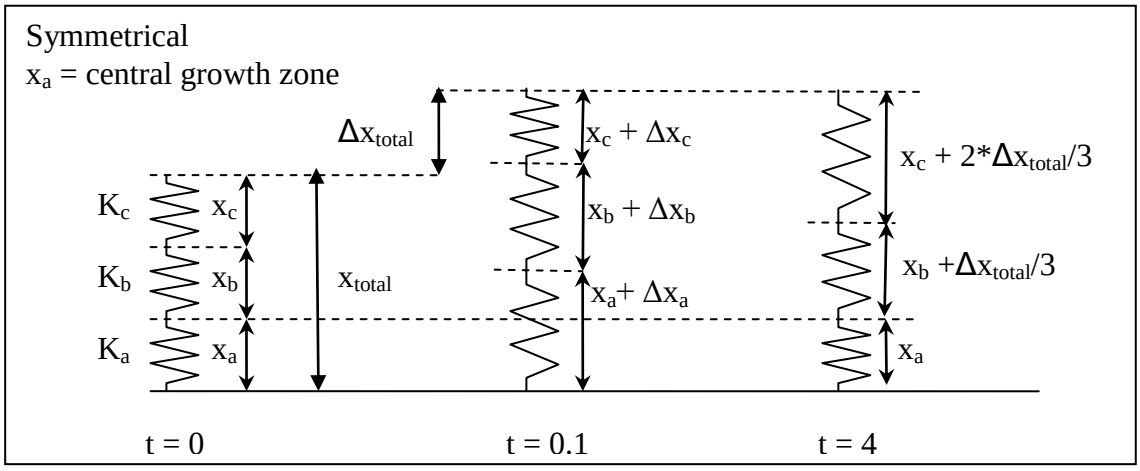

Figure 9-2 Representation of model 1 tissue extension and differentiation

The three tissue types were the central growth zone (CGZ) of granulation tissue (x_a), fibrocartilage (x_b) and boney callus (x_c). These have stiffnesses K_a, K_b and K_c respectively. Initially they were all one unit length and were extended by a total of ΔX_{total} every 4hours. Any individual increase in length depended on their respective stiffnesses.

$$X_{total} = x_a + x_b + x_c$$

$$\Delta X_{total} = \Delta x_a + \Delta x_b + \Delta x_c$$

if $K_a < K_b < K_c$

then $\Delta x_a > \Delta x_b > \Delta x_c$

It has been shown clinically that at an optimum rate of distraction the CGZ will stay a constant size (Ilizarov, 1989b) but in this model, if another extension were to take place

immediately, the CGZ would continue to extend the most, as it had the lowest stiffness. To address this, between each distraction the distributions of elastic extension were changed such that length x_a remained constant by increasing x_b and x_c (Figure 9.2). The proportion of x_a taken by x_b compared to x_c was varied and could be dependent on strain. Stiffnesses were 1N/mm, 5N/mm and 500N/mm for K_a, K_b and K_c respectively, where relative values were taken from data used by Lacroix and Prendergast, 2002; Claes and Hiegele, 1999; Isaksson *et al.*, 2006. The value used for ΔX_{total} was the standard 0.25mm and the full model can be found in Appendix F(i).

9.3.2 Model outputs

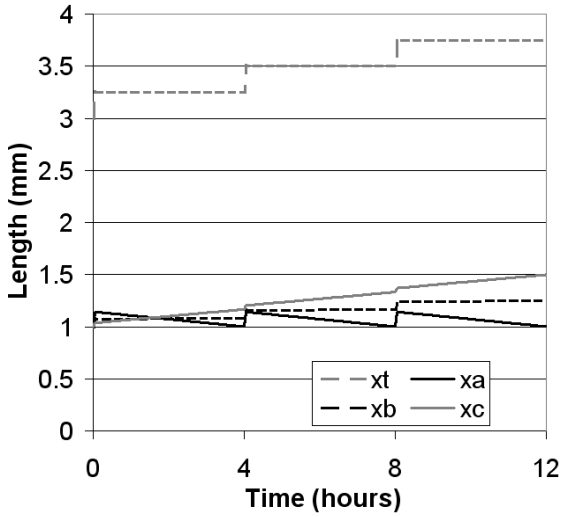

Figure 9-3 Lengths of springs a,b and c along with the total length

Figure 9-3 shows the lengths of each of the springs (x_a, x_b and x_c) extending over time, both as a result of the three steps of total length increase (x_t) and due to the changing proportions covered by each spring in order to keep the central growth zone (x_a) a constant size before distractions. In tissue terms, each distraction in the model resulted in immediate proliferation of cells then gradual differentiation of cells. New tissue was 'formed' (i.e. there was a change in length) in all three sections and then differentiated over time from section a to section b and c. This did not exactly mirror the biological method as new tissue would only be grown in the CGZ i.e. $\Delta x_a = \Delta x_t$, and $\Delta x_b = \Delta x_c = 0$. The model was tested under different rates of extension. If the rate was increased then the length of the CGZ increased as it did not have time to differentiate fully. If no additional distraction took place, differentiation continued to occur until $x_a = 0$. These two cases corresponded to the clinical cases of non-union and premature consolidation of the callus.

The rate at which the tissue differentiated could be dependent on factors such as strain or total tissue length.

As stated in the introduction, in this work the mechanical aspects of the distraction process - principally the reaction force - were of greatest importance. However, using this initial model, the load increase from each extension stayed constant as the tissue stiffness remained constant and so a more sophisticated model was required to approximate the loads within the tissues.

9.4 Model 2 – cell concentration

9.4.1 Model description

The model described in section 9.3 was improved to allow the stiffness of the tissues to change depending on the cell concentration level within each tissue. This was a 1D simplified version of the 'cell density' for areas and volumes used in 2D and 3D mechanobiological models. The system involved representing each of the tissues as a line with cells as shown in Figure 9-4. Each of the three zones behaved as a different tissue type with different stiffness, similar to the previous spring model, the total stiffness being calculated from the individual stiffnesses of the three zones. If extended, the strain in the CGZ stimulated cell proliferation. Proliferation only took place in the CGZ, not in the other zones.

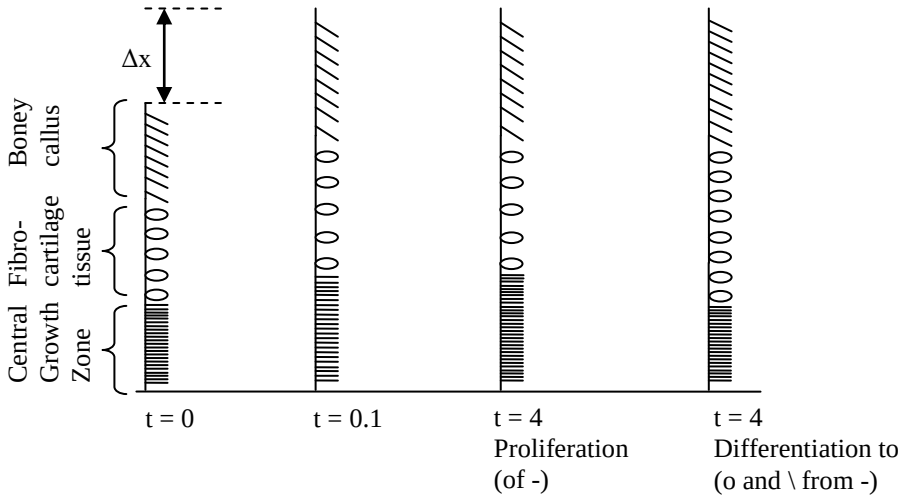

Figure 9-4 Simplified 1-D model using tissue concentration

From Figure 9-4, during distraction all three areas became less concentrated (t=0.1) due to elongation, particularly the CGZ (-) which lengthened the most (lowest stiffness). Over

time, and driven by strain and cell concentration, cells proliferated in the CGZ and simultaneously differentiated to other zones (t=4). This reduced the number of cells in the CGZ back to the original concentration. Correspondingly, the increase in the number of cells in the other two zones helped to maintain their concentration. This allowed cell proliferation to be distinct from differentiation.

For all zones there existed an optimum concentration and, as concentration was proportional to stiffness, this optimum stiffness referred to the stiffnesses defined in section 9.3.1. Decreasing the concentration decreased the stiffness of the tissue and vice versa. Under optimal distraction conditions (rate of 1mm/day) the stiffness of the whole system remained constant. The Simulink model can be found in Appendix F(ii).

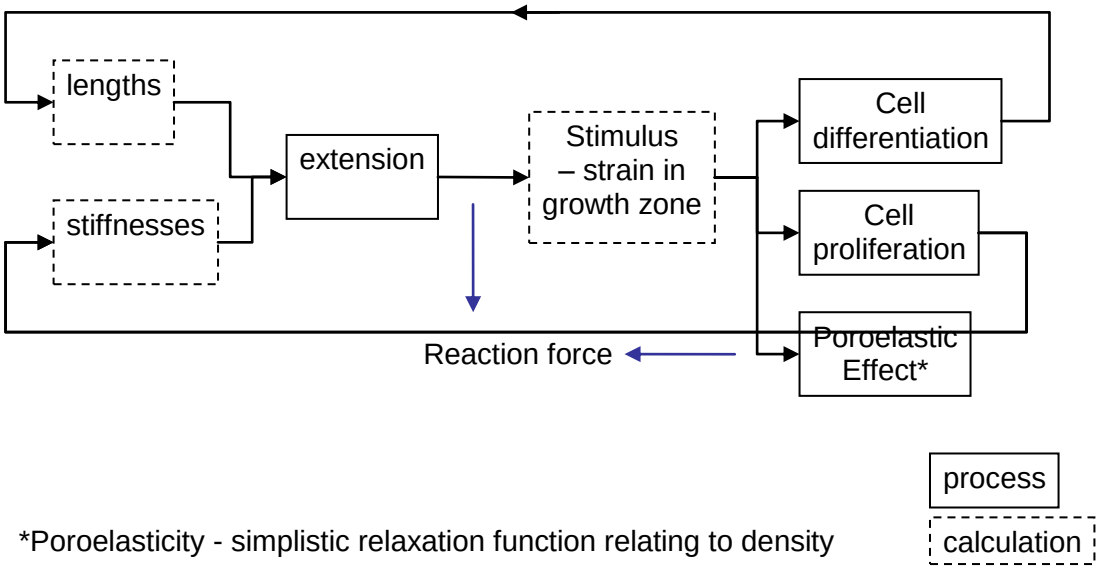

Figure 9-5 Process diagram for simplified mechanoregulation model

9.4.2 Model outputs

The tissue was extended at the same frequency (4steps/day) but using different rates of distraction. The effect of the rate of distraction on the lengths and stiffnesses of the tissues was analysed. Resulting lengths of each of the different tissues were plotted after a total extension of 3.5mm (Figure 9-6) for rates of 0.5-2mm/day.

The results show that as the rate increases the length of fibrous tissue (xb) increases and the CGZ increases whereas the length of boney tissue decreases.

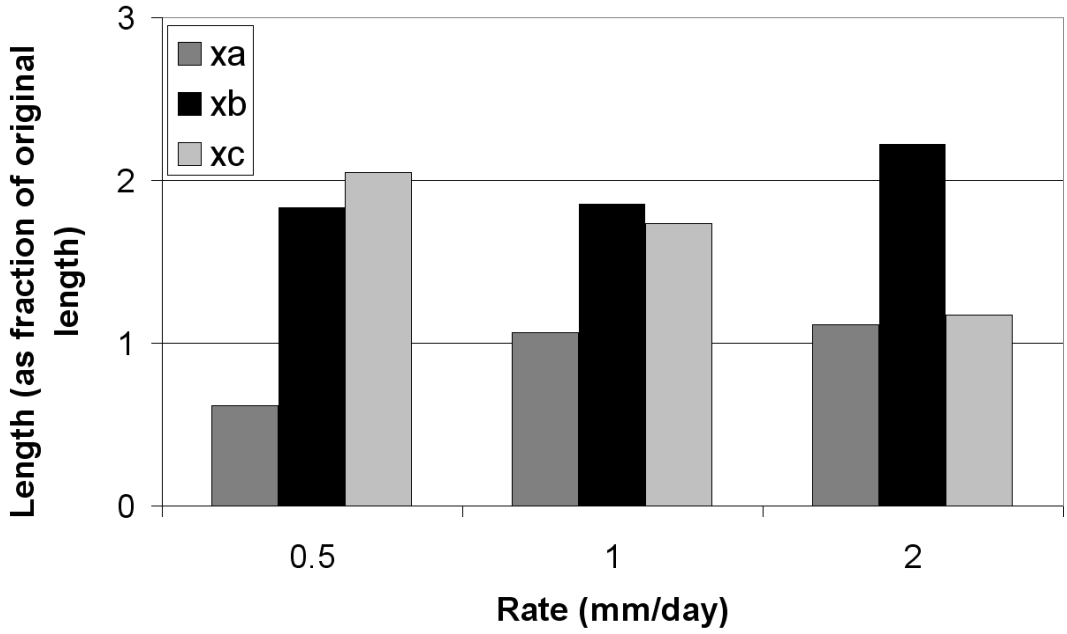

Figure 9-6 Lengths of tissues over time for varying distraction rates

X_a (representing the CGZ) remained relatively constant. Simulated outputs for a rate of 0.5mm/day showed a decrease in length of CGZ while at the higher rate of 2mm/day there was an increase in the length of the CGZ. As the length of the CGZ started to increase, the strain gradually decreased resulting in a levelling to a resting length around 50% greater than its original length. A notable increase in fibrous tissue was seen for the fast rate of 2mm/day while the length of boney tissue remained fairly constant for all rates.

Stiffnesses of both the fibrous tissue (k_b) and boney tissue (k_c) both increased when the rate was slow and decreased when the rate was high as expected. Although the total stiffness was influenced, it was still dominated by the stiffness of the newly formed tissue (k_a) due to the springs being in series (Figure 9-7).

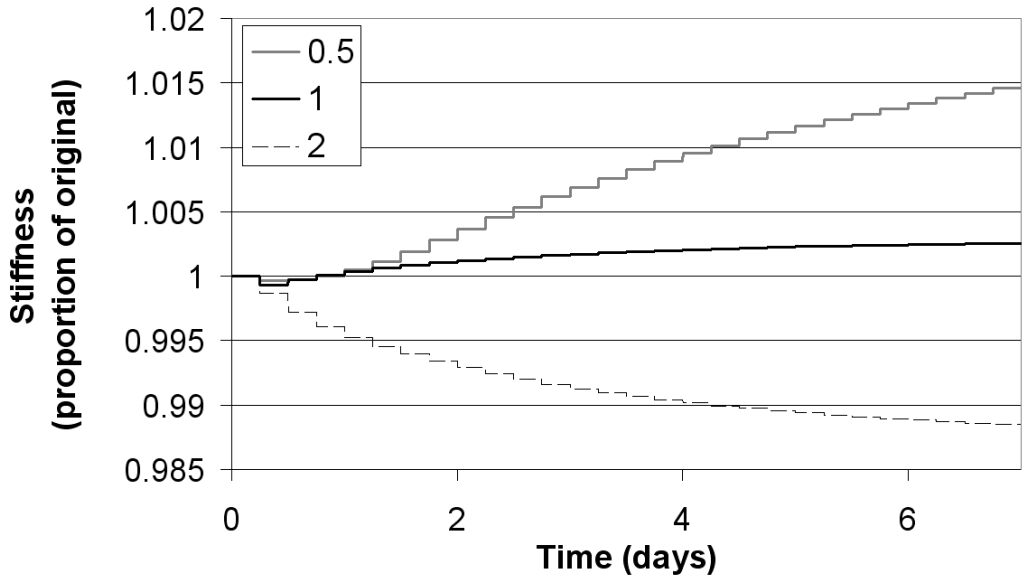

Figure 9-7 Total stiffness change depending on distraction rate

9.5 Model 3 - cell distribution

9.5.1 Model description

Although it was thought that tissue pattern was of little significance, the distribution of tissues with varying stiffness in series influenced the forces seen and therefore required further consideration. Isaksson's mechanoregulation model for DO (Isaksson *et al.*, 2007) could be said to present a relatively axial arrangement, with the different tissues in layers moving proximally and distally from the distraction gap. The model used by Reina-Romo *et al.* (2009a) instead shows a more radial arrangement of tissues. Most importantly the histograms from a study by Ohyama *et al.* (1994) show a combination of the two (Figure 9-8a). Reaction force was determined by stiffness in the axial direction but was influenced by the radial distribution of the tissues and was subsequently represented by springs in series and parallel, giving a total stiffness that was no longer dominated by the weakest tissue (Figure 9-8b).

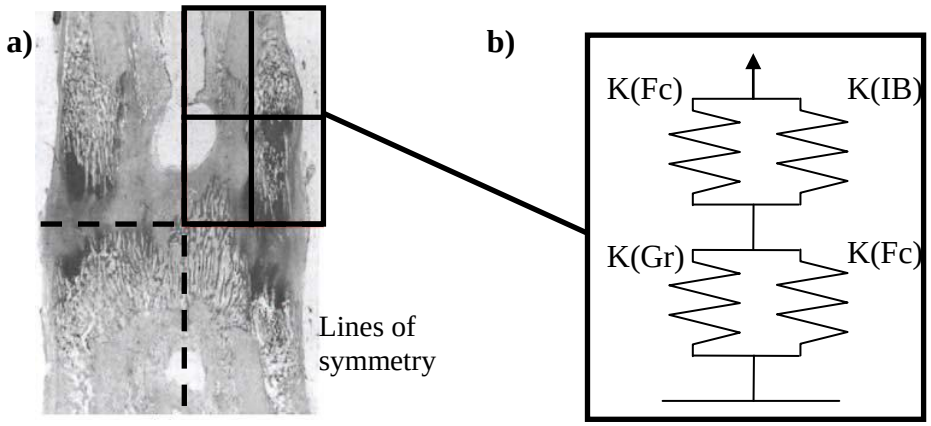

From Ohyama et al., (1994)

Figure 9-8 a) Histology sample of rabbit distraction zone b) Proposed simplified 1D model

The histology sample of the distraction zone for a rabbit (Figure 9-8a) show a high level of axial symmetry and thus could be modelled as illustrated in Figure 9-8b. The sample pattern shows a higher proportion of cartilage cells towards the exterior of the bone and more bone cells towards the top of the image, away from the growth zone (Ohyama *et al*., 1994). Consequently the spring representing the granulation tissue was positioned on the central axis with the boney cells spring towards the exterior.

An additional change to this model was that the rate of proliferation was determined not only by the strain in the CGZ but also by the density in this zone. In the same way the differentiation was controlled by the strain and cell concentrations within both the CGZ and other tissues. The model can be found in Appendix F(iii)

9.5.2 Model outputs

The model outputs for the four tissues are displayed as four blocks instead of springs, using colour gradient to give a qualitative representation of tissue stiffness alongside the quantitative value of tissue length (Figure 9-9a).

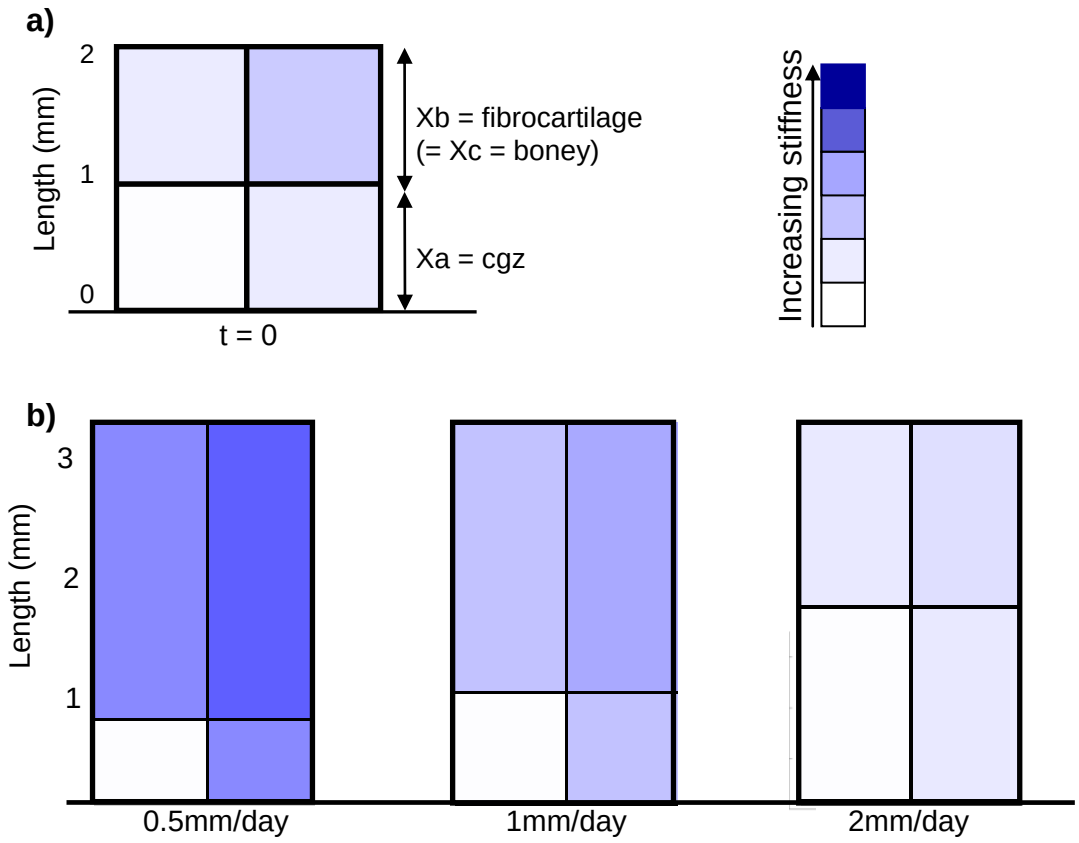

Figure 9-9 a) Model at t=0 b) Model outputs for extension of tissues to 3mm with varying distraction rates

As shown in Figure 9-9b above, a rate of <1mm/day decreased the size of the growth zone, indicating possible premature consolidation, while increasing the rate above 1mm/day increased the size of the growth zone – a precursor to malunion. The model predicts that the stiffness of the fibrous tissue and boney tissue would increase for low rates while decreasing for higher rates, as suggested by experimental data (Ilizarov, 1989b). This change in stiffness changes the load increase during distraction.

Some authors have included a short term effect in their models called a 'poroelastic effect', representing fluid flow through the tissues and resulting in a temporary force increase. This was added to the model, (made relative to cell concentrations) bringing a degree of shorter term changes to the regenerate model alongside those experienced with the soft tissue model. The cumulative reaction force was predicted to decrease with higher extension but the immediate peak due to extension increased with the larger step size (Figure 9-10).

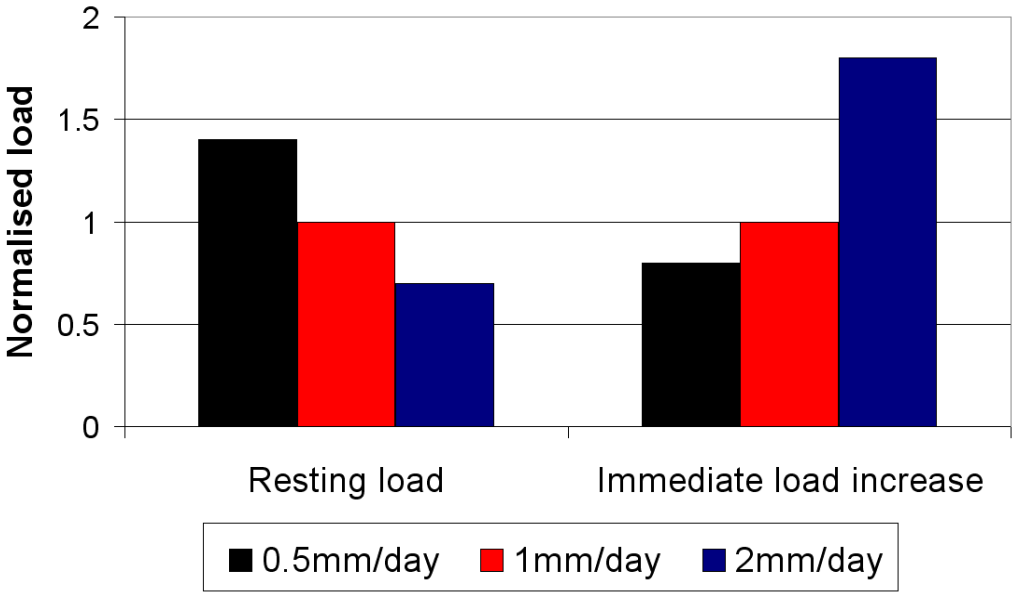

Figure 9-10 Normalised loads (to 1mm/day) after 30mm lengthening for varying distraction rates

Normalising the load to the values for a rate of 1mm/day highlighted the change in both resting load and immediate load increase when the rate increases or decreases. The resting load (i.e. the pre-distraction load) increased with a rate of 0.5 but the immediate load increase was less than for higher rates. This model gave a simple method of changing the immediate load increase from the callus tissue that would eventually be coupled with the tissue model which simulates the immediate load increase from the soft tissue.

9.6 Discussion

The development of a simplified mechanobiological model to modify the stiffnesses according to distraction rate has been described. During the development assumptions were made regarding some of the biological events and parameter values as their true nature is, as yet, uncertain. The mechanical stimuli for cell proliferation and differentiation have not been explicitly defined, especially the specific levels at which tissues select different differentiation pathways or rates of proliferation. In the four spring tissue models the stimulus for proliferation was taken to be strain within the CGZ alongside its concentration. This was similar to other authors (Reina-Romo *et al.*, 2009a), although they took the second invariant of the deviatoric strain tensor which was not

possible in a one dimensional model). There was a direct relationship between strain and rate of differentiation to certain saturation levels (Figure 9-11). The interfragmentary strain theory developed by Perren (1979) suggested that tissue could not reside in an area that is subject to higher strains than it can withstand, the implication being that high strains may prevent proliferation or differentiation to specific tissues. In this case, the link between strain and proliferation could be more akin to Figure 9-11. Here, the proliferation and differentiation are never above optimum and become zero at the extremes of strain.

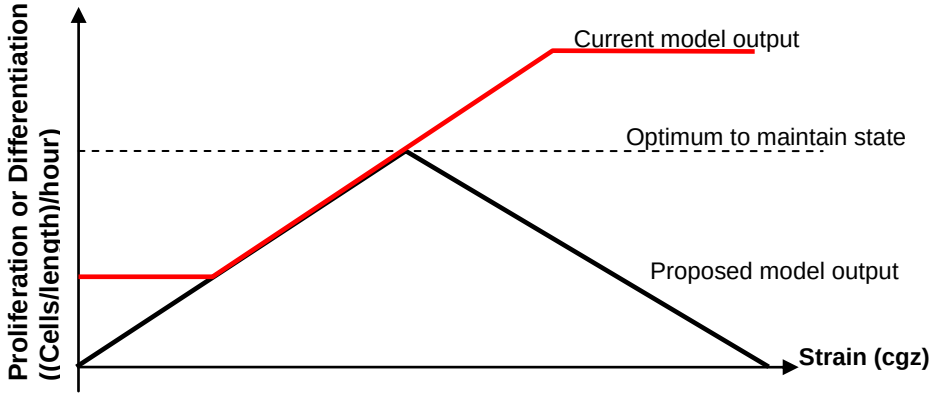

Figure 9-11 Proliferation and differentiation related to strain in the CGZ

Using this relationship (Figure 9-11), the increase per hour is constant (Figure 9-12a), but this may better be represented as a non-constant increase over time to the saturation level, or indeed the optimum level (Figure 9-12b).

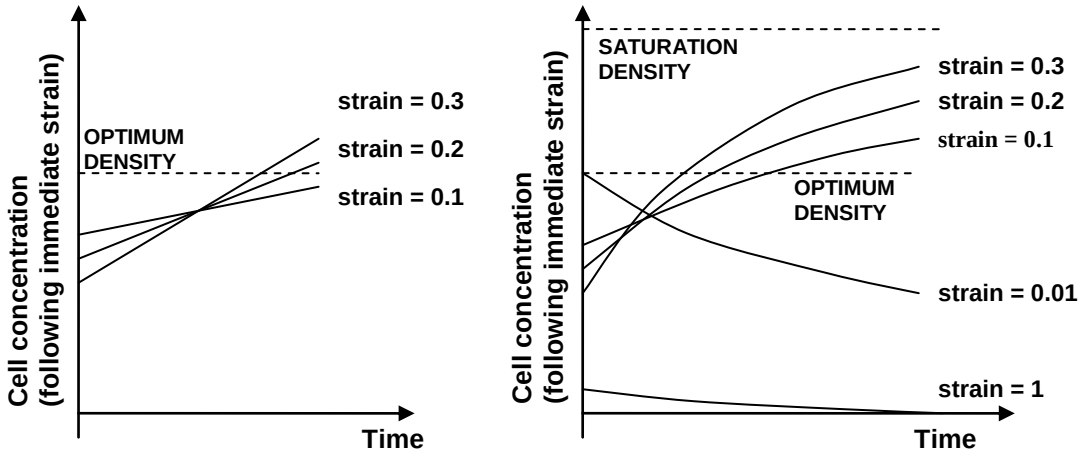

Figure 9-12 Proliferation rates over time a) current model b) alternative model

The material properties of the tissue were based on values from other numerical models of this kind. Isaksson *et al*. (2009) studied the effect of material properties on the models and found that some parameters were more influential than others, with the Youngs modulus of cartilage having a significant effect on the mechanical stability and amount of bone formation at each stage, proving the requirement for accuracy in selection of material stiffness values.

The poroelastic effect has been modelled by Morgan *et al*,. (2006) who predicted a reduction in total pressure of over 70% within the first 20minutes, with fluid velocities reaching zero after 10minutes. Their timescale was 12hr and only one step was simulated therefore no longer term healing effects were modelled. Two models (Reina-Romo *et al*., 2009b; Isaksson *et al*., 2007) analyse the reaction force from each step of distraction, however only one correlated their computation results with those found experimentally. The other predicted a decrease in reaction force throughout the distraction period when in fact this tends to increase (Isaksson *et al*., 2007).

Frequency of distraction affected the poroelastic force addition but was not a focus of the model as clinical data is limited. It is known that the regenerated tissues, including nerves, can be improved in quality when high frequency distraction is used but the effect this has on the long term tissue stiffness and resultant resistance to loading is, as yet, unclear. Because of the long term nature of this model the output (load) did not considerably vary from minute to minute as in the viscoelastic model. It was therefore acceptable to obtain the extension over four (or eight) hours and take this as the input to the model instead of a continuous input.

In summary, the model has been able to show clinically relevant characteristics such as an increase in fibrous tissue when distraction rates were high and an increase in high stiffness boney tissue when rates were low. Additionally, the tissue stiffness was found to increase if rates were low which resulted in higher resistive forces. Alongside further quantitative validation, this simplified mechanobiological model could be used as a tool, alongside the existing tissue model (Chapter 7) to suggest changes in tissue stiffness (k_1 and k_2) that occur during DO, where these parameters may be result of combining the stiffnesses of more than one tissue type.

Chapter 10

Model Application

10.1 Introduction

The numerical models of both the distraction device and tissue have been developed to enable a representation of the complete mechanical environment during limb lengthening. Previous Chapters describe the validation of elements of the model completed using data from experimental testing. Although the healing model proposed in Chapter 9 plays an important part in understanding the longer term tissue characteristics and consequent loading, there is insufficient clinical data to validate the quantitative output of the model so the focus here was on the short-term implementation of the models from Chapters 5-8. Following their validation, the practical implementation of the complete model is now shown. In this Chapter, published data of clinical loads during lengthening are used to calibrate the tissue model. A comparison has been made between two existing data sets and the resultant model values. Once calibrated, the model can then be used to predict future loading patterns for two different lengthening devices. Additionally, the numerical model can be used to predict the influence of device design changes for performance optimisation purposes. With the availability of more clinical data sets, the model will become increasingly viable as a method for predicting the range of forces during lengthening using a variety of devices and lengthening regimes.

10.2 Calibrating model to clinical data

10.2.1 Materials

Two sets of well-established clinical data from widely cited sources were selected for use. These are referred to as data set A (Simpson *et al*., 1996), and data set B (Aarnes *et al.*, 2002a) for clarity. Both research groups used load cells mounted in an external fixator to monitor the forces during lengthening procedures *in vivo*. Lengthening was carried out by 0.25mm increments. Data set A provided continuous load data for 3hrs after each extension. Data set B gave pre- and post-distraction forces for four-hourly distractions during daytime hours lasting three days. No additional data points were given between the pre- and post-distraction values but suggestion was made in their discussion that the decay was likely to have been exponential. Despite this observation, linear interpolation between recorded points is implied by drawing straight lines between data points. Nevertheless, it can be seen that the trends strongly support their argument. (An animal tissue study was conducted to attempt to collect *ex vivo* data to support the existing clinical data and, although outputs were interesting, the load results for manual and automated extension were not truly comparative. Details can be found in Appendix G.)

10.2.2 Methods

The model can be calibrated using either of these data sets. This is done by the evaluation of the parameters k_1, k_2 and η_2 as described in Chapter 7. The differences in the data sets (described in 10.2.1) means that they can be used to show variation in tissue forces expected from different patients during distraction. Additionally, the fact that one data set provides load data for three days allows it to be used for further validation of the tissue model.

The hypothesis was that, once calibrated using specific data, the model outputs are not transferable to different patients using different devices for different indications. To test this hypothesis the model was calibrated to data set A, model outputs were plotted alongside data set B and the differences analysed.

To assess the capability of the model to predict future loading patterns using clinical measurements, data set B was used. This provided tissue loads for three full days of lengthening. The model was calibrated using the data from one day of lengthening (day 44), then the predicted loads for the following two days (days 45, 46) were compared to measured values.

10.2.3 Results

The continuous data from data set A demonstrated the viscoelastic nature of tissue very well. The data shows that the load increase of 50N from an applied 0.25mm elongation reduced exponentially by 40N over a period of 2hrs (Figure 10-1).

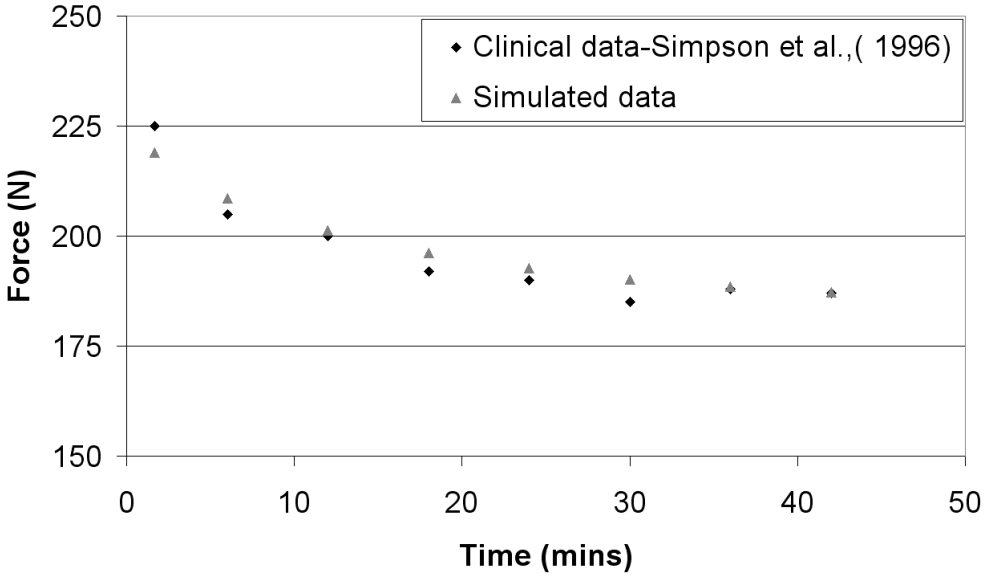

Figure 10-1 Simulating clinical data from Simpson *et al.* (1996)

Eight data points at six minute intervals were used to define the exponential decay for both the experimental and modelled relaxation curve. The correlation coefficient (R^2) between predicted and experimental data was calculated to be 0.92, giving an indication of the ability of the model to predict the experimental data points. Thus, the model can be satisfactorily calibrated to clinical data for load relaxation in tissues.

The calibrated model output for one extension (using data set A) was extrapolated to four extensions for comparison with data set B. This extrapolated set of results shows that the load stopped decreasing some way before the next 4 hourly distraction, and thus there was no residual loading to be included in the next step.

Figure 10-2 shows that, when calibrated using data set A for one patient, the simulated model could not be used to predict the loads during lengthening for other patients.

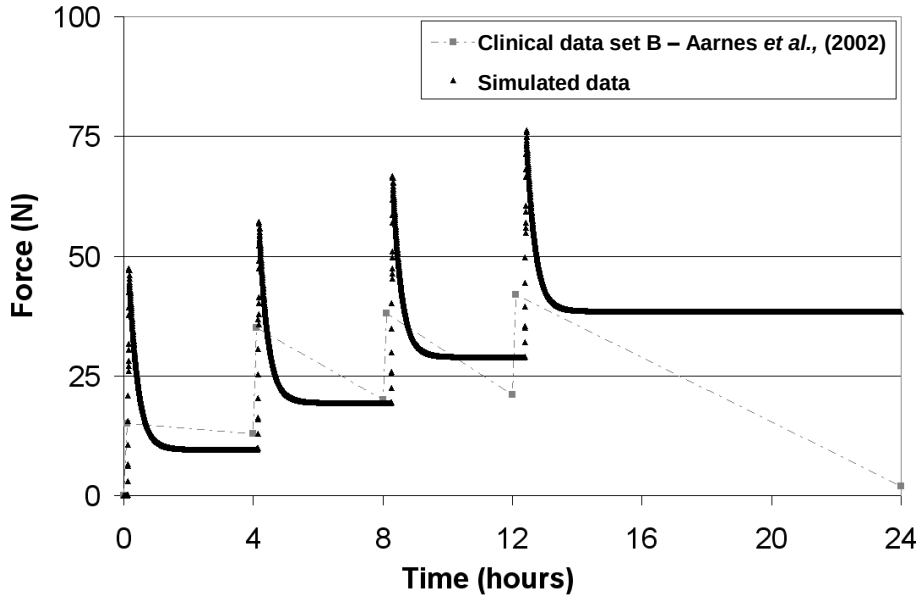

Figure 10-2 Comparing one day of data from Aarnes *et al.*, (2002a) with simulated output using tissue properties from Simpson *et al.*, (1996).

It is clear that, contrary to data set A, there was some residual load relaxation associated with data set B as relaxation overnight (12hrs) was considerably larger than during the day (4hrs) (Figure 10-2).

The calibrated model predicted peaks of more than double those recorded in data set B. This was attributed to both the elastic and viscous components of the model. Firstly, the final settled value at 24hrs was 36N above the value found by data set B which proved that the elastic component was larger. However, this larger elastic load did not fully explain the larger immediate increase which must have been the result of a larger viscous load than experienced by the tissue described by data set B. The viscous load in data set A also relaxed more quickly, i.e. had a lower value of η_2.

The model was then calibrated to data set B using the same parameters k_1, k_2 and η_2 as before but where k_1 (elastic stiffness) was a tenth of the value from data set A, k_2 was more than double and η_2 was five times larger (viscoelastic components). The output of the simulation with these values is given in Figure 10-3.

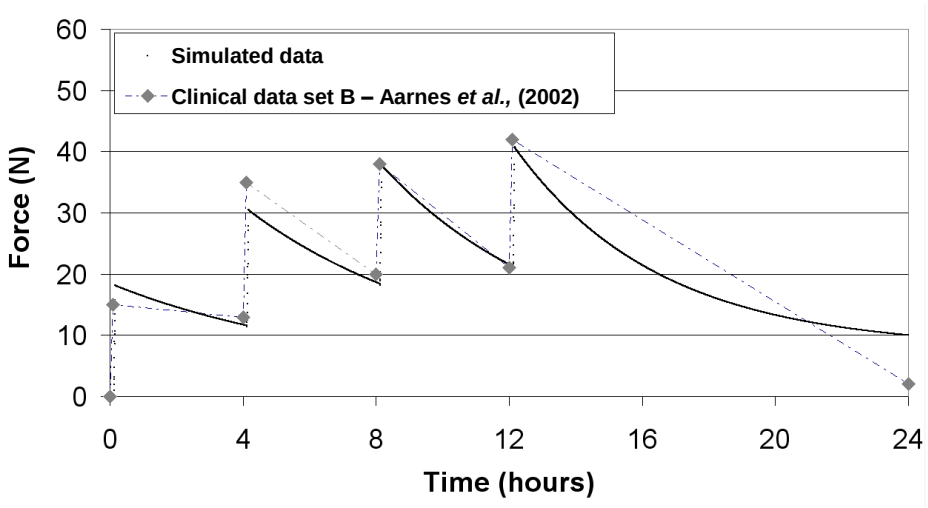

Figure 10-3 Tissue properties to fit data from Aarnes *et al.*, (2002a) for one day of lengthening

The simulation described all four immediate load increases to within 3.5N (20%), where two were within 10% of the actual increase. Three of the four relaxation values were within 2N of the actual loads. The largest error was the final value after relaxation overnight where simulated relaxation was 22% less than recorded. It has been suggested that overnight relaxations may be different than daytime relaxations (Younger *et al.*, 1994) which may be due to a lack of ambulation/load bearing on the tissue and this might explain the error in the final relaxation value. Any attempts to vary the parameter values throughout the course of one day based on the data currently available would not be accurate and require much deeper investigation.

The force decay following the first step of the day was markedly smaller than the subsequent decays (2N after step 1 compared to 17N after step 3), highlighting the need to account for the cumulative relaxations. The simulation emulates this well, seen clearly in the increased rate of load relaxation after each extension. If for the purposes of this comparison a linear decay is assumed, the simulation showed an average rate of load decrease was 1.5N/hr after the first extension but 4.25N/hr after the third i.e. increasing after each extension.

In order to test whether this same model could be applied to any day of lengthening for that patient, the calibrated model outputs were compared to the loads during the next two days of extension as recorded in data set B (Figure 10-4) where the starting values were reduced to that of day 44. The simulated data fit well with day 45 but for day 46 the error

was consistently over 25%. This suggested that there may be residual relaxations over consecutive days.

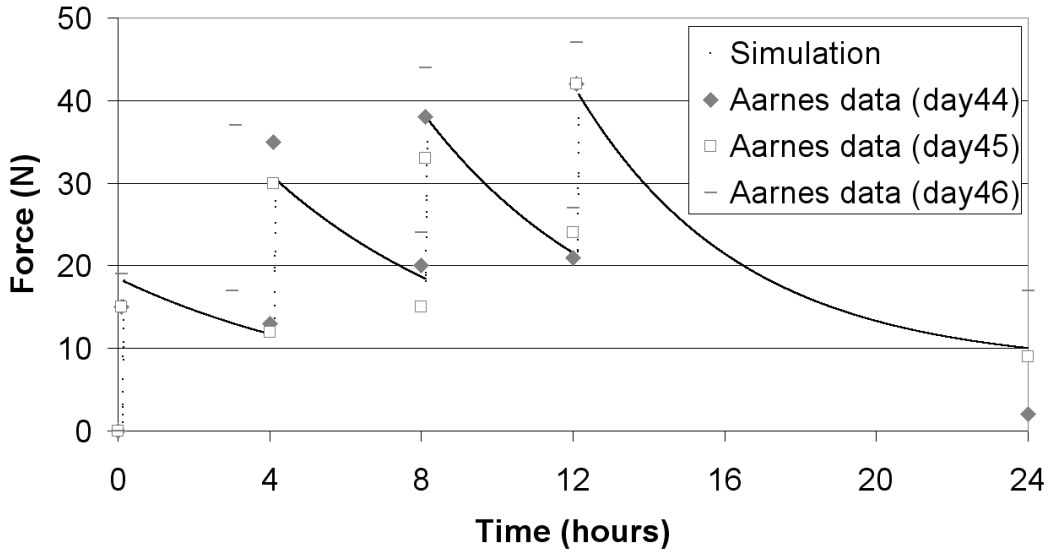

Figure 10-4 Comparing day 44 material properties to subsequent days

Thus, the calibrated model was run for three days, predicting the load pattern for days 45 and 46. In Figure 10-5 this model output is compared to the clinical data for the three days of lengthening. The average error in load relaxation (i.e. difference between peak and the pre-distraction value for the next step) was high at 90% but, when data for the first step of each day was excluded, the average error decreased to 17% (where 5 out of 6 relaxations had an error of under 12%). It should be noted that errors were increased due to the fact that measured loads did not show a regular pattern of increase. The causes of irregularity could include varying external loading through physiotherapy or ambulation, imprecise extensions or inaccurate measurements.

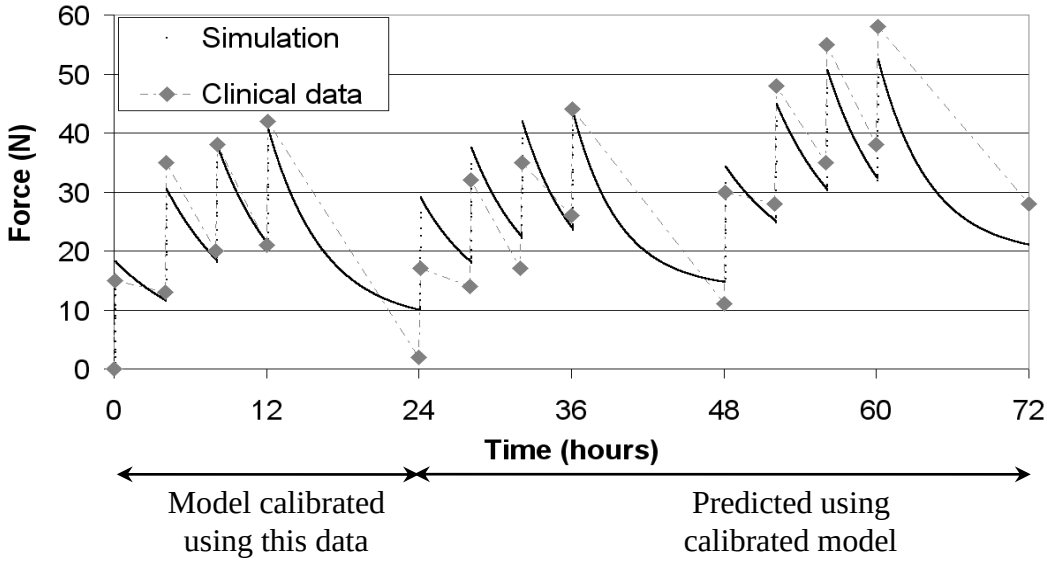

Figure 10-5 Simulated loading compared to measured clinical data (Aarnes *et al.*, 2002a)

Further model validation has been achieved through this calibration procedure, demonstrating the ability of the model to use clinical data to establish specific model parameters (k_1, k_2 and η_2) and, using the calibrated model, to predict tissue forces from subsequent distractions. This model could be used to analyse the effect of different lengthening regimes on the forces through the tissue, predicting the change in loading due to larger step increases, higher frequency distraction or even the effect of different devices.

10.3 Predicting performance for an automated device

10.3.1 Materials

Calibrated model predictions for tissue loading during stepwise lengthening with a manual fixator have been shown but new sophisticated lengthening devices, such as the device described in previous Chapters, can provide a more continuous method of extension aiming to reduce high peak forces through the tissue that have the potential to cause pain and tissue degradation. The numerical model simulating tissue loads was developed such that the tissue extension (model input) did not have to be immediate i.e. the input could be continuously variable.

Consequently the calibrated tissue model was assembled with the numerical model of the automated device to predict the loading patterns for the same 'tissue' when subject to a

different device that employed a different distraction regime. This gave a direct comparison between the tissue forces expected for two different devices distracting the same tissue. This can never be possible using clinical methods as tissue properties vary between patients and potentially between two distraction sites for the same patient.

10.3.2 Method

The starting load was set to 200N to ensure that the device was under clinically relevant loading. Firstly the tissue model, previously calibrated to clinical data set B, was assembled with the numerical model of the device. Set B was selected as it comprised data for a longer time span than data set A, allowing 72 hours of experimental data to be compared directly to simulated results. To find the effect of different tissue properties, the tissue model was then calibrated to data set A which had higher elastic and viscous components.

Finally, the effect of distraction rate on residual relaxations was analysed by doubling the rate of voltage increase for the device model. For this analysis data set A was used. This was because calibration in 10.2.3 showed that, due to a higher degree of viscoelasticity, the load increase during extensions was larger and therefore would highlight the effect of a rate increase more clearly.

10.3.3 Results

Results showed that, because the extension was gradual when using the automated device, the fluctuation in load per cycle was <0.1N. This resulted in a linear load increase, the gradient of the line being the tissue elasticity constant k_1 (Figure 10-6).

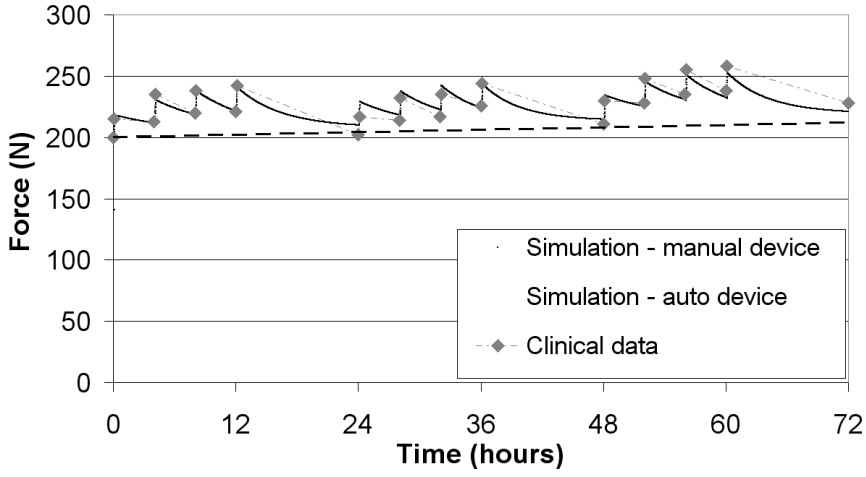

Figure 10-6 Predicted loads for automated device

The maximum number of cycles required to extend 1mm was 53, equating to an average of 20microns per cycle. This was using low device stiffness in the model i.e. lowest extension per cycle (this device variation is described in Chapter 8).

The tissue model was then calibrated using data set A and, as expected, the gradient was significantly larger being directly related to the elastic stiffness (k_1 for data A was ten times k_1 for data B as described in 10.2.3). The variation in load per cycle is shown in Figure 10-7. Interestingly, although the viscous load increase per cycle was over 1N, full relaxation did occur. When analysing the load profile alongside the device extension profile, it was seen that there was a large degree of relaxation during the short device discharge phase. This viscous relaxation continued during the initial slow extension of the next cycle but when the extension rate became larger the load increased too. (Note that the extension rate is not necessarily constant, it is the actuator voltage that increases linearly which, depending on device stiffness, may result in non-linear extension.)

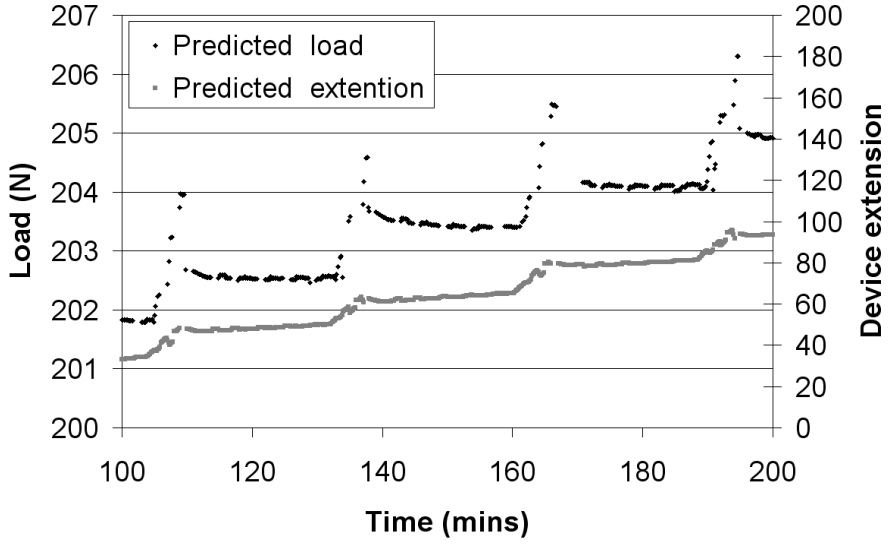

Figure 10-7 Predicted load and extension for tissue model calibrated to data set A.

The hypothesis was that by doubling the rate of distraction, the full relaxation may not take place and that residual relaxations would be built up. This was found to be true. Figure 10-8 shows that, in this case, the load increase during charging was larger by 30-40% and that the slope of the relaxation curve was greater during the first stage of actuator charging than in Figure 10-7. Consequently, some residual relaxation was expected. This was quantified by pausing device extension at the end of one charging cycle (190mins) and allowing full load relaxation to occur. The final settled value was 2.5N below the

expected pre-distraction value (i.e. the load at the beginning of the next charging phase had the device continued to extend).

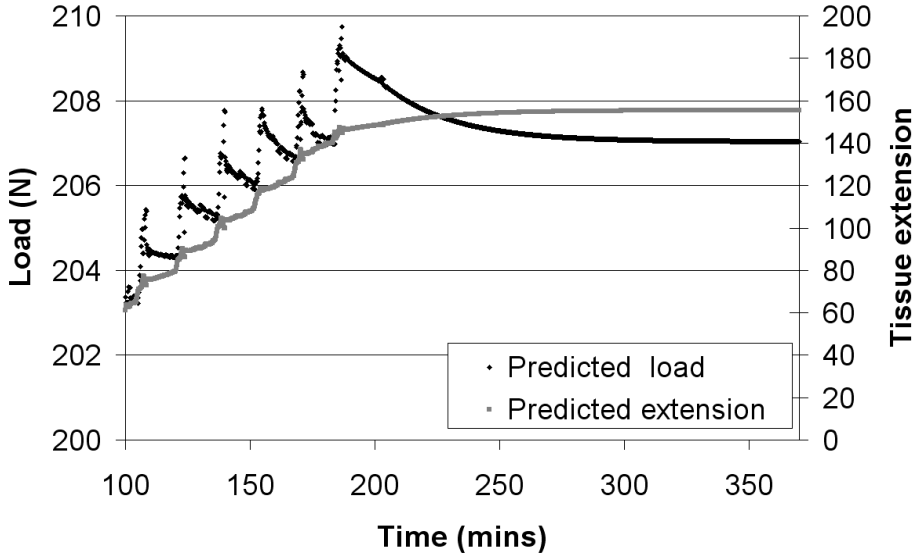

Figure 10-8 Predicted load and extension of tissue with rate doubled

This study has shown that even for a continuously extending device, increasing the rate of distraction can affect the viscoelastic tissue loading and create residual relaxations that will not fully relax until extension is complete. That said, the immediate load increases are still small (3N) compared to traditional step-wise lengthening where load increases have been measured at over 100N (Simpson *et al.*, 1996).

10.4. Influence of changes to device design

The efficiency of electromechanical devices is of importance as it directly relates to battery power and product lifespan. The model can be used to examine the effect of making design changes and has the potential for reducing both design times and financial expenditure when compared to experimental means.

Quantification of the losses within devices, through various simulations, can identify the greatest contributor to reduced efficiency. This information can then be used to optimise the device design.

The parameters selected for analysis were contact device stiffness, backlash, motor torque, actuator power and thread pitch. Where appropriate the values have been modified to assess their impact on performance. In general this modification was a doubling of the value in order to see a step change in output.

The impact of these device changes on the tissue response was also assessed.

10.4.1 Stiffness and backlash

Throughout the device design (Chapter 4) the stiffness of the device has been known to have a significant influence on the performance of the device, specifically the extension of the device per cycle. This is true of many devices using other methods of actuation and it is important to identify the key contributors to the device stiffness. The term 'device stiffness' used here includes all compliant interfaces alongside the deflection of parts themselves when under load. The number of parts and interfaces within lengthening devices varies and, with the introduction of smart devices over traditional manual devices, the complexity of load transfers and moving parts may result in more complex analysis required to find the sources of inefficiency.

One-way mechanisms are an integral part of many recent limb lengthening devices and a degree of backlash is expected during the reset phase primarily due to non-congruent faces. Backlash results in a loss of efficiency that should not only be quantified (Chapter 6) but further analysed to check if significant improvements can be made to device performance by modifying individual parts or interfaces e.g. decreasing manufacturing tolerances.

Within the numerical model of the device, the stiffness models were positioned in four locations, two relating to the stiffnesses during charging (kc1 and kc2) and two relating to the stiffnesses during device reset and discharging (kc3 and kc4). These positions are located primarily between the nuts and their associated interfaces as described in Chapter 4.

By manipulating these constants, the model can be used to predict the change in efficiency were the stiffnesses of these interfaces/parts to be changed.

Maximum device extension for a 'perfect' system (i.e. one in which there are no losses due to compliances) can be calculated using theoretical values. The maximum travel of the actuator under no load was 96microns but when subjected to load during its extension, the maximum travel decreased due to the stiffness of the actuator itself. The stiffness in this case was 17 N/micron which, for a 200N static load, resulted in a maximum travel of about 84microns per cycle.

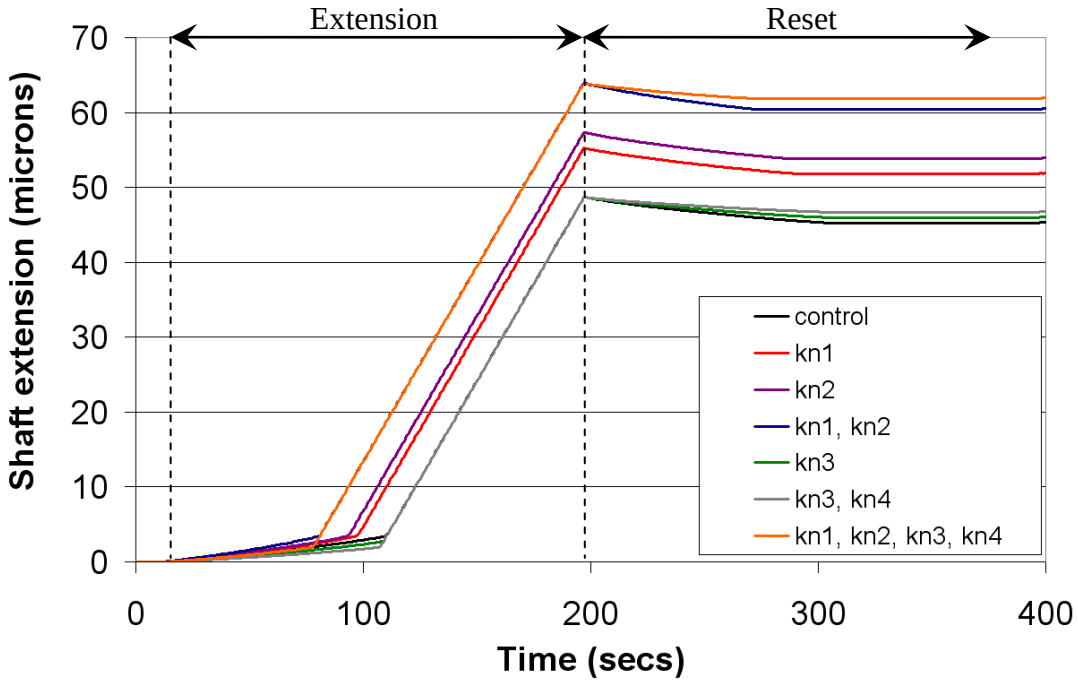

Figure 10-9 Influence of changing device stiffness values on extension profile over one cycle.

Using values for kc1-kc4 found through model validation (Chapter 6) the device extension profile is shown in Figure 10-9 (control). The device extension per cycle was measured at around half (54%) of the maximum actuator extension.

The first investigation highlighted the critical components or contact zones in order that they might be the focus of performance improvement. The method used was to double each of the kc1-kc4 values in turn and find the increase in device extension. The stiffness models were non-linear and therefore this did not necessarily result in half the deflection. Figure 10-9 shows that for the stiffnesses involved during charging, this doubling of stiffness resulted in the device extension rising to 72% of actuator extension. This was a significant area of loss and highlighted that focus for improvement should be given to these components and interfaces, specifically those characterised by kn2 (the greatest contributor) which includes the yoke-nut-shaft interface.

If, instead, the stiffnesses involved during reset/discharge were doubled, then the extension was improved by 2%. If setback was eliminated altogether then the extension would be improved by 4%. Comparing this to the performance increase when analysing the stiffnesses involved in charging, it can be seen that more focus should be on the reduction of loss at these other interfaces. This may not be the case for all one way

mechanisms within devices as the setback during reset may have a more significant contribution to overall loss of efficiency.

10.4.2 Actuator

Actuation methods within distraction devices vary and are often constrained by criteria such as size, weight, cost and power consumption. It is often not possible to assess different actuators due to high component costs and the implications on the geometry of other parts. In selecting the piezo-electric actuator used in the device, special consideration was given to the extension under no-load, the blocking load and the diameter with the intention of selecting an actuator with minimum diameter for maximum extension and load capabilities.

Obviously, a change in the maximum stroke of the actuator would influence the device performance (and would be related to actuator stiffness). It was found that by doubling the stroke of the actuator, the extension per cycle increased by 186% while halving the stroke decreased the extension to 7% of the original extension (Figure 10-10).

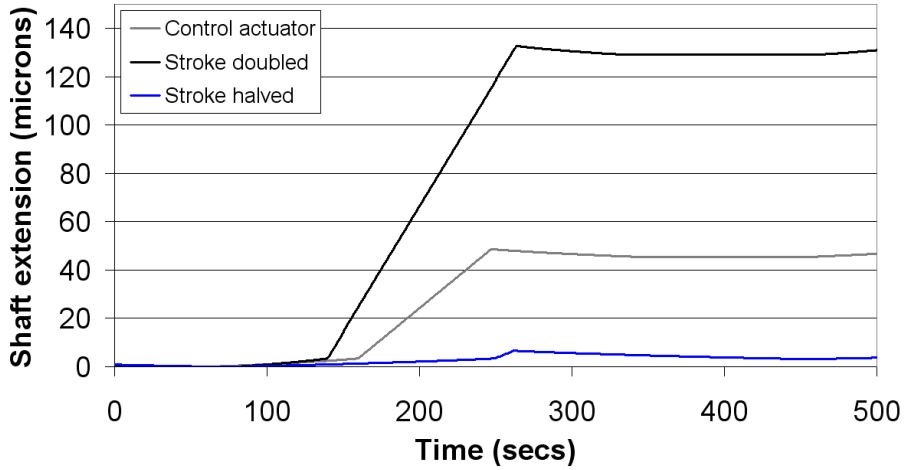

Figure 10-10 Influence of actuator stroke on device extension profile over one cycle

This showed that the loss due to compliance was closer to an absolute value than a percentage of the maximum stroke. The range of loss was found to be 45-63microns over the three tests.

However, selection of an arbitrary alternative travel or blocking load value would be useless if no alternative actuator was commercially available. Consequently a comparison was made between an alternative actuator (manufactured by PI, part no. P-216.90) with a block force of 4500N and maximum stroke of 180microns (Figure 10-11).

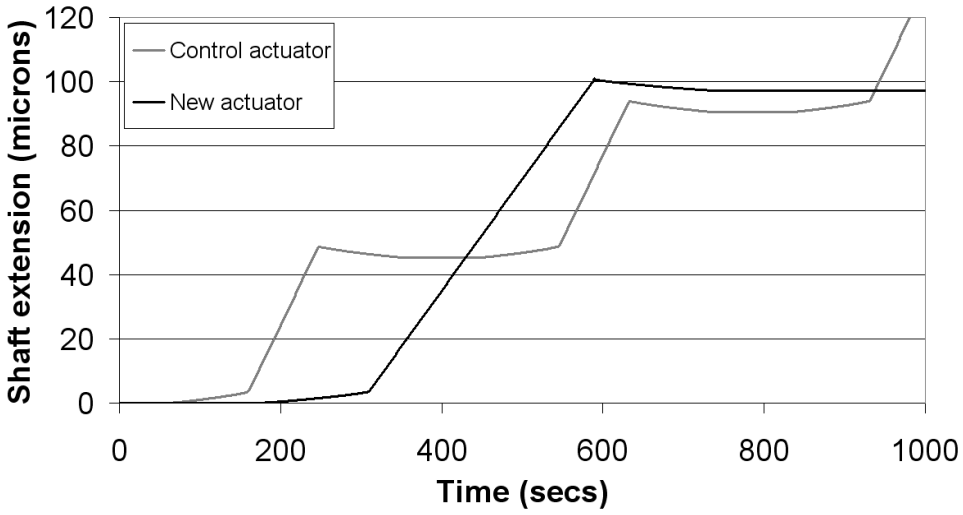

Figure 10-11 Influence of new PI actuator on device extension profile over one cycle

The actuator took longer to charge as the fully charged voltage was higher (4500V compared to 2000V) and the increase in voltage per second remained as in previous tests. Extension per cycle was ~100microns and actual loss from device stiffness (50microns) was within the previously described range.

The main drawback of using this more powerful actuator would be that the diameter was considerably larger than the current actuator, resulting in an increase in bulk as well as weight, both affecting patient comfort.

10.4.3 Thread pitch

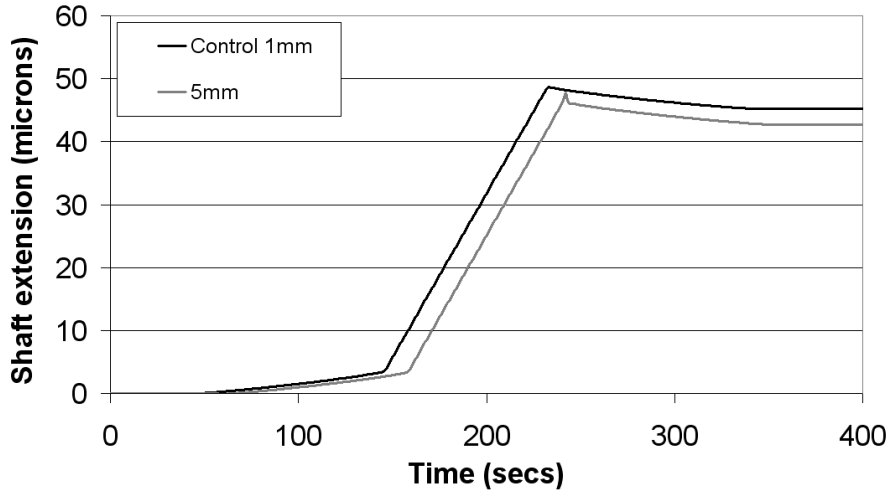

Figure 10-12 Influence of thread pitch on device extension profile over one cycle

The impact of changing the thread pitch of the shaft was analysed using the simulation. It was doubled and halved (0.5mm, 2mm) with only small impact on extension per cycle

(<0.3%). It was only when the pitch was increased to 4-5mm that a larger influence seen (2.3% and 2.8% respectively). Figure 10-12 shows that the extension was very slightly less during charging (1%) and that the setback was greater (22%) with the sharp decline at the beginning of actuator discharge suggesting that the motor rotation was not adequate to take up the full slack. This can be explained by the higher frictional force opposing its rotation from the larger angle.

10.4.4 Motor torque

Taking up the slack in a one way system is often done using a motor. It is important to understand the motor requirements and the effect of a different motor torque on the system output. In this case it was found that increasing the motor torque by 25% increased the extension of the device by around 3microns over 6 cycles (1.1%) (Figure 10-13).

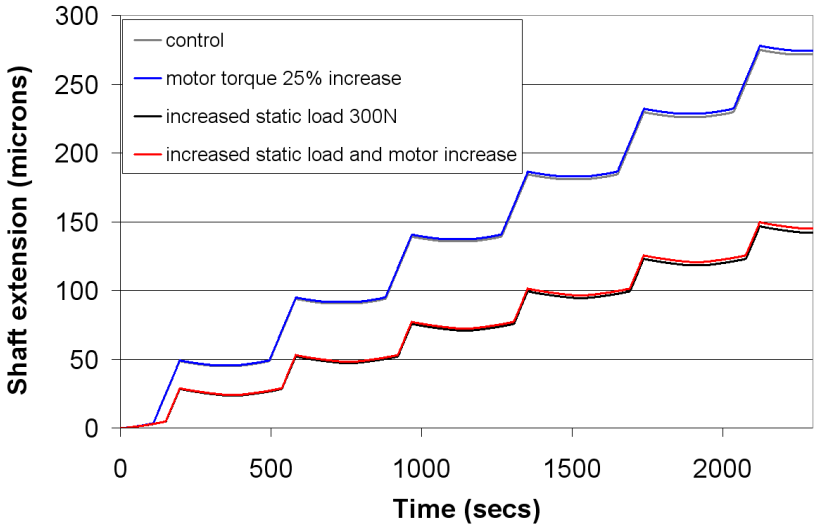

Figure 10-13 Influence of motor torque on device performance over one cycle

If the torque was increased by more than this, the motor started to drive the shaft forward. At higher loads (300N) the absolute difference was the same so the percentage difference was larger at 2.1%.

10.4.5 Additional parameters

Other parameters such as component mass had minimal affect on the performance of the device in this case as mass only affected acceleration of the parts. The frequency was too low for small changes in acceleration to have an effect on the extension of this device. Chapter 8 described the effect of pin stiffness and it was found that the longer the pin, the lower stiffness and lower immediate tissue extension.

10.4.6 Impact on tissue forces

The main influence on device extension per cycle was found to be the stiffness of components and interfaces during actuator charging. Therefore, the influence that this stiffness had on tissue forces during the running of the device was assessed by doubling kc1 and kc2 - the two largest contributors to the loss of extension per cycle. Figure 10-14 shows that the device extension remained non-linear. Extension per cycle increased as expected, which in turn increased the viscous loading through the tissue and the resultant relaxation.

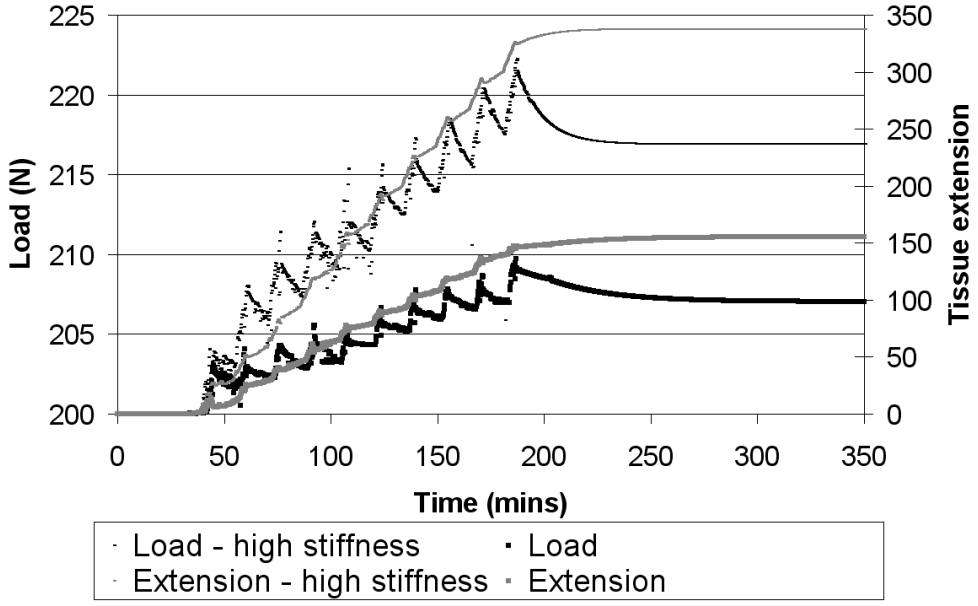

Figure 10-14 Influence on load and extension of increasing device stiffness components kc1 and kc2

Consequently, the values of kc1-kc4 were increased to imitate near infinite stiffness. The resulting profiles are shown in

Figure 10-15.

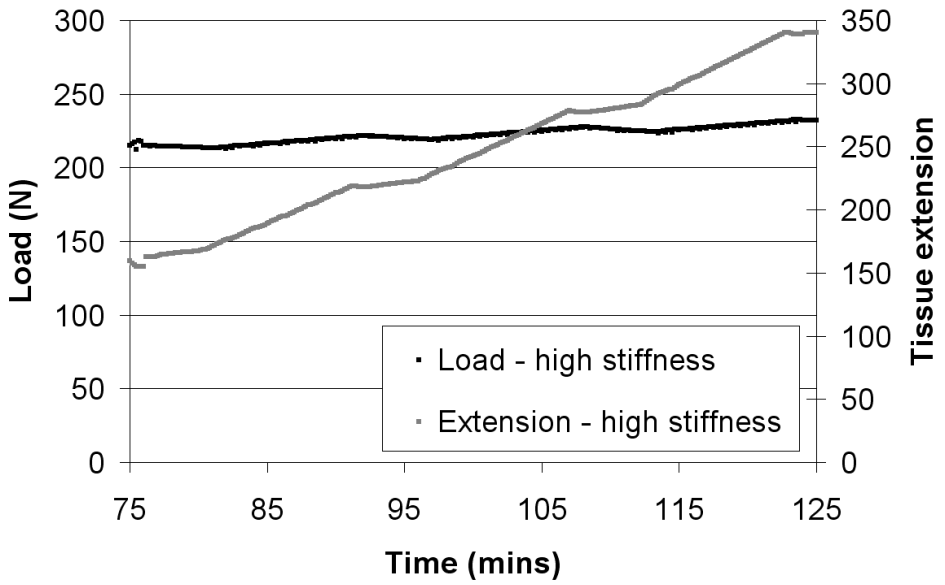

Figure 10-15 Influence on load and extension profiles for high device stiffness

It is clear that the load profile has a shorter relaxation phase and has greater linearity than previous simulations (Figure 10-14) but there remains a portion of the charge cycle that is of a lower rate. This is where the compression of the piezo actuator itself is taking place and is one component stiffness that cannot be eliminated.

Obviously achieving a device with zero internal compliance is not possible due to the materials themselves having a modulus, but reduction of interface compliances is possible in many device designs and consideration should be given to this especially when using automated devices as these can have an effect on the tissue loading values.

10.5 Discussion

The application of the numerical model has been described in this Chapter. The main purpose of the model is to aid the development of limb lengthening devices. This has been done by:-

1. predicting the types of loads that devices will be under through use of a tissue model with time-dependent characteristics (effect of tissue forces on device)
2. predicting the impact of device changes on their performance and on tissue loading (effect of device on tissues)

The first application was focused on predicting the forces that lengthening devices are subject to. It was shown that the model was able to characterise the forces during one day of lengthening in the clinical environment, resulting in model calibration for two specific clinical data sets. This confirmed that the load relaxation was not always fully complete between distractions and that in order to best model the tissue forces, the residual relaxation must be accounted for, as described in Chapter 7. This model was then used to predict loads during a further two days of lengthening, taking residual relaxations into account. Clinical data did not follow a regular pattern but the simulated relaxation values were almost always within 12% of measured values. It was also found that tissue forces varied greatly between patients so an indication of the tissue properties was required before accurate predictions could be made. In-built load measurement is becoming a common feature of limb lengthening devices (Wee et al., (2011), Shevtsov and Vasilyevich Popkov (2002)) and thus tissue characteristics can be monitored more frequently providing more data so that further confidence in the model can be gained.

The second application focused on analysing the effect of device design on performance and the resultant impact on the tissue. Comparison was made between the tissue loads when using two methods of distraction - a manual device and the automated lengthening device. This has allowed direct comparison of the forces invoked by the two different distraction devices in the same mechanical environment. As expected, the model predicted the reduction of peak forces when using a continuous lengthening regime. Some authors describe a quasi-continuous lengthening regime where lengthening is once per minute (Aarnes et al., 2002a; Ilizarov, 1989), or sixty extension cycles (Shevtsov and Popkov, 2002) or where each step is always 2.6μm no matter the frequency (Wee et al., 2011). It was found that for continuous lengthening by the automated device at a rate of 1mm/day, the residual relaxations were insignificant. Interestingly, when the rate was increased to just 2mm/day, residual relaxations after each cycle, although small, could be clearly seen. This is partly due to the fact that for this specific device the extension was not linear despite linear actuator charging. In fact, there was a ‘fast’ and ‘slow’ portion during which the tissue loading was clearly different. The ‘slow’ portion was as a result of device compliances which had to be ‘taken up’ by the actuator before there was extension of the shaft, and thus tissue, in the ‘fast’ portion. If the extension of the device, and therefore tissue, had been linear, it is estimated that the residual relaxations would be much lower, or may even be eliminated at a rate of 2mm. It is likely that there would be a rate at which residual relaxation are impossible to eliminate, even with entirely linear

extension. This would obviously vary for different tissue characteristics, but for the high stiffness tissue properties used here, it is suggested that this would be not much higher than the 2mm/day extension previously used in the simulation (Figure 10-8). A rate of 2mm/day is at the high end of current clinical extension rates, but it is hoped that by linearising the extension and allowing soft tissue accommodation, the healing of the regenerate might hasten and faster distraction rates might then be possible. Therefore, it is suggested that these device compliances should be reduced to maintain a low load with low residual relaxations during extension.

The impact of changing the device stiffness has been analysed using the device model along with other, more device-specific parameters. The effect that modifying these parameters had on the performance of the device (which in this case was defined by its extension per charging cycle) has been determined. This would not have been possible without the use of the model. This process highlighted that, for this specific device, the improvement that would have the largest impact on performance would be an increase in stiffness of the shaft-nut component and interface, perhaps achieved by narrowing the acceptable machining tolerances for these parts. Many of the modifications made to the device model resulted in such small changes that the impact on performance (i.e. extension per cycle) and tissue loading would be minimal. This type of knowledge has the potential to save considerable time and effort during development. Conversely, for some parameters such as stiffness during charging, the change in extension per cycle was large enough to influence tissue loading and these interactions could be examined and modified where appropriate. It was found that, even if the current automated device had near infinite stiffness, the extension could not be entirely linear when charging the actuator linearly (as the actuator itself has a stiffness associated with it). However, through the use of the control system, it may be possible to have an elevated rate of voltage increase across the actuator at the beginning of the charging cycle that results in improved linearity of shaft extension, and thus a reduced viscous load increase.

It has been seen that these models can be extremely useful in the development of devices and especially in quantifying the load range that the device will be exposed to, assessing the impact of the device on the load through the tissues and analysing the influence of iterative changes to design. Thus it is a tool that can improve new distraction devices such that the high complication rates associated with this procedure can be reduced. Further applications include:-

1. the ability to use the model to aid selection of the most appropriate battery for a specific device. With the increasing development of automated devices consideration must be given to the impact of the size and weight of batteries on device design and thus use of the model would be extremely valuable in the assessment of battery requirements.
2. the simulation of various distraction rates and frequencies to identify distraction regimes that reduce the power consumption of automated devices without compromising tissue load levels.
3. the design of the decision making algorithm for smart devices (such as the one under development) i.e. when pattern of forces is known, what changes should be made to the distraction regime. It is hoped that there will be wider availability of clinical load data through the use of instrumented devices. This data can then be analysed and used within the model to determine the appropriate limits for change and consequences of finding particular trends of loading. Using the model these limits could be more specific to the patient and their indication, resulting in reduced errors and thus a more robust device.
4. the development of optimum patient specific distraction regimes in order to improve regenerate and soft tissue quality whilst reducing extension time. Again, with the use of a large clinical data bank, the load and extension predictions from the model could allow predictions to be made without the initial model calibration, i.e. based on patient demographics and clinical indication.

Thus it has been shown that the model has the ability to significantly improve the development process for new distraction devices, particularly automated devices with control systems. The potential of the model for use in optimisation of distraction regimes and patient specific treatments has been identified, with the aim of reduced extension time and better physiological outcomes for the patient.

Chapter 11

Conclusions and further work

11.1 Main conclusions

Loading through tissues during limb lengthening varies greatly over the course of the procedure. Therefore, distraction devices are subject to a range of forces that, as shown through this work, are also dynamic in nature. Consequently, during their development, distraction devices should be tested within an environment that is similar to that in which they will be finally used. Alongside consideration of the ability of the device to withstand the changing forces or the effects on 'performance', attention should also be given to the effects of different devices on the loading through the tissues themselves and the impact of this on the final tissue quality. It has been suggested that the mechanical properties of tissues (such as stiffness) during lengthening may be an indicator for the ability of the tissues to adapt to the process of distraction (Aarnes *et al.,* 2002a) and thus there is increasing interest in recording the loads during tissue extension.

Integrating monitoring of tissue loading and extension into the device design alongside the ability to change the regime based on these findings has been accomplished through the development of a new 'smart' device. Testing of such a device requires special consideration of the impact of the device on the tissue in order to change the regime based on past loading and extension patterns. Thus the immediate impact of the device extension on the tissue has been assessed.

In this work, a method of evaluating the loads through distraction devices and tissues was developed in the form of a numerical model. Model validation was achieved using a fluid-based mechanical test rig to mimic the time-dependent properties of the tissue. The application of the model to the clinical field showed that following calibration using load data for one day, predictions could be made for the forces during the two subsequent days.

The model could also be used to predict forces for varying distraction frequencies. Manual lengthening frequency is four times per day but automated devices have been developed that can extend almost continuously. A newly developed automated distraction device was used within this work for loading comparison with traditional devices. The automated device analysed within this work was developed as a smart device; to record the forces during distraction and adapt the regime accordingly (although the smart nature was not analysed here and thus the rate of actuator charge was linear). Hence the tissue would be kept under optimal loading conditions. Other authors (Wee *et al.*, 2011) are attempting different distraction regimes in animal studies but, through the use of this model, it is proposed that the degree of animal testing can be reduced.

Therefore, a numerical model of the new automated lengthening device was built. This was used alongside the tissue model to predict forces during automated distraction. It was found that the device model outputs were more accurate when the pins were eliminated than when pins were included. This was due to cyclic variations within the device when offset loading was applied. Although it had been expected that the additional pin stiffness would influence the loads and extensions transferred to the tissue, it was not clear that the bending within the device so greatly affect the internal contact stiffnesses and that the influence on the performance (measured by extension per cycle) of the device would be so large. Another feature of the device model was its ability to quantify stiffnesses within the device (of components and at interfaces) and assess their impact on tissue loading. This was valuable in selecting the most significant contributors to overall compliance and thus proposing where design improvements should be focussed.

This model gave an indication of short-term forces but it was understood that a longer-term load response to extension should also be included. Thus a simplified healing model was developed that was based on prior complex mechanobiological models. With further validation this could become part of the larger tissue model, changing the values of stiffness parameters as the extension progressed.

11.2 Contributions to the field

- The first validated simplified numerical model to predict tissue forces during limb lengthening has been designed that can be used for evaluation of distraction devices and the short-term forces developed in the tissue as a result of distraction.
- The model can allow for various rates and frequencies of distraction as it does not assume complete load relaxation between extensions.

- A separate validated numerical model of an automated lengthening device was developed
- This model is applicable to other devices by varying its stiffness parameters, pin parameters as well as other more device specific parameters
- The joining of these two models allows for evaluation of distraction devices within a dynamic mechanical environment representing changing tissue forces.
- The model was calibrated using clinical data to allow direct comparison between the forces generated by different lengthening devices.
- The models provide the opportunity to assess the effects of iterative changes to device design on device performance and thus optimisation of efficiency/power
- Additional analysis of the effects of these device changes on loads and extensions of tissues without cost or expense of experimental trials using mechanical or animal testing
- A simplified mechanobiological healing model focussing on the stiffness of regenerated callus tissue that, with further validation through clinical data, can be used alongside the short-term models to predict longer-term changes to tissue stiffness as a result of biological changes within the regenerated bone tissue.

11.3 Further Work

1. More clinical data is required to predict the loading patterns with no initial tissue characterisation. Thus fitting load cells to existing manual lengthening appliances as well as more modern continuous devices would provide data that could result in a bank of data with associated information such as clinical indications and patient demographics. This would allow for initial predictions and then has the potential for pattern matching to optimise regimes.
2. The model does not include the influence of weight bearing on device performance or tissues. Clinical data that specifies the level of ambulation of patients or monitors the load including ambulatory forces could help to understand the influence of this important factor.
3. A numerical representation of the decision making of the control system within Simulink could help to define rate decision points i.e.

a) changing rate as a result of changing resistance (if the extension per cycle is X, resulting in an approximate load of Y, then the next rate of voltage increase across the piezo actuator will be Z)

b) alerting for clinical evaluation and potential intervention if the change in resistance is extreme or beyond specific limits

4. The device has the potential for superimposing a high frequency extension signal over the continuous lengthening which have been shown to increase fracture healing rates (Goodship *et al*., 1985). This proposal requires biological confirmation therefore animal studies would be required.
5. Determining the source of resistance has always been a source of discussion and it may be that monitoring the forces within tissues (particularly relaxation profiles and patterns) alongside the extensions could give an indication of the type of tissue (material type) under tension and therefore would give rise to better regimes to allow for either soft tissue accommodation or callus formation.

APPENDICES

APPENDIX A –AUTOMATED DEVICE PIC PROGRAM

The PIC program was written in C language but flow diagrams are given here to clarify the function. This program goes through an initialisation phase and 4 separate 'states'. Subroutines are also used and these are given separately following the main program.

Parameters

id - inrush delay
time in milliseconds required to miss motor inrush current
hvz - high voltage zero calibration point
hvs - high voltage slope calibration parameter
hvm - high voltage max
maximum voltage applied to the piezo - trip point. when exceeded - program proceeds to the next state=motor torquing
hvd - high voltage discharge limit
voltage at which the piezo is considered discharged. trip point to next state - motor torqueing
ds - distance slope
calibration parameter for dvrt linear position sensor. Note - no zero point calibration - device autozeroes
rp - ramp period
controls ramp generation - is the number of seconds required per micron of movement
imc - init motor count
specifies the no of times the motor initialisation routine runs during start up
mpl - motor pulse length
length in milliseconds of the second motor torque

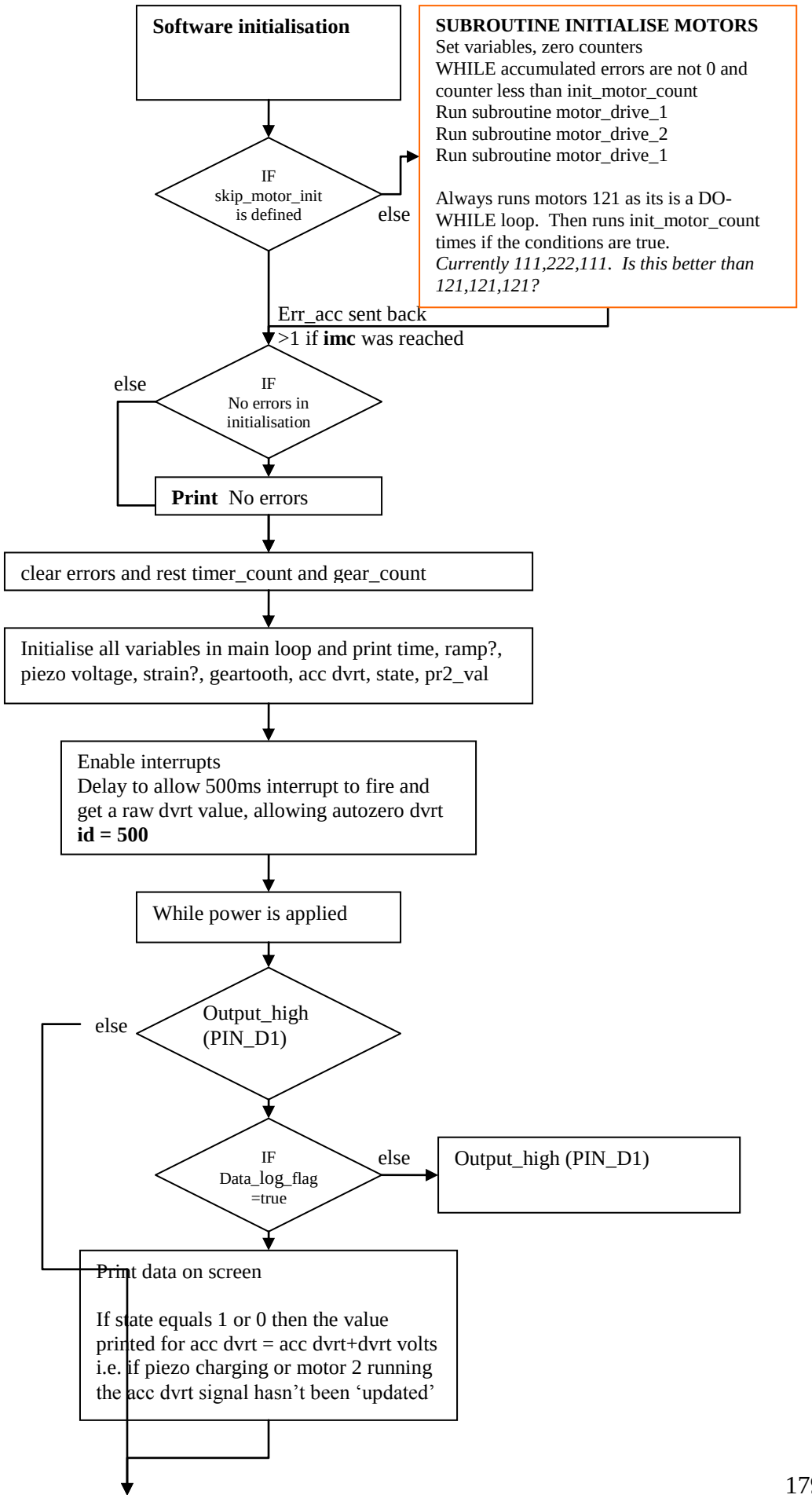
Software initialisation
IF skip_motor_init is defined
else
SUBROUTINE INITIALISE MOTORS
Set variables, zero counters
WHILE accumulated errors are not 0 and counter less than init_motor_count
Run subroutine motor_drive_1
Run subroutine motor_drive_2
Run subroutine motor_drive_1
Always runs motors 121 as its is a DO-WHILE loop. Then runs init_motor_count times if the conditions are true.
Currently 111,222,111. Is this better than 121,121,121?
Err_acc sent back
>1 if imc was reached
else
IF No errors in initialisation
Print No errors
clear errors and rest timer_count and gear_count
Initialise all variables in main loop and print time, ramp?, piezo voltage, strain?, geartooth, acc dvrt, state, pr2_val
Enable interrupts
Delay to allow 500ms interrupt to fire and get a raw dvrt value, allowing autozero dvrt
id = 500
While power is applied
else
Output_high (PIN_D1)
IF Data_log_flag =true
else
Output_high (PIN_D1)
Print data on screen
If state equals 1 or 0 then the value printed for acc dvrt = acc dvrt+dvrt volts
i.e. if piezo charging or motor 2 running the acc dvrt signal hasn't been 'updated'

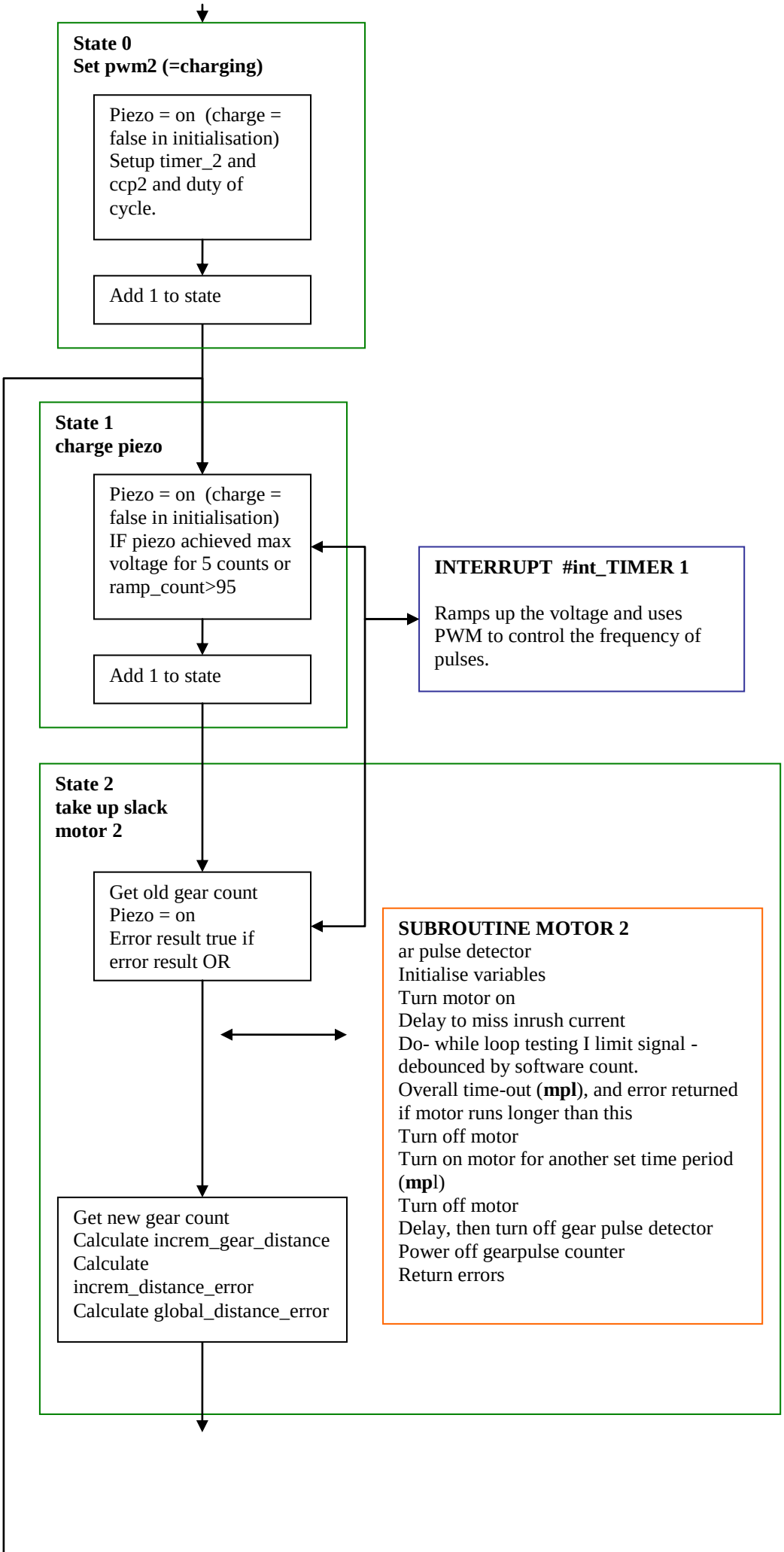
State 0
Set pwm2 (=charging)
Piezo = on (charge = false in initialisation)
Setup timer_2 and ccp2 and duty of cycle.
Add 1 to state
State 1
charge piezo
Piezo = on (charge = false in initialisation)
IF piezo achieved max voltage for 5 counts or ramp_count>95
Add 1 to state
INTERRUPT #int_TIMER 1
Ramps up the voltage and uses PWM to control the frequency of pulses.
State 2
take up slack
motor 2
Get old gear count
Piezo = on
Error result true if error result OR
SUBROUTINE MOTOR 2
ar pulse detector
Initialise variables
Turn motor on
Delay to miss inrush current
Do- while loop testing I limit signal - debounced by software count.
Overall time-out (mpl), and error returned if motor runs longer than this
Turn off motor
Turn on motor for another set time period (mpl)
Turn off motor
Delay, then turn off gear pulse detector
Power off gearpulse counter
Return errors
Get new gear count
Calculate increm_gear_distance
Calculate increm_distance_error
Calculate global_distance_error

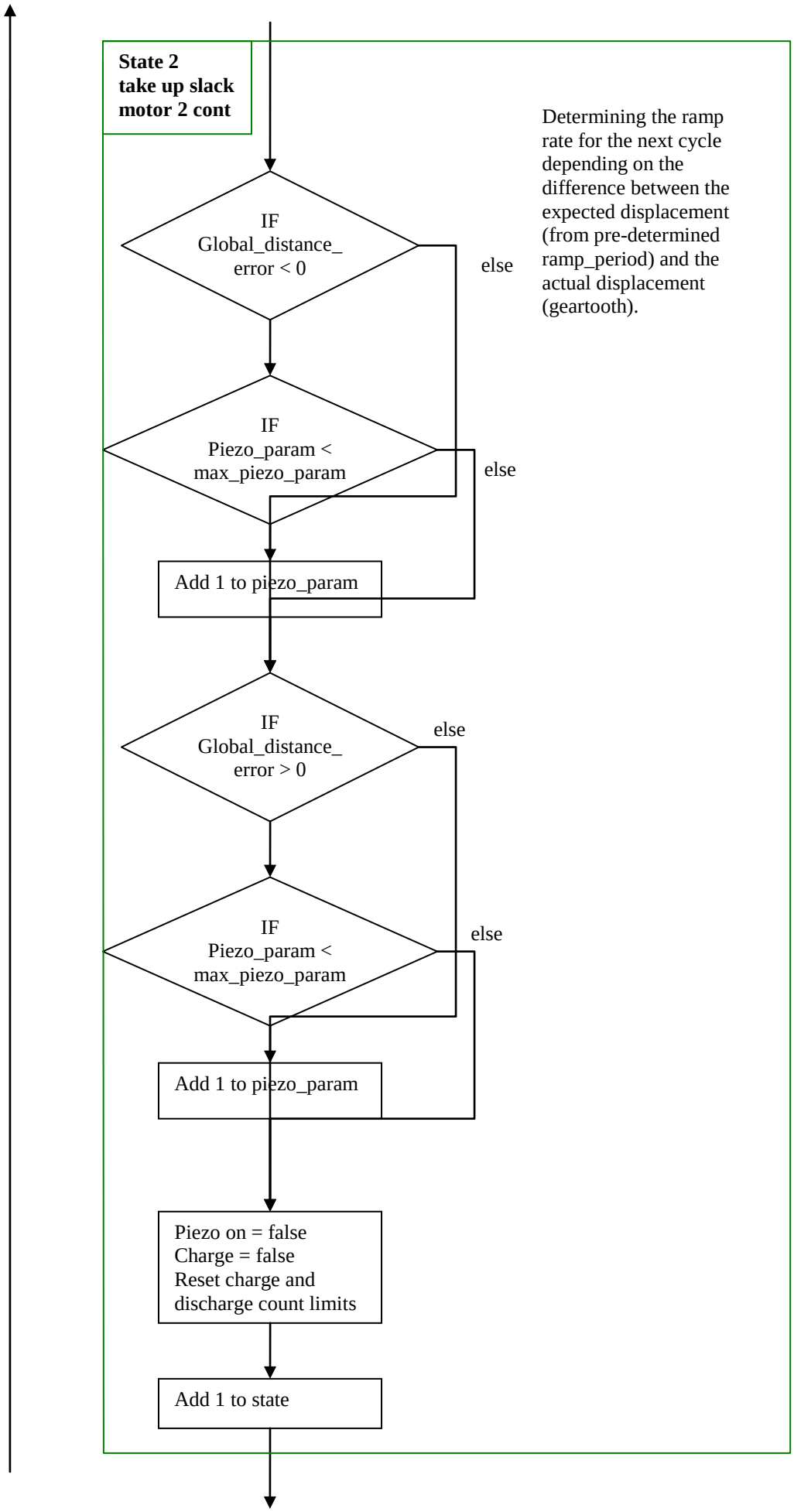
State 2
take up slack
motor 2 cont
Determining the ramp rate for the next cycle depending on the difference between the expected displacement (from pre-determined ramp_period) and the actual displacement (geartooth).
IF
Global_distance_
error < 0
else
IF
Piezo_param <
max_piezo_param
else
Add 1 to piezo_param
IF
Global_distance_
error > 0
else
IF
Piezo_param <
max_piezo_param
else
Add 1 to piezo_param
Piezo on = false
Charge = false
Reset charge and
discharge count limits
Add 1 to state

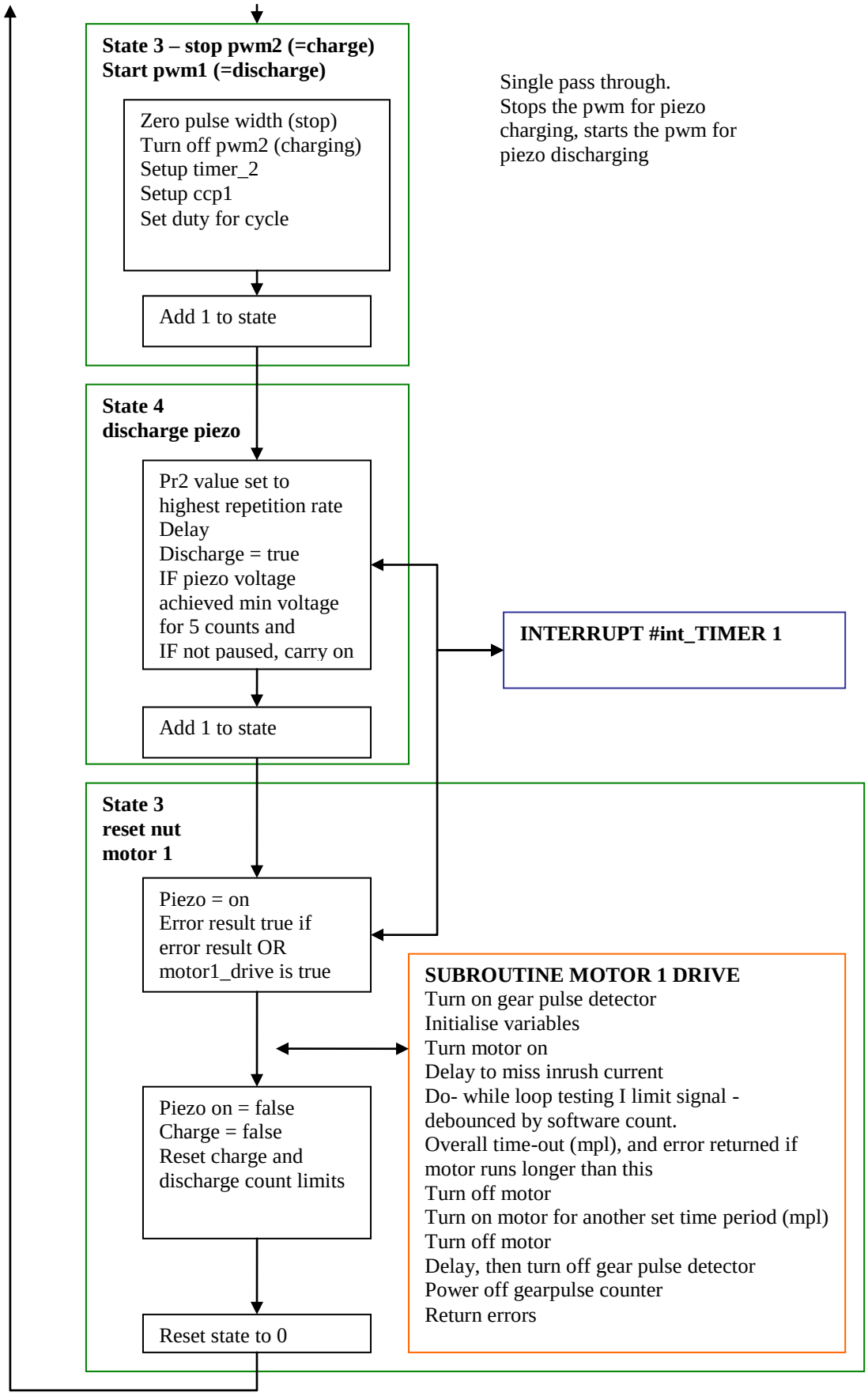
State 3 – stop pwm2 (=charge)
Start pwm1 (=discharge)
Zero pulse width (stop)
Turn off pwm2 (charging)
Setup timer_2
Setup ccp1
Set duty for cycle
Add 1 to state
Single pass through.
Stops the pwm for piezo charging, starts the pwm for piezo discharging
State 4
discharge piezo
Pr2 value set to highest repetition rate
Delay
Discharge = true
IF piezo voltage achieved min voltage for 5 counts and
IF not paused, carry on
Add 1 to state
INTERRUPT #int_TIMER 1
State 3
reset nut
motor 1
Piezo = on
Error result true if error result OR motor1_drive is true
SUBROUTINE MOTOR 1 DRIVE
Turn on gear pulse detector
Initialise variables
Turn motor on
Delay to miss inrush current
Do- while loop testing I limit signal - debounced by software count.
Overall time-out (mpl), and error returned if motor runs longer than this
Turn off motor
Turn on motor for another set time period (mpl)
Turn off motor
Delay, then turn off gear pulse detector
Power off gearpulse counter
Return errors
Piezo on = false
Charge = false
Reset charge and discharge count limits
Reset state to 0

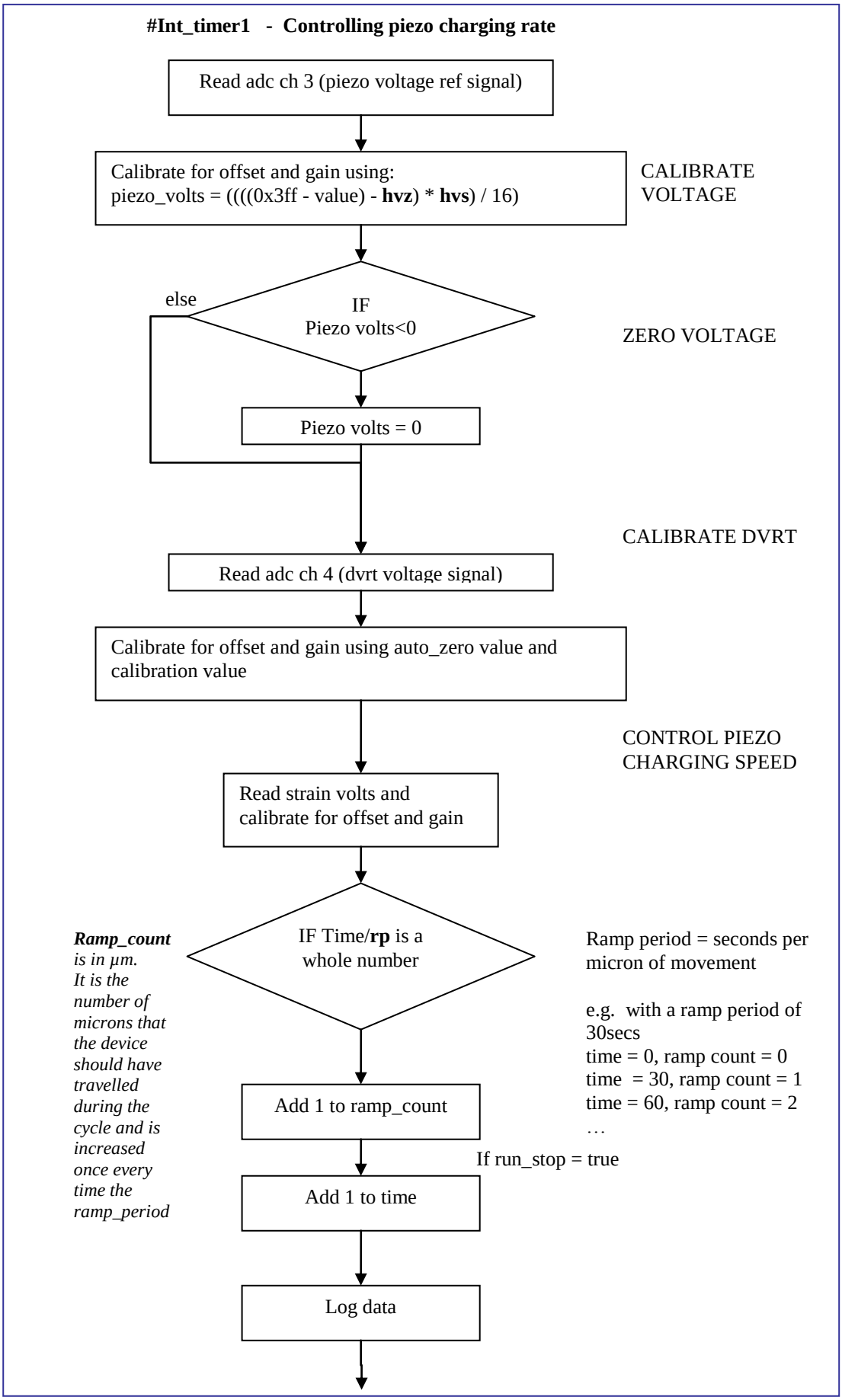
#Int_timer1 - Controlling piezo charging rate
Read adc ch 3 (piezo voltage ref signal)
Calibrate for offset and gain using:
piezo_volts = ((((0x3ff - value) - hvz) * hvs) / 16)
CALIBRATE VOLTAGE
else
IF
Piezo volts<0
ZERO VOLTAGE
Piezo volts = 0
CALIBRATE DVRT
Read adc ch 4 (dvrt voltage signal)
Calibrate for offset and gain using auto_zero value and calibration value
CONTROL PIEZO CHARGING SPEED
Read strain volts and calibrate for offset and gain
IF Time/rp is a whole number
Ramp period = seconds per micron of movement
e.g. with a ramp period of 30secs
time = 0, ramp count = 0
time = 30, ramp count = 1
time = 60, ramp count = 2
…
Ramp_count is in µm. It is the number of microns that the device should have travelled during the cycle and is increased once every time the ramp_period
Add 1 to ramp_count
If run_stop = true
Add 1 to time
Log data

Controlling piezo charging rate (2)

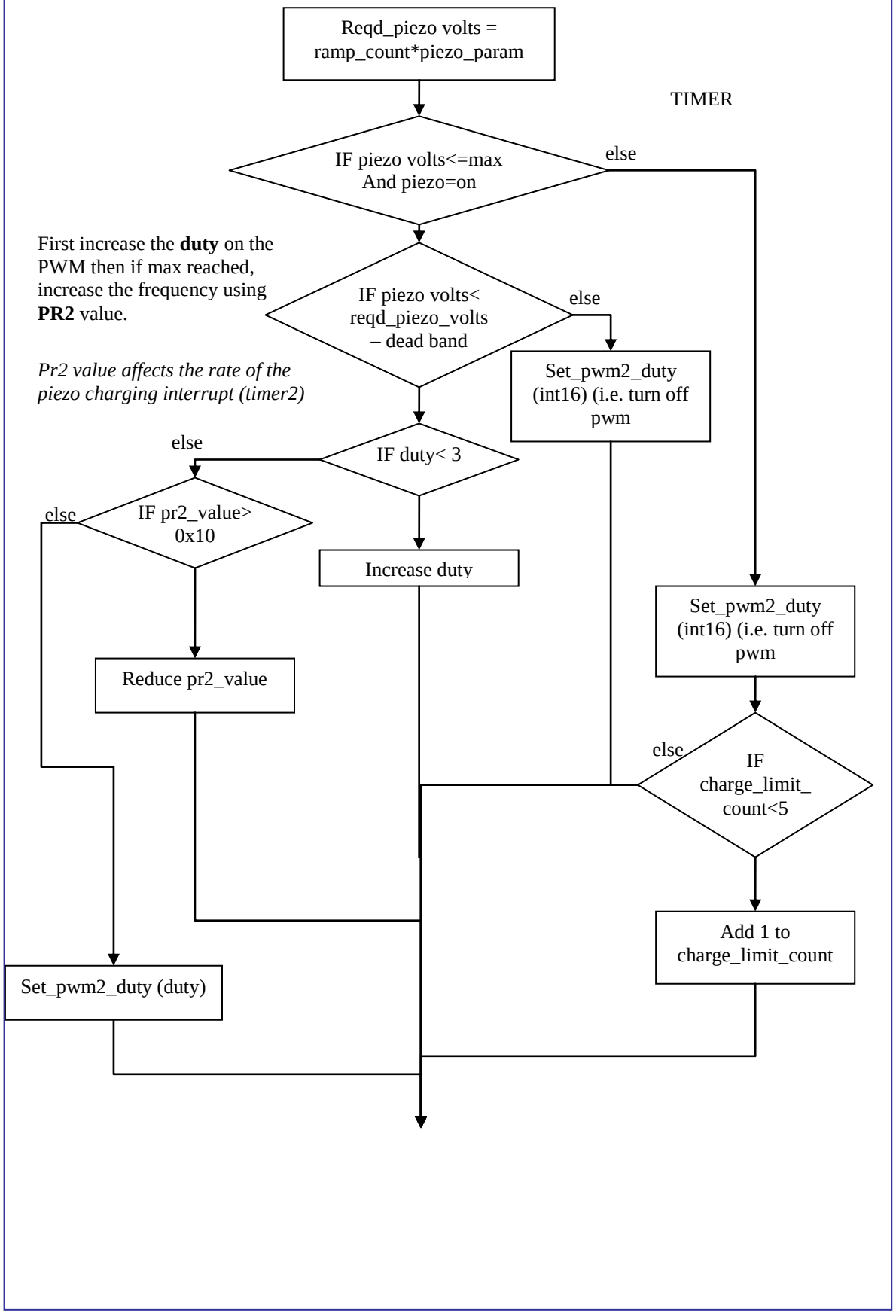

#Int1 Piezo discharging

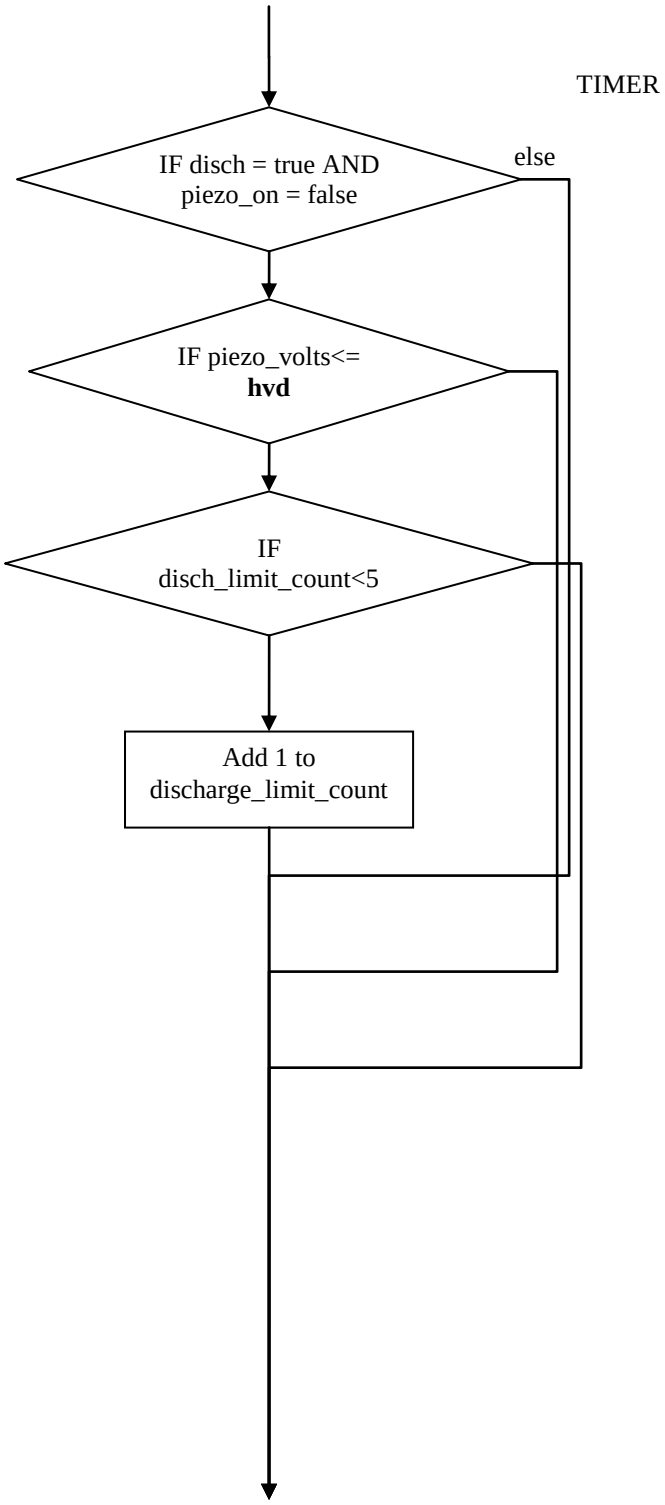

APPENDIX B: ENGINEERING DRAWINGS FOR PROTOTYPE DEVICE

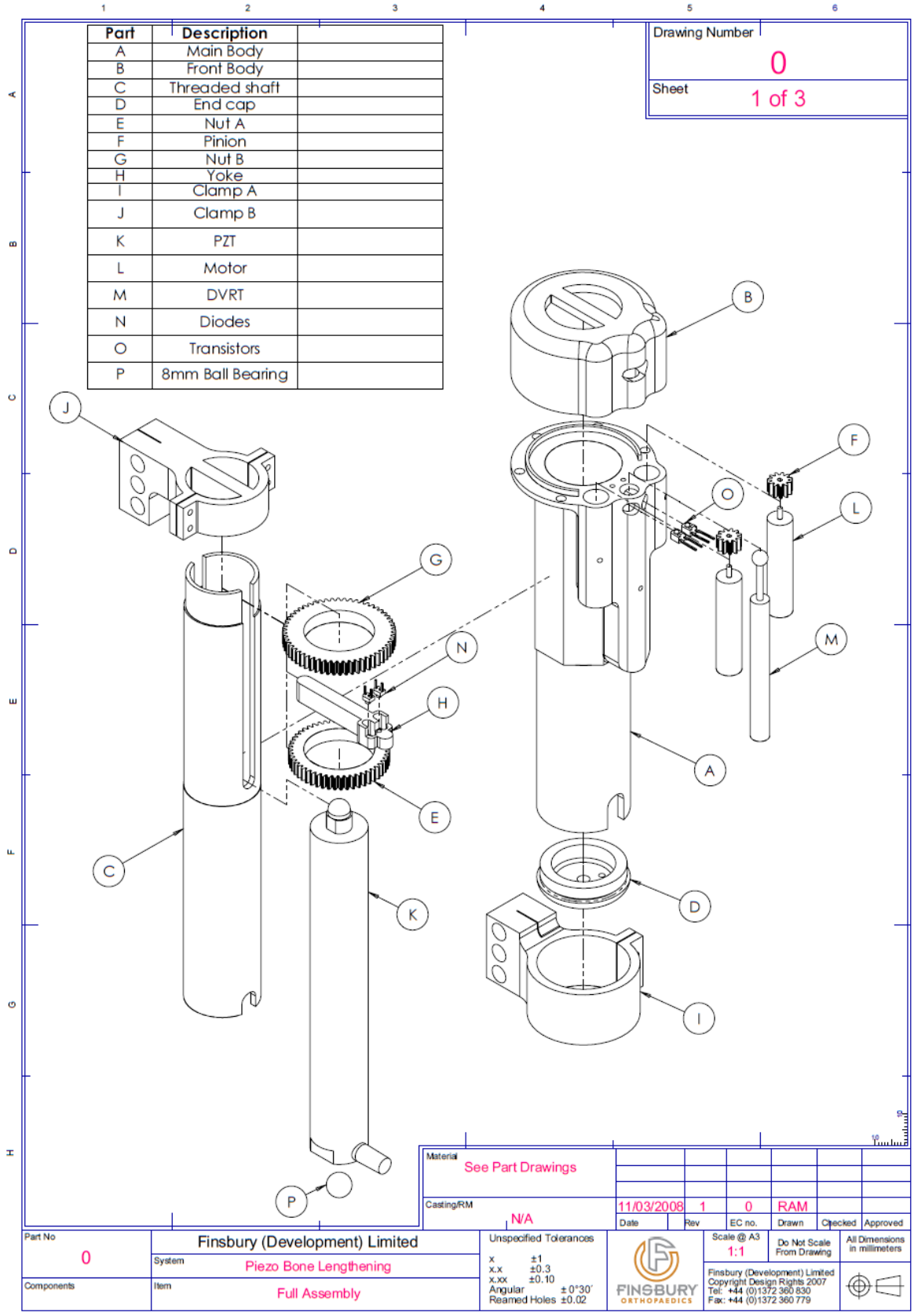

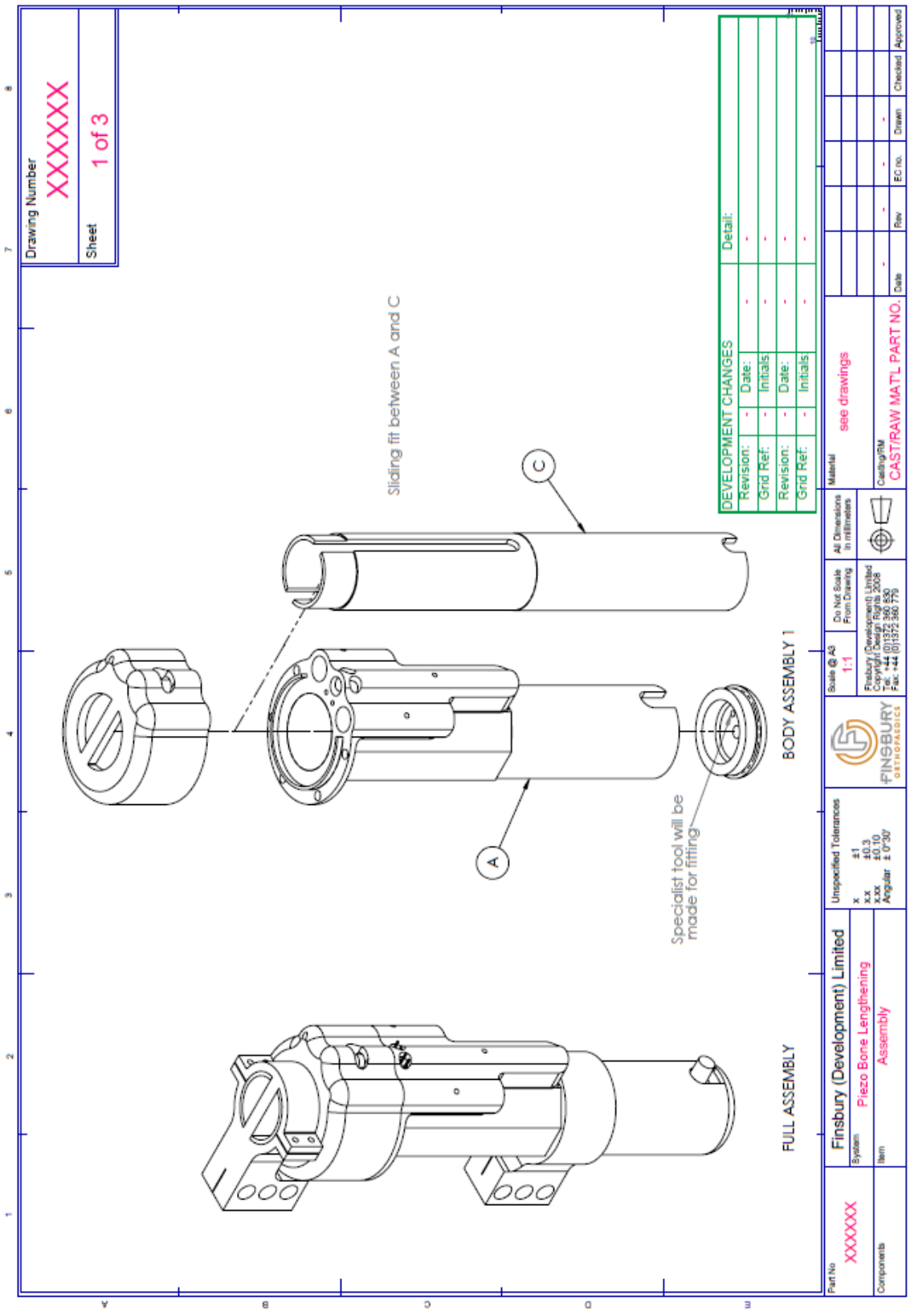
Drawing Number
XXXXXX
Sheet 1 of 3
Sliding fit between A and C
Specialist tool will be made for fitting
BODY ASSEMBLY 1
FULL ASSEMBLY
DEVELOPMENT CHANGES
Detail:
Revision: - Date: - -
Grid Ref: - Initials - -
Revision: - Date: - -
Grid Ref: - Initials - -
Material see drawings
Casting/RM CAST/RAW MATL PART NO.
Finsbury (Development) Limited
System Piezo Bone Lengthening
Item Assembly
Components
Part No XXXXXX
Unspecified Tolerances
x ±1
x.x ±0.3
x.xx ±0.10
Angular ± 0°30'
Scale @ A3 1:1
Do Not Scale From Drawing
All Dimensions In millimeters
Finsbury (Development) Limited
Copyright Design Rights 2008
Tel: +44 (0)1372 380 830
Fax: +44 (0)1372 386 779
FINSBURY ORTHOPAEDICS
Date - Rev - EC no. - Drawn - Checked - Approved

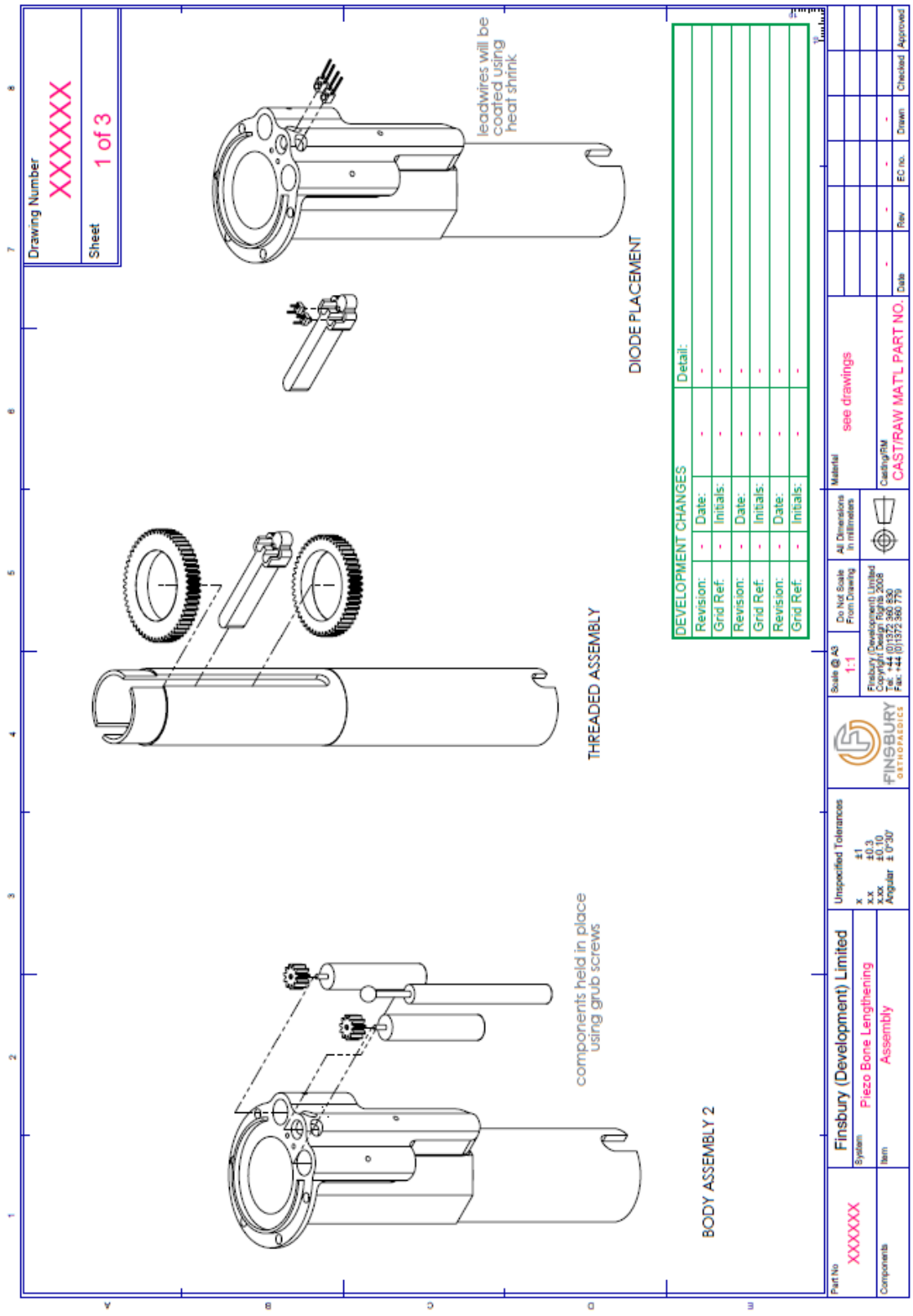
Drawing Number
XXXXXX
Sheet 1 of 3
leadwires will be coated using heat shrink
DIODE PLACEMENT
THREADED ASSEMBLY
components held in place using grub screws
BODY ASSEMBLY 2
DEVELOPMENT CHANGES
Detail:
Revision: - Date: -
Grid Ref: - Initials: -
Revision: - Date: -
Grid Ref: - Initials: -
Revision: - Date: -
Grid Ref: - Initials: -
Material
see drawings
Casting/RM
CAST/RAW MATL PART NO.
Part No
XXXXXX
Components
Finsbury (Development) Limited
System
Piezo Bone Lengthening
Item
Assembly
Unspecified Tolerances
x ±1
xx ±0.3
xxx ±0.10
Angular ± 0°30'
Scale @ A3
1:1
Do Not Scale From Drawing
All Dimensions in millimeters
Finsbury (Development) Limited
Copyright Design Rights 2008
Tel: +44 (0)1372 380 830
Fax: +44 (0)1372 380 779
FINSBURY ORTHOPAEDICS
Date
Rev
EC no.
Drawn
Checked
Approved

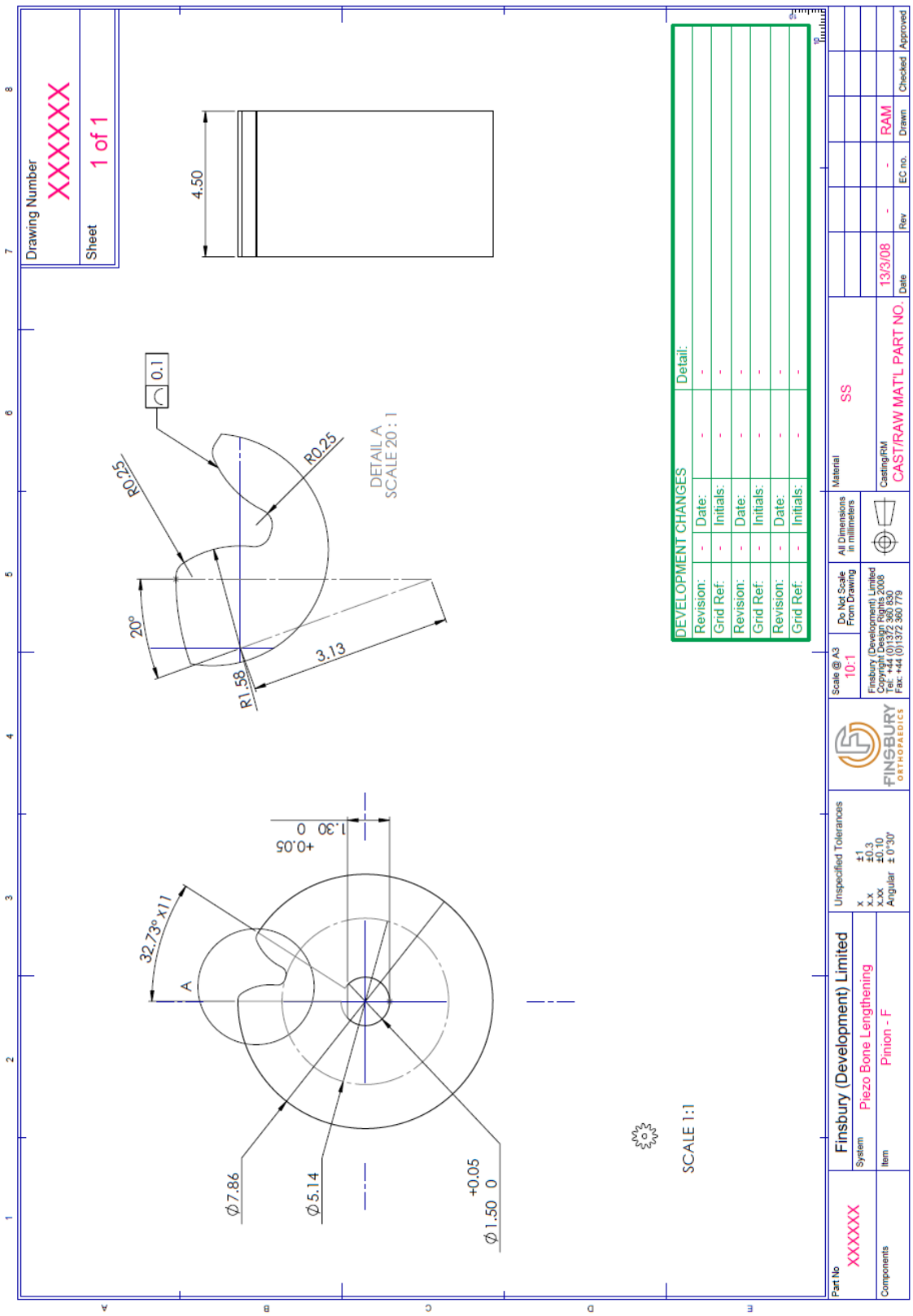
Drawing Number
XXXXXX
Sheet 1 of 1
4.50
0.1
R0.25
R0.25
20°
3.13
R1.58
DETAIL A
SCALE 20 : 1
DEVELOPMENT CHANGES
Detail:
Revision: - Date: - Initials: - Grid Ref: -
Revision: - Date: - Initials: - Grid Ref: -
Revision: - Date: - Initials: - Grid Ref: -
Revision: - Date: - Initials: - Grid Ref: -
32.73° x11
A
Ø7.86
Ø5.14
Ø1.50 +0.05 0
1.30 +0.05 0
SCALE 1:1
Material SS
Casting/RM CAST/RAW MAT'L PART NO.
Date 13/3/08
Rev -
EC no. -
Drawn RAM
Checked
Approved
All Dimensions in millimeters
Do Not Scale From Drawing
Scale @ A3 10:1
Finsbury (Development) Limited
Copyright Design Rights 2008
Tel: +44 (0)1372 360 830
Fax: +44 (0)1372 360 779
FINSBURY ORTHOPAEDICS
Unspecified Tolerances
x ±1
x.x ±0.3
x.xx ±0.10
Angular ± 0°30'
Part No XXXXXX
Finsbury (Development) Limited
System Piezo Bone Lengthening
Item Pinion - F
Components

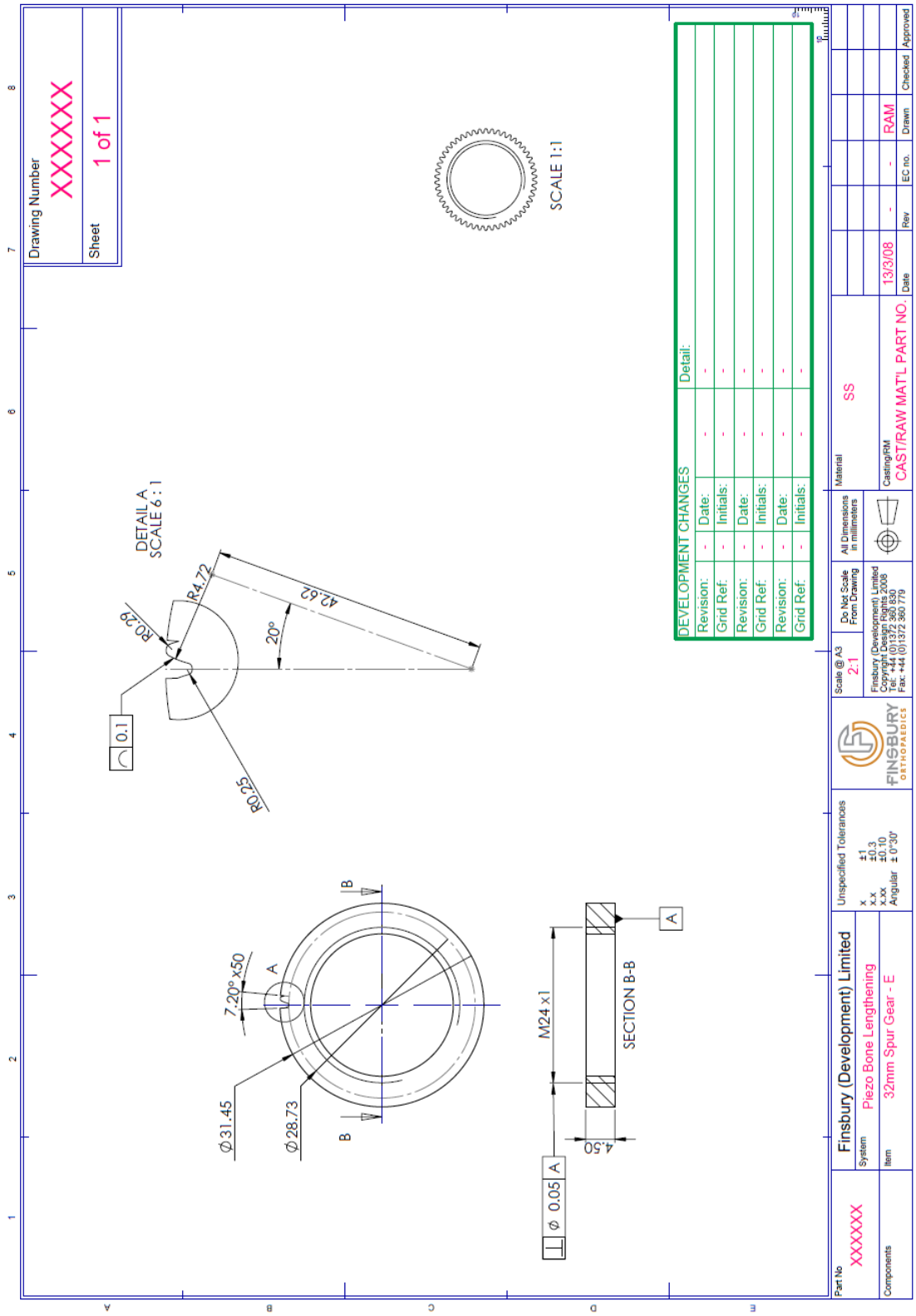
Drawing Number
XXXXXX
Sheet 1 of 1
SCALE 1:1
DETAIL A
SCALE 6 : 1
R0.25
R4.72
42.62
20°
R0.25
0.1
7.20° x50
A
B
Ø31.45
Ø28.73
B
M24 x1
SECTION B-B
4.50
A
⌖ Ø 0.05 A
DEVELOPMENT CHANGES
Detail:
Revision: - Date: -
Grid Ref: - Initials: -
Revision: - Date: -
Grid Ref: - Initials: -
Revision: - Date: -
Grid Ref: - Initials: -
Revision: - Date: -
Grid Ref: - Initials: -
Scale @ A3 2:1
Do Not Scale From Drawing
All Dimensions in millimeters
Material SS
Casting/RM CAST/RAW MAT'L PART NO.
Finsbury (Development) Limited
Copyright Design Rights 2008
Tel: +44 (0)1372 360 630
Fax: +44 (0)1372 360 779
FINSBURY ORTHOPAEDICS
Unspecified Tolerances
x ±1
x.x ±0.3
x.xx ±0.10
Angular ± 0°30'
Part No XXXXXX
Components
Finsbury (Development) Limited
System Piezo Bone Lengthening
Item 32mm Spur Gear - E
Date 13/3/08
Rev -
EC no. -
Drawn RAM
Checked
Approved

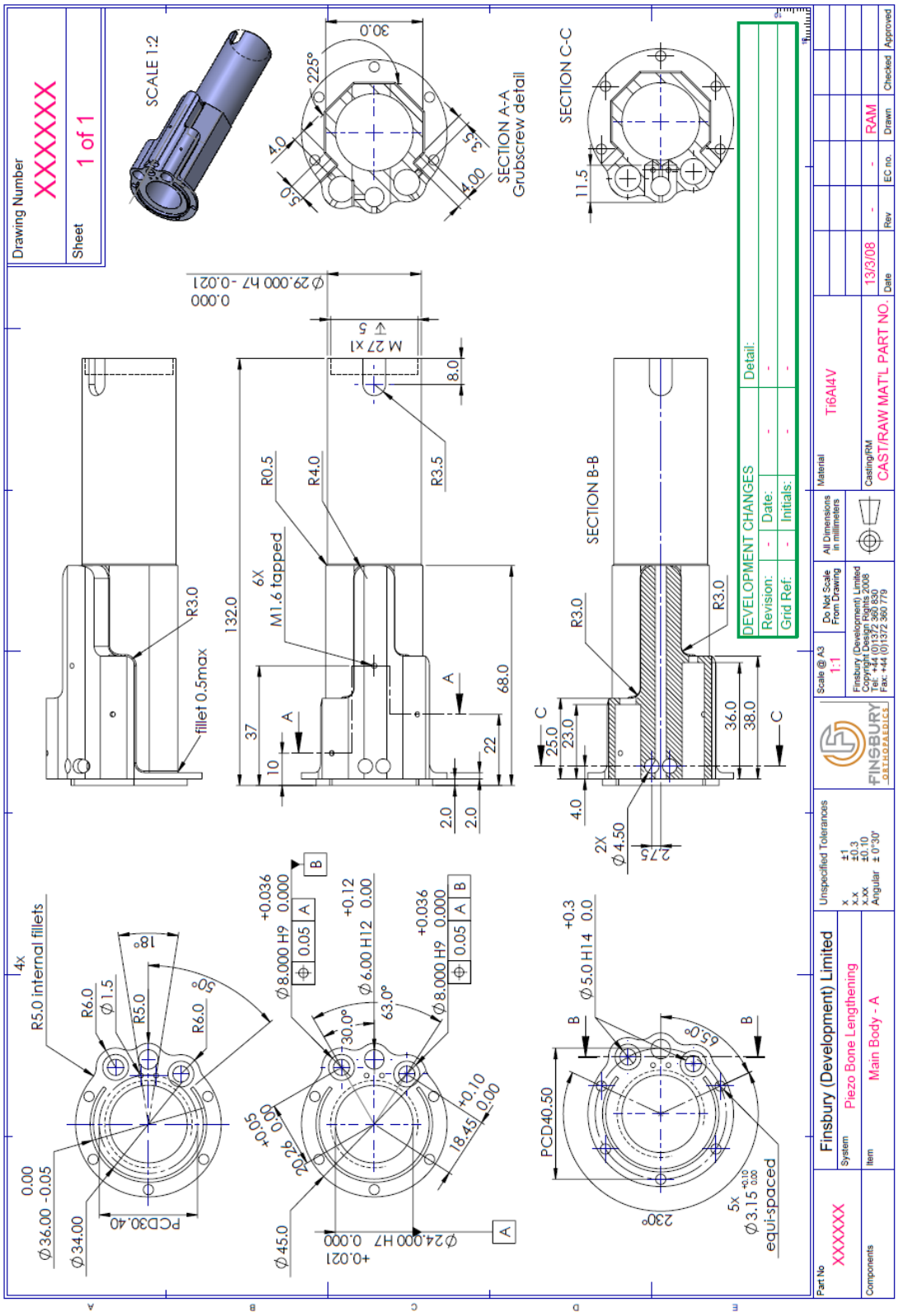
Drawing Number
XXXXXX
Sheet 1 of 1
SCALE 1:2
SECTION A-A
Grubscrew detail
SECTION C-C
SECTION B-B
DEVELOPMENT CHANGES
Detail:
Revision:
Date:
Grid Ref:
Initials:
Material Ti6Al4V
Casting/RM
CAST/RAW MAT'L PART NO.
All Dimensions in millimeters
Do Not Scale From Drawing
Scale @ A3 1:1
Unspecified Tolerances
Finsbury (Development) Limited
System Piezo Bone Lengthening
Item Main Body - A
Components
Part No XXXXXX
Date 13/3/08
Rev -
EC no. -
Drawn RAM
Checked
Approved
4x R5.0 internal fillets
PCD30.40
PCD40.50
6X M1.6 tapped
M 27 x1
fillet 0.5max
equi-spaced

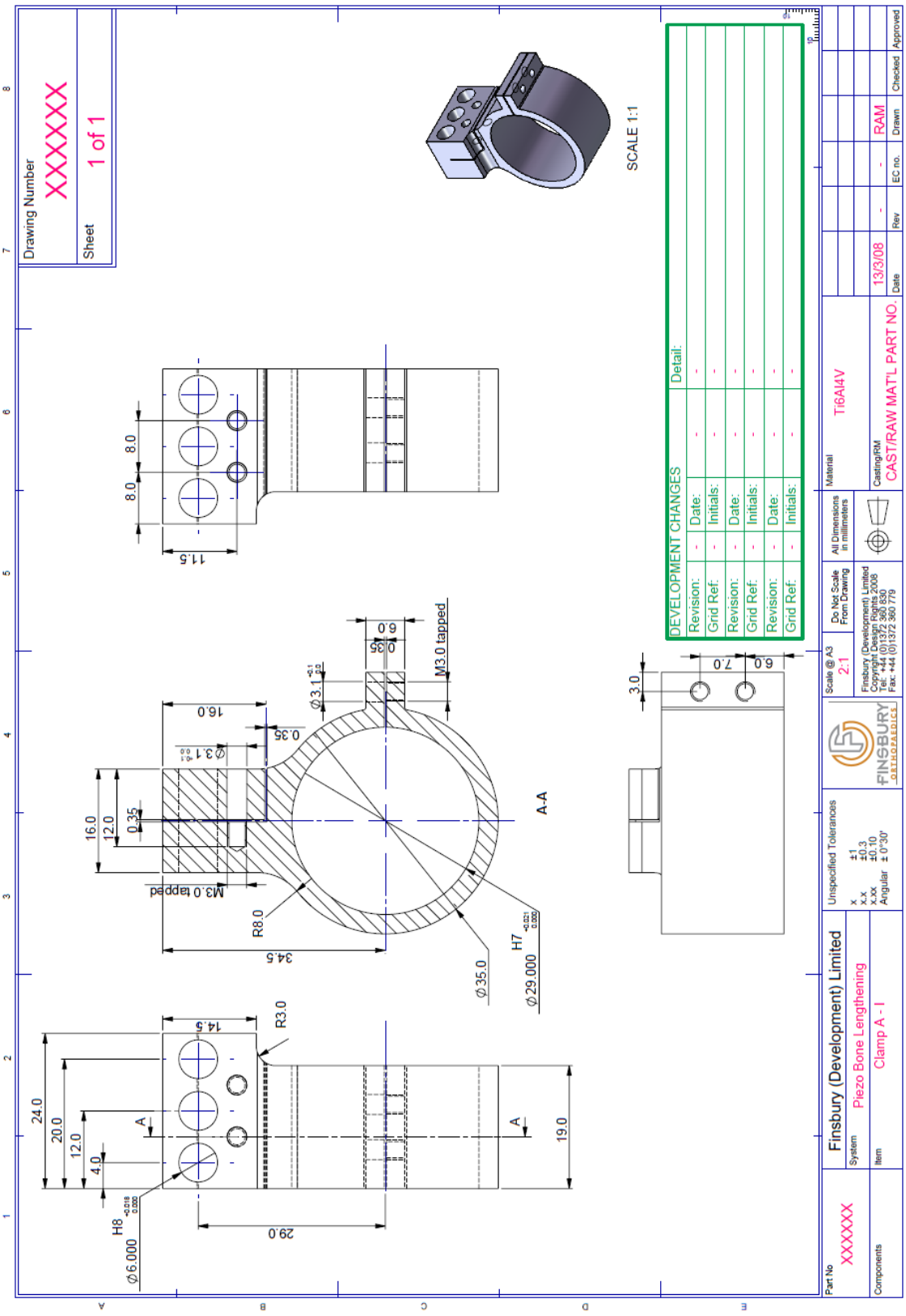
Drawing Number
XXXXXX
Sheet 1 of 1
SCALE 1:1
DEVELOPMENT CHANGES
Detail:
Revision: - Date: -
Grid Ref: - Initials: -
Revision: - Date: -
Grid Ref: - Initials: -
Revision: - Date: -
Grid Ref: - Initials: -
Material Ti6Al4V
Casting/RM CAST/RAW MAT'L PART NO.
All Dimensions in millimetres
Do Not Scale From Drawing
Scale @ A3 2:1
Unspecified Tolerances
x ±1
x.x ±0.3
x.xx ±0.10
Angular ± 0°30'
Finsbury (Development) Limited
Copyright Design Rights 2008
Tel: +44 (0)1372 360 830
Fax: +44 (0)1372 360 779
FINSBURY ORTHOPAEDICS
Part No XXXXXX
System Piezo Bone Lengthening
Item Clamp A - I
Components
Rev - 13/3/08 Date
EC no. - Drawn RAM Checked Approved
A-A
M3.0 tapped
R8.0
R3.0
Ø35.0
Ø29.000
Ø6.000
24.0
20.0
12.0
4.0
29.0
19.0
16.0
34.5
14.5
11.5
8.0
3.0
7.0
6.0

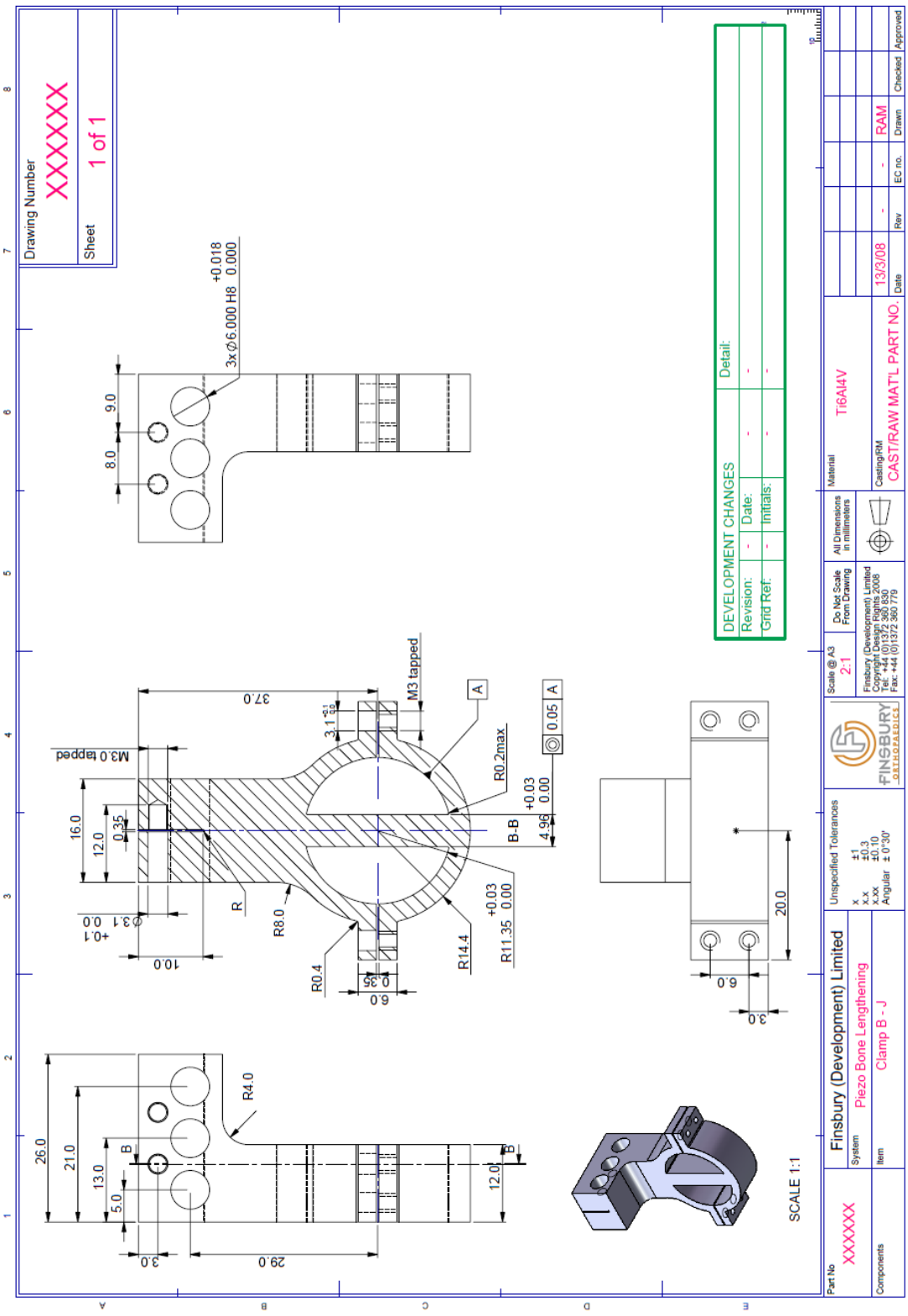
Drawing Number
XXXXXX
Sheet 1 of 1
DEVELOPMENT CHANGES
Detail:
Revision: - Date: - Initials: -
Grid Ref: - - -
3x Ø6.000 H8 +0.018 0.000
9.0
8.0
37.0
M3 tapped
M3.0 tapped
16.0
12.0
0.35
Ø3.1 +0.1 0.0
10.0
R
R8.0
R0.4
R0.2max
R14.4
R11.35 +0.03 0.00
B-B
4.96 +0.03 0.00
0.05 A
6.0
3.0
20.0
6.0
3.0
R4.0
26.0
21.0
13.0
5.0
B
29.0
12.0
SCALE 1:1
Part No XXXXXX
Components
Finsbury (Development) Limited
System Piezo Bone Lengthening
Item Clamp B - J
Unspecified Tolerances
x ±1
x.x ±0.3
x.xx ±0.10
Angular ± 0°30'
FINSBURY ORTHOPAEDICS
Scale @ A3 2:1
Do Not Scale From Drawing
All Dimensions in millimeters
Material Ti6Al4V
Casting/RM CAST/RAW MATL PART NO.
Date 13/3/08
Rev -
EC no. -
Drawn RAM
Checked
Approved

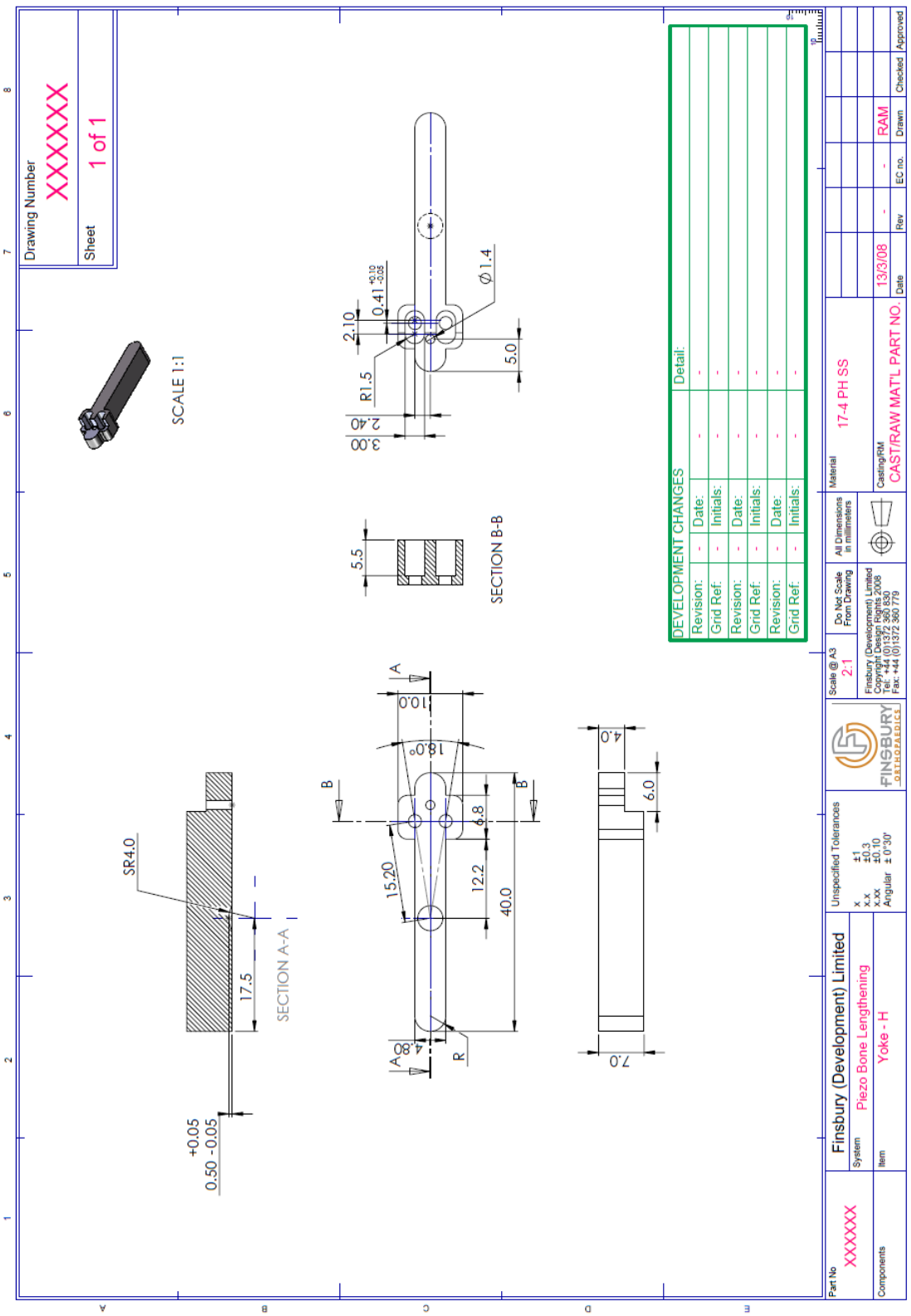
Drawing Number
XXXXXX
Sheet 1 of 1
SCALE 1:1
SECTION A-A
SECTION B-B
SR4.0
17.5
+0.05
0.50 -0.05
10.0
18.0°
15.20
12.2
40.0
6.8
4.80
R
4.0
6.0
7.0
2.10
0.41 +0.10 -0.05
R1.5
2.40
3.00
Ø1.4
5.0
5.5
DEVELOPMENT CHANGES
Detail:
Revision:
Grid Ref:
Date:
Initials:
Scale @ A3 2:1
Do Not Scale From Drawing
All Dimensions in millimeters
Material 17-4 PH SS
Casting/RM CAST/RAW MAT'L PART NO.
Finsbury (Development) Limited
Unspecified Tolerances
x ±1
x.x ±0.3
x.xx ±0.10
Angular ±0°30'
FINSBURY ORTHOPAEDICS
Part No XXXXXX
System Piezo Bone Lengthening
Item Yoke - H
Components
Date 13/3/08
Drawn RAM
Checked
Approved

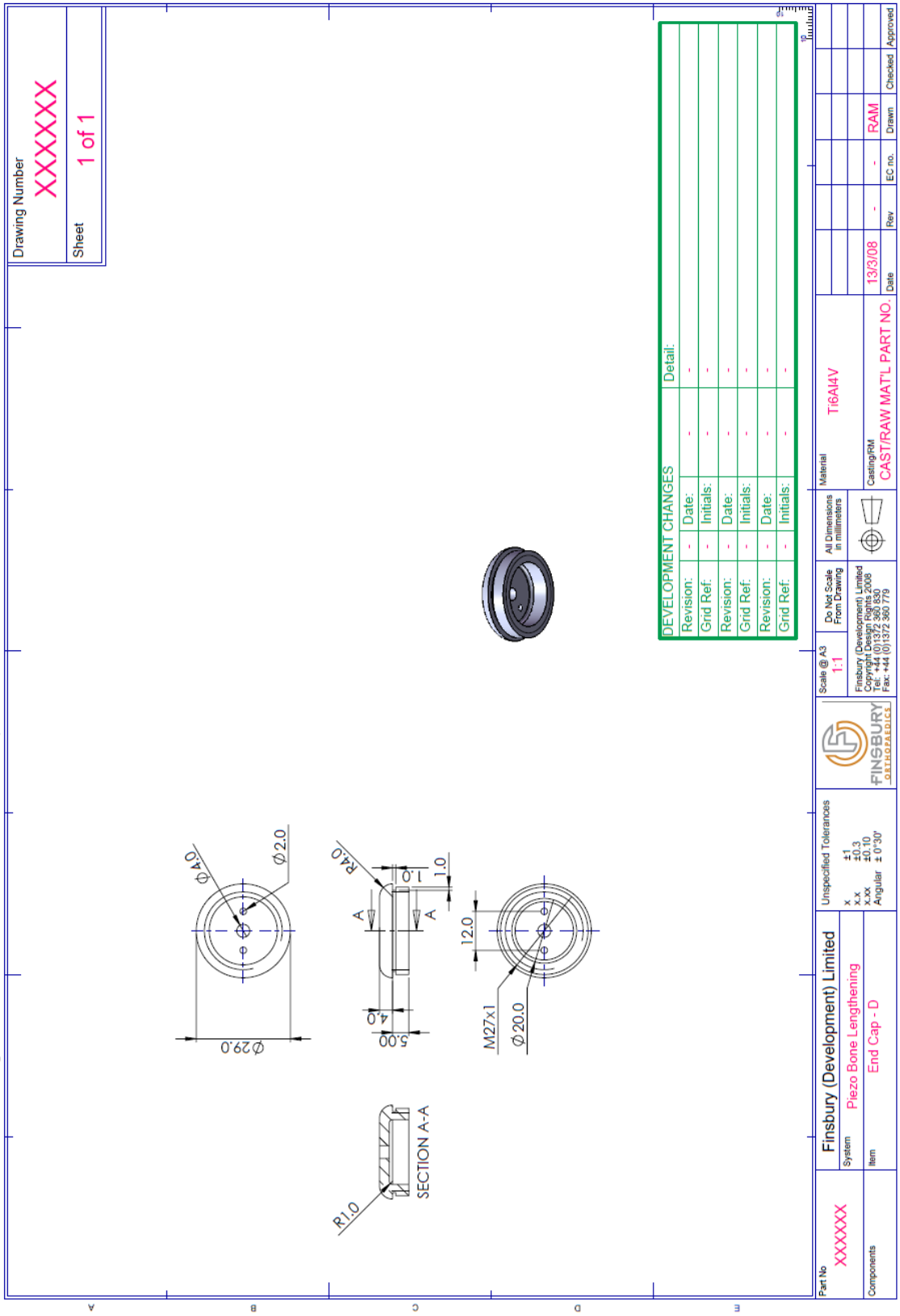
Drawing Number
XXXXXX
Sheet 1 of 1
DEVELOPMENT CHANGES
Detail:
Revision: - Date: - -
Grid Ref: - Initials: - -
Revision: - Date: - -
Grid Ref: - Initials: - -
Revision: - Date: - -
Grid Ref: - Initials: - -
Ø4.0
Ø2.0
Ø29.0
R4.0
1.0
1.0
A
A
5.00
4.0
12.0
M27x1
Ø20.0
R1.0
SECTION A-A
Scale @ A3 1:1
Do Not Scale From Drawing
All Dimensions in millimeters
Material Ti6Al4V
Casting/RM CAST/RAW MAT'L PART NO.
Unspecified Tolerances
x ±1
x.x ±0.3
x.xx ±0.10
Angular ± 0°30'
FINSBURY ORTHOPAEDICS
Finsbury (Development) Limited
Copyright Design Rights 2008
Tel: +44 (0)1372 360 830
Fax: +44 (0)1372 360 779
Part No XXXXXX
System Piezo Bone Lengthening
Item End Cap - D
Components
Date 13/3/08
Rev -
EC no. -
Drawn RAM
Checked
Approved

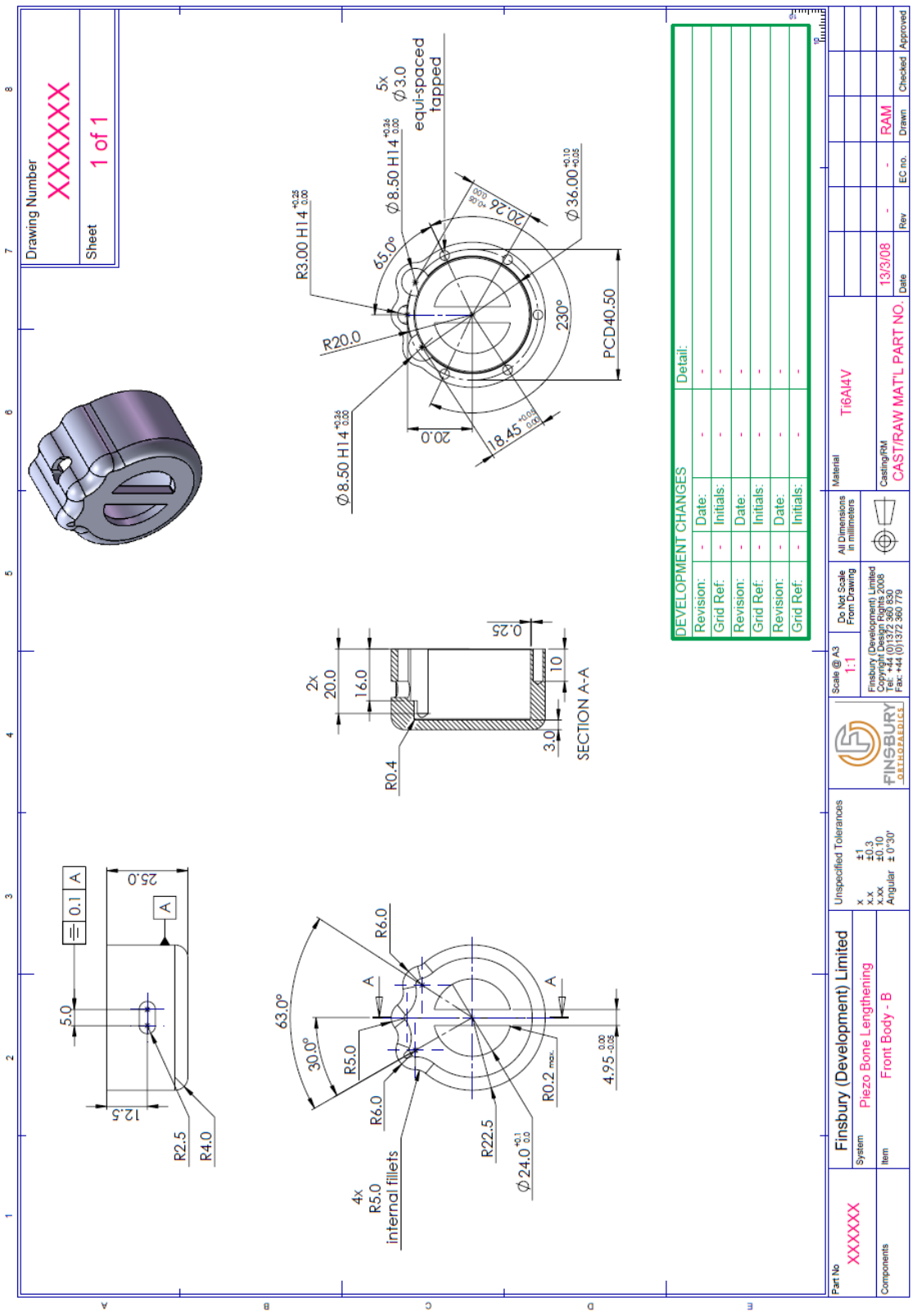
Drawing Number
XXXXXX
Sheet 1 of 1
R3.00 H14 +0.25 0.00
R20.0
Ø8.50 H14 +0.36 0.00
5x Ø3.0 equi-spaced tapped
Ø8.50 H14 +0.36 0.00
65.0°
20.26 +0.05 0.00
Ø36.00 +0.10 +0.05
230°
PCD40.50
20.0
18.45 +0.05 0.00
Ø8.50 H14 +0.36 0.00
DEVELOPMENT CHANGES
Detail:
Revision: - Date: -
Grid Ref: - Initials: -
Revision: - Date: -
Grid Ref: - Initials: -
Revision: - Date: -
Grid Ref: - Initials: -
2x 20.0
16.0
0.25
10
3.0
R0.4
SECTION A-A
63.0°
30.0°
R6.0
R5.0
R6.0
4x R5.0 internal fillets
R22.5
Ø24.0 +0.1 0.0
R0.2 max.
4.95 0.00 -0.05
0.1 A
25.0
5.0
12.5
R2.5
R4.0
Part No XXXXXX
Components
System Piezo Bone Lengthening
Item Front Body - B
Unspecified Tolerances
x ±1
x.x ±0.3
x.xx ±0.10
Angular ± 0° 30'
FINSBURY
Scale @ A3 1:1
Do Not Scale From Drawing
Finsbury (Development) Limited
Copyright Design Rights 2008
Tel: +44 (0)1372 360 360
Fax: +44 (0)1372 360 779
All Dimensions in millimeters
Material Ti6Al4V
Casting/RM CAST/RAW MAT'L PART NO.
Date 13/3/08
Rev -
EC no. -
Drawn RAM
Checked
Approved

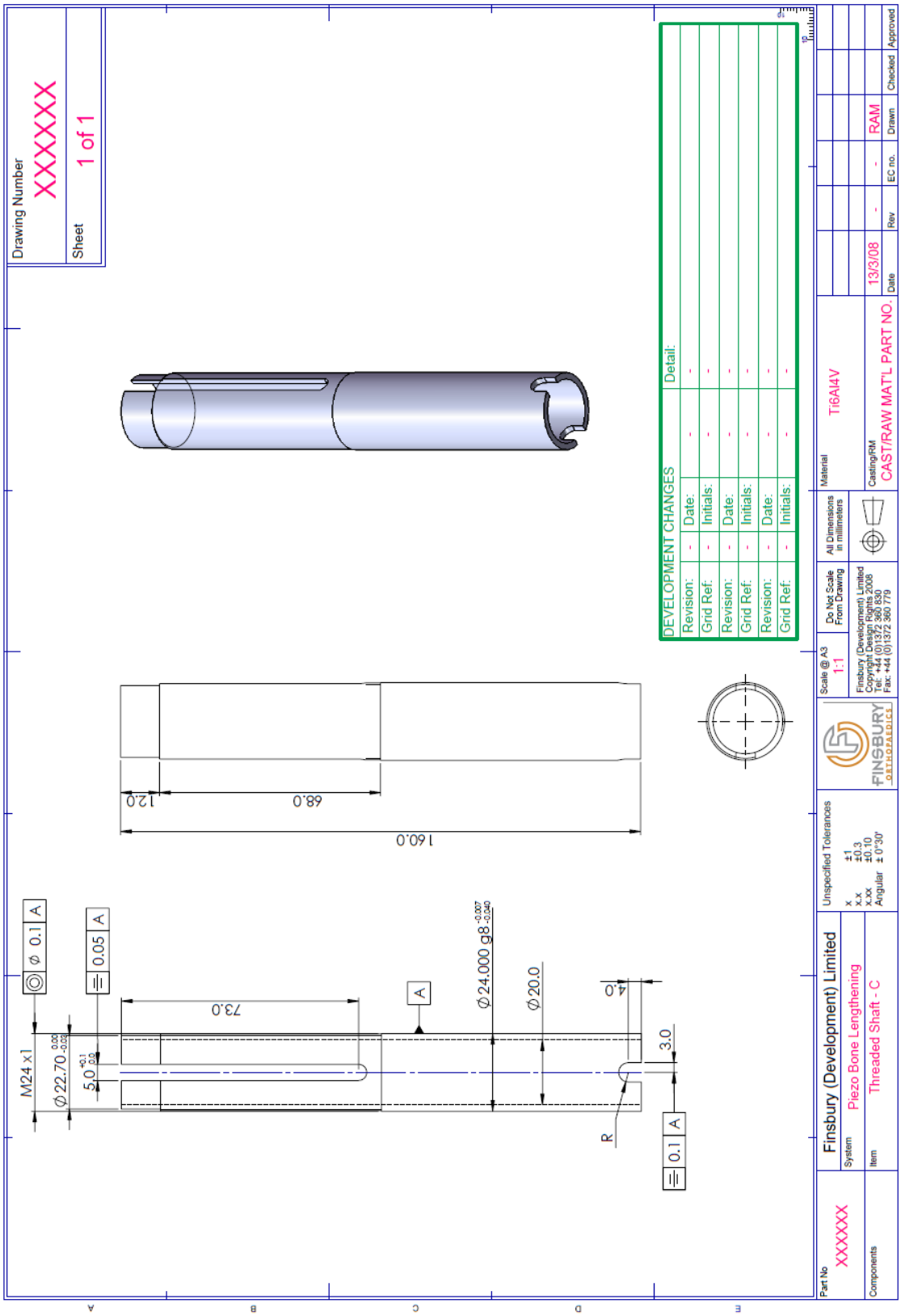
Drawing Number
XXXXXX
Sheet
1 of 1
DEVELOPMENT CHANGES
Detail:
Revision:
Date:
Grid Ref:
Initials:
Material
Ti6Al4V
Casting/RM
CAST/RAW MATL PART NO.
All Dimensions in millimeters
Do Not Scale From Drawing
Scale @ A3
1:1
Finsbury (Development) Limited
Unspecified Tolerances
Part No
XXXXXX
Components
System
Piezo Bone Lengthening
Item
Threaded Shaft - C
FINSBURY
ORTHOPAEDICS
Date
13/3/08
Rev
EC no.
Drawn
RAM
Checked
Approved
160.0
68.0
12.0
73.0
M24 x1
Ø22.70
5.0
Ø24.000 g8
Ø20.0
4.0
3.0
R
0.1 A
0.05 A
Ø 0.1 A

APPENDIX C – MODELLING OF THE DEVICE

APPENDIX C(i) - MODEL DEVELOPMENT
A full 1-D model of the components and their interactions was built.

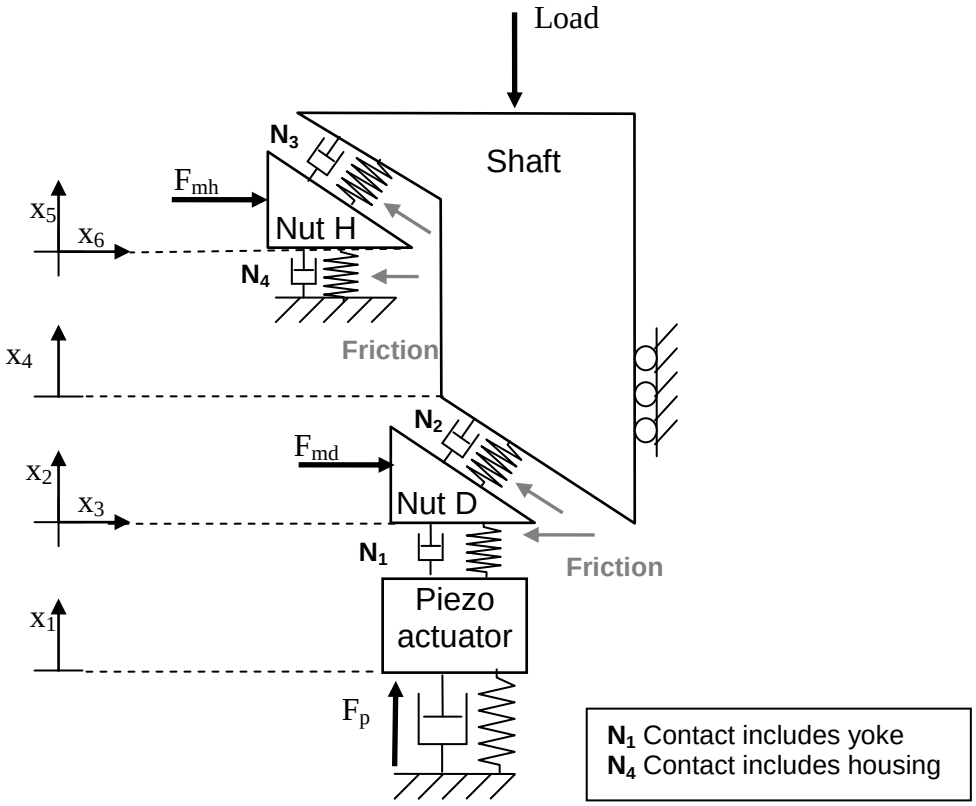

Then, based on the free body diagram for each component, equations of motion were written:

Piezo actuator	$m_1\ddot{x}_1 = F_p - N_1 - k_1x_1 - cx_2$
Driving Nut - horizontal	$m_2\ddot{x}_2 = F_{motor} - \mu_2N_2\cos\theta - N_2\sin\theta - \mu_1N_1 - \dot{x}_2c_{motor}$
Driving nut - vertical	$m_3\ddot{x}_3 = N_1 - N_2\cos\theta + \mu_2N_2\sin\theta$
Shaft	$m_4\ddot{x}_4 = N_2\cos\theta + N_3\cos\theta - \mu_2N_2\sin\theta - \mu_3N_3\sin\theta - F_1 - \dot{x}_4c_{shaft}$
Holding nut - horizontal	$m_5\ddot{x}_5 = F_{mb} - N_3\sin\theta - \mu_3N_3\cos\theta - \mu_4N_4 - \dot{x}_5c_{motor}$
Holding nut - vertical	$m_6\ddot{x}_6 = -N_3\cos\theta + \mu_3N_3\sin\theta + N_4$

APPENDIX C(ii) DEVICE MODEL DESCRIPTION

Piezo actuator (x_1)

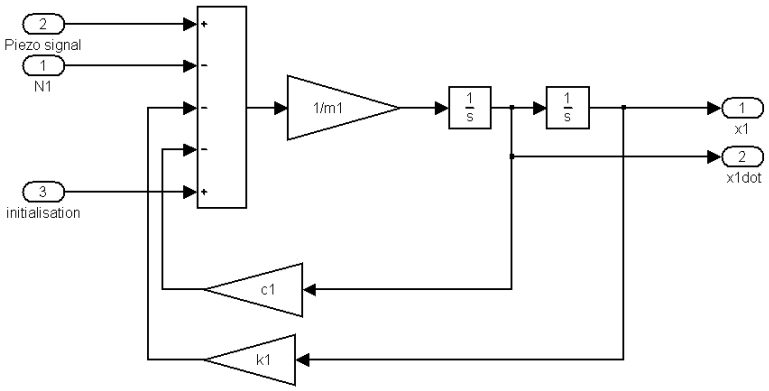

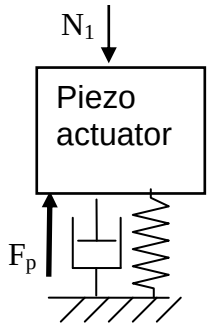

Driving nut (x_2)

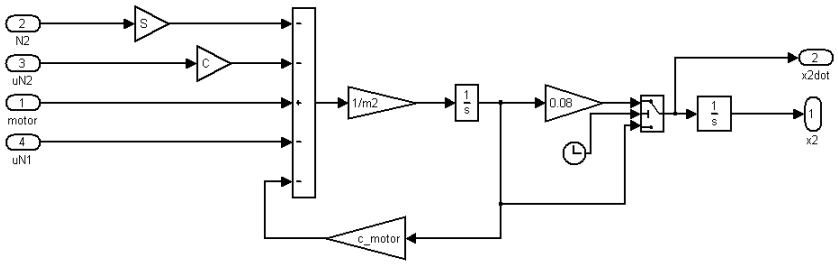

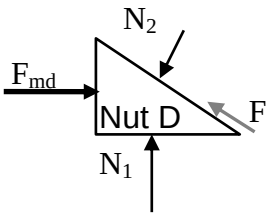

Driving nut (x_3)

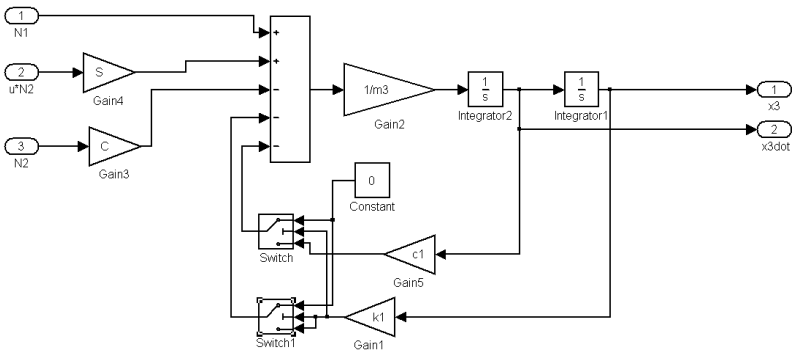

Shaft (x_4)

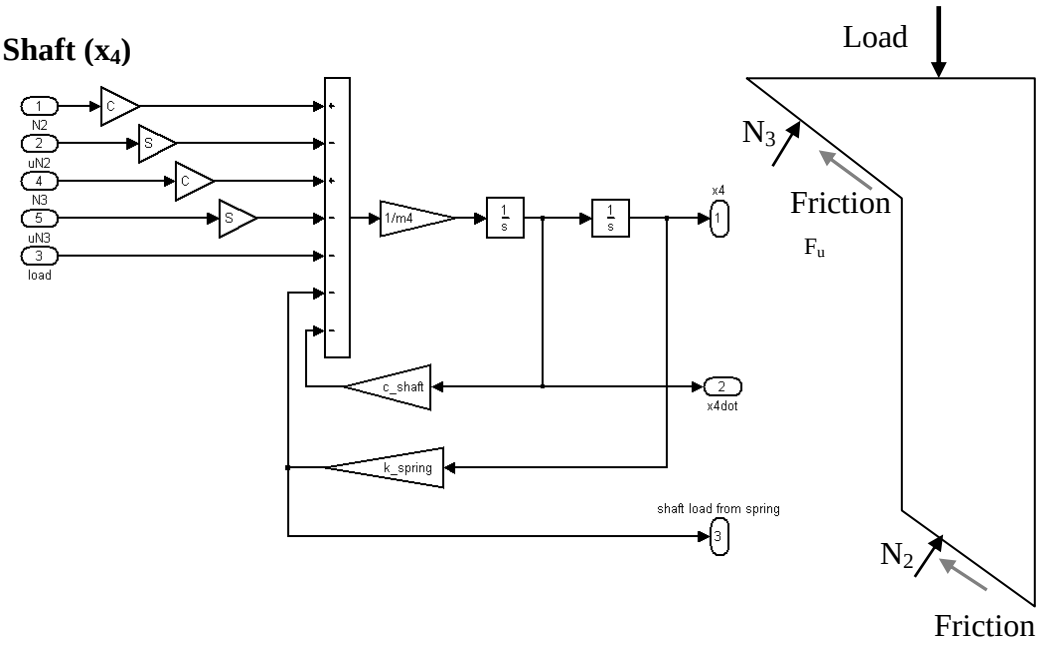

Holding Nut (x_5)

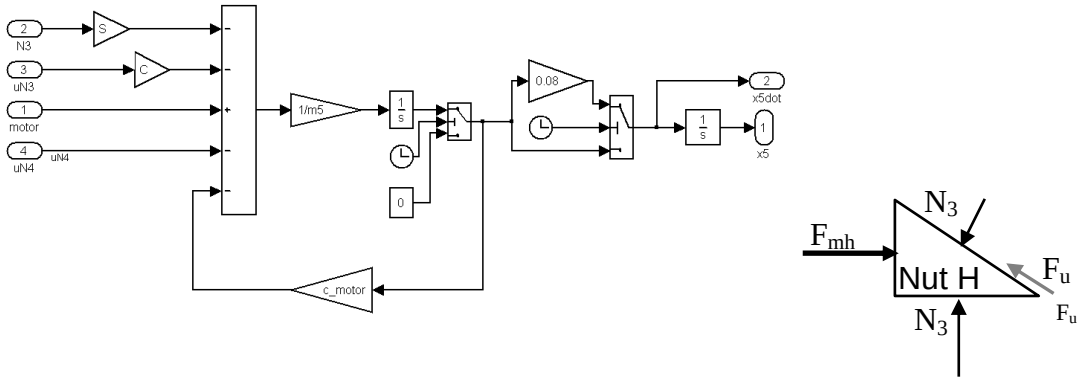

Holding Nut (x_6)

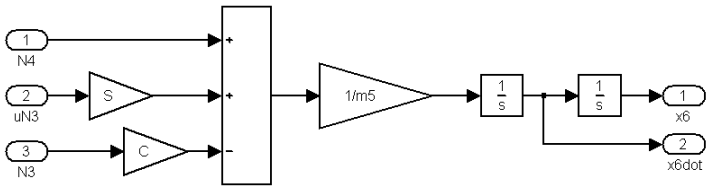

N_1, piezo actuator-driving nut

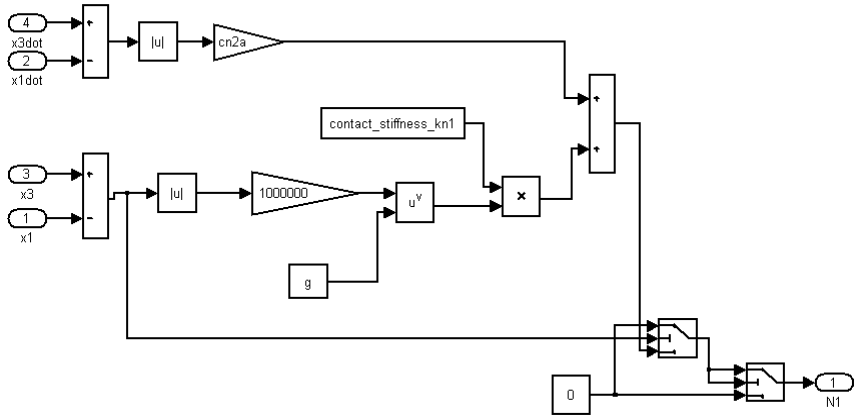

N_2, driving nut-shaft

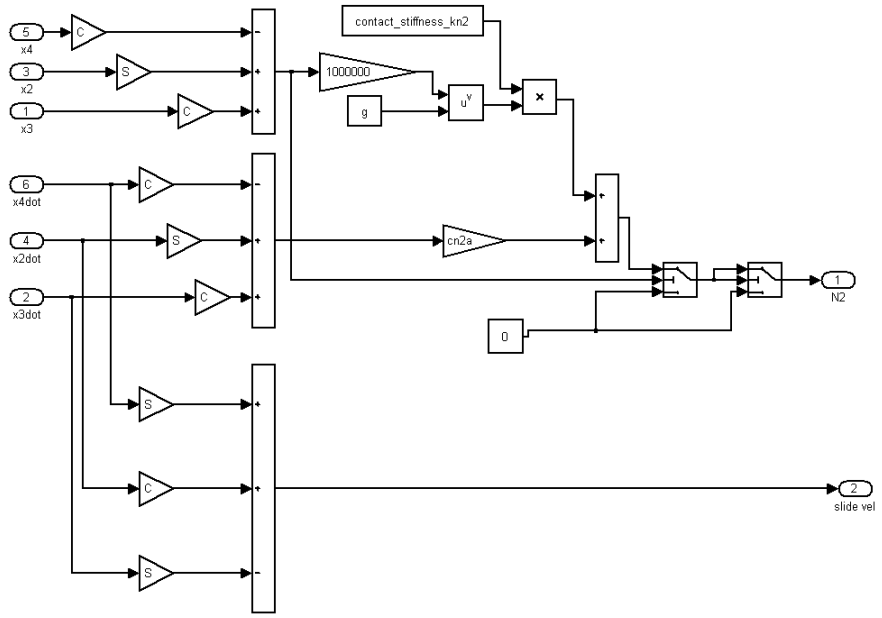

N_3, holding nut-shaft

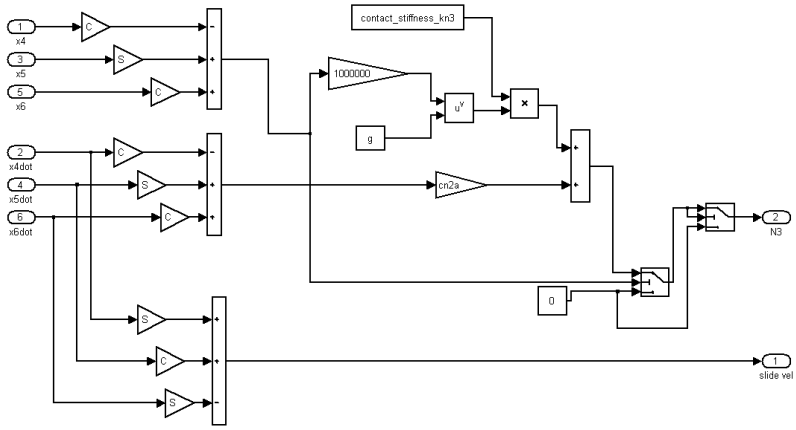

N_4, holding nut

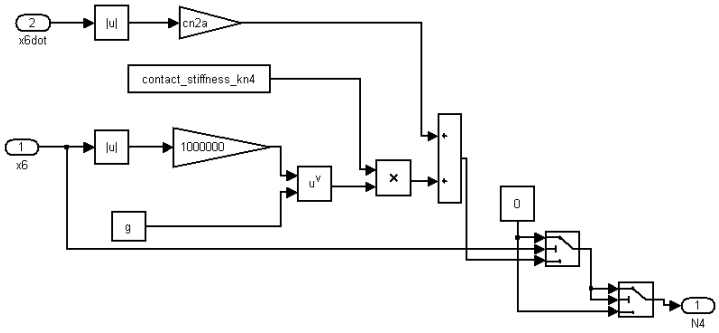

Friction

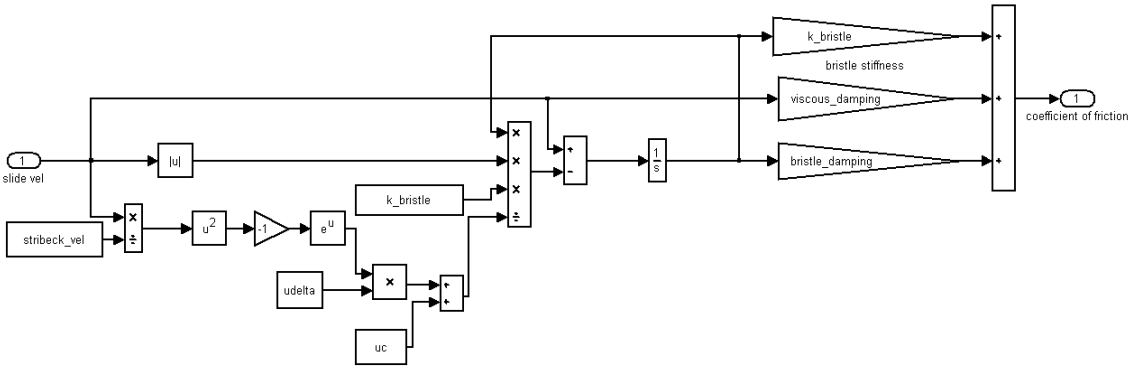

Piezo signal control

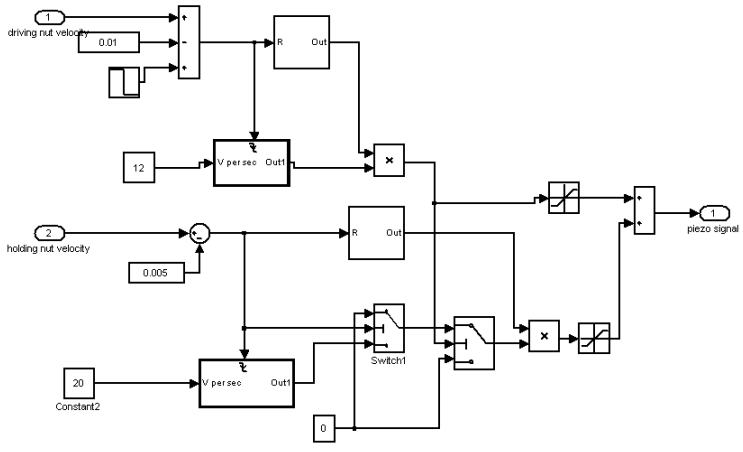

Full device model

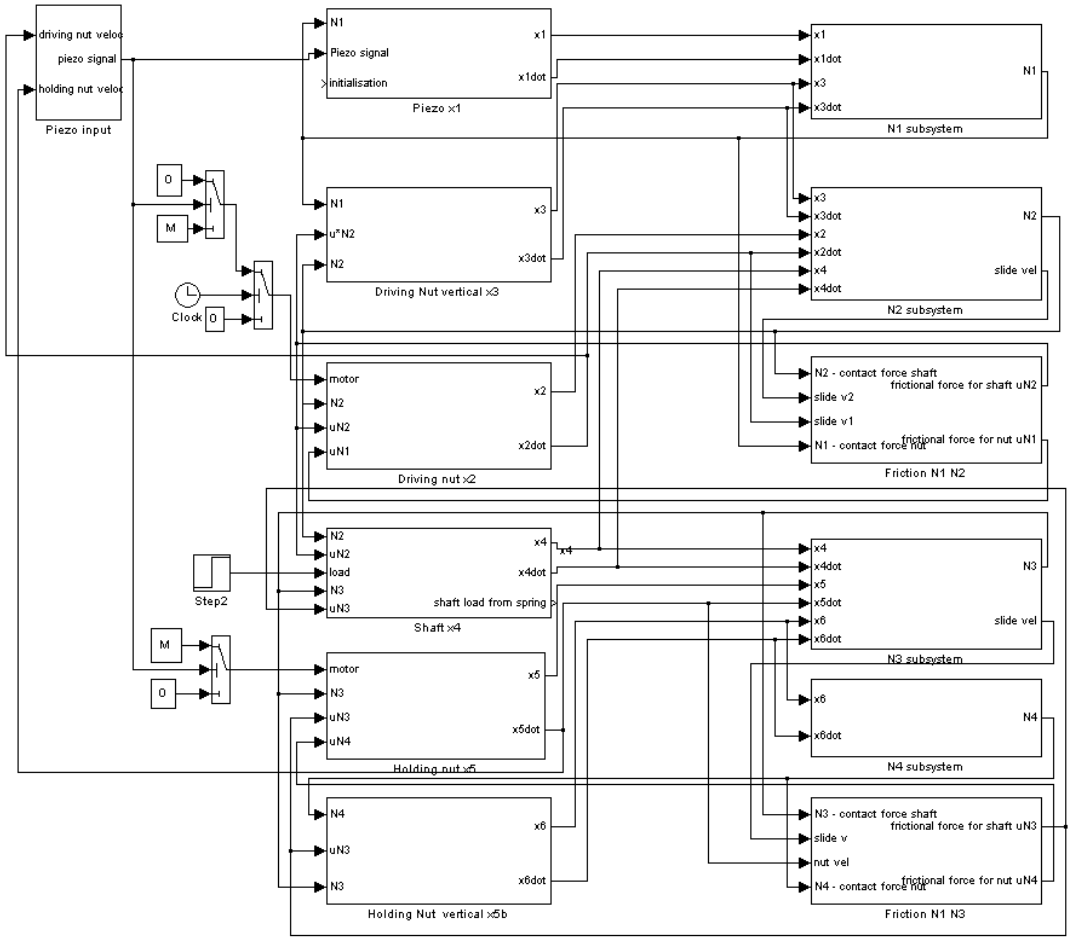

Configuration parameters
- Solver
Solver type - ode23s (stiff/Mod. Rosenbrock)
Variable step
Max step size limited to 0.5 *(stops solution missing crucial steps in simulation)*
100 allowable minimum step size violations
1000 consecutive zero crossings
Data import/export
Export component displacements every second

Initialisation function
M = 1

C = 0.99991123
S = 0.01333215

m1 = 0.1
m2 = 0.018
m4 = 0.05
m5 = 0.018

contact_stiffness_kc1 = 10
contact_stiffness_kc2 = 10
contact_stiffness_kc3 =10
contact_stiffness_kc4 = 10
cn2a =3
g = 1.6
k_spring = 0

k1 = 16667000
c1 = 150000

c_shaft = 50
c_motor = 4

uc = 0.3
udelta = 0.5
k_bristle =5000
viscous_damping = 0.001
bristle_damping = 1
stribeck_vel = 0.000001

APPENDIX C(iii) TISSUE MODEL OUTLINE (USINS PINS)

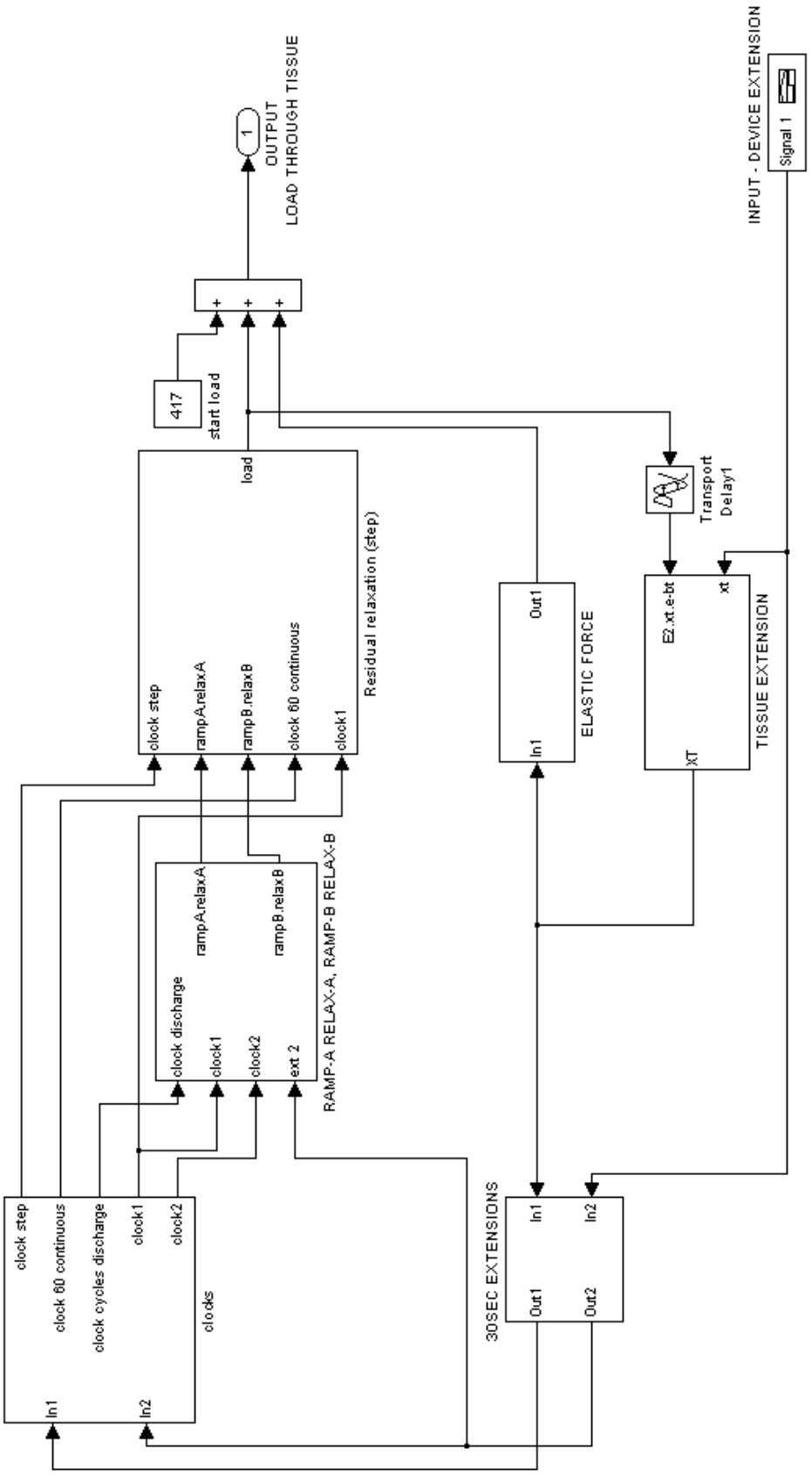

APPENDIX D: BASIC VISCOELASTIC MODELS

The spring-dashpot representations of viscoelasticity described in Chapter 3 can be modelled in the same way as was used for the contact models when modelling the devices. This builds upon the simple spring model (for an elastic material) to a material with time dependency. As before, equations are turned into block diagrams and the simulink model of a maxwell unit is shown below (Figure C1). The transfer function is an approximated linearisation of the derivative block as the solver cannot find the exact linearisation due to the blocks inability to be represented as a state space system (dynamic equation is y=u').

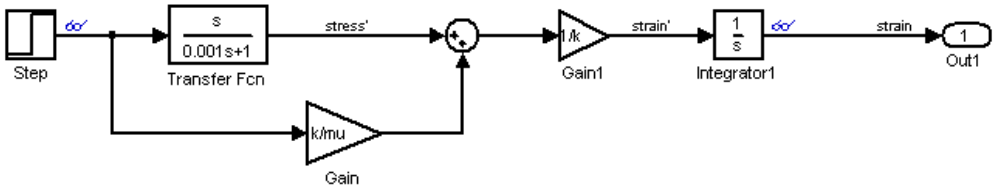

(a)

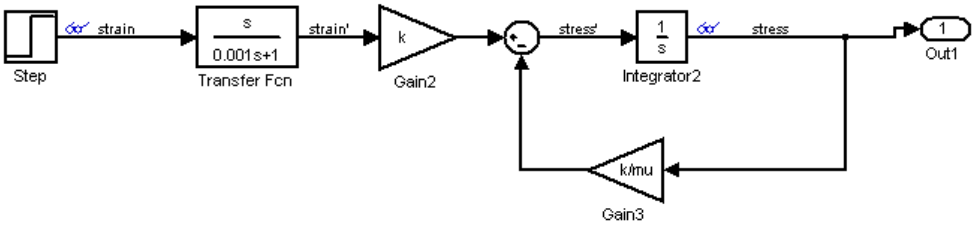

(b)

Figure D1. Maxwell step stress model (a) and step strain model (b)

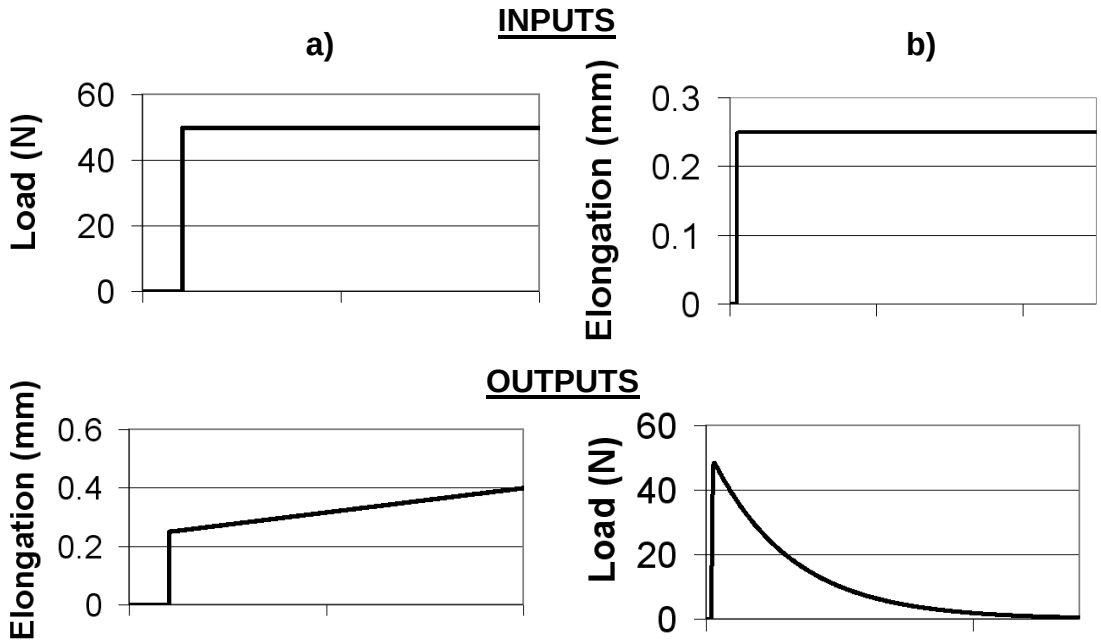

Figure D2. Load output from step distraction model, elongation output from step load model. μ and E are the same in both cases

A unit step is applied to each of the models at t=1 and the outputs are shown in Figure C2. The response to step stress can be termed a 'creep response' and as discussed in Chapter3 the expected strain response from the Maxwell element is not typically viscoelastic, instead a constant linear increase is observed with no asymptote reached. Conversely the stress response shows the relaxation characteristic curve. Values of k and μ can be modified to change the peak force or relaxation time.

Similarly, the Simulink Voigt model is shown in Figure C3.

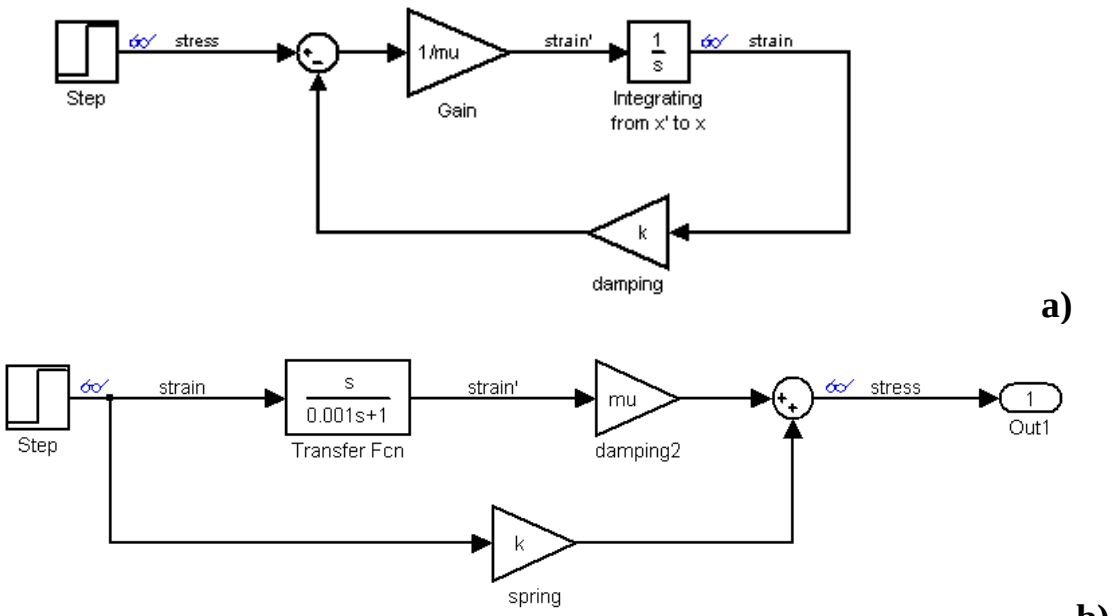

Figure D3. Voigt step stress model (a) and step strain model (b)

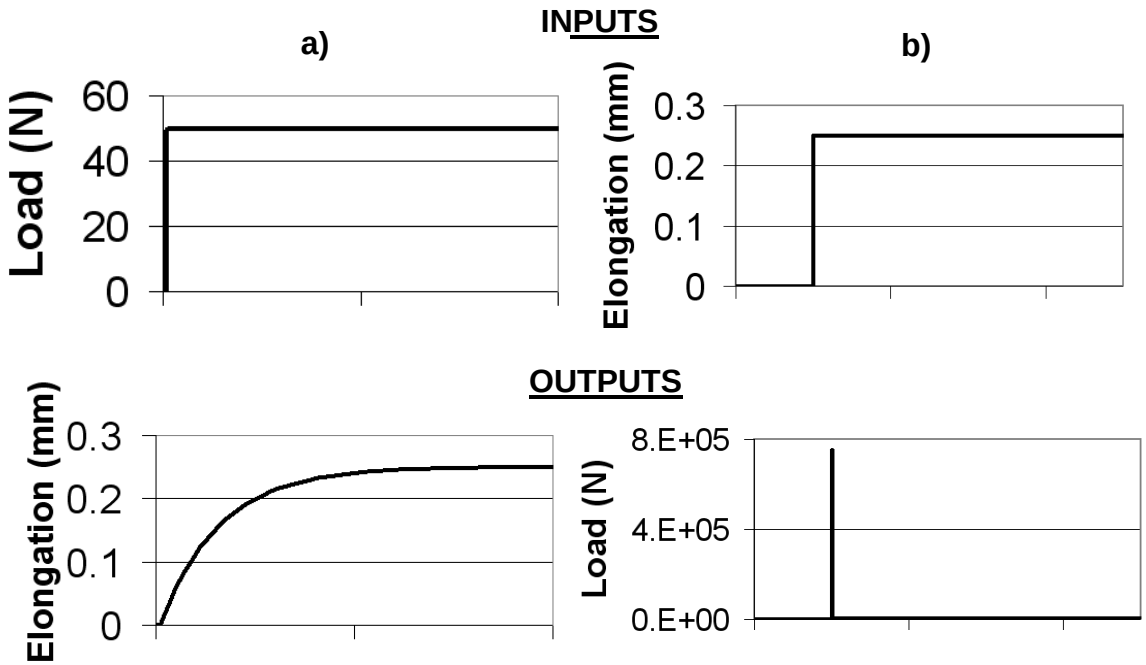

Figure D4. a) Strain output from step stress model, stress output from step strain model. μ and E are the same in both cases

Again a unit step is applied and the outputs are shown in Figure C4. This time the strain output from step stress (a) is representative of a viscoelastic system whereas the stress output from step strain shows an instantaneous relaxation due to the presence of the dashpot.

A combination of these two models is called the Standard Linear Solid model which can be built using the following relationships, allowing the system to be defined in terms of only total stress, total strain and their derivatives.

$$\varepsilon = \varepsilon_1 + \varepsilon_2 \qquad \text{(A)}$$
$$\varepsilon_1 = \varepsilon_D \qquad \text{(B)}$$
$$\sigma = \sigma_2 \qquad \text{(C)}$$
$$\sigma = \sigma_1 + \sigma_D \qquad \text{(D)}$$
$$\varepsilon_1 = \sigma_1 / E_1 \qquad \text{(E)}$$
$$\varepsilon_2 = \sigma_2 / E_2 \qquad \text{(F)}$$
$$\dot{\varepsilon}_D = \sigma_D / \eta_D \qquad \text{(G)s}$$

This allows the following

$$\varepsilon + \frac{\eta_D}{E_1}\dot{\varepsilon} = (\frac{1}{E_1} + \frac{1}{E_2})\sigma + \frac{\eta_D}{E_1}\frac{1}{E_2}\dot{\sigma}$$

$$\varepsilon + \tau_\sigma \dot{\varepsilon} = D_R\sigma + \tau_\varepsilon D_R \dot{\sigma}$$

Where:

τ_σ is relaxation time at constant stress

τ_ε is relaxation time at constant strain

D_R is relaxed compliance

This can be expressed in block format (Figure C5). Inputs of step stress and step strain both result in a standard viscoelastic response as shown in Figure C6. The terms stress and strain have been replaced by load and elongation for the purposes of the one dimensional model.

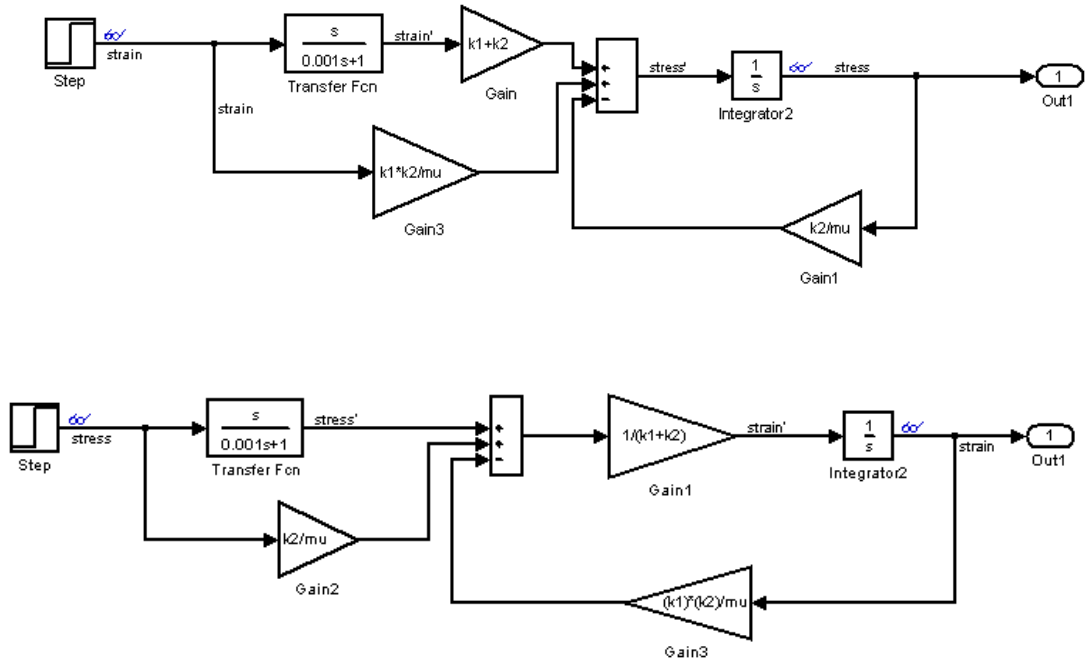

Figure D5. Standard Linear step strain model (a) and step stress model (b)

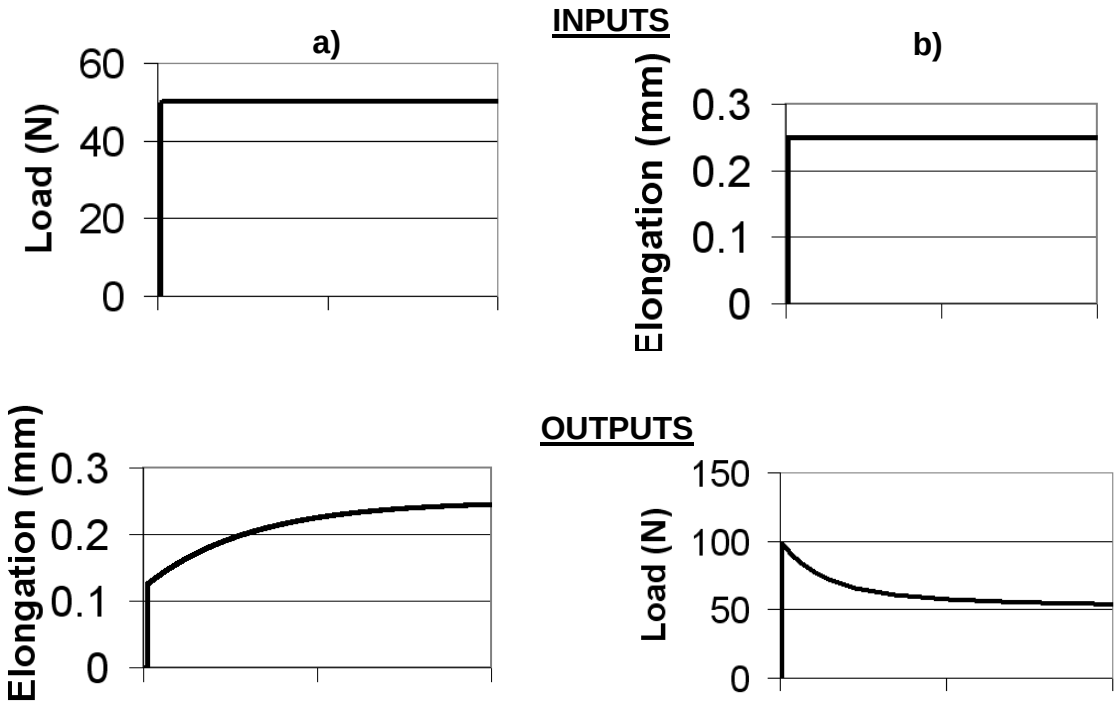

Figure D6. Load output from step elongation model, load output from step elongation model. μ and E are the same in both cases

In this case both the stress relaxation and creep are modelled.

In order for these models have physical significance they are commonly used with the technique of curve fitting to experimental data. Curve fitting normally requires the use of

many Voigt elements in series or Maxwell elements in parallel. These are called the generalised Maxwell (or Maxwell-Weichert) and generalised Kelvin-Voigt.

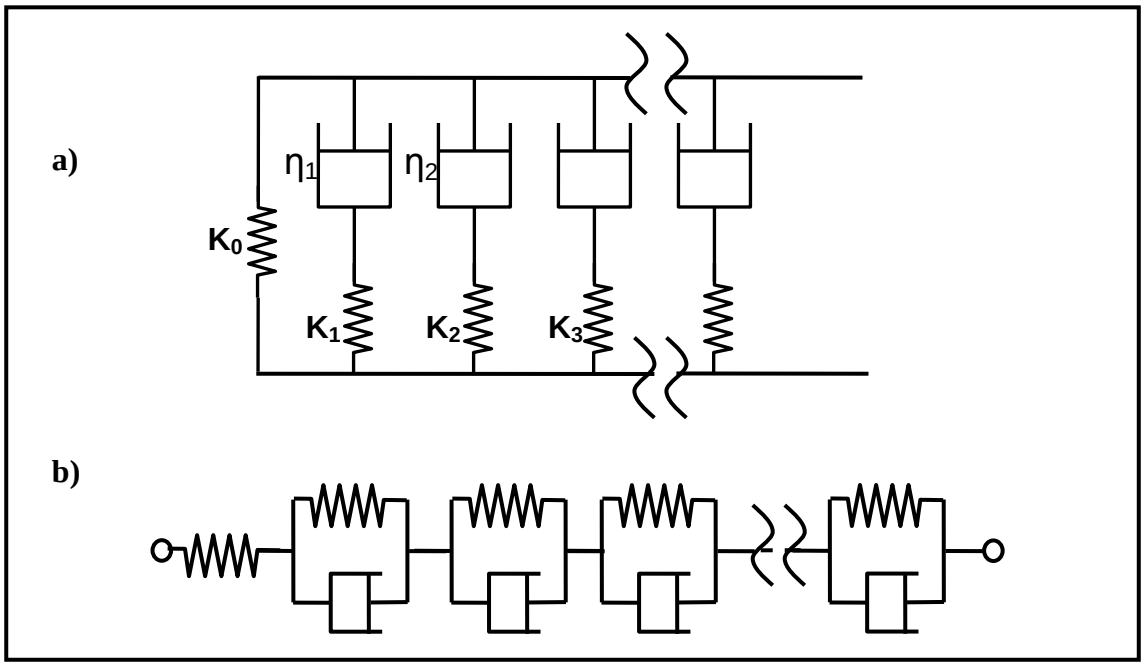

Figure D7. Generalised Maxwell model (a) and Generalised Voigt model (b)

Accordingly, the Standard Linear Solid model can be described as a Generalised Maxwell-Weichert model of the first order. For the tissue models, the input will be extension and the output load therefore the Generalised Maxwell equation was used.

$$L(t) = K_1*\delta + K_2*\delta*e^{(-K_2*t/\eta_2)} + ... + K_n*\delta*e^{(-K_n*t/\eta_n)}$$

APPENDIX E: TEMPERATURE EFFECTS

When running tests over a period of time to mimic daily extensions performed clinically, loads measured between the piston and the device were found to increase after the expected immediate relaxation had taken place.

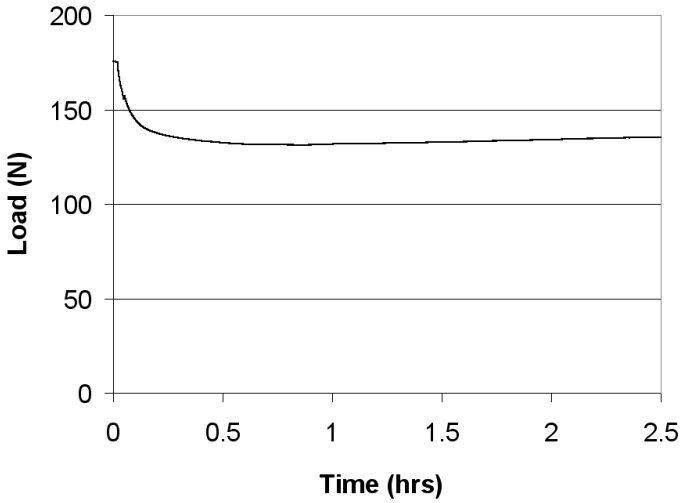

Figure E1 Rise in load following immediate load relaxation

By measuring over a longer time period it was found that the hydraulic system was experiencing cyclic changes in load over the course of 24hrs. Room temperature was logged using a thermocouple over the course of a day and is shown in Figure D2 plotted against the load changes in the closed system. Thus the load changes were attributed to a pressure variation from water expansion due to temperature changes.

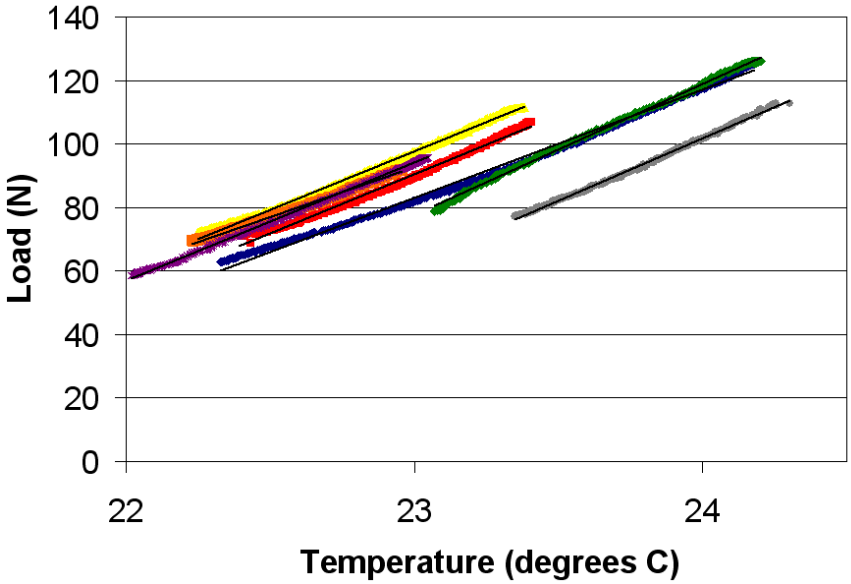

Figure E2. The relationship between Load and temperature

In order to correct for temperature effects, the load was monitored over 3days and the average load increase per degree was measured as 36.2N/degree with a standard deviation of 4.0. However, further testing revealed that there was a small degree of fluid loss through the value due to higher pressure. Consequently it was clear that test durations had to be reduced to keep this temperature effect to a minimum.

APPENDIX F – HEALING MODEL

The outline of each of the proposed numerical models.for healing are given below:

APPENDIX F (i) OUTLINE OF HEALING MODEL 1

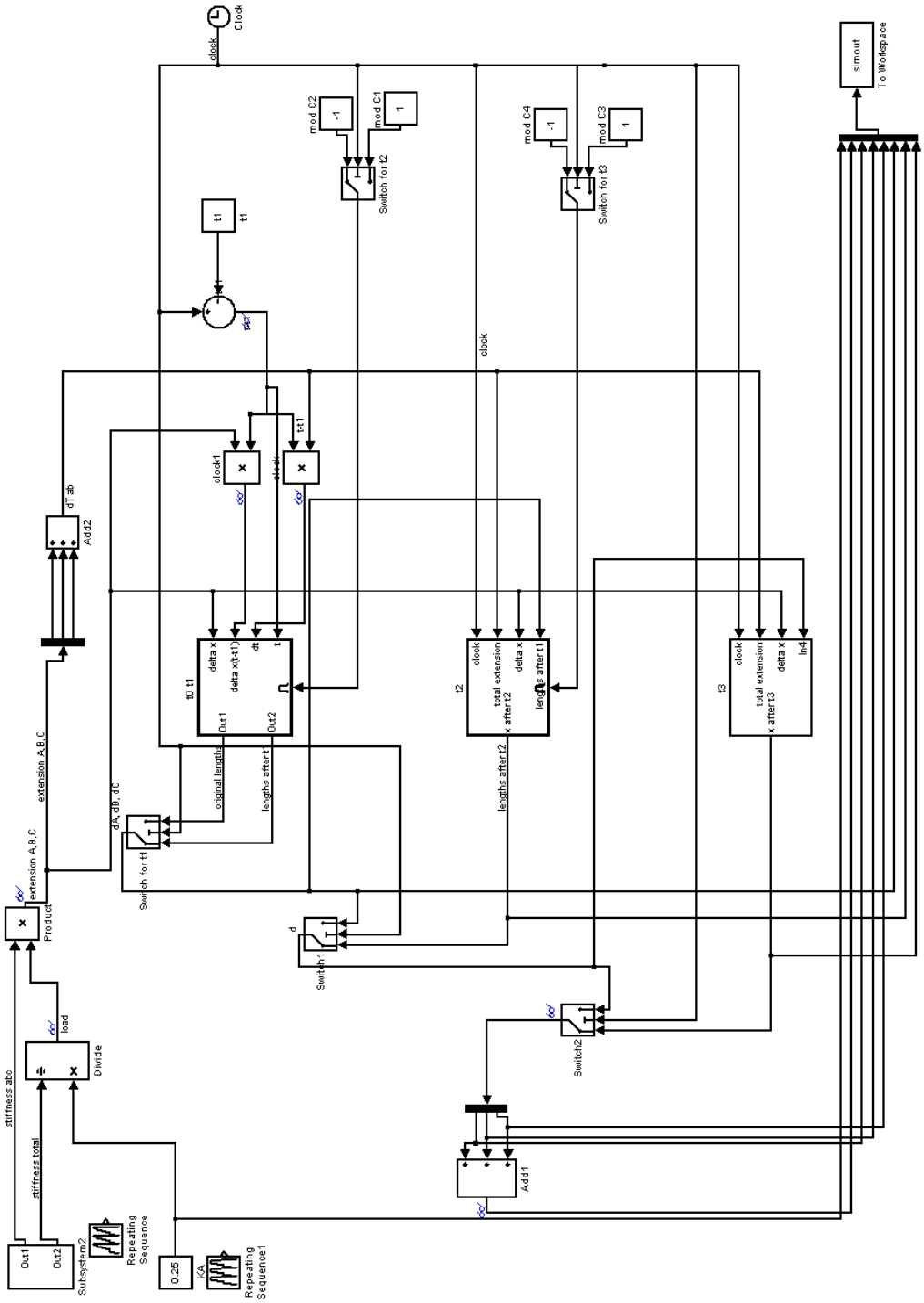

APPENDIX F (ii) OUTLINE OF HEALING MODEL 2

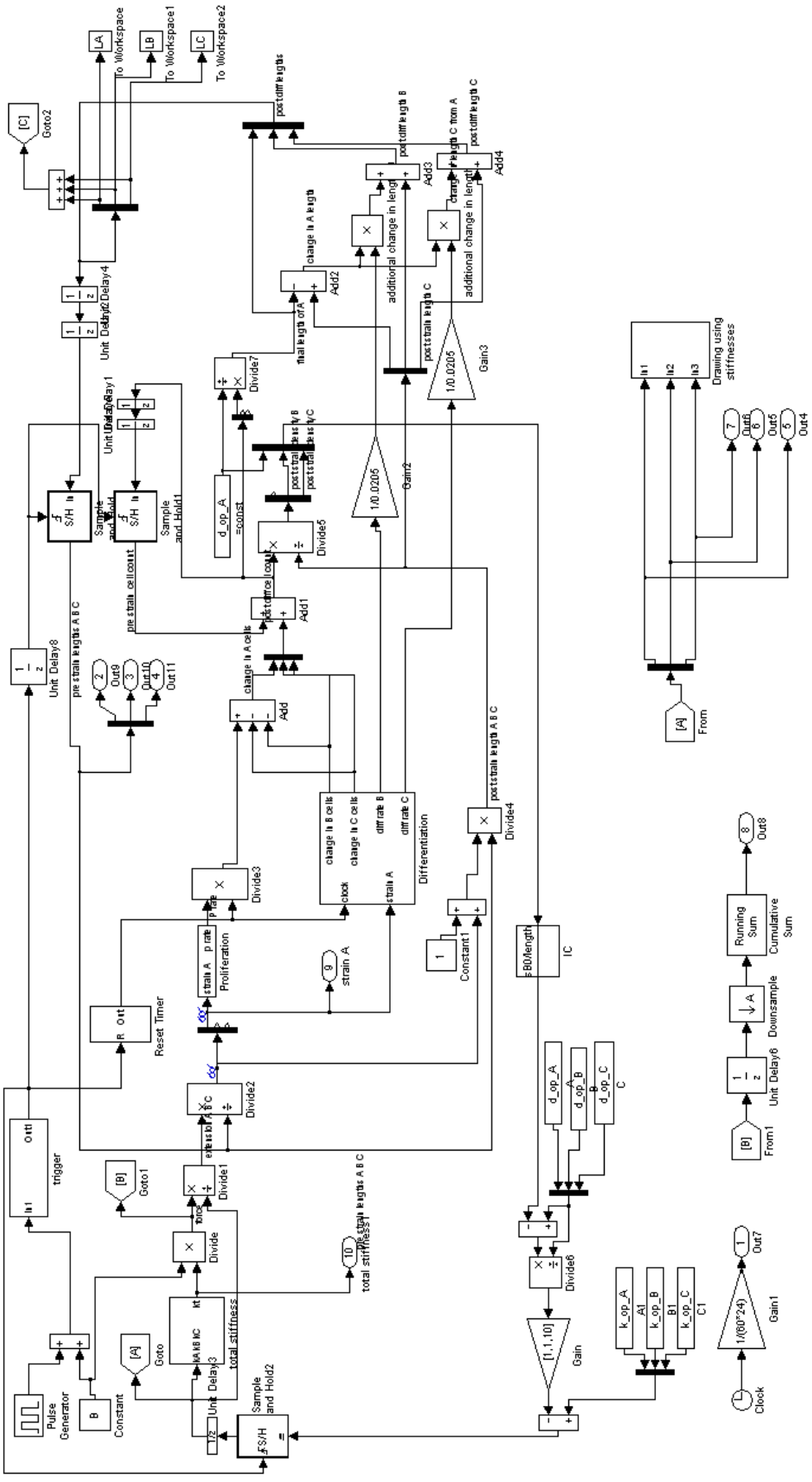

APPENDIX F (iii) OUTLINE OF HEALING MODEL 3

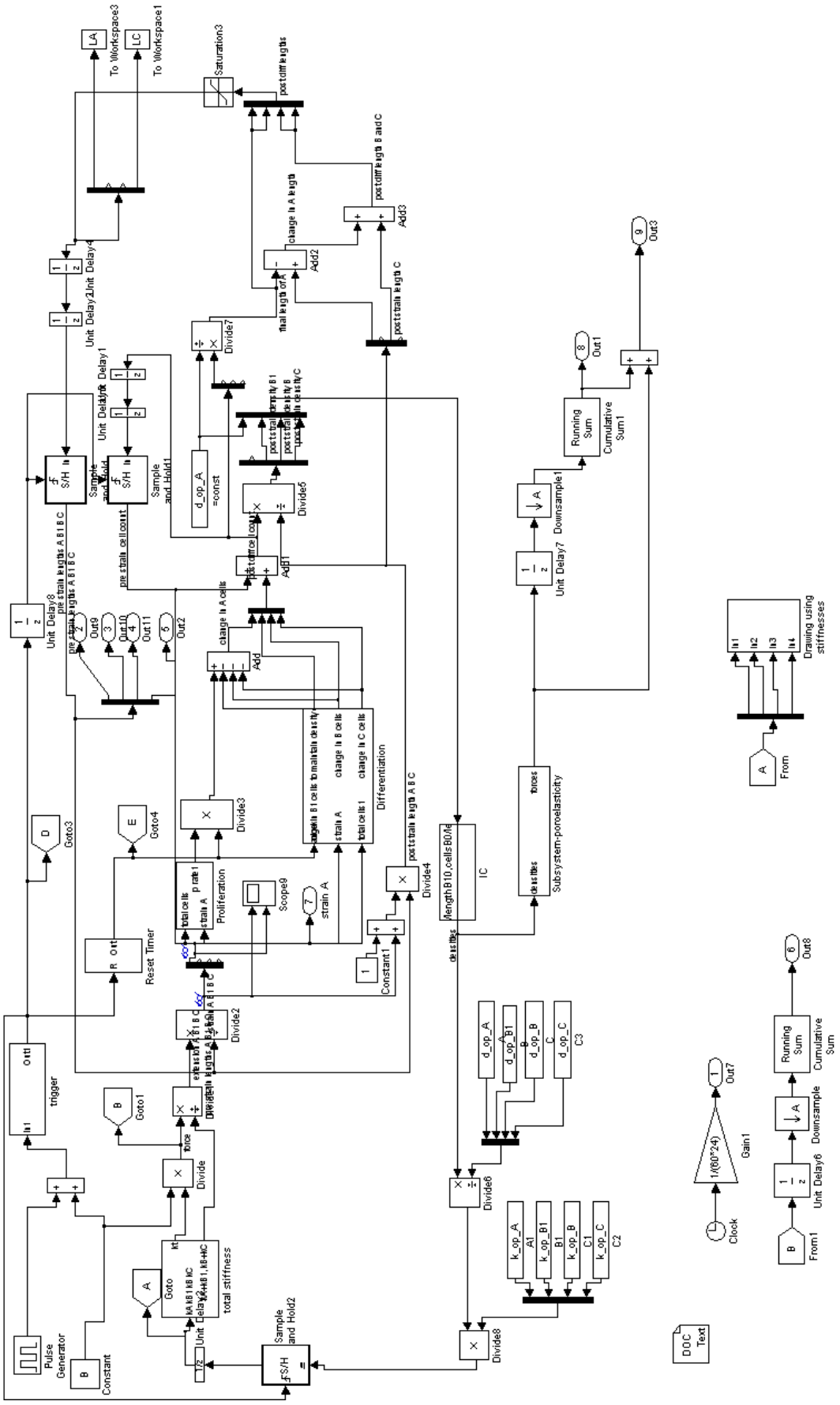

APPENDIX G – ANIMAL TISSUE STUDY

An animal tissue study was conducted to attempt to compare the loads between the two devices and to identify issues of using the device in a near clinical environment.

The hind legs of a lamb were sourced and used as soon after slaughter as possible (2-3days) to maintain mechanical properties. They were not separated to ensure comparability. The PBL device was mounted on one leg, manual device on the other. Operative technique was found from literature and surgical guides for external fixation devices. Tissue was separated down to the bone, 4mm stainless steel pins were inserted, an osteotomy performed and the device placed on the pins. Two pins per site were to be used but, due to poor clamp design, only one pin per site gave ample holding in the PBL bone.

A preload of 50-60N was applied to both of the limbs by an initial extension of the device. This was more difficult in the PBL device as the fastest extension possibly was selecting the 2sec/micron ramp rate, which results in approx 2mm/hour. Consequently the alternative was to move the clamp manually along the body of the device before clamping which did not always result in the correct preload.

The traditional manual lengthening device was extended by 4x1mm per day. The automated device provided quasi-continuous distraction at the same rate (4mm/day). This elevated rate was chosen to highlight the viscoelastic tendencies of the tissue and to ensure a load increase was visible.

Loads were measured using load cell bobbin within the manual device and an instrumented (strain gauged) component in the automated device.

Of course the study has its limitations (including no resistance from the bone regenerate, no healing during extension, no vascularisation) but even so, the aim can be achieved of having a first real tissue comparison as well as identifying the issues surrounding use in biological tissues.

Figure G1. Manual device (right leg) and automated device on left leg of lamb

The load response of the tissue during the stepwise test gave a characteristic viscoelastic response with obvious stress relaxation taking place (Figure F2).

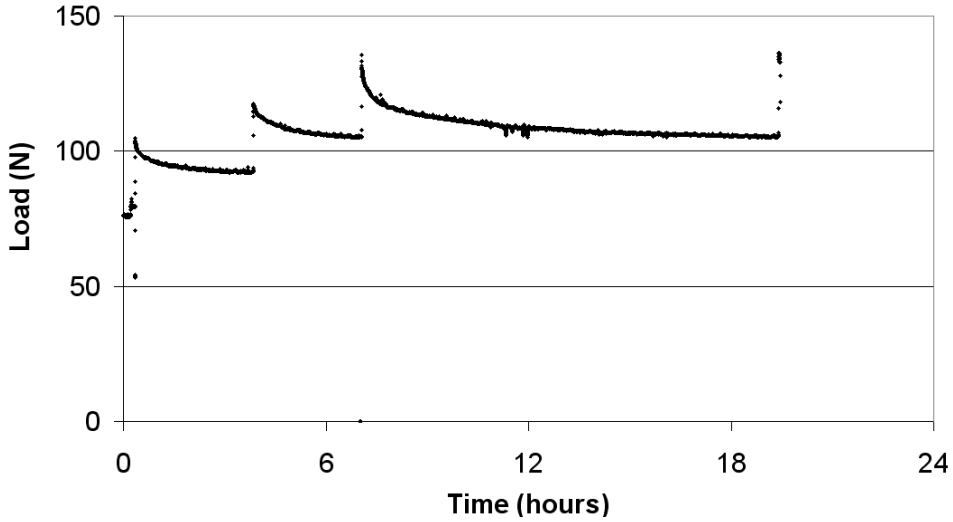

Figure G2 – Manual device load values at rate 4mm/day. Viscoelastic response is clear.

The load increased sharply after each 1mm extension then reduced gradually before the next cycle i.e. the initial load of cycle 2 = relaxation load of cycle 1. The graph shows the highly viscoelastic nature of the tissue as expected. The relaxation was 50% complete after 3hrs but was 95% complete after 12hrs.

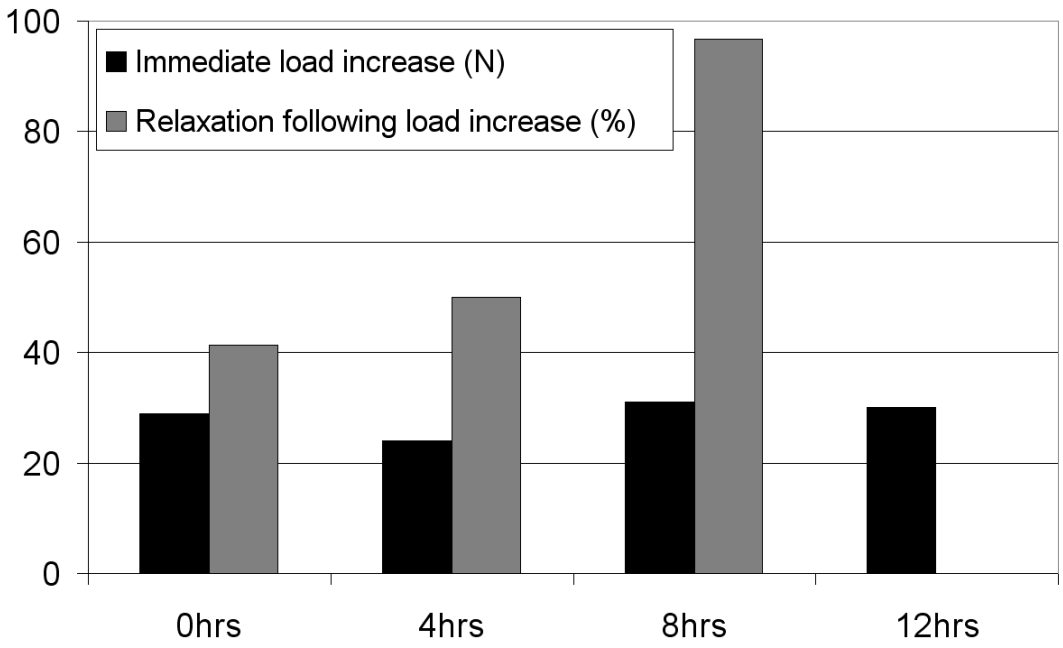

Figure G3. Percentage increase and relaxations due to rate of 4mm/day

This suggests that soft tissue relaxation is incomplete between daytime distractions and that the longer break overnight is used to achieve full relaxation. Of course the extensions in this test were larger than clinical norm but the absolute load increases per step were within the range measured clinically.

Unfortunately these loads were not able to be compared to the automated device as the load data for the device was erroneous. This was mainly due to the undesirable movement of the gauged component. However, load limits could be extracted it was noted that the load did not go above that of the manual device.

Although a comparison could not be made the study showed that relaxations are likely to be incomplete between daily distractions with manual devices and that the load during automated continuous distraction remained lower than that of stepwise lengthening.

REFERENCES

Aarnes, G.T., Steen, H., Ludvigsen, P., Kristiansen, L.P., Reikerås, O. (2002a) Tissue response during monofocal and bifocal leg lengthening in patients, *Journal of Orthopaedic Research,* 20 (1), pp.137-141

Aarnes, G.T., Steen, H., Ludvigsen, P., Kristiansen, L.P., Reikerås, O. (2002b) High frequency distraction improves tissue adaptation during leg lengthening in humans, *Journal of Orthopaedic Research,* 20 (4), pp.789-792

Aarnes, G.T., Waanders, N.A., Huiskes, R., Goldstein, S.A. (2005) In vivo assessment of regenerate axial stiffness in distraction Osteogenesis, *Journal of Orthopaedic Research,* 23, pp.494-498

Antoci, V., Ono, C.M., Antoci, V.Jr, Raney, E.M. (2006) Axial deformity correction in children via distraction Osteogenesis, *International Orthopaedics,* 30, pp.278–283

Aronson, J. and Harp, J.H. (1994) Mechanical forces as predictors of healing during tibial lengthening by distraction osteogenesis, *Clinical Orthopaedics and Related Research,* 301, pp.73-79

ASTM F1541 – 02 (2007) e1, Standard Specification and Test Methods for External Skeletal Fixation Devices

Babic J. and Lenarcic, J. (2004) In vivo determination of triceps surae muscle–tendon complex viscoelastic properties, *European Journal of Applied Physiology,* 92, pp.477–484

Baidya, K.P., Ramakrishna, S., Rahman, M., Ritchie, A. (2001) Advanced textile composite ring for Ilizarov external Ring fixator, *Proceedings of the Institution of Mechanical Engineers Part H,* 215, pp.11-23

Baumgart, R., Betz, A., Schweiberer, L. (1997) A fully implantable motorized intramedullary nail for limb lengthening and bone transport, *Clinical Orthopaedics & Related Research,* 343, pp.135–143

Benirschke, S.K., Mirels, H., Jones, D., Tencer, A.F. (1993) The use of resonant frequency measurements for the noninvasive assessment of mechanical stiffness of the healing tibia, *Journal of Orthopaedic Trauma,* 7 (1), pp.64-71

Betz, A., Hax, P.-M., Hierner, R., Kortmann, H.-R. (2008) Lengthening correction of the lower extremities with fully implantable marrow distraction nails. System comparison by means of case studies, *Trauma und Berufskrankheit,* 10 (1), pp.45-54

Biedermann, R., Kirschbichler, K., Kaufmann, G., Mattesich, M., Frischhut, S., Krismer, M. (2006) Deformity correction and limb lengthening by external fixation. Is the Taylor Spatial Frame superior to other devices?, *Journal of Bone and Joint Surgery,* 88-B, Supp I, pp.125

Boccaccio, A., Prendergast, P.J.,Pappalettere, C., Kelly, D.J. (2008) Tissue differentiation and bone regeneration in an osteotomized mandible: a computational analysis of the latency period, *Medical and Biological Engineering and Computing*, 46, pp.283–298

Cai, G., Saleh, M., Coulton, L., Yang, L. (2004) Distraction-resisting force during tibial diaphyseal lengthening and consolidation—a study on a rabbit model, *Clinical Biomechanics,* 19, pp.733–737

Canudas de Wit, C., Olsson, H., Åström, K.J., Lischinsky, P. (1995) A new model for control of systems with friction, *IEEE Transactions on Automatic Control*, 40 (3), pp.419-425

Carter, D.R., Blenman, P.R., Beaupre, G.S. (1988) Correlations between mechanical stress history and tissue differentiation in initial fracture healing, *Journal of Orthopaedic Research,* 6, pp.736-748

Carter D.R., Beaupre G.S., Giori N.J., Helms J.A. (1998) Mechanobiology of Skeletal Regeneration, *Clinical Orthopaedics and Related Research*, 355S, pp.41-55

Claes, L.E., Heigele, C.A., Neidlinger-Wilke, C., Kaspar, D., Seidl, W., Margevicius, K.J., Augat, P. (1998) Effects of mechanical factors on the fracture healing process, *Clinical Orthopaedics and Related Research,* 355-S, pp.S132-S147

Claes, L.E. and Heigele, C.A. (1999) Magnitudes of local stress and strain along bony surfaces predict the course and type of fracture healing, *Journal of Biomechanics*, 32, pp.255-266

Claes, L. (2007) Biomechanical mechanisms and considerations of Distraction Osteogenesis, *53rd Annual meeting of the Orthopaedic Research Society,* Distraction Osteogenesis – a most advanced form of tissue engineering.

Codivilla, A. (1905) On the means of lengthening, in the lower limbs, the muscles and tissues which are shortened through deformity. Reprinted in *Clinical Orthopaedics and Related Research,* (2008), 466, pp.2903–2909

Cole, J.D., Justin, D., Kasparis, T., DeVlught, D., Knobloch, C. (2001) The intramedullary skeletal kinetic distractor (ISKD): first clinical results of a new intramedullary nail for lengthening of the femur and tibia, *Injury*, 32, pp.129-13

Cowin S.C. and Moss, M.L., (2001) Mechanosensory mechanisms in bone, in: Bone Mechanics Handbook, Second Edition, Edited by Cowin S.C., Boca Raton, CRC press

Cunningham, J.L., Evans, M., Harris, J.D., Kenwright, J. (1987) The measurement of stiffness of fractures treated with external fixation, *Engineering in Medicine*, 16 (4), pp.229-232

Currey, J.D. (2002) Bones: Structure and Mechanics, Princeton University Press, Princeton, NJ

Dahl, P.R. (1968) A solid friction model. Technical Report TOR-0158H3107–18I-1. Prepared for The Aerospace Corporation, El Segundo, CA

Doblare, M., Garcıa, J.M., Gomez, M.J. (2004) Modelling bone tissue fracture and healing: a review, *Engineering Fracture Mechanics*, 71, pp.1809–1840

Dhar, P.R. and Zu, J.W. (2007) Design of a resonator device for in vivo measurement of regional tissue viscoelasticity, *Sensors and Actuators- A*, 133, pp.45–54

Encylopaedia Britannica online, Art. Muscles of human leg www.britannica.com/EBchecked/media/101369/Posterior-view-of-the-right-leg-showing-the-muscles-of> Accessed 5/9/2011

Eveleigh, R.J (1997) Biomechanical Evaluation of IM nails during simulated fracture healing. PhD Thesis, University of Bath, England

Fadel, M. and Hosny, G. (2005) The Taylor spatial frame for deformity correction in the lower limbs, *International Orthopaedics*, 29 (2), pp.125-129

Figueiredo, U.M., Watkins, P.E., Goodship, A.E. (1993) The effects of micromotion in distraction osteogenesis, *Transactions of the Annual Meeting - Orthopaedic Research Society*, 18 (130)

Fink, B. (1996) Osteogenesis and its influencing factors during treatment with the Ilizarov method, *Clinical Orthopaedics and Related Research*, 323, pp.261-272

Fischgrund, J., Paley, D., Suter, C. (1994) Variables affecting time to bone healing during limb lengthening, *Clinical Orthopaedics and Related Research,* 301, pp.31-37.

Forriol, F., Goenaga, I., Mora, G., Vinolas, J., Canadel, J. (1997) Measurement of bone lengthening forces; an experimental model in the lamb, *Clinical Biomechanics,* 121, pp.17-21

Fragomen, A.T. and Rozbruch, S.R. (2007) The Mechanics of External Fixation. *Hospital for Special Surgery Journal*, 3 (1), pp.13-29

Fukashiro, S., Noda, M., Shibayama, A. (2001) In vivo determination of muscle viscoelasticity in the human leg, *Acta Physiologica Scandinavica,* 172 (4), pp.241–248

Fung, Y.C. (1983) *Biomechanics: Mechanical properties of living tissues*. Second Edition, Springer, New York.

Gardner, T.N., Evans, M., Kenwright, J. (1997a) A biomechanical study on five unilateral external fracture fixation devices, *Clinical Biomechanics,* 12 (2), pp.87-96

Gardner, T.N., Evans, M., Simpson, A.H.R.W., Kyberd, P.J., Kenwright, J. (1997b) A method of examining the magnitude and origin of 'hard' and 'soft' tissue forces resisting limb lengthening, *Medical Engineering and Physics,* 19, pp.405-411

Gardner, T.N., Evans, M., Simpson, H., Kenwright, J. (1998) Force-displacement behaviour of biological tissue during distraction Osteogenesis, *Medical Engineering and Physics,* 20 (9) pp.708-715

Gardner, T.N., Stoll, T., Marks., L., Mishra, S., Knothe Tate., M. (2000) The influence of mechanical stimulus on the pattern of tissue differentiation in a long bone fracture - FEM study, *Journal of Biomechanics,* 33, pp.415-425

Gasser, B., Boman, B., Wyder, D., Shneider, E. (1990) Stiffness characteristics of the circular Ilizarov device as opposed to conventional external fixator, *Journal of Biomechanical Engineering*, 112, pp.15-21

Gaul, L. and Nitsche, R. (2000) Friction Control for Vibration Suppression, *Mechanical Systems and Signal Processing*, 14 (2), pp.139–150.

Gomez-Benito, M.J., Garcı´a-Aznar, J.M., Kuiper, J.H., Doblare, M. (2005) Influence of fracture gap size on the pattern of long bone healing: a computational study, *Journal of Theoretical Biology*, 235, pp.105–119

Goodship, A.E. and Kenwright, J. (1985) The influence of induced micromovement upon the healing of experimental tibial fractures, *Journal of Bone and Surgery,* 67-B (4), pp.650-655

Greenwood, J.A. and Williamson, J.B.P. (1966) Contact of Nominally Flat Surfaces, *Proceedings of the Royal Society of London. Series A, Mathematical and Physical Sciences*, 295 (1442), pp.300-319

Guichet, J.-M. and Casar, R.S. (1997) Mechanical characterization of a totally intramedullary gradual elongation nail, *Clinical Orthopaedics and Related Research*, 337, pp.281-290

Guichet, J.-M., Deromedis, B., Donnan, L.T., Peretti, G., Lascombes, P., Bado, F. (2003) Gradual femoral lengthening with the albizzia intramedullary nail, *Journal of Bone and Joint Surgery - Series A,* 85 (5), pp.838-848

Haessig Jr. D.A. and Friedland, B. (1990) On the modeling and simulation of friction. *Proceedings of the American Control Conference*, pp.1256-1261

Hankemeier, S., Go¨sling, T., Pape, H.C., Wiebking, U., Krettek, C. (2005) Limb lengthening with the Intramedullary Skeletal Kinetic Distractor (ISKD), *Operative Orthopadie und Traumatologie,* 17 (1), pp.79-101

Hente, R., Cordey, J., Perren, S.M. (2003) In vivo measurement of bending stiffness in fracture healing, *BioMedical Engineering OnLine*, 29 (8)

Hertz, H. (1896) Miscellaneous Papers, *On the contact of elastic solids.* New York, Macmillan and Co. Ltd

Huiskes, R. and Chao, E.Y.S. (1986) Guidelines for External Fixation Frame Rigidity and Stresses, *Journal of Orthopaedic Research*, 4, pp.68-75

Huiskes, R., Van Driel, W.D., Prendergast, P.J., Søballe, K. (1997) A biomechanical regulatory model for periprosthetic fibrous-tissue differentiation, *Journal Of Materials Science: Materials In Medicine*, 8, pp.785-788

IEC 60601-1-4 Ed. 1.1 b: (2000) Medical electrical equipment - Part 1-4: General requirements for safety - Collateral Standard: Programmable electrical medical systems

Ilizarov, G.A. (1989a) The tension-stress effect on the genesis and growth of tissues. Part I. The influence of stability of fixation and soft-tissue preservation, *Clinical Orthopaedics and Related Research*, 238, pp.249-281.

Ilizarov, G.A. (1989b) The tension-stress effect on the genesis and growth of tissues: Part II. The influence of the rate and frequency of distraction, *Clinical Orthopaedics and Related Research*, 239, pp.263-285

Ilizarov, G.A. (1990) Clinical application of the tension-stress effect for limb lengthening, *Clinical Orthopaedics and Related Research*, 250, pp.8-26.

Institute for limb lengthening and complex reconstruction. Hospital for special surgery, Weill Cornell Medical College. Image: Femur lengthening in a child with a growth-plate injury.
http://www.limblengthening.com/casehistories/ch06/ch06.html# Accessed 10/5/07

Isaksson, H., Wilson,W., van Donkelaar, C.C., Huiskes, R., Ito, K. (2006) Comparison of biophysical stimuli for mechano-regulation of tissue differentiation during fracture healing, *Journal of Biomechanics,* 39, pp.1507–1516

Isaksson, H., Comas, O., Donkelaar, C.C., Mediavilla, J., Wilson, W., Huiskes, R., Ito, K. (2007) Bone regeneration during distraction osteogenesis: Mechano-regulation by shear strain and fluid velocity, *Journal of Biomechanics,* 40, pp.2002–2011

Isaksson, H., van Donkelaar, C.C., Ito, K. (2009) Sensitivity of tissue differentiation and bone healing predictions to tissue properties, *Journal of Biomechanics*, 42, pp.555–564

Jacobson, B. (2003) The Stribeck Memorial lecture, *Tribology International,* 36, pp.781–789

Kenawey, M., Krettek, C., Liodakis, E., Wiebking, U., Hankemeier, S. (2011) Leg lengthening using intramedullary skeletal kinetic distractor: Results of 57 consecutive applications, *Injur*y, 42, pp.150-155

Krawczyk, A., Kuropka, P., Kuryszko, J., Wall A., Dragan S., Kulej M. (2007) Experimental studies on the effect of osteotomy technique on the bone regeneration in distraction Osteogenesis, *Bone*, 40, pp.781-791.

Krieg, A.H., Lenze, U., Speth, B.M., Hasler, C.C. (2011) Intramedullary leg lengthening with a motorized nail: Indications, challenges, and outcome in 32 patients, *Acta Orthopaedica*, 82 (3), pp.344–350

Kuiper, J.H., Ashton, B.A., Richardson, J.B. (2000) Computer simulation of fracture callus formation and stiffness restoration. *Proceedings of the 12th conference of the European Society of Biomechanics*, Dublin, p.61

Lauterburg, M.T., Exner, G.U., Jacob H.A.C. (2006) Forces involved in lower limb lengthening: an in vivo biomechanical study, *Journal of Orthopaedic Research*, 24, pp.1815–1822

Lacroix, D. and Prendergast, P.J. (2002) A mechanoregulation model for tissue differentiation during fracture healing: analysis of gap size and loading, *Journal of Biomechanics*, 35, pp.1163–1171

Leidinger, B., Winkelmann, W., Roedl, R. (2006) Limb lengthening with a fully implantable mechanical distraction intramedullary nail, *Zeitschrift fur Orthopadie und Ihre Grenzgebiete*, 144 (4), pp.419-426

Leong, P.L. and Morgan, E.F. (2008) Measurement of fracture callus material properties via nanoindentation , *Acta Biomaterialia*, 4, pp.1569–1575

Love, J., Yang, L., Saleh, M. (2003) The effect of soft tissue tension on osteotomy stability during distraction, *Journal of Bone and Joint Surgery*, 87-B, Supp_III, p.232

Loverich, J.J., Koopmann G.H., Lesieutre, G.A. (2007) A New Piezoelectric Actuator Using a Feed-screw for Quasi-static Motion Accumulation – Part II: Mathematical Modeling and Design Optimization, *Journal of Intelligent Material Systems and Structures*, 0, pp.1-10

Machirajua, C., Phana, A.-V., A.W. Pearsall, A.W., Madanagopalb, S. (2006) Viscoelastic studies of human subscapularis tendon: Relaxation test and a Wiechert model, *Computer methods and programs in biomedicine*, 83, pp.29–33

Magnusson, S.P., Aagaard, P., Rosager, S., Poul Dyhre-Poulsen, P., Kjaer, M. (2001) Load–displacement properties of the human triceps surae aponeurosis in vivo, *Journal of Physiology*, 531 (1), pp.277–288

Manner, H.M., Huebl, M., Radler, C., Ganger, R., Petje, G., Grill, F. (2007) Accuracy of complex lower-limb deformity correction with external fixation: a comparison of the Taylor Spatial Frame with the Ilizarov Ring fixator, *Journal of Childrens Orthopaedics*, 1, pp.55–61

Marieb, E.N. and Hoehn, K (2010) Human Anatomy and Physiology. Eighth Edition. Pearson Education, Inc. San Francisco, USA

Markel, M.D., Wikenheiser., M.A., Chao, E.Y.S. (1990) A Study of Fracture Callus Material Properties: Relationship to the Torsional Strength of Bone, *Journal of Orthopaedic Research,* 8, pp.843-850

Matsuura, M., Lounici, S., Inoue, N., Walulik, S., Chao, E.Y. (2003) Assessment of External Fixator Reusability Using Load- and Cycle-Dependent Tests, *Clinical Orthopaedics & Related Research*, 406 (1), pp275-281

McDonald, S.J., Dooley, P.C., McDonald, A.C., Schuijers, J.A., Ward, A.R., Grills, B.L. (2009) Early Fracture Callus Displays Smooth Muscle-Like Viscoelastic Properties Ex Vivo: Implications for Fracture Healing, *Journal of Orthopaedic Research*, 27 (11) pp.1508-13

McNally, M (2008) Nuffield Orthopaedic Centre, Oxford. Private Communication

Moorcroft, C.I., Ogrodnik, P.J., Thomas, P.B.M., Wade, R.H. (2001) Mechancial properties of callus in human tibial fractures: a preliminary investigation, *Clinical Biomechanics,* 16, pp.776-782

Mora, G. and Forriol, F. (2000) Mechanical analysis of the healing of different osteotomies fixed externally, *International Orthopaedics*, 24, pp.295–298

Morgan, E.F., Longaker, M.T., Carter, D.R. (2006) Relationships between tissue dilatation and differentiation in distraction, *Osteogenesis Matrix Biology*, 25, pp.94 – 103

Morin, A.J. (1833) New friction experiments carried out at metz in 1831-1833, *Proceedings of the French Royal Academy of Sciences*, 4, pp.1–128

Nakamura, K., Matsushita, T., Okazaki, H., Kurokawa, T. (1997) Soft tissue responses to limb lengthening, *Journal of Orthopaedic Science*, 2, pp.191-197

National Institute for Clinical Excellence (2006a) Interventional Procedures. Programme. Interventional procedure overview of intramedullary distraction for lower limb lengthening – 358

National Institute for Clinical Excellence (2006b) Intramedullary distraction for lower limb lengthening, Guidance document, ISBN 1-84629-325-1

National Institute for Health and Clinical Excellence (2006c) 358 – Intramedullary distraction for lower limb lengthening, Comments table.

Noonan, K.J., Leyes M., Forriol, F., Canadell, J. (1998) Distraction Osteogenesis of the Lower Extremity with Use of Monolateral External Fixation: A Study of Two Hundred and Sixty-one Femora and Tibiae, *The Journal of Bone and Joint Surgery*, 80, pp.793-806

Ogrodnik, P.J., Moorcroft, C.I., Thomas, P.B.M. (2007) An automated system for measuring multi-dimensional, time dependent mechanical properties of a human tibial fracture, *Medical Engineering & Physics*, 29, pp.1049–1055

Ohnishi, I., Kurokawa, T., Sato, W., Nakamura, K. (2005) Measurement of the tensile forces during bone lengthening, *Clinical Biomechanics,* 20 (4), pp.421-427

Ohyama M., Miyasaka Y., Sakurai M.,Yokobori A.J., Sasaki S. (1994) The mechanical behavior and morphological structure of callus in experimental callotasis. *Biomedical Materials and Engineering,* 4, pp.273–281

Olsson, H., Åström, K.J., Canudas de Wit, C., Gäfvert, M., Lischinsky, P. (1998) Friction Models and Friction Compensation, *European Journal of Control,* 4 (3), pp.176-195

Onions, R.A. and Archard J. F. (1973) The contact of surfaces having a random structure, *Journal of Physics D: Applied Physics,* 6 (3), pp.289-304

Orthofix (1999) Operative Technique Limb reconstruction system. Part A: General Principles

Paley, D., Herzenberg, J.E., Paremain, G., Bhave, A. (1997) Femoral lengthening over an intramedullary nail. A matched-case comparison with Ilizarov femoral lengthening, *Journal of Bone and Joint Surgery,* 79 (10), pp.1464-1480

Pauwels, F. (1960) Eine neue theorie über den einfluß mechanischer reize auf die differenzierung der stützgewebe. Translated as "A new theory concerning the influence of mechanical stimuli on the differentiation of the supporting tissues." *Zeitschrift fur Anatomie und Entwicklungsgescichte,* 121, pp.478-515

Perren S.M. (1979) Physical and biological aspects of fracture healing with special reference to internal fixation. *Clinical Orthopaedics and Related Research,* 138, pp.175–196

Physik Instrumente (2005) The World of Micro- and Nanopositioning, Catalogue

Podolsky, A. and Chao, E.Y.S. (1993) Mechanical performance of Ilizarov circular external fixators in comparison with other external fixators, *Clinical Orthopaedics and Related Research,* 293, pp.61-70

Pouliquin J.C., Pauthier F, Ucla E, Kassis B., Coelin J.L., Langlais, J. (1994) Tension measurements during lengthening of the lower limbs in children and adolescents, *Journal of Pediatric Orthopaedics, Part B,* 3, pp.107–113.

Prendergast, P.J., Huiskes, R., Soballe, K. (1997) Biophysical stimuli on cells during tissue differentiation at implant interfaces, *Journal of Biomechanics,* 30, pp.539–548

Reina-Romo, E., Gómez-Benito, M.J. , García-Aznar, J.M. , Domínguez, J. , Doblaré, M. (2009a) Modeling distraction osteogenesis: Analysis of the distraction rate, *Biomechanics and Modeling in Mechanobiology,* 8 (4), pp.323-335

Reina-Romo E., Gómez-Benito, M.J., García-Aznar, J.M., Doblaré, M. (2009b) Growth mixture model of distraction osteogenesis: effect of pre-traction stresses, *Biomechanics and Modeling in Mechanobiology,* 9 (1), pp.103-115

Richardson, J.B., Kenwright J., Cunningham J.L. (1992) Fracture stiffness measurement in the assessment and management of tibial fractures, *Clinical Biomechanics*, 7, pp.75–79

Shepherd, L.E., Zalavras, C.G., Shean, C. (2001) Femoral lengthening techniques, *Operative Techniques in Orthopaedics*, 11 (3), pp.178-186.

Shevtsov V.I., Vasilyevich Popkov A. (2002), Limb lengthening in automatic mode, *Ortopedia Traumatologia Rehabilitacja* , 4 (4), pp.403-412

Simpson, A.H.R.W., Cunningham, J.L, Kenwright, J. (1996) The forces which develop in the tissues during leg lengthening. A clinical study, *The Journal of Bone and Joint Surgery*, 78-B (6), pp.979-983

Singare, S., Li, D., Liu, Y., Wu, Z., Wang, J. (2006) The effect of latency on bone lengthening force and bone mineralization: An investigation using strain gauge mounted on internal distractor device, *Biomedical Engineering Online,* 5 (18), p.8

Singh S., Lahiri A., Iqbal M. (2006) The results of limb lengthening by callus distraction using an extending intramedullary nail (Fitbone) in non-traumatic disorders, *Journal of Bone and Joint Surgery*, 88-B, pp.938-942

Smith and Nephew Richards Inc. (1991) Method and apparatus for the fixation of bone fractures, limb lengthening and the correction of deformities. United States Patent No. 5062844, Filed on 1990-09-07

Snyder, C.C., Levine, G.A., Swanson, H.M., Browne Jr, E.Z. (1973) Mandibular lengthening by gradual distraction: preliminary report, *Plastic and Reconstructive Surgery***,** 51 (5), pp.506-508

Takano, Y., Ueno, M., Kiguchi, K., Itou., J, Mawatari, M., Hotokebuchi, T. (2008) Development of a Knee Joint Motion Simulator to Evaluate Deep Knee Flexion of Artificial Knee Joints, *Conference Proceedings IEEE Engineering in Medicine and Biology Society*, pp.4571-4574

Taylor, K.F., Rafiee, B., Inoue, N., McHale, K.A., Howard, R.S., Chao, E.Y.S. (2005) Linear increase in axial stiffness of regenerate callus during limb lengthening, *Clinical Orthopaedics and Related Research*, 435, pp.239-244

Thonse, R., Herzenberg, J.E., Standard, S.C., Paley, D. (2005) Limb Lengthening with a Fully Implantable, Telescopic, Intramedullary Nail, *Operative Techniques in Orthopaedics*, 15, pp.355-362

Tjernstrom, B., Thoumas, K.-A., Pech, P. (1992) Bone remodeling after leg lengthening: Evaluation with plain radiographs, and computed tomography and magnetic resonance imaging scans, *Journal of Pediatric Orthopaedics*, 12 (6), pp.751-755

Tortora, G.J. and Grabowski, S.R. (2002) Principles of anatomy and physiology, Tenth edition, John Wiley & Sons, New York

Waanders, N.A., Richards, M., Steen, H., Kuhn, J.L., Goldstein, S.A., Goulet, J.A. (1998) Evaluation of the mechanical environment during distraction Osteogenesis, *Clinical Orthopaedics And Related Research*, 349, pp.225-234

Watanabe, Y., Takai, S., Arai, Y., Yoshino, N., Hirasawa, Y. (2006) Prediction of mechanical properties of healing fractures using acoustic emission, *Journal of Orthopaedic Research*, 19 (4), pp.548-553

Watson , M.A. (2002) Mechanics of the Ilizarov external fixation system: a finite element based study, PhD Thesis, University of Aberdeen

Wee, J., Mackenzie, W.G., Richardson, D.W., Akins, R., Dodge, G.R., Rahman, T., Levine, D., Seliktar, R. (2008) Optimizing limb lengthening using an autodistractor and force measurement, *9th Biennial Conference on Engineering Systems Design and Analysis*

Wee J., Rahman T., Akins R.E., Seliktar R., Levine D.G., Richardson D.W., Dodge G.R., Thabete A.M., Holmes L., Mackenzie W.G. (2011) Using distraction forces to drive an autodistractor during limb lengthening, *Medical Engineering & Physics*, 33, pp.1001–1007

White, S.H. and Kenwright, J. (1991) The importance of delay in distraction of osteotomies, *Orthopaedic Clinics of North America*, 22 (4), pp.569-79.

Wittenstein Intens GmbH, 2008 – Fitbone device image www.wittenstein-intens.de/img/fitbone.jpg Accessed 19/09/2011

Wolfson, N., Hearn, T.C., Thomason, J.J., Armstrong, P.F. (1990) Force and Stiffness changes during Ilizarov Leg Lengthening, *Clinical Orthopaedics and Related Research*, 250, pp.58-60

Yasui, N., Kojomoto, H., Shimizu, H., Shimomura, Y. (1991) The effect of distraction upon bone, muscle, and periosteum, *Orthopaedic Clinics of North America*, 22, pp.563–567

Younger, A. (1990) Forces measured during femoral lengthening in children, Thesis, Master of Science, University of Aberdeen

Younger, A.S.E., Mackenzie, W.G., Morrison, J.B. (1994) Femoral forces during limb lengthening in children, *Clinical Orthopaedics and Related Research*, 301, pp.55-63

Zimmermann, B.M., Betz, A.M., Ziegler, R.M. (2007) Pain during limb lengthening by a fully implantable distraction nail: Causes and therapeutic possibilities, *Pravention und Rehabilitation*, 19 (4), pp.152-157

PUBLICATIONS

MacInnes R.A., Taylor A., Hobson P. R., Brown C.J. (2008) Pre-Clinical Assessment Of A Smart Piezo-Actuated Limb Lengthening Device, *Bath Biomechanics Symposium,* Bath, UK

MacInnes, R.A., Brown, C.J., Hobson, P.R., A. Taylor, A (2009) Predicting Tissue Forces during Distraction Osteogenesis, *International Conference on the Mechanics of Biomaterials and Tissues,* Florida, USA